A Theoretical Study of some Elementary Steps Involved in Catalytic Cycles by Enzymes and Transition Metal Complexes

酵素及び遷移金属錯体の触媒サイクルに含まれる
素反応過程に関する理論的研究

学位論文

熊本大学大学院　自然科学研究科
生産科学専攻　武蔵泰雄

A THEORETICAL STUDY OF SOME ELEMENTARY STEPS INVOLVED IN CATALYTIC CYCLES BY ENZYMES AND TRANSITION METAL COMPLEXES

YASUO MUSASHI

1994

Contents

Carboxybiotin

Chapter 5 CO_2 Insertion Into a Rh(I)-H Bond

Chapter 6 CO_2 Insertion into a M-H Bond (M = Rh and Cu)

Chapter 7   **Oxidative Addition of The Si-X σ-Bond
to (X = H, C, or Si) Palladium (0) and
Platinum (0) Complexes**

Chapter 1

General Introduction

1.1 Background

The catalyst is of importance in many fields, such as synthetic and organic chemistry, biochemistry, and industrial chemistry. In general, the catalyst promotes the chemical reactions by activating chemically inactive or less active molecules, and stabilizing reactive intermediates and/or transition states. There are recent increasing interests on catalyses of the transition-metal complexes and enzymes. This is because transition-metal complexes and enzymes perform various catalytic reactions under mild reaction conditions, and several times, those reactions are highly selective. However, enzyme is generally expensive and much sensitive to reaction conditions; for instance, they are active at only moderate temperature and in the neutral pH region. Therefore, intensive efforts have been made to develop artificial enzymic catalysts that can be used under reaction conditions of wide range. Also, in transition metal catalysts, there remain several points to be solved; for instance, separation of products from substrates and catalysts, use of less expensive metals unlike rhodium and platinum, use of simple ligand, etc. In order to develop such useful catalyst, we need detailed information on the geometry, electronic state, and bonding nature of the intermediate involved in catalytic reactions. However, isolation, identification, and characterization of the intermediates are very difficult because the amount of intermediate is very small and its reactivity is high in general.

Under these circumstances, theoretical study is expected

to offer valid information not only on the geometry, electronic structure, and bonding nature of the intermediate but also on the transition state of the catalytic reaction. In this thesis, we present theoretical studies on several elementary processes involved in catalytic reactions by enzymes and transition metal complexes. The ab initio MO method is mainly employed here, in which the electron correlation effects are considered with the second ~ fourth order Møller-Plesset perturbation (MP2 ~ MP4) and single and double excitation-configuration interaction (SD-CI) methods. Detailed knowledge obtained in this thesis is expected to be useful for designing a good catalyst for CO_2 fixation.

In this chapter, reactions examined here are reviewed, the first is coenzyme-catalyzed carboxylation and decarboxylation reactions, the second is the CO_2 insertion reaction into transition metal-hydride and alkyl bonds, and the third is the oxidative addition of the Si-X σ-bond to transition metal complexes. Also, the aims of the present study are described.

1.2 Coenzyme Catalyses of Carboxylation and Decarboxylation

The coenzyme is, in general, necessary as a cofactor in the enzymic reaction and plays an important catalytic function. In enzymic reactions, there are two typical reactions related to CO_2 fixation; one is decarboxylation of pyruvate anion and the other is transcarboxylation reactions. These decarboxylation and transcarboxylation are considered to be important not only as metabolic functions but also as useful function for CO_2 fixation.[1-11]

In decarboxylation reactions, thiamin diphosphate (TDP, vitamin B_1) shown in Figure 1.1 is a coenzyme of pyruvate

2
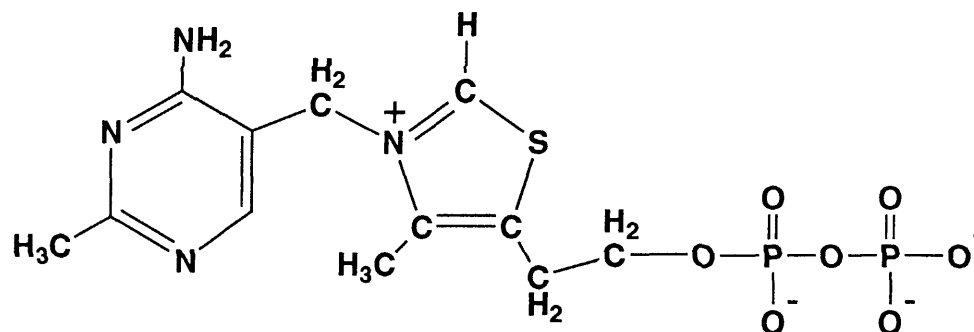
Figure 1.1 Thiamin Diphosphate (TDP)

decarboxylase which catalyzes the conversion of pyruvate to acetaldehyde and carbon dioxide (eq 1.1).[12] This reaction can be seen as electrophilic substitution of carbon dioxide for proton at an acyl carbon.[12]

$$CH_3C(O)COO^- \ + \ H^+ \ \rightarrow \ CH_3C(O)H \ + \ CO_2 \tag{1.1}$$
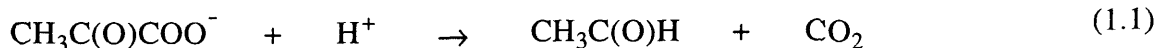
In general, the carbon atom of carbonyl is favorable for nucleophilic substitution rather than electrophilic substitution, because of its electropositive character. In fact, this type of reaction is chemically unprecedented. In spite of such unfavorable situation, the enzymic system of TDP reacts with pyruvate to form a lactyl-TDP (LTDP, Figure 1.2), in which electron density increases at the carbon atom of the carbonyl group, to accelerate the proton attack to the carbonyl carbon atom. It has been experimentally reported that the coenzyme of TDP is important in decarboxylation of pyruvate and TDP itself can catalyzes its decarboxylation.[13]

Although many experimental works have been carried out on TDP, there still remain several issues to be examined as follows;
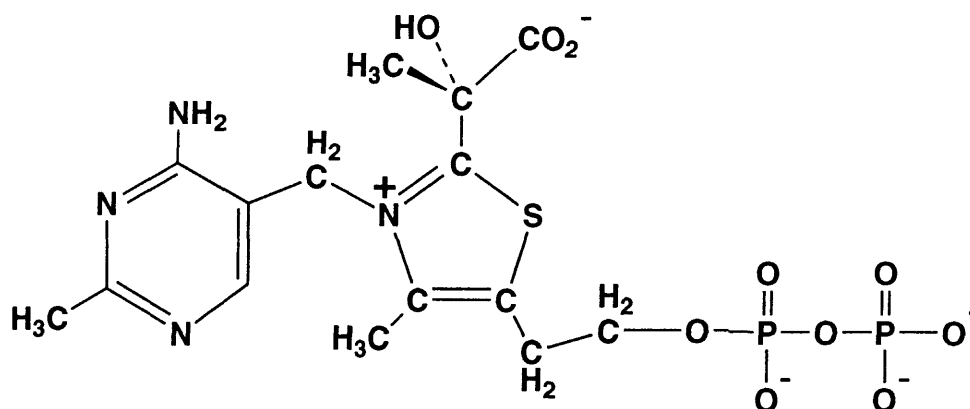
Figure 1.2 Lactyl-Thiamin Diphosphate (LTDP)
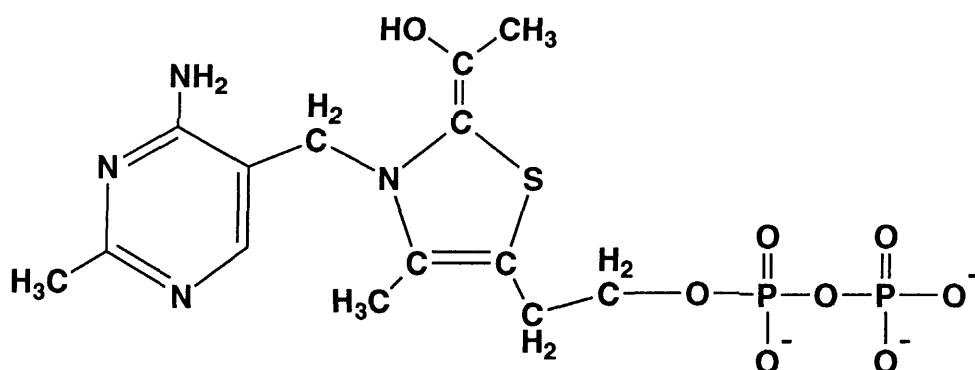
Figure 1.3 Enamine intermediate

(1) Geometry of LTDP (Figure 1.2) has not been known because LTDP is high by reactive species and its life time is only a few minutes.[14]

(2) It has not been fully investigated whether an enamine intermediate (Figure 1.3) is involved in the reaction or not.

(3) Geometry of transition state, activation energy, and reaction energy of decarboxylation of LTDP have not been fully investigated.

Transcarboxylation is catalyzed by biotin (vitamin H, see Figure 1.4). This is a coenzyme which catalyzes the bond formation between the carboxylate group derived from bicarbonate (HCO_3^-) and a carbon atom adjacent to a carbonyl group. The reaction mechanism is summarized as follows;[15-17]

$$Biotin + ATP + HCO_3^- \rightarrow Biotin \cdot CO_2^- + ADP + HPO_4^{2-} \qquad (1.2)$$

$$Biotin \cdot CO_2^- + H_3C \cdot \overset{O}{\overset{\|}{C}}CO_2H + B \rightarrow {}^-O_2CH_2C \cdot \overset{O}{\overset{\|}{C}}CO_2H + Biotin + BH \quad (1.3)$$
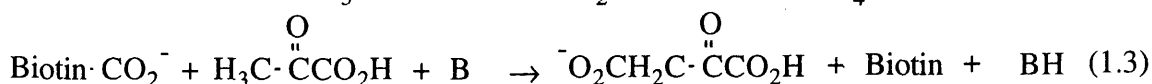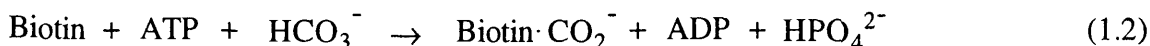
First, carboxybiotin is formed from biotin, HCO_3^-, adenosine triphosphate (ATP) (eq 1.2), accompanied with conversion of ATP to adenosine diphosphate (ADP), and inorganic phosphate.[18,19] Then, the carboxyl group transfers from carboxybiotin to an α-carbon of the carbonyl compound (eq 1.3).[20-22]

Interestingly, two kinds of intermediate were proposed in biotin carboxylation; one is N-carboxybiotin (Figure 1.5A) and the other is O-carboxybiotin (Figure 1.5B). Imoto et al. reported that imidazolidone ring is less reactive for carbon dioxide[23] and Caplow found that carbonyl group of carboxybiotin is less electrophilic.[24] These experimental results suggested that biotin-dependent carboxylation proceeds via the O-carboxybiotin.[25] On the other hand, Lane et al. obtained the experimental result that supports the existence of N-carboxylated species in biotin-dependent enzymic reaction by confirming the enzyme activity of N-carboxybiotin derivative isolated.[26] Thus, N-carboxylation mechanism has been undoubtedly accepted now.

Considering the above-mentioned discussion presented in experimental field, following issues should be examined to understand well the mechanism of biotin-dependent catalytic reaction;
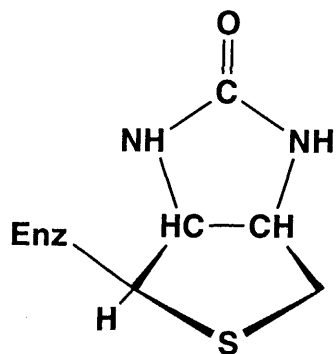
Figure 1.4 d-(+)-Biotin
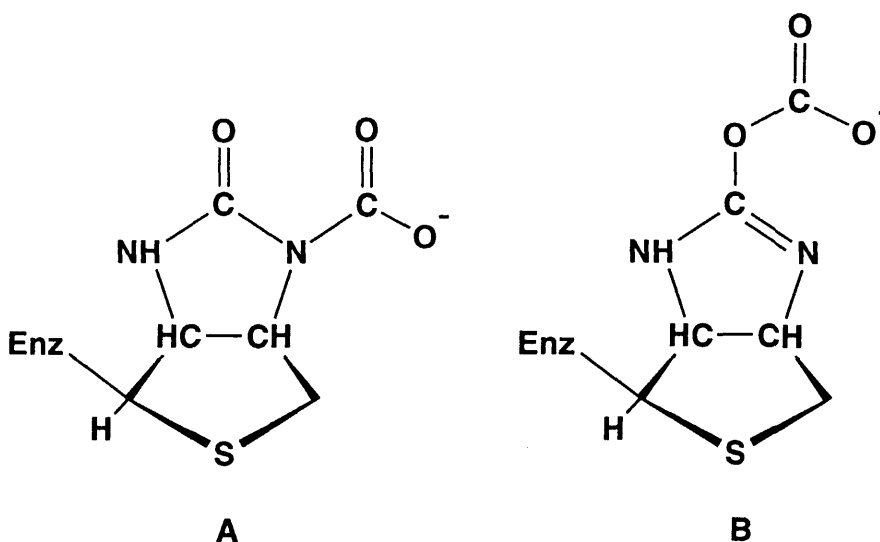
Figure 1.5 N-carboxybiotin **A** and O-carboxybiotin **B**

(1) Geometry, reactivity, and electronic structure of N-carboxybiotin.

(2) Comparison of N-carboxylation with O-carboxylation.

1.3 Catalyses of Transition-metal Complexes Related to CO_2 Fixation

Recently, chemical fixation of CO_2[27] becomes of great importance because of increase in the concentration of CO_2 in the atmosphere.

6

In electrochemical[28-41] and photochemical[42-46] reduction of CO_2 *catalyzed by transition-metal complexes or enzyme*, CO_2 *is* converted into useful substances such as carbon monoxide, methanol, formic acid, oxalic acid, organic acids, and methane.

In spite of many experimental works, only a few processes using CO_2 as raw material for carbon source have been developed. Considering this unsuccessful situation in the CO_2 fixation, detailed theoretical information on the reactions of CO_2 is necessary to find an excellent catalyst for the CO_2 fixation; for instance, geometry, bonding nature, and electronic structure of intermediate and transition state, the activation energy, and the reaction energy, are useful and indispensable for further development of the chemistry of CO_2 fixation.

In the many reactions of CO_2, insertion of CO_2 into a M-R (R = hydride, alkyl, or alkoxide)[47-53] bond (eq 1.4) is

$$(L)_nM\text{-}R \quad + \quad CO_2 \quad \rightarrow \quad (L)_nM(\eta^1\text{-}OC(O)R)$$

$$\rightarrow \quad (L)_nM(\eta^2\text{-}O_2CR) \quad\quad (1.4)$$

expected to be utilized for constructing the good catalytic system since many transition metal catalytic cycles involve the insertion reactions of alkene, alkyne, and carbonyl into a M-R bond. In fact, formyl or carboxyl group is formed through the insertion reaction of CO_2, and they would play an important role as a precursor or an intermediate of catalytic CO_2 fixation. From those reasons, many experimental works have been actively carried out on the CO_2 insertion into the M-R bond.[54-63]

In contrast to these experimental works, only a few theoretical works on the insertion of CO_2 have been reported, to our knowledge. From theoretical works, we can

expect to obtain several informations on the CO_2 insertion into the M-R bond, as follows;

(1) Changes in geometry, electron distribution, and bonding nature,

(2) The activation energy and the reaction energy,

(3) Reactivity of transition-metal-hydride and alkyl complexes in the CO_2 insertion, and

(4) Differences in reactivity between CO_2 and C_2H_4 in the insertion reaction.

1.4 Oxidative Addition of the Si-X σ-Bond to Transition-metal Complex

Oxidative addition of the saturated σ-bond (eq 1.5) to transition-metal complexes is of importance in activation of saturated compound.[64,65] For instance, the oxidation addition of the C-H bond to transition metal complex is considered to be involved in activation of alkane.[66] In fact, the C-H bond activation of hydrocarbon was

$$(L)_nM \quad + \quad H-CH_2R \quad \rightarrow \quad (L)_nM(H)(CH_2R) \quad\quad (1.5)$$

experimentally found by Graham,[67] Bergman,[68] and Jones[69] and their co-workers. Mechanistic studies on this C-H bond activation have elucidated that the C-H bond activation is achieved by oxidative addition of the C-H bond to the coordinatively unsaturated transition-metal complex.[66]

Under these circumstances, several interesting theoretical works on the oxidative addition of H_2, CH_4, C_2H_6, have been carried out with the molecular orbital (MO) method.[70-76] In these studies, the detailed knowledge including the geometry of transition state, activation energy, the reaction energy has been presented.

Similar to the oxidative addition of the C-H σ-bond, the oxidative addition of Si-X σ-bond (X = H, CH_3, or SiH_3) (eq 1.6) is of importance in catalytic syntheses of various

$$(L)_nM \quad + \quad H_3Si-SiH_3 \quad \rightarrow \quad (L)_nM \overset{SiH_3}{\underset{SiH_3}{\diagdown}} \qquad (1.6)$$

organosilicon compounds; for instance, the Si-H oxidative addition is involved as a key process in transition-metal catalyzed hydrosilylation of alkene.[77-80] Also, the Si-Si oxidative addition is involved in bis-silylation of alkene and alkyne.[81-90]

Sakaki and his collaborator have investigated the oxidative addition of CH_4 and SiH_4 with $Pt(PH_3)_2$, by using ab initio MO method.[91] They showed that Si-H oxidative addition occurs much more easily with the lower activation energy and the larger exothermicity than the C-H oxidative addition.[91] Although palladium (0) complexes have often been used as catalysts in the bis-silylation,[64a,76,82-87,88c,89] previous theoretical work revealed that the Pd(0) complex was unfavorable for the oxidative addition of H-H and C-X (X = H, CH_3) bonds.[92]

In this regard, it is necessary to investigate theoretically the oxidative addition of the Si-X σ-bond to the palladium (0) complex, in particular, to clarify the reason that the Si-H and Si-Si oxidative addition to palladium (0) complexes can proceed unlike the C-H and H-H oxidative addition. The detailed knowledge on these issues is expected to be useful to construct a efficient catalytic system for synthetic reaction of organosilicon compounds.

9

1.5 Aims of the present study

As described above, there remain many issues to be theoretically solved in catalytic reactions of enzymes and transition metal complexes. Aims of this thesis are summarized as follows.

In chapter 2, decarboxylation function of thiamin diphosphate was theoretically investigated. Aims of this chapter are;

1) to obtain detailed knowledge on geometry changes and energy changes in decarboxylation of 2-lactylthiazolium cation,

2) to offer theoretical evidence of the enamine intermediate, and

3) to make clear the differences in reactivity between 2-lactylthiazolium cation and the other two lactylazolium, 2-lactyloxazolium and 2-lactylimidazolium.

In chapter 3, carboxyimidazolidone was theoretically investigated as a model of carboxybiotin. The main purposes are;

1) to present information necessary for systematic theoretical investigation of biotin,

2) to present such detailed information as CO_2 binding energy, geometry, bonding nature, electron distribution, and reactivity of carboxyimidazolidone,

3) to compare N-carboxyimidazolidone with O-carboxy-imidazolidone, and

4) to examine the stability of the η^2-side-on carboxy-imidazolidone.

In chapter 4, theoretical investigation on the CO_2

insertion into the Cu(I)-H and Cu-CH$_3$ bonds is presented, in comparing it with the similar C$_2$H$_4$ insertion into the Cu(I)-H and Cu(I)-CH$_3$ bonds. Following issues are mainly discussed;

1) to offer detailed knowledge on the CO$_2$ insertion into the Cu-R bond, such as geometry change, electron redistribution, and transition state structure,

2) to estimate the activation energy and the reaction energy,

3) to compare the CO$_2$ insertion with the C$_2$H$_4$ insertion, and

4) to explain the difference in the insertion reaction between CO$_2$ and C$_2$H$_4$.

In chapter 5, insertion of CO$_2$ into the Rh(I)-H bond of RhH(PH$_3$)$_3$ is theoretically investigated. Also, in this chapter, detailed knowledge on the CO$_2$ insertion into the Rh(I)-H bond is presented like in chapter 4;

1) to make clear geometry change, electron distribution, and changes in bonding nature in the CO$_2$ insertion into the Rh(I)-H bond,

2) to estimate activation energy and reaction energy of CO$_2$ insertion into the Rh(I)-H bond, and

3) to compare the Rh(I) complex with the Cu(I) complex in the CO$_2$ insertion based on the energy decomposition analysis.

In chapter 6, the similar CO$_2$ insertion into the Rh(III)-H bond of [RhH$_2$(PH$_3$)$_3$]$^+$ is theoretically investigated with the following purposes;

1) to estimate activation energy and reaction energy of CO$_2$ insertion into the Rh(III)-H bond,

1) to clarify the differences in reactivity between high and low oxidation states of Rh in CO$_2$ insertion, and

2) to predict a favorable transition-metal complex for CO_2 insertion.

In chapter 7, an oxidation addition of the Si-X (X = H, C, and Si) bond to the Pd(0) complex is theoretically investigated. Following aims are mainly examined.

1) to offer detailed information on the oxidative addition, such as the geometry of transition state, the activation energy, and the reaction energy,

2) to compare the reactivity of the Pd(0) complex with that of the Pt analogue, and

3) to clarify the reason that the activation energy of the Pd(0) reaction system is lower than that of the Pt reaction system, in spite of the lower exothermicity.

References

(1)   L.O. Krampitz, "Thiamin Diphosphate and Its Catalytic Functions," Marcel Dekker, New York (1970).

(2)   A. A. Gallo, J. J. Mieyal, and H. Z. Sable, In "Bioorganic Chemistry," ed by E. E. van Tamelen, Academic, New York (1978), Vol. 4, pp. 147-177.

(3)   R. Kluger, Ann. N. Y. Acad. Sic., **378**, 63 (1982).

(4)   R. R. Williams and T. D. Spies, "Vitamin B1 and Its Use in Medicine," Macmillan, New York (1938).

(5)   W. H. Sebrell, Ann. N. Y. Acad. Sci., **98**, 563 (1962).

(6)   W. B. Bradley, Ann. N. Y. Acad. Sci., **98**, 602 (1962).

(7)   F. A. Robinson "The Vitamin Co-factors of Enzyme Systems," Pergamon, Oxford (1966).

(8)   R. A. LaRossa and J. V. Schloss, J. Biol. Chem., **259**, 8753 (1984).

(9)   P. V. Attwood and D. B. Keech, Curr. Top. Cell. Regul., **23**, 1 (1984).

(10)   H. Dugas and C. Penney, "Bioorganic Chemistry," "A Chemical Approach to Enzyme Action," Springer, New York (1981), pp. 458-477.

(11)   H. G. Wood and R. E. Barden, Annu. Rev. Biochem., **46**, 385 (1977).

(12)   R. Breslow, J. Am. Chem. Soc., **80**, 3719 (1958).

(13)   R. Kluger, J. Am. Chem. Soc., **87**, 863 (1987).

(14)   R. Kluger, J. Chin, and T. Smith, J. Am. Chem. Soc., **103**, 884 (1981).

(15)   J. R. Knowles, Annu. Rev. Biochem., **58**, 195 (1989).

(16)   G. R. J. Thatcher and R. Kluger, Adv. Phys. Org. Chem., **25**, 99 (1989).

(17)   R. Kluger, Chem. Rev., **90**, 1151 (1990).

(18)   F. Lynen, J. Knappe, E. Lorch, G. Jütting, and E. Ringelmann, Angew. Chem., **71**, 481 (1959).

(19) (a) R. Kluger and S. D. Taylor, <u>J. Am. Chem. Soc.</u>, **113**, 996 (1991). (b) S. D. Taylor and R. Kluger, <u>J. Am. Chem. Soc.</u>, **115**, 867 (1993).

(20) J. Réty and F. Lynen, <u>Biochem. Z.</u>, **342**, 256 (1993).

(21) (a) J. Stubbe and R. H. Abeles, <u>J. Biol. Chem.</u>, **252**, 8338 (1977). (b) J. Stubbe, S. Fish, and R. H. Abeles, <u>J. Biol. Chem.</u>, **255**, 236 (1980).

(22) (a) D. Kuo and I. A. Rose, <u>J. Am. Chem. Soc.</u>, **104**, 3235 (1977). (b) D. Kuo and I. A. Rose, <u>J. Am. Chem. Soc.</u>, **115**, 387 (1985).

(23) E. Imoto, "Kouso Ruiji Kinou wo Motsu Yuhki Hannou I," "Kagaku no Zoukan 110," Nankodo (1976), p. 71.

(24) M. Caplow, <u>J. Am. Chem. Soc.</u>, **87**, 5774 (1965).

(25) T. C. Bruice and A. F. Hegarty, <u>Proc. Natl. Acad. Sci. U. S.</u>, **65**, 805 (1970).

(26) R. B. Guchhait, S. E. Polakis, P. Bimroth, E. Stoll, J. Moss, and M. D. Lane, <u>J. Biol. Chem.</u>, **249**, 6633 (1974).

(27) (a) D. J. Darensbourg and R. A. Kudaroski, <u>Adv. Organomet. Chem.</u>, **22**, 129 (1983). (b) D. A. Palmer and R. van Eldik, R. <u>Chem. Rev.</u>, **83**, 651 (1983). (c) D. Walther, <u>Coord. Chem. Rev.</u>, **79**, 135 (1987). (d) A. Behr, <u>Angew. Chem., Int. Ed. Engl.</u>, **27**, 661 (1988). (e) P. Braustein, D. Matt, and D. Nobel, <u>Chem. Rev.</u>, **88**, 747 (1988). (f) A. R. Culter, P. K. Hanna, and J. C. Vites, <u>Chem. Rev.</u>, **88**, 1363 (1988). (g) A. Behr "Carbon Dioxide Activation by Metal Complexes," VCH Publishing, Weinheim, West Germany (1988).

(28) S. Meshitsuka, M. Ichikawa, and K. Tamaru, <u>J. Chem. Soc., Chem. Commun.</u>, **1974**, 158.

(29) (a) K. Hiratsuka, H. Sasaki, and S. Toshima, <u>Chem. Lett.</u>, **1977**, 1137. (b) K. Takahashi, K. Hiratsuka,

H. Sasaki, and S. Toshima, <u>Chem. Lett.</u>, **1979**, 305.

(30) B. Fisher and R. Eisenberg, <u>J. Am. Chem. Soc.</u>, **102**, 7363 (1980).

(31) M. Tezuka, T. Yajima, A. Tsuchiya, Y. Matsumoto, Y. Uchida, and M. Hidai, <u>J. Am. Chem. Soc.</u>, **104**, 6834 (1982).

(32) (a) M. Beley, J. -P. Collin, R. Ruppert, and J. -P. Sauvage, <u>J. Chem. Soc., Chem. Commun.</u>, **1984**, 1315. (b) M. Beley, J. -P. Collin, R. Ruppert, and J. -P. Sauvage, <u>J. Chem. Soc., Chem. Commun.</u>, **108**, 7461 (1986).

(33) S. Kapusta and N. Hackerman, <u>J. Electrochem. Soc.</u>, **131**, 1511 (1984).

(34) C. M. Lieber and N. S. Lewis, <u>J. Am. Chem. Soc.</u>, **106**, 5033 (1984).

(35) S. Slater and J. H. Wagenknecht, <u>J. Am. Chem. Soc.</u>, **106**, 5367 (1984).

(36) (a) C. M. Bolinger, B. P. Sullivan, K. Conrad, J. A. GIlbert, N. Story, and T. J. Meyer. <u>J. Chem. Soc., Chem. Soc.</u>, **1985**, 796. (b) T. R. O'Toole, L. D. Margerum, T. D. Westmoreland, W. J. Vining, R. W. Murray, and T. J. Meyer, <u>J. Chem. Soc., Chem. Commun.</u>, **1985**, 1416.

(37) S. Daniele, P. Ugo, G. Bontempelli, and M. Florani, <u>J. Electroanal. Chem. Interfacial Electrochem.</u>, **219**, 259 (1987).

(38) (a) H. Ishida, H. Tanaka, K. Tanaka, and T. Tanaka, <u>Chem. Lett.</u>, **1987**, 597. (b) H. Ishida, H. Tanaka, K. Tanaka, and T. Tanaka, <u>J. Chem. Soc., Chem. Commun.</u>, **1987**, 131.

(39) P. A. Christensen, A. Hamnett, A. V. G. Muir, <u>J. Electroanal. Chem. Interfacial Electrochem.</u>, **241**, 361

(1988).

(40)   M. R. M. Bruce, E. Megehee, B. P. Sullivan, H. Thorp, T. R. O'Toole, A. Downard, and T. J. Meyer, Organometallics, **7**, 238 (1988).

(41)   H. C. Hurrell, A. -L. Mogstad, D. A. Usifer, K. T. Potts, and D. H. Abruna, Inorg. Chem., **28**, 1080 (1989).

(42)   J. Hawecker, J. -M. Lehn, and R. Ziessel, J. Chem. Soc., Chem. Commun., **1983**, 56.

(43)   (a) I. Willner, D. Mandler, and A. Riklin, J. Chem. Soc., Chem. Commun., **1986**, 1022. (b) K. A. Belmore, R. A. Vanderpool, J. -C. Tsai, M. A. Khan, and K. M. Nicholas,J. Am. Chem. Soc., **110**, 2004 (1988).

(44)   (a) H. Ishida, K. Tanaka, and T. Tanaka, Chem. Lett., **1987**, 1035.   (b) H. Ishida, T. Terada, K. Tanaka, and T. Tanaka, Inorg. Chem., **29**, 905 (1990).

(45)   N. D. Silavwe, A. S. Goldman, R. Ritter, and D. R. Tyler, Inorg.Chem., **28**, 1231 (1989).

(46)   J. -M. Lehn and R. Ziessel, J. Organomet. Chem., **382**, 157 (1990).

(47)   (a) M. E. Vol'pin, Pure Appl. Chem., **30**, 607 (1972). (b) I. S. Kolomnikov, G. Stepovska, S. Tyrlik, and M. E. Vol'pin, Zh. Obshch. Khim., **42**, 1652 (1972).   (c) I. S. Kolomnikov, G. Stepovska, S. Tyrlik, and M. E. Vol'pin, Zh. Obshch. Khim., **44**, 1743 (1974).   (d) I. S. Kolomnikov, G. Stepovska, S. Tyrlik, and M. E. Vol'pin, J. Gen. Chem. USSR (Engl. Transl.), **44**, 1710 (1974).

(48)   I. S. Kolomnikov and M. Kh. Grioryan, Russ. Chem. Rev. (Engl. Transl.), **47**, 334 (1978).

(49)   A. L. Lapidus and Y. Y. Ping, Russ. Chem. Rev. (Engl. Transl.), **50**, 63 (1981).

(51) R. Ziessel, <u>Nouv. J. Chim.</u>, **7**, 613 (1983).

(52) D. J. Darensbourg and C. Ovalles, <u>CHEMTECH</u>, **1985**, 636.

(53) D. Walther, <u>Coord. Chem. Rev.</u>, **79**, 135 (1987).

(54) (a) S. Inoue and N. Takeda, <u>Bull. Chem. Soc. Jpn.</u>, **50**, 984 (1977). (b) T. Aida and S. Inoue, <u>J. Am. Chem. Soc.</u>, **105**, 1304 (1983). (c) F. Kojima, T. Aida, and S. Inoue, <u>J. Am. Chem. Soc.</u>, **108**, 391 (1986) (d) T. Aida, M. Ishikawa, and S. Inoue, <u>Macromolecules</u>, **19**, 8 (1986). (e) Y. Hirai, T. Aida and S. Inoue, <u>J. Am. Chem. Soc.</u>, **111**, 3062 (1989). (f) M. Komatsu, T. Aida, and S. Inoue, <u>J. Am. Chem. Soc.</u>, **113**, 8492 (1991).

(55) A. Rokicki and W. Kuran, <u>J. Macromol. Sci. Rev. Macromol. Chem.</u>, **135**, C21 (1981).

(56) K. Soga, E. Imai, and I. Hattori, <u>Polym. J.</u>, **13**, 407 (1981).

(57) S. Gambarotta, S. Strologo, C. Floriani, A. Chiesi-Villa, and C. Guastini, <u>J. Am. Chem. Soc.</u>, **107**, 6278 (1985).

(58) (a) E. Carmona, P. Palma, M. Paneque, and M. L. Poveta, <u>J. Am. Chem. Soc.</u>, **108**, 6424 (1986).
(b) E. Carmona, E. Gutiérrez-Puebla., J. M. Marin, A. Monge, M. Paneque, M. L. Poveta, and C. Ruiz, <u>J. Am. Chem. Soc.</u>, **111**, 2883 (1989).

(59) P. Braunstein, D. Matt, and D. Nobel, <u>J. Am. Chem. Soc.</u>, **110**, 3207 (1988).

(60) D. J. Darensbourg and C. Ovalles, <u>J. Am. Chem. Soc.</u>, **109**, 3330 (1989).

(61) K. T. Aye, L. Gelmini, N. C. Payne, J. J. Vittal, and R. J. Puddephatt, <u>J. Am. Chem. Soc.</u>, **112**, 2464 (1990).

(62) (a) C. Amatore and A. Jutand, J. Am. Chem. Soc., 113, 2819 (1991). (b) C. Amatore and A. Jutand, J. Electroanal. Chem., 306, 141 (1991).

(63) J. C. Tsai and K. M. Nicholas, J. Am. Chem. Soc., 114, 5117 (1992).

(64) (a) T. D. Tilley, "The Chemistry of Organic Silicon Compounds," ed by S. Patai and Z. Rappoport, John Wiley & Sons, New York (1989), pp. 1415. (b) I. Ojima, "The Chemistry of Organic Silicon Compounds," ed by S. Patai and Z. Rappoport, John Wiley & Sons, New York (1989), pp. 1479.

(65) F. Seitz and M. S. Wrighton, Angew. Chem., Int. Ed. Engl., 27, 289 (1988).

(66) (a) A. E. Shilov, "Activation of Saturated Hydrocarbons by Transition Metal Complexes," D. Reidel Publishing, Dordrecht (1984). (b) R. G. Bergman Science, 223, 902 (1984). (c) R. H. Crabtree, Chem. Rev., 85, 245 (1985). (d) M. L. H. Green and D. O'Hare, Pure Appl. Chem., 57, 1897 (1985). (e) W. D. Jones and F. J. Feher, Acc. Chem. Res., 22, 91 (1989).

(67) (a) J. K. Hoyano and W. A. Graham, J. Am. Chem. Soc., 104, 3723 (1982). (b) J. K. Hoyano, A. D. McMaster, and W. A. G. Graham, J. Am. Chem. Soc., 105, 7190 (1983).

(68) (a) A. H. Janowicz and R. G. Bergman, J. Am. Chem. Soc., 104, 352 (1983). (b) . H. Janowicz and R. G. Bergman, J. Am. Chem. Soc., 105, 3929 (1983). (c) R. A. Perana and R. G. Bergman, Organometallics, 3, 508 (1984). (d) M. Wax, J. M. Stryker, J. W. Buchanan, C. A. Kovac, and R. G. Bergman, J. Am. Chem. Soc., 106, 1211 (1984). (e) A. H. Janoxixz, R. A. Periana, J. W. Buchanan, C. A. Kovac, J. M. Stryker, M. J. Wax, and

R. G. Bergman, <u>Pure Appl. Chem.</u>, **56**, 13 (1984). (f) R. A. Periana and R. G. Bergman, <u>J. Am. Chem. Soc.</u>, **106**, 7272 (1984).

(69)   (a) W. D. Jones and F. J. Feher, <u>J. Am. Chem. Soc.</u>, **104**, 4240 (1982). (b) W. D. Jones and F. J. Feher, <u>Organometallics</u>, **2**, 562 (1983). (c) W. D. Jones and F. J. Feher, <u>Organometallics</u>, **2**, 686 (1983). (d) W. D. Jones and F. J. Feher, <u>J. Am. Chem. Soc.</u>, **106**, 1650 (1984). (e) W. D. Jones and F. J. Feher, <u>Inorg. Chem.</u>, **23**, 2376 (1984). (f) W. D. Jones and F. J. Feher, <u>J. Am. Chem. Soc.</u>, **105**, 620 (1985).

(70)   M. R. A. Blomberg, U. Brandemark, and P. E. Siegbahn, <u>J. Am. Chem. Soc.</u>, **105**, 5557 (1983).

(71)   S. Obara, K. Kitaura, and K. Morokuma, <u>J. Am. Chem. Soc.</u>, **106**, 7428 (1984).

(72)   (a) J. J. Low and W. A. Goddard, <u>Organometallics</u>, **5**, 609 (1986). (b) J. J. Low and W. A. Goddard, <u>J. Am. Chem. Soc.</u>, **108**, 6115 (1986).

(73)   N. Koga and K. Morokuma, <u>J. Phys. Chem.</u>, **94**, 5454 (1990).

(74)   (a) M. R. A. Blomberg, P. E. M. Siegbahn, U. Nagashima, and J. Wennerberg, <u>J. Am. Chem.Soc.</u>, **113**, 424 (1991). (b) M. R. A. Blomberg, P. E. M. Siegbahn, and M. Svensson, <u>J. Phys. Chem.</u>, **95**, 4313 (1991). (c) M. R. A. Blomberg, P. E. M. Siegbahn, and M. Svensson, <u>J. Am. Chem. Soc.</u>, **114**, 6095 (1992).

(75)   J. -Y. Saillard and R. Hoffmann, <u>J. Am. Chem. Soc.</u>, **106**, 2206 (1984).

(76)   T. Ziegler, C. Tschinke, L. Fan, A. D. Becke, <u>J. Am. Chem. Soc.</u>, **111**, 9177 (1989).

(77)   (a) D. L. Lichtenberger and A. Rai-Chaudhuri, <u>J. Am. Chem. Soc.</u>, **111**, 3583 (1989). (c) D. L. Lichtenberger

and A. Rai-Chaudhuri, <u>J. Am. Chem. Soc.</u>, **112**, 2492 (1990).

(78) U. Schbert, <u>Adv. Organomet. Chem.</u>, **30**, 151 (1990).

(79) D. M. Hester, J. Sun, A. W. Harper, and G. K. Yang, <u>J. Am. Chem. Soc.</u>, **114**, 5234 (1992).

(80) H. Rabaa, J. -Y. Saillard, and U. Shubert, <u>J. Organomet. Chem.</u>, **330**, 397 (1987).

(81) (a) K. Yamamoto, J. Okinoshima, and M. Kumada, M. <u>J. Organomet. Chem.</u> **27**, C31 (1971). (b) H. Okinoshima, K. Yamamoto, and M. Kumada, <u>J. Organomet. Chem.</u>, **86**, C27 (1975). (c) K. Tamao, S. Okazaki, and M. Kumada, <u>J. Organomet. Chem.</u>, **146**, 87 (1978).

(82) (a) H. Sakurai, Y. Kamiyama, and Y. Nakadaira, <u>J. Am. Chem. Soc.</u>, **97**, 931 (1975). (b) H. Sakurai, T. Kobayashi, and Y. Nakadaira, <u>J. Organomet. Chem.</u>, **162**, C43 (1978). (c) H. Sakurai, Y. Eriyama, Y. Kamiyama, and Y. Nakadaira, <u>J. Organomet. Chem.</u>, **264**, 229 (1984).

(83) (a) H. Matsumoto, K. Shono, A. Wada, I. Matsubara, H. Watanabe, and Y. Nagai, <u>J. Organomet. Chem.</u>, **199**, 185 (1980). (b) H. Watanabe, M. Saito, N. Sutou, and Y. Nagai, <u>J. Chem. Soc., Chem. Commun.</u>, **1981**, 617. (c) H. Watanabe, M. Saito, K. Kishimoto, J. Inose, and Y. Nagai, <u>J. Organomet. Chem.</u>, **225**, 343 (1982).

(84) C. W. Carlson and R. West, <u>Organometallics</u>, **2**, 1801 (1983).

(85) D. Seyferth, E. W. Goldman, and J. Escudié, <u>J. Organomet. Chem.</u>, **271**, 337 (1984).

(86) (a) T. Hayashi, A. Yamamoto, T. Iwata, and Y. Ito, <u>J. Chem. Soc., Chem. Comm.</u>, **1987**, 398. (b) T. Hayashi, Y. Matsumoto, and Y. Ito, <u>J. Am. Chem. Soc.</u>, **110**, 5579 (1988). (c) M. Murakami, P. G. Andersson, M.

20

Suginome, and Y. Ito, <u>J. Am. Chem. Soc.</u>, **113**, 3987 (1991).

(87) (a) T. Hayashi, A. M. Kawamoto, T. Kobayashi, and M. Tanaka, <u>J. Chem. Soc., Chem. Comm.</u>, **1990**, 563.   (b) T. Hayashi, T. Kobayashi, A. M. Kawamoto, H. Yamashita, and M. Tanaka, <u>Organometallics</u>, **9**, 280 (1990).   (c) H. Yamashita, M. Catellani, and M. Tanaka, <u>Chem. Lett.</u>, **1991**, 241.   (d) H. Yamashita and M. Tanaka, <u>Chem. Lett.</u>, **1992**, 1547.

(88) (a) Y. Tsuji, R. M. Lago, S. Tomohiro, and H. Tsuneishi, <u>Organometallics</u>, **11**, 2353 (1992).   (b) Y. Obora, Y. Tsuji, and T. Kawamura, <u>Organometallics</u>, **12**, 2853 (1993).

(89) (a) Y. Ito, S. Nishimura, and M. Ishikawa, <u>Tetrahedron Lett.</u>, **28**, 1293 (1987).   (b) Y. Ito, M. Suginome, and M. Murakami, <u>J. Am. Chem. Soc.</u>, **110**, 3692 (1988).

(90) H. Yamashita, N. P. Reddy, and M. Tanaka, <u>Chem. Lett.</u>, **1993**, 315.

(91) (a) S. Sakaki and M. Ieki, <u>J. Am. Chem. Soc.</u>, **113**, 5063 (1991).   (b) S. Sakaki and M. Ieki, <u>J. Am. Chem. Soc.</u>, **115**, 2373 (1993).

(92) (a) J. J. Low and W. A. Goddard III, <u>J. Am. Chem. Soc.</u>, **108**, 6115 (1986).   (b) J. J. Low and W. A. Goddard III, <u>Organometallics</u>, **11**, 5063 (1991).

Part I

Coenzyme Catalyses of Carboxylation and Decarboxylation

Decarboxylation of 2-Lactylthiazolium Cation

2.1 Introduction

Thiamin diphosphate (TDP) is a coenzyme participating in the enzymatic decarboxylation of pyruvate.[1] The reaction mechanism of the pyruvate decarboxylation has been proposed by Breslow, as shown in Scheme 2.1.[2] In this mechanism, lactyl-TDP (LTDP), an enamine (or 2α-carboanion) species, and hydroxyethyl-TDP (HETDP) are involved as key intermediates. So far, there have been reported several experimental results supporting this reaction mechanism. For instance, HETDP was isolated from yeast pyruvate decarboxylase.[3] In addition, Krampitz et al. succeeded the chemical synthesis of HETDP and reported that HETDP was converted to acetaldehyde and thiamin diphosphate by wheat germ pyruvate decarboxylase.[4] Also, LTDP and lactylthiamin (a model of LTDP) were chemically synthesized, and their reaction behaviors have been investigated.[5,6] In particular, experimental results of Lienhard et al.[7] are worthy of note, here; the decarboxylation of 2-lactyl-3,4-dimethylthiazolium cation proceeds with the high activation barrier of 31.2 kcal/mol in water but with the very small activation barrier in ethanol. From these results, they proposed that the desolvation action of the enzyme might be a major cause of catalysis in thiamine pyrophosphate-dependent enzymatic reactions.

Although several important results have been reported
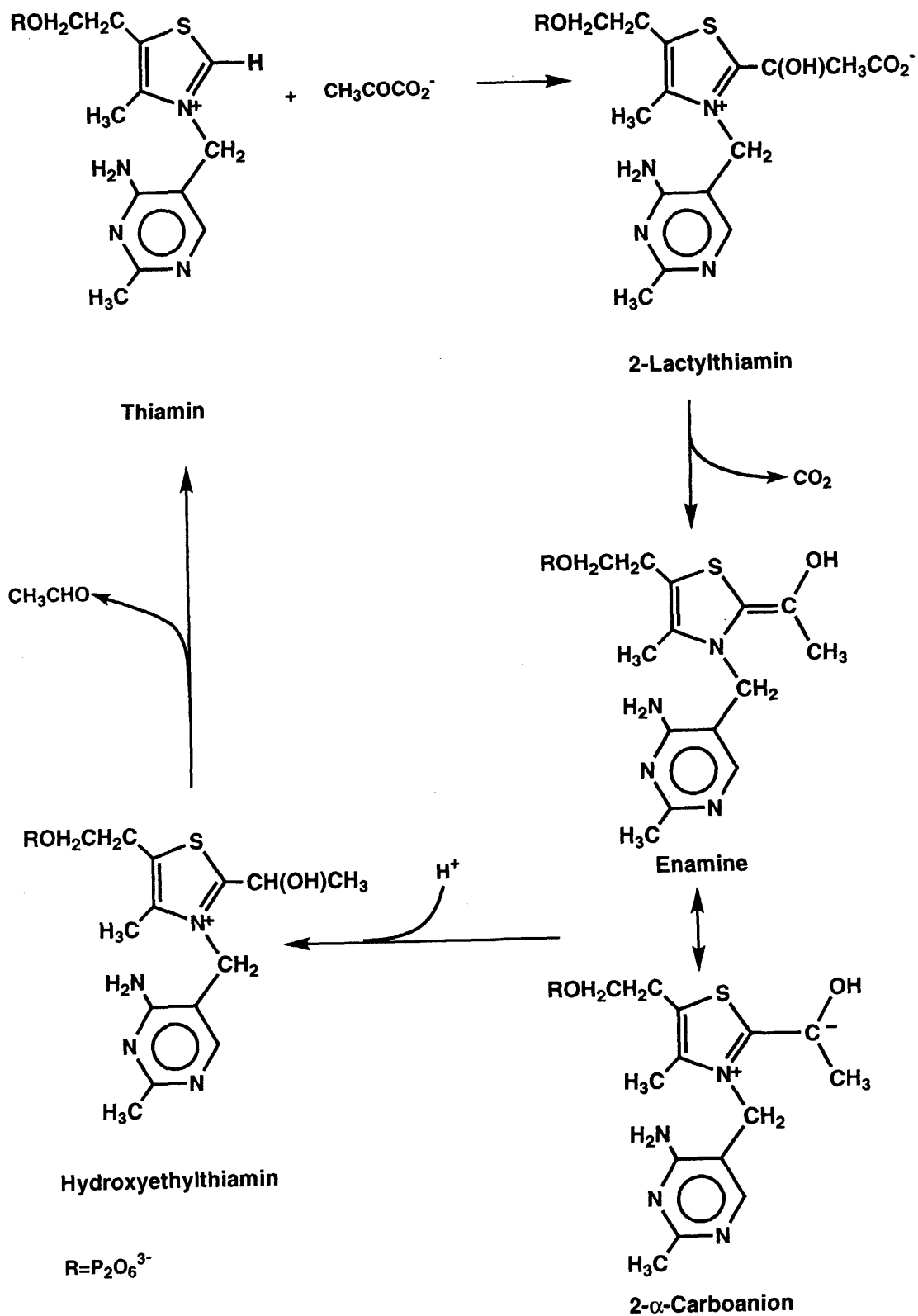
Scheme 2.1

on LTDP and HETDP as described above, the enamine intermediate has not been chemically synthesized and its existence has not been directly confirmed yet, probably owing to its high reactivity. Recently, Kluger et al. provided experimental support to the enamine intermediate.[8] In addition, there has been reported Jordan's interesting result indicating that the enamine intermediate is indeed on the reaction pathway.[9] Molecular orbital calculations are also expected to offer several valid informations on the enamine species.

In this chapter, AM1 and ab initio MO/MP2 calculations are carried out on the decarboxylation reaction of 2-lactylthiazolium, a model of LTDP. Also, decarboxylation reactions of 2-lactyloxazolium and 2-lactylimidazolium are investigated, in an attempt to compare their reactivities with the 2-lactylthiazolium reactivity. It is our intention with this chapter to present (1) good understanding of the decarboxylation reaction of 2-lactylthiazolium, (2) theoretical evidence of the enamine intermediate, and (3) a clear comparison of the decarboxylation reactivity between thiazolium, oxazolium, and imidazolium cations.

2.2 Computational Details

AM1 calculations were carried out with MOPAC program (version 3.0),[10] where AM1 standard parameters[11] were employed except for MNDO parameters used for the S atom.[12] Ab initio closed-shell Hartree-Fock (HF) and MP2 calculations were performed with Gaussian 82 and 86 programs.[13] MINI-1 basis set[14a,b] was used for geometry

optimization at the HF level. 6-31G[15] and MIDI-4[14a,c] basis sets were employed for MP2 calculations.

In AM1 calculations, geometries of reactants, transition states, and products were optimized with Davidon-Fletcher-Powell method, where the azolium ring was assumed to be planar. This assumption seems reasonable because 2-lactylthiazolium is destabilized in energy by the out-of-plane distortion of its N-H bond. Geometry changes caused by the decarboxylation were investigated, taking the $C^{2\alpha}$-CO_2 distance as a reaction coordinate (see Figure 2.1 for C^2, $C^{2\alpha}$, etc.).

In ab initio MO calculations, geometries were optimized with the energy gradient method at the HF level, where the geometry of the thiazolium ring was taken to be the same as it in the AM1-optimized structure of 2-lactylthiazolium.[17a,c] This assumption is reasonable when the early stage of the decarboxylation is investigated, because AM1 calculations showed that geometry changes of the thiazolium ring were very small upon going to the TS from 2-lactylthiazolium. MP2 calculations were performed with all the core orbitals excluded from the active space.

2.3 Results and Discussion
2-3-1 Decarboxylation Reaction of 2-Lactylthiazolium

The geometry of 2-lactylthiazolium (**1**) optimized with the AM1 method is shown in Figure 2.1. This optimized geometry agrees well with the experimental structure of phosphalactylthiamin (methyl 2-hydroxy-2-(2-thiamin)ethylphosphonate).[17b] The energy change caused by
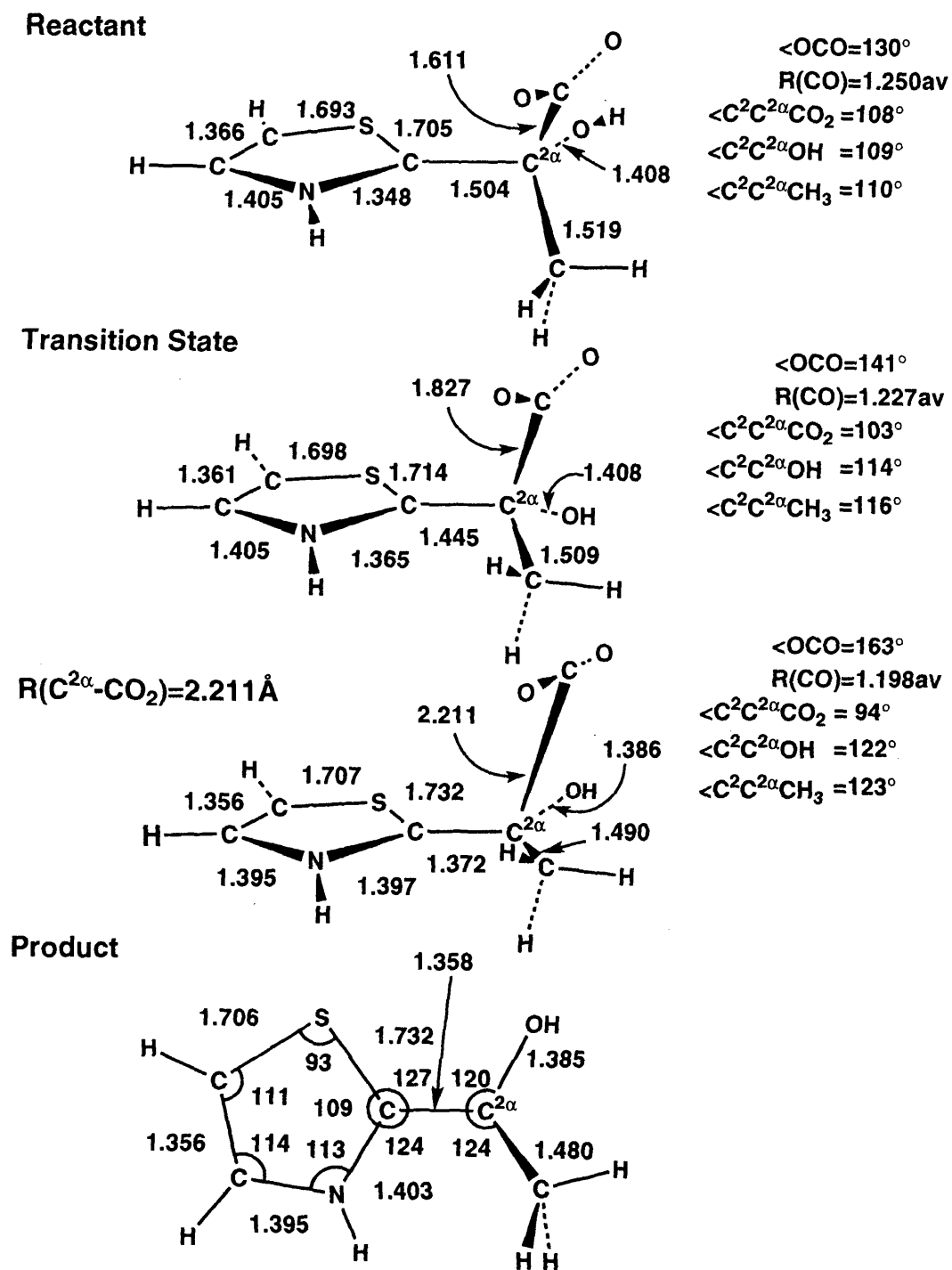
Figure 2.1 Geometry changes caused by decarboxylation of 2-lactylthiazolium (bond distance in Å and bond angle in degree).
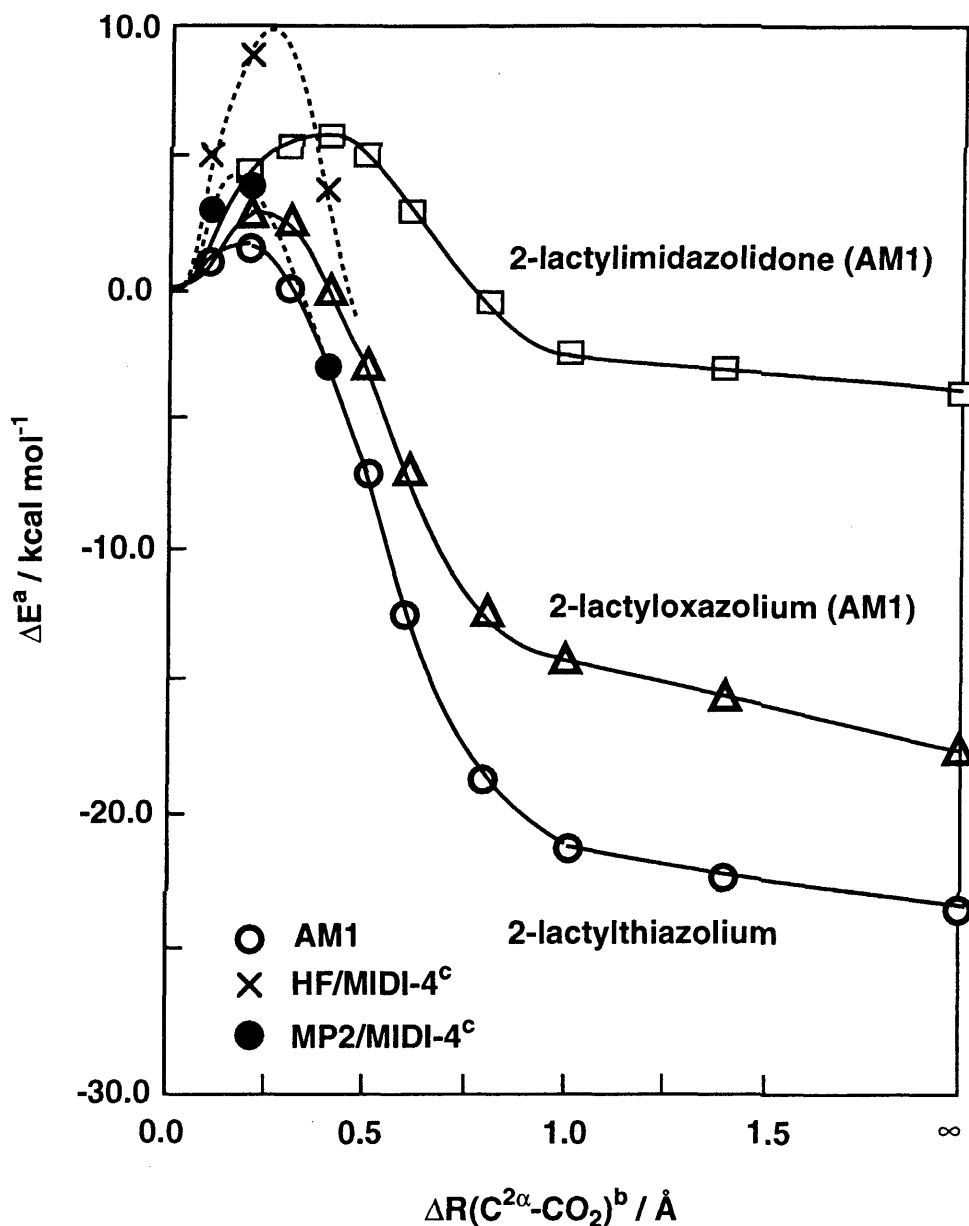
Figure 2.2 Energy changes caused by decarboxylations of 2-lactylthiazolium, 2-lactyloxazolium, and 2-lactylimidazolium.

a) ΔE represents total energy changes from 2-lactylthiazolium, 2-lactyloxazolium, and 2-lactylimidazolium.   b) $\Delta R(C^{2a}-CO_2)$ means lengthning of the $C^{2a}-CO_2$ distance from 2-lactyl-azoliums. c)   Results of HF/6-31G and MP2/6-31G are very close to results of HF/MIDI-4 and MP2/MIDI-4, respectively.

the decarboxylation of 2-lactylthiazolium is given in Figure 2.2 as a function of the $C^{2\alpha}-CO_2$ distance. AM1 calculations indicate that the $C^{2\alpha}-CO_2$ distance lengthens at the transition state (TS) by ca. 0.2 Å, like ab Initio MO/MP2 calculations. Thus, we can consider that the AM1 method presents reliable results on this decarboxylation reaction. Geometries of the TS (**2**) and the product (**4**) of this decarboxylation are also shown in Figure 1.1. Going to **4** from **1**, the C^2-N distance is getting longer, the $C^2-C^{2\alpha}$ distance is getting shorter, and the OCO, $C^2C^{2\alpha}CH_3$ and $C^2C^{2\alpha}OH$ angles gradually open. These results mean that the $C^2-C^{2\alpha}$ single bond is changing to the double bond, the $C^2=N$ double bond to the single bond, and the CH_3 and OH groups are going into the plane of the $C^2=C^{2\alpha}$ double bond. Lengthening the $C^{2\alpha}-CO_2$ distance to 2.211 Å (i.e., going to the late stage of the reaction), the $C^2-C^{2\alpha}$ distance shortens to 1.363 Å and the C^2-N distance lengthens to 1.397 Å, as shown by **3** in Figure 1.1. These distances of the $C^2-C^{2\alpha}$ and C^2-N bonds are similar in magnitude to those of the C=C double and C-N single bonds, respectively, indicating that **3** is characteristic of the enamine compound. Also, the product (**4**) apparently takes the enamine structure (Figure 1.1). Thus, these results provide us with the theoretical evidence that the enamine intermediate is indeed on the reaction pathway.

AM1 calculations show that the activation barrier of this decarboxylation is considerably small (E_a = 1.5 kcal/mol). Although somewhat large activation barriers, 8.9 and 9.0 kcal/mol, are evaluated by HF/MIDI-4 and HF/6-31G

Table 2.1 Activation Barrier (E_a) and Exothermicity (E_{exo}) of Decarboxylations of 2-Lactylazoliums. (kcal/mol)

	Method	$R_{C2\alpha-CO2}$	E_a	E_{exo}
2-lactylthiazolium				
	AM1	0.22	1.5	23.8
	HF/MIDI-4	0.25	8.9	_[b]
	HF/6-31G	0.25	9.0	_[b]
	MP2/MIDI-4	0.17	3.9	_[b]
	MP2/6-31G	0.18·	4.4	_[b]
2-lactylthiazolium[c] with 2 H_2O	AM1	0.30	5.6	14.7
2-lactylthiazolium[d] with 3 H_2O	AM1	0.32	19.0	-2.1[e]
2-lactyloxazolium	AM1	0.18	2.8	18.1
2-lactylimidazolium	AM1	0.42	6.4	3.9

a) Bond lengthening at TS. b) Not calculated.[18] c) 2 molecules of water were added to the reaction system.[19a] d) 3 molecules of water were added to the reaction system.[19b] e) endothermic

calculations respectively, inclusion of electron correlation by the MP2 method substantially decreases the activation barrier to 3.9 (MP2/MIDI-4) and 4.4 kcal/mol (MP2/6-31G), as shown in Table 2.1 Corresponding to this small activation barrier, the exothermicity (E_{exo}) calculated for this
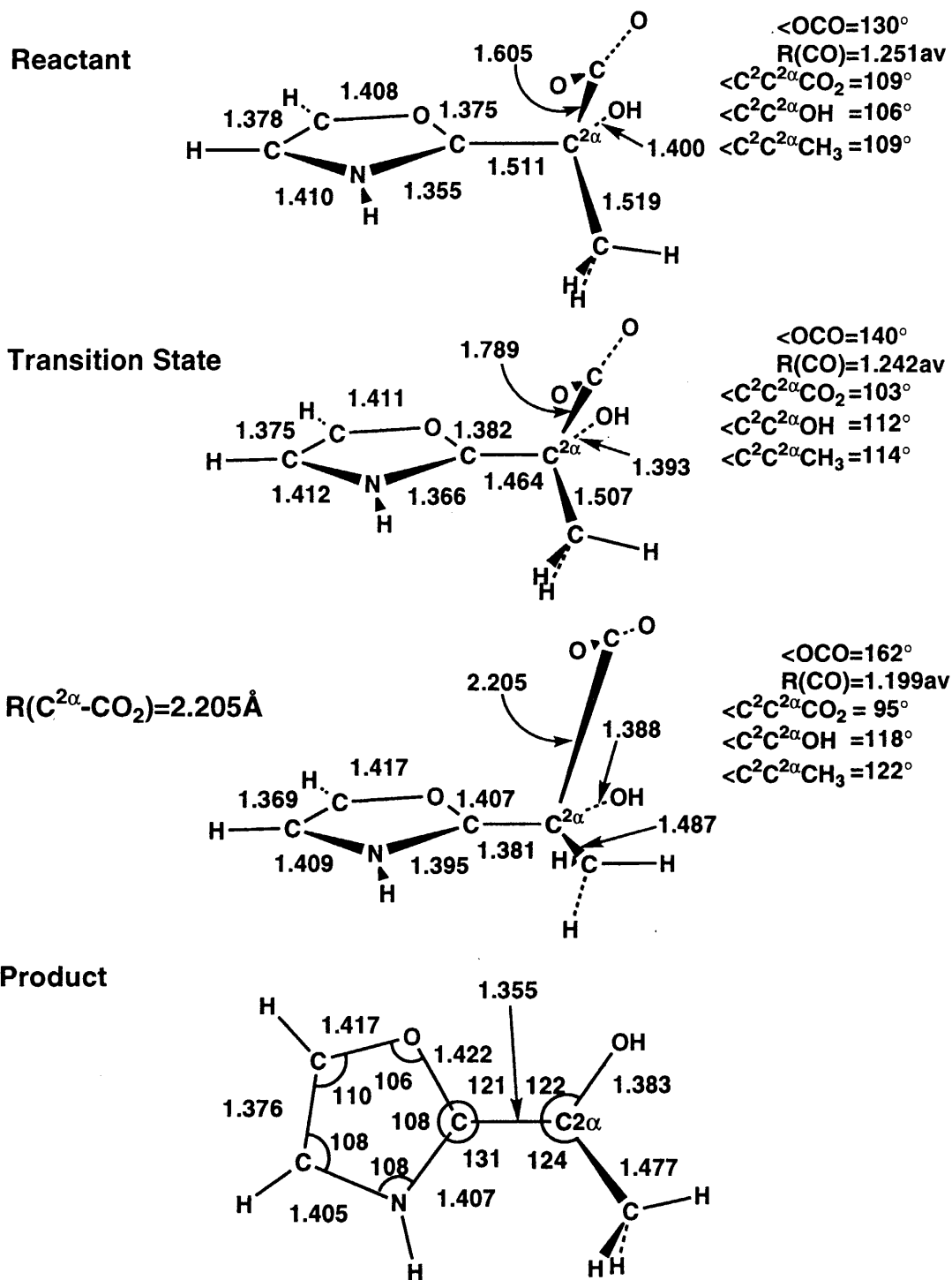
decarboxylation is extremely large; $E_{exo} = 23.8$ kcal/mol (AM1 calculation).[18] All these results suggest that the decarboxylation of 2-lactylthiazolium proceeds very easily in non-polar solvents. In such a polar solvent as water, the situation would change. 2-Lactylthiazolium is considered as a zwitter-ion because the CO_2 part is negatively charged and the thiamin ring is positively charged. On the other hand, products (enamine and CO_2) are neutral. Thus, a polar solvent stabilizes 2-lactylthiazolium more than the products, which would increase the activation barrier and decrease the exothermicity. In order to examine how water molecules influence this decarboxylation, we carried out AM1 calculations on this decarboxylation reaction in the presence of several water molecules. First, let us investigate the case where two water molecules interact with the CO_2 part of 2-lactylthiazolium. Positions of water molecules are roughly optimized.[19a] These two water molecules increase the activation barrier to 5.6 kcal/mol and decrease the exothermicity to 14.7 kcal/mol. Then, let us investigate the case where one additional water molecule is placed so as to interact with the N atom of the thiazolium ring. Again, the position of this water molecule is roughly optimized,[19b] whereas the positions of the other two water molecules are not re-optimized. This new water molecule further increases the activation barrier to 19.0 kcal/mol and significantly decreases the exothermicity to -2.1 kcal/mol (i.e., the reaction becomes endothermic). These results are consistent with Lienhard's experiment that

31

the decarboxylation reaction of a lactylthiazolium
derivative, 2-(1-carboxy-1-hydroxyethyl)-3,4-
dimethylthiazolium chloride, proceeds very rapidly in
ethanol but very slowly in water.[7] In other words, the
desolvation of the reaction system seems one of the
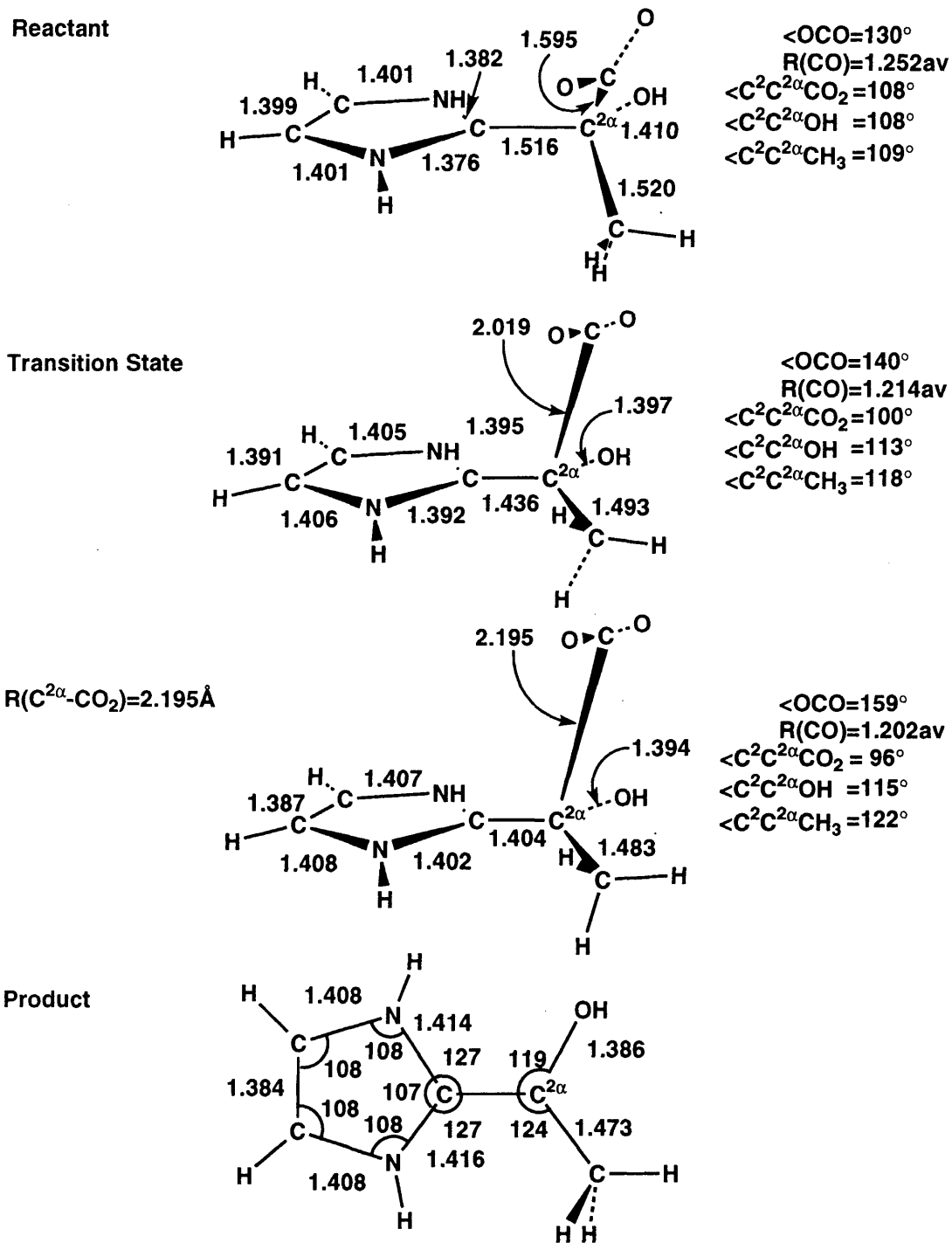important roles of thiamin diphosphate.

2-3-2 Decarboxylation Reactions of 2-Lactyloxazolium and 2-Lactylimidazolium

These decarboxylation reactions are investigated with
the AM1 method, where the $C^{2\alpha}$-CO_2 distance is taken as a
reaction coordinate like in the decarboxylation of
2-lactylthiazolium. Geometry changes caused by these
decarboxylations are given in Figures 2.3 and 2.4. As these
decarboxylations proceed (i.e., as the $C^{2\alpha}$-CO_2 distance
lengthens), the C^2-N distance is getting longer, the C^2-$C^{2\alpha}$
distance is getting shorter, and the OCO, $C^2C^{2\alpha}CH_3$ and $C^2C^{2\alpha}OH$
angles gradually open, like in the decarboxylation of 2-
lactylthiazolium. Consequently, 2-lactyloxazolium and 2-
lactylimidazolium change to **7** (Figure 2.3) and **11** (Figure
2.4) respectively, at the late stage of the reaction. Both
7 and **11** are characteristic of enamine compounds.
Furthermore, products (**8** and **12**) of these reactions take the
enamine structure like the product **4** of the 2-lactyl-
thiazolium decarboxylation.

The activation barrier calculated with the AM1 method
increases in the order 2-lactylthiazolium (1.5 kcal/mol) <
2-lactyloxazolium (2.8 kcal/mol) < 2-lactylimidazolium (6.4
kcal/mol), and the exothermicity decreases in the order

Reactant

<OCO=130°
R(CO)=1.251av
<$C^2C^{2\alpha}CO_2$ =109°
<$C^2C^{2\alpha}OH$ =106°
<$C^2C^{2\alpha}CH_3$ =109°

Transition State

<OCO=140°
R(CO)=1.242av
<$C^2C^{2\alpha}CO_2$ =103°
<$C^2C^{2\alpha}OH$ =112°
<$C^2C^{2\alpha}CH_3$ =114°

$R(C^{2\alpha}-CO_2)=2.205\text{Å}$

<OCO=162°
R(CO)=1.199av
<$C^2C^{2\alpha}CO_2$ = 95°
<$C^2C^{2\alpha}OH$ =118°
<$C^2C^{2\alpha}CH_3$ =122°

Product

Figure 2.3 Geometry changes caused by decarboxylation of 2-lactyloxazolium (bond distance in Å and bond angle in degree).

33

Reactant

<OCO=130°
R(CO)=1.252av
<$C^2C^{2\alpha}CO_2$=108°
<$C^2C^{2\alpha}OH$ =108°
<$C^2C^{2\alpha}CH_3$ =109°

Transition State

<OCO=140°
R(CO)=1.214av
<$C^2C^{2\alpha}CO_2$=100°
<$C^2C^{2\alpha}OH$ =113°
<$C^2C^{2\alpha}CH_3$=118°

$R(C^{2\alpha}-CO_2)=2.195$Å

<OCO=159°
R(CO)=1.202av
<$C^2C^{2\alpha}CO_2$ = 96°
<$C^2C^{2\alpha}OH$ =115°
<$C^2C^{2\alpha}CH_3$ =122°

Product

Figure 2.4 Geometry changes caused by decarboxylation of 2-lactylimidazolium (bond distance in Å and bond angle in degree).

34

2-lactylthiazolium (23.8 kcal/mol) > 2-lactyloxazolium (18.1 kcal/mol) > 2-lactylimidazolium (3.9 kcal/mol). Thus, the decarboxylation of 2-lactylthiazolium proceeds the most easily but that of 2-lactylimidazolium proceeds with the most difficulty in these three decarboxylations.

It is interesting to compare geometries of the TS in these decarboxylations. As described above, the C^2-$C^{2\alpha}$ bond changes to its double bond but the C^2-N bond changes to its single bond upon going to the product from the reactant. To indicate how much the C^2-$C^{2\alpha}$ single bond changes to its double bond at the TS, a factor f_1 is defined as follows; $f_1 = R(C-C)_P - R(C-C)_{TS} / R(C-C)_R - R(C=C)_P$, where such subscripts as, P, R, and TS, represent product, reactant, and transition state, respectively. Apparently, f_1 is 0 % for the C^2-$C^{2\alpha}$ single bond and 100 % for the C^2=$C^{2\alpha}$ double bond. Also, a factor, f_2, is defined on the C^2-N bond, to illustrate how much the C^2=N double bond changes to its single bond at the TS; $f_2 = R(C=N)_R - R(C-N)_{TS} / R(C=N)_R - R(C-N)_P$. Apparently, f_2 is 0 % for the C^2=N double bond and 100 % for the C^2-N single bond. These factors, f_1 and f_2, are considered as measures indicating the character of TS. As listed in Table 2.2, these f_1 and f_2 exhibit interesting differences between 2-lactylimidazolium and the other two; f_1=38 % and f_2=31 % in the decarboxylation of 2-lactylthiazolium, f_1=30 % and f_2=21 % in the decarboxylation of 2-lactyloxazolium, f_1=58 % and f_2=40 % in the decarboxylation of 2-lactylimidazolium. These results suggest that the decarboxylation of 2-lactylimidazolium reaches TS more late than the other decarboxylations.

Table 2.2 Measures of C^2-$C^{2\alpha}$ bond lengthening (f_1) and C^2-N^3 bond shortening (f_2), and Pauling's bond order (n) of the C^2-$C^{2\alpha}$ and C^2-N^3 bonds at the transition state of the decarboxylation of 2-lactylaozliums.

	Measure of change in bond distance		Pauling's bond order	
	$f_1{}^a$	$f_2{}^b$	$n_{C2-C2a}{}^c$	$n_{C2-N3}{}^c$
2-lactylthiazolium	38 %	31 %	1.323	1.615
2-lactyloxazolium	30 %	21 %	1.232	1.727
2-lactylimidazolium	58 %	40 %	1.466	1.516

a) f_1 is the measure indincating how much the C^2-$C^{2\alpha}$ bond changes to the double bond from the single bond (see text).

b) f_2 is the measure indincating how much the C^2-N bond changes to the single bond from the double bond (see text).

c) Pauling's bond order; $n=\exp[(R_1-R_n)/C]$, where R_1 and R_n are bond lengths for bonds of order unity and n, respectively. C is estimated so as that n=1 for the single bond and n=2 for the double bond.

Pauling's bond order is also useful in discussing the character of TS. As shown in Table 2.2, the decarboxylation of 2-lactylimidazolium exhibits the greater value of the C^2-$C^{2\alpha}$ bond order and the smaller value of the C^2-N one at the TS than the other decarboxylations, indicating that in the 2-lactylimidazolium decarboxylation, the C^2-$C^{2\alpha}$ single bond changes to its double bond and the C^2=N double bond changes to its single bond at the TS, to a greater extent, than in the other decarboxylations. These results again

suggest that the decarboxylation of 2-lactylimidazolium reaches TS more late than the others.

2-3-3 Electron Redistribution in These Decarboxylations and Factors Determining the Reactivity of Azolium

As the decarboxylation proceeds, the electron density of the CO_2 part decreases but that of the azolium ring increases, as clearly shown in Figure 2.5. The greatest change is caused by the decarboxylation of 2-lactylthiazolium. This means that the thiazolium ring is the most electron-withdrawing (i.e. the least electron-donating) in these three azoliums.

It is worthwhile investigating whether or not the decarboxylation reactivity is related to the electron-withdrawing character of the azolium ring. The more the azolium ring is electron-withdrawing, the more its π^* orbital lies low in energy. Thus, let us inspect the relation between the π^* orbital of the azolium ring and the decarboxylation reactivity of 2-lactylazolium. Since a neutral CO_2 molecule eliminates from 2-lactylazolium, 2-lactylazolium is considered to consist of CO_2 and such a remaining fragment as 2-hydroxyethylthiazolium (**10**), 2-hydroxyethyloxazolium (**11**), and 2-hydroxyethylimidazolium (**12**). These fragments, **10**, **11**, and **12**, are calculated with the AM1 method, where their geometries are taken to be the same as in the TS. Here, we should notice HOMO of 2-hydroxyethylazolium because the charge transfer from Lewis base to CO_2 is considered important to the CO_2 binding with

37
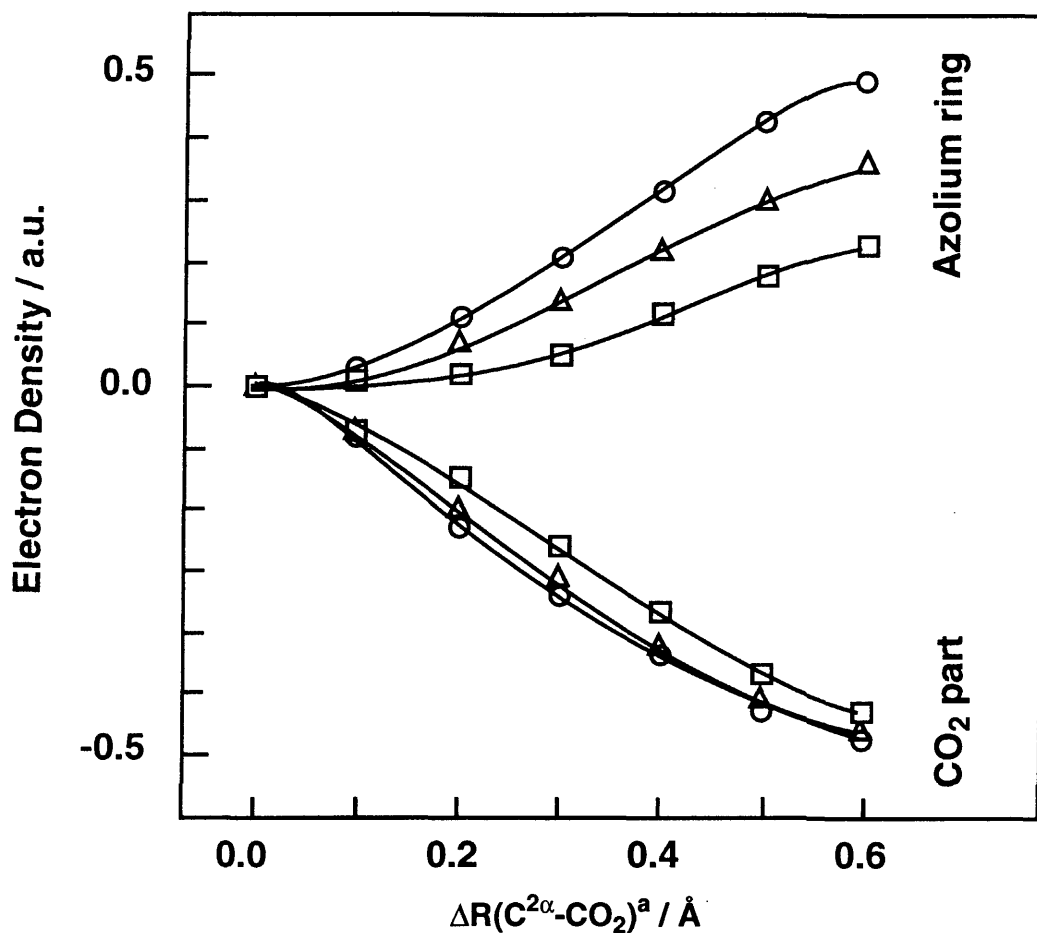
Figure 2.5 Changes in electron density of the CO_2 part and azolium-ring caused by decarboxylations of 2-lactylthiazolium, 2-lactyloxazolium, and 2-lactylimidazolium.

a) $\Delta R(C^{2\alpha}\text{-}CO_2)$ means lengthning of the $C^{2\alpha}\text{-}CO_2$ distance caused by the decatboxylation from 2-lactylazoliums.

the base.[20] As schematically shown in Figure 2.6, their HOMO mainly consists of the $C^{2\alpha}p_\pi$ orbital into which the π^* orbital of the azolium ring mixes in a bonding way. Because the π^* orbital of the azolium ring rises in energy in the order thiazolium < oxazolium < imidazolium, the bonding
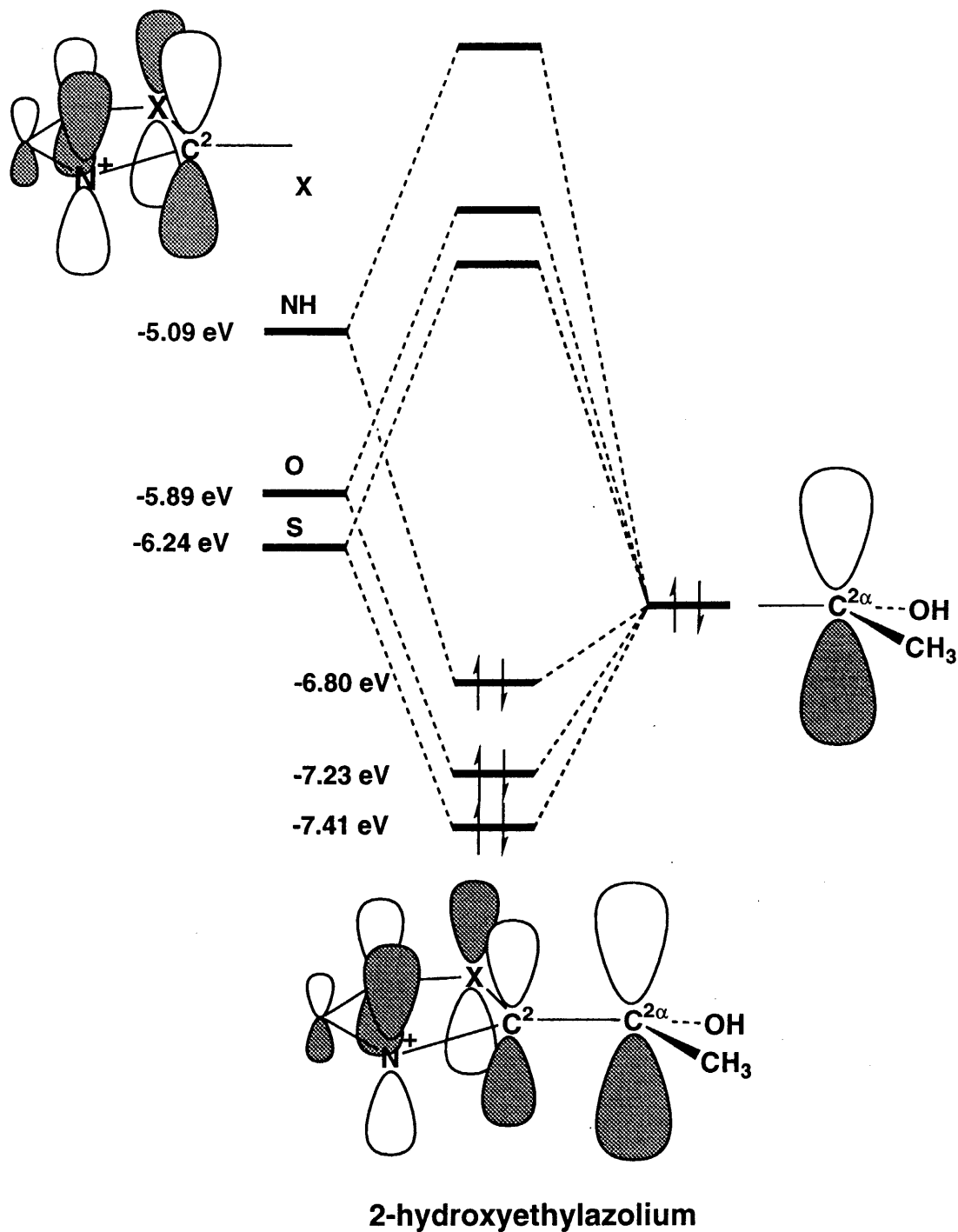
Figure 2.6 Schematical representation of interaction between CO_2 and the $C^{2\alpha}$ atom at Transition State.

mixing between the π^* orbital of the azolium ring and the $C^{2\alpha}p_\pi$ orbital weakens in the order **10** > **11** > **12**, and therefore, HOMO of 2-hydroxyethylazolium rises in energy in the order **10** < **11** < **12**, as shown in Figure 2.6. Thus, the charge transfer from 2-hydroxyethylazolium to CO_2 becomes strong in the order **10** < **11** < **12**, which leads to the weakest $C^{2\alpha}$-CO_2 interaction in 2-lactylthiazolium and the strongest $C^{2\alpha}$-CO_2 interaction in 2-lactylimidazolium. Consequently, the decarboxylation of 2-lactylthiazolium proceeds the most easily but that of 2-lactylimidazolium occurs with the most difficulty in these 2-lactylazoliums examined.

In summary, the decarboxylation reactivity of 2-lactylazolium can be related to the electron-withdrawing ability of the azolium ring, as follows: Since the π^* orbital of the thiazolium ring lies at the lowest energy level in these azoliums examined, thiazolium is the most electron-withdrawing, and at the same time, HOMO of 2-hydroxyethylthiazolium lies at the lowest energy level in these 2-hydroxyethylazoliums. In 2-lactylthiazolium, therefore, the CO_2 binding with the $C^{2\alpha}$ atom is the weakest in these 2-lactylazoliums, which results in the easiest decarboxylation of 2-lactylthiazolium. In other words, the greatest decarboxylation reactivity of 2-lactylthiazolium comes from the most electron-withdrawing ability of the thiazolium ring. These results are consistent with Breslow's proposal that the thiazolium ring serves as an electron sink for the decarboxylation process.[2]

Finally, let us discuss briefly the reason that the π^*

orbital of the thiazolium ring lies at the lowest energy level in these azoliums. Compared to the O atom of oxazolium and the NH group of imidazolium, the S atom of thiazolium possesses highly polarizable and diffuse orbitals, which would stabilize the π^* orbital of the thiazolium ring in energy and would enhance the electron-withdrawing ability of the thiazolium ring.

2.4 Conclusions

AM1 and ab initio MO/MP2 calculations are carried out on the decarboxylation reaction of 2-lactylthiazolium, a model of thiamin diphosphate. For the decarboxylation, the calculated activation barrier (E_a) is very small and the calculated exothermicity (E_{exo}) is considerably large; E_a = 1.5 kcal/mol (AM1), 3.9 kcal/mol (MP2/MIDI-4), 4.4 kcal/mol (MP2/6-31G), and E_{exo} = 23.8 kcal/mol (AM1). Two water molecules interacting with the CO_2 part of 2-lactylthiazolium increase the activation barrier to 5.6 kcal/mol and decrease the exothermicity to 14.7 kcal/mol. An additional water molecule interacting with the thiazolium ring further increases the activation barrier to 19.0 kcal/mol and significantly decreases the exothermicity to -2.1 kcal/mol (i.e., the reaction is endothermic). This result agrees well with Lienhard's experiment.

As the decarboxylation proceeds, the C^2-$C^{2\alpha}$ and C^2-N bonds are changing to the corresponding double and single bonds, respectively, and the product takes the typical enamine structure. This theoretical result, as well as Jordan's experiments, clearly indicates that the enamine is

41

indeed on the reaction pathway.

   Decarboxylation reactions of 2-lactyloxazolium and
2-lactylimidazolium are investigated, to compare their
reactivities with that of 2-lactylthiazolium. Products of
their decarboxylations also take the enamine structure. In
their decarboxylations, the activation barrier is slightly
higher than that of 2-lactylthiazolium; 2.8 kcal/mol for 2-
lactyloxazolium and 6.4 kcal/mol for 2-lactylimidazolium
(AM1 calculation). The exothermicity is somewhat smaller in
2-lactyloxazolium (18.1 kcal/mol) and significantly smaller
in 2-lactylimidazolium (3.9 kcal/mol) than in 2-
lactylthiazolium. Thus, the decarboxylation reactivity
decreases in the order thiazolium > oxazolium > imidazolium.
This decreasing order is interpreted in terms of the π^*
orbital of the azolium ring. Since the energy level of its
π^* orbital lowers in the order imidazolium > oxazolium >
thiazolium, HOMO of 2-hydroxyethylazolium lowers in the same
order, which results in the most weak $C^{2\alpha}$-CO_2 binding of 2-
lactylthiazolium. Accordingly, the decarboxylation of 2-
lactylthiazolium proceeds the most easily. The π^* orbital
of the azolium ring would be stabilized in energy by highly
polarizable and diffuse orbitals of the S atom.

References

(1) (a) S. Mizuhara and P. J. Handler, <u>J. Am. Chem. Soc.</u>, **80**, 5893 (1958). (b) L. O. Krampitz, <u>Annu. Rev. Biochem.</u>, **38**, 213 (1969). (c) L. O. Krampitz, "Thiamin Diphosphate and Its Catalytic Functions," Marcel Dekker, New York (1970). (c) A. A. Gallo, J. J. Mieyal, and H. Z. Sable, "Bioorganic Chemistry," Acadmic Press, New York (1978), Vol. 4, pp. 147-177. (d) R. Kluger, <u>Chem. Rev.</u>, **87**, 863 (1987). (e) A. Schellenberger and R. L. Schowen, Eds., "Thiamin Pyrophosphate Biochemistry," CRC Press, Boca Raton, FL (1988).

(2) R. Breslow, <u>J. Am. Chem. Soc.</u>, **80**, 3719 (1958).

(3) H. Holzer and K. Beaucamp, <u>Biochim. Biophys. Acta</u>, **46**, 225 (1961).

(4) L. O. Krampitz and G. J. Greull, <u>J. Cell. Comp. Physiol.</u>, **54**, 101 (1959), Suppl.1.

(5) R. Kluger, J. Chin, and T. J. Smyth, <u>J. Am. Chem. Soc.</u>, **103**, 884 (1981).

(6) R. Kluger and T. J. Smyth, <u>J. Am. Chem. Soc.</u>, **103**, 1214 (1981).

(7) J. Crosby, R. Stone, and G. E. Lienhard, <u>J. Am. Chem. Soc.</u>, **92**, 2891 (1970).

(8) (a) R. Kluger, K. Karimian, G. Gish, W. A. Pangborn, and G. DeTitta. <u>J. Am. Chem. Soc.</u>, **109**, 618 (1987). (b) R. Kluger, K. Karimian, and K. Kitamura, <u>J. Am. Chem. Soc.</u>, **109**, 6368 (1987).

(9) (a) F. Jordan, Z. H. Kudzin, and C. B. Rios, <u>J. Am. Chem. Soc.</u>, **109**, 4415 (1987). (b) N. Annan, R. Paris,

and F. Jordan, <u>J. Am. Chem. Soc.</u>, **111**, 8895 (1989).
(c) F. G. Bordwell, A. V. Satish, F. Jordan, C. B.
Rios, and A. C. Chung, <u>J. Am. Chem. Soc.</u>, **112**, 792
(1990). (d) G. Barletta, A. C. Chung, F. Jordan, and
J. M. Schlegel, <u>J. Am. Chem. Soc.</u>, **112**, 8144 (1990).
(e) X. Zeng, A. Chung, M. Haran, and F. Jordan, <u>J. Am.
Chem. Soc.</u>, **113**, 5842 (1991).

(10) J. J. P. Stewart, MOPAC Version 3.0, QCPE 455, 1983.

(11) M. J. S. Dewar, E. G. Zeobisch, E. F. Healy, and J. J.
P. Stewart, <u>J. Am. Chem. Soc.</u>, **107**, 3902 (1985).

(12) (a) M. J. S. Dewar, M. L. McKee, and H. S. Rzepa, <u>J.
Am. Chem. Soc.</u>, **100**, 3607 (1978). (b) M. J. S. Dewar
and M. L. McKee, <u>J. Comp. Chem.</u>, **4**, 542 (1983).

(13) (a) <u>Gaussian 82</u>; J. S. Binkley, M. J. Frish, and J. A.
Pople, Carnegie-Mellon Quantum Chemistry Publishing
Unit, Pittsburgh, PA (1984). (b) Gaussian 86; M. J.
Frisch, J. S. Binkley, H. B. Schlegel, K.
Raghavachari, C. F. Melius, R. L. Martin, J. J. P.
Stewart, F. W. Bobrowicz, C. M. Rohlfing, L. R. Kahn,
D. J. DeFrees, R. A. Whiteside, D. J. Fox, E. M.
Fleuder, and J. A. Pople, Carnegie-Mellon Quantum
Chemistry Publishing Unit, Pittsburg, PA (1986).

(14) (a) S. Huzinaga, J. Andzelm, M. Klobukowski, E.
Radzio-Andzelm, Y. Sakai, and H. Tatewaki, "Gaussian
Basis Sets for Molecular Calculations," Elsevier,
Amsterdam (1984). (b) The (3s/1s) set of H is taken
from the following ref.; F. B. Van Duijneveldt,
"Gaussian Basis Sets for the Atoms H-Ne for Use in
Molecular Calculations," <u>IBM J. Res. Dev.</u>, **1971**, 945.

(c) The (3s)/[2s] set of H is taken from the following ref.; T. H. Dunning, *J. Chem. Phys.*, **53**, 2823 (1970).

(15) W. J. Hehre, L. Random, P. V. R. Schleyer, and J. A. Pople, "Ab Initio Molecular Orbital Theory," Wiley, New York (1986), Chap. 4.

(16) (a) R. Fletcher and M. J. D. Powell, *Comput. J.*, **6**, 163 (1963). (b) W. C. Davidon, *Comput. J.*, **10**, 406 (1968).

(17) (a) The optimized geometry of the thiazolium ring by the AM1 method agrees well with the experimental structure.[17b] The ab initio MO method overestimated bond lengths of the thiazolium ring by 0.06 Å ~ 0.2 Å, when either MINI-1, STO-3G, or 3-21G was employed. Only when a d-polarization function is added on the S atom, the optimized geometry agrees well with the experimental structure.[17b] (b) A. Turano, W. Furey, J. Pletcher, M. Sax, D. Pike, and R. Kluger, *J. Am. Chem. Soc.*, **104**, 3089 (1982). (c) In ab initio MO calculations, the reaction coordinate, $C^{2\alpha}$-CO_2 distance, is increased with an increment of 0.2 Å, and the geometry was optimized at each $C^{2\alpha}$-CO_2 distance. The TS was located by least-square fitting of total energies.

(18) Since the structure of the thiazolium's five-membered ring is considerably different between **1** and the enamine product, the thiazolium ring in the product should be re-optimized for calculation of the exothermicity. However, such optimization is much time-consuming in ab initio MO calculations, because
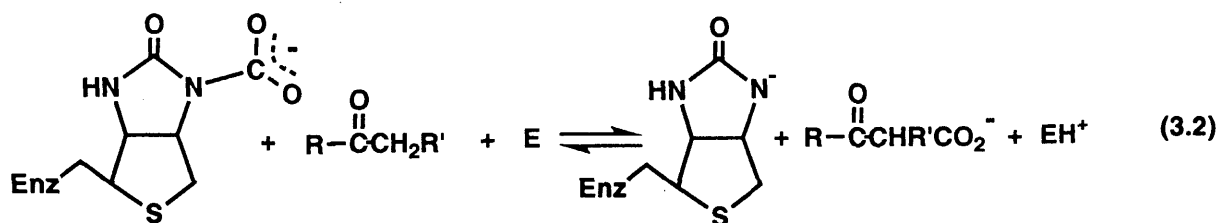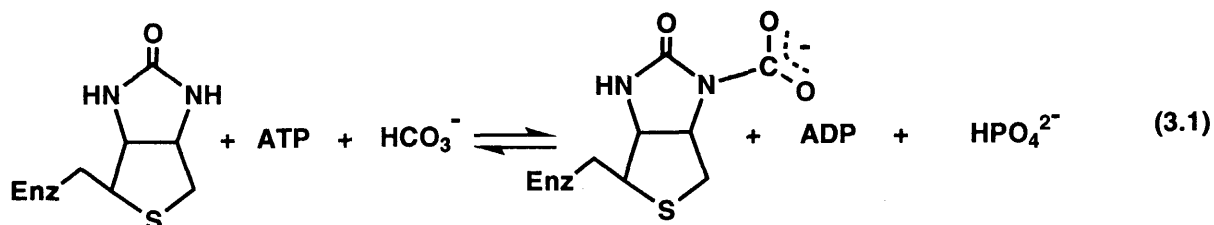
use of a d-polarization function is indispensable to *obtain good geometry of the five-membered ring.*[17a] Thus, the exothermicity was not calculated by the ab initio MO/MP2 method.

(19)   (a) Water molecules are placed in the CO_2 plane, where waters approach the O atom of CO_2 with the H atom in the lead. The approaching angle of H_2O (<COH) and the distance between O of CO_2 and H of H_2O are optimized. (b) A water molecule is placed above the thiazolium ring, perpendicularly to the ring, where the O atom of water molecule approaches the N atom of thiazolium. The N-O distance and the approaching angle of H_2O are optimized.

(20)   (a) S. Sakaki, K. Kitaura, and K. Morokuma, <u>Inorg. Chem.</u>, **21**, 760 (1982). (b) *S. Sakaki and A. Dedieu,* <u>Inorg. Chem.</u>, **26**, 3278 (1987). (c) S. Sakaki, N. Koga, and K. Morokuma, <u>Inorg. Chem.</u>, **29**, 3110 (1990).

<center>

Structure and Bonding Nature of

Carboxyimidazolidone,

**a Model of Carboxybiotin.**

</center>

3.1 Introduction

The reaction mechanism of the biotin-mediated CO_2 metabolism has been actively investigated as reviewed recently,[1] because biotin serves as a cofactor in a number of important enzymic carboxylation reactions of organic substrates.[2-4] For instance, the pioneering work of Lynen et al. clearly indicated that enzymic carboxyl-transfer reaction proceeds via a carboxybiotin intermediate.[2] The reaction mechanism accepted now is summarized as follows;[1] (1) N-carboxybiotin is formed from biotin, bicarbonate, and ATP (eq 3.1), accompanied with conversion of ATP to ADP

$$\text{biotin} + \text{ATP} + \text{HCO}_3^- \rightleftharpoons \text{N-carboxybiotin} + \text{ADP} + \text{HPO}_4^{2-} \tag{3.1}$$

$$\text{N-carboxybiotin} + \text{R}-\overset{\text{O}}{\underset{\|}{\text{C}}}\text{CH}_2\text{R}' + \text{E} \rightleftharpoons \text{biotin}^- + \text{R}-\overset{\text{O}}{\underset{\|}{\text{C}}}\text{CHR}'\text{CO}_2^- + \text{EH}^+ \tag{3.2}$$

and inorganic phosphate,[2,3] and then (2) the carboxyl group transfers from N-carboxybiotin to an organic substrate with the deprotonation of substrate by either enzyme or biotin

itself (eq 3.2).[4-6] Although many elegant experimental works *have been carried out to clarify the reaction mechanism,*[1] there still remain several important issues to be examined. One of those issues is the reactivity of N-carboxybiotin. Because N-carboxybiotin is considered to be inherently unreactive,[7] it must be activated to perform the carboxyl-transfer reaction. Kluger et al.[8] proposed that the carboxyl group becomes reactive by the rotation around the N-CO_2 bond because such rotation would destroy the resonance preserved in the most stable planar conformation. The other proposal was presented by Perrin and Dwyer, in which the CO_2 group of carboxybiotin is considered to be activated by proton donor or cationic species.[9] Detailed knowledge on geometry, stability, bonding nature, and electron distribution of carboxybiotin would be helpful to discuss the reaction mechanism. Not only experimental works but also theoretical works are necessary to present such knowledge. However, only a few of theoretical works have been carried out to our knowledge,[8,10] in which rather simple compounds were adopted as a model of biotin.

In this chapter, we carried out ab initio MO/MP4, SD-CI, and coupled cluster with double substitution (CCD) calculations of N-carboxyimidazolidone **1**, O-carboxy-imidazolidone **2**, and the η^2-side-on carboxyimidazolidone **3**, where imidazolidone was adopted here as a model of biotin (Scheme 3.1). Our purposes of this chapter are (1) to offer fundamental knowledge necessary for systematically theoretical investigation of biotin; for instance, reliability of model, basis set effects, and correlation effects on geometry and stability, (2) to present such

N-Carboxybiotin

O-Carboxybiotin

1   **2**   **3**
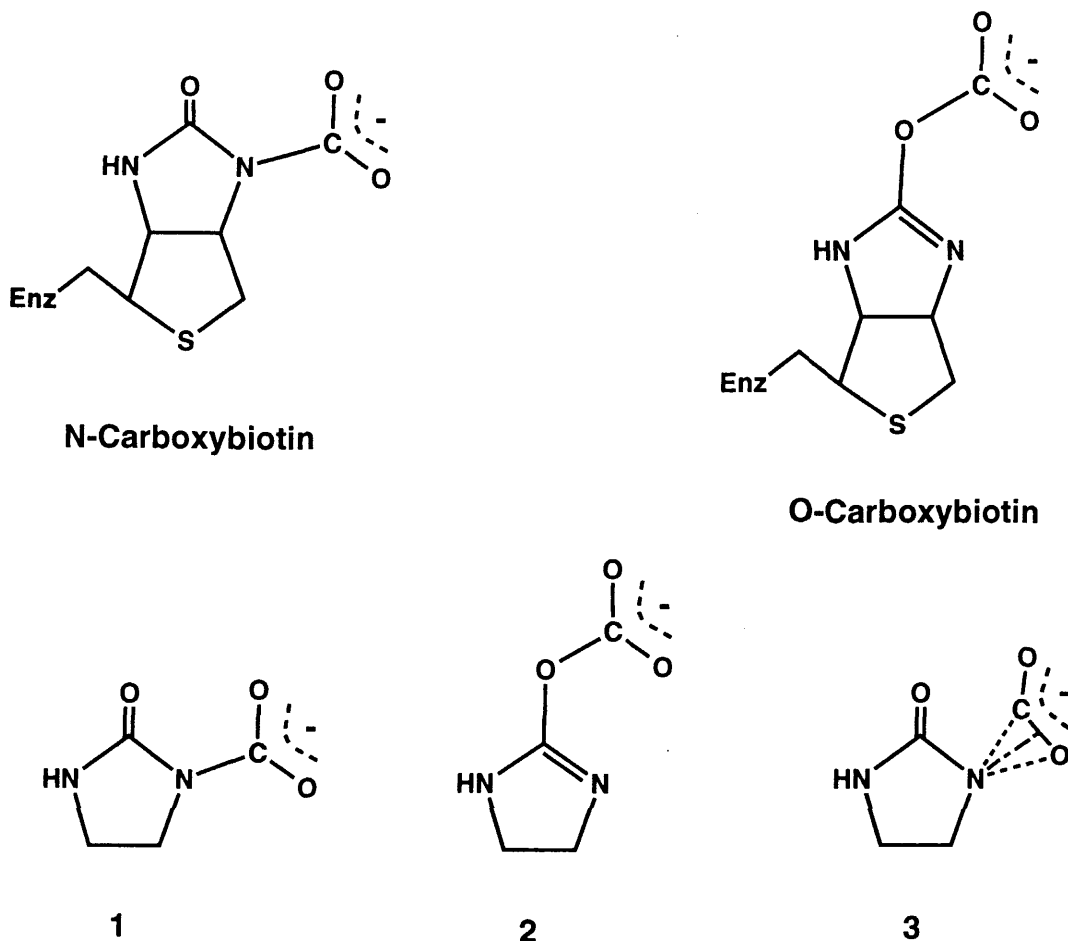
Scheme 3.I

detailed information of imidazolidone and carboxy-
imidazolidone as geometry, bonding nature, electron
distribution, and reactivity, (3) to make a clear comparison
between N-carboxyimidazolidone and O-carboxyimidazolidone,
because O-carboxybiotin was proposed previously[11] but any
information has not been reported on it, and (4) to examine
the stability of the η^2-side-on carboxyimidazolidone; this
structure has not been discussed at all, whereas both η^1-C
and η^2-side-on CO_2 adducts have been reported in transition-

metal complexes.[12]

3.2 Computational Details

Ab initio closed-shell Hartree-Fock (HF), MP2 to MP4SDQ, SD-CI, and CCD calculations were carried out with Gaussian 86[13a] and 92[13b] programs. 3-21G,[14] 6-31G,[15] and 6-31+G[16] basis sets were used in these calculations, where d-polarization functions[17] were added to N and O of imidazolidone. In SD-CI calculations, the contribution of higher-order excited configurations were estimated, according to Davidson,[18] Davidson-Silver,[19] and Pople et al.[20] In CCD calculations, the contribution of single and triple substitutions was evaluated through forth-order with CCD wave functions.[21] In all the calculations at the correlated level, core orbitals were excluded from the active space.

Geometry optimization was performed with the energy gradient method at HF and MP2 levels, using 3-21G set. In the optimization, the five-membered ring of imidazolidone was assumed to be in the C_s symmetry because the five-membered ring of methylbiotin has been experimentally reported to be planar.[22] Such important geometrical parameters as the $N-CO_2$ distance of N-carboxyimidazolidone **1**, the $O-CO_2$ distance of O-carboxyimidazolidone **2**, and the geometry of the CO_2 part were re-optimized at the MP2 level, using 3-21G set, where the geometry of imidazolidone was assumed to be the same as the HF-optimized structure. This assumption seems reasonable, as will be discussed below.

Full geometry optimization of η^2-side-on carboxy-imidazolidone **3** led to **1**. Thus, the geometry of **3** was optimized at R(N-X) = 2.0, 2.2 and 2.4 Å under the

3
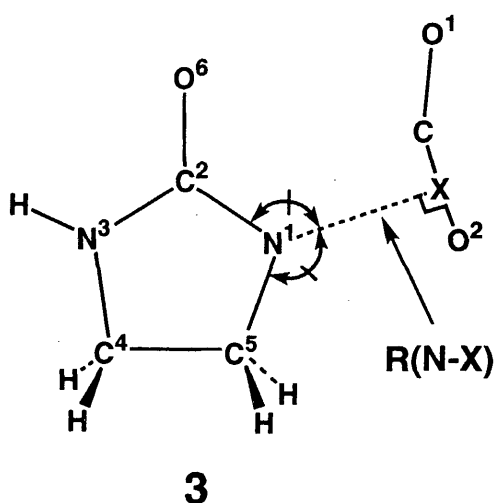
Scheme 3.2

constraint that the N–X line bisecting the $C^2N^1C^5$ angle is perpendicular to the C=O bond, where X is the center of the C=O bond (see Scheme 3.2).

In order to investigate the interaction between CO_2 and deprotonated imidazolidone, we carried out energy decomposition analysis proposed by Morokuma et al.[23] In this analysis, the interaction energy (INT) is defined as the stabilization energy of carboxyimidazolidone relative to imidazolidone⁻ and CO_2 taking their distorted structures in carboxyimidazolidone (eq 3.3), where deprotonated imidazolidone is abbreviated as imidazolidone⁻ and negative charge of carboxyimidazolidone is not described here for brevity. The deformation energy (DEF) is defined as the destabilization energy which is necessary to distort CO_2 and imidazolidone⁻ from their equilibrium structures to their distorted structures taken in **1** and **2** (eq 3.4);

$$INT = E_t(Imd\text{-}CO_2) - E_t(Imd)_{dist} - E_t(CO_2)_{dist}, \qquad (3.3)$$

DEF = $E_t(Imd)_{dist} - E_t(Imd)_{eq} + E_t(CO_2)_{dist} - E_t(CO_2)_{eq}$,   (3.4)

where Imd means imidazolidone⁻, and subscripts of "eq" and "dist" represent the equilibrium structure and the distorted one respectively. BE is the sum of INT and DEF, which corresponds to the negative value of usual binding energy (eq 3.5). INT is further divided into several chemically meaningful terms at the HF level, as shown in eq 3.6.

$$BE = INT + DEF$$

$$= E_t(Imd-CO_2) - E_t(Imd)_{eq} - E_t(CO_2)_{eq} \qquad (3.5)$$

$$INT = ES + EX + CTPLXA(Imd \rightarrow CO_2)$$

$$+ CTPLXB(Imd \rightarrow CO_2) + R \qquad (3.6)$$

ES is the electrostatic (coulombic) interaction between imidazolidone⁻ and CO_2. EX is the exchange repulsion arising from Pauli exclusion principle between imidazolidone⁻ and CO_2. CTPLXA consists of the charge transfer (CT) from imidazolidone⁻ to CO_2, the polarization of CO_2, and their coupling term. CTPLXB consists of the CT from CO_2 to imidazolidone⁻, the polarization of imidazolidone⁻, and their coupling term. R is a higher order coupling term. From the definition, a negative value means stabilization in energy for all these terms (vice versa). Although this analysis is based on the HF approximation, the bonding nature of **1** and **2** would be reliably compared by this analysis because the relative stabilities of **1** and **2** are essentially the same at both HF and correlated levels (vide infra). IMSPAC program was used for this analysis.[24]

3.3 Results and Discussion
3-3-1 A Comparison of Biotin with Imidazolidone

First, we will examine whether imidazolidone can be

O
| 1.200
1.370 C 1.367
H—N 106 N—H
115   115
1.442 102 102 1.449
1.580
H₃C H C 1.582 C H H
1.561   1.547
H 1.836 S 1.817 H

(A) Methylbiotin

O
| 1.202
1.369 C 1.369
H—N 106 N—H
115   115
1.450 102 102 1.450
C 1.573 C
H H H

(B) Imidazolidone

O^6
| 1.233
1.432 C^2 1.315
H—N^3 111 N^1
113 109
1.429 99 108 1.449
C^4 C^5
H 1.589 H

HF-level

O^6
| 1.258
1.466 C^2 1.336
H—N^3 110 N^1
113 109
1.428 99 109 1.450
C^4 C^5
H 1.618 H

MP2-level

(C) Deprotonated imidazolidone
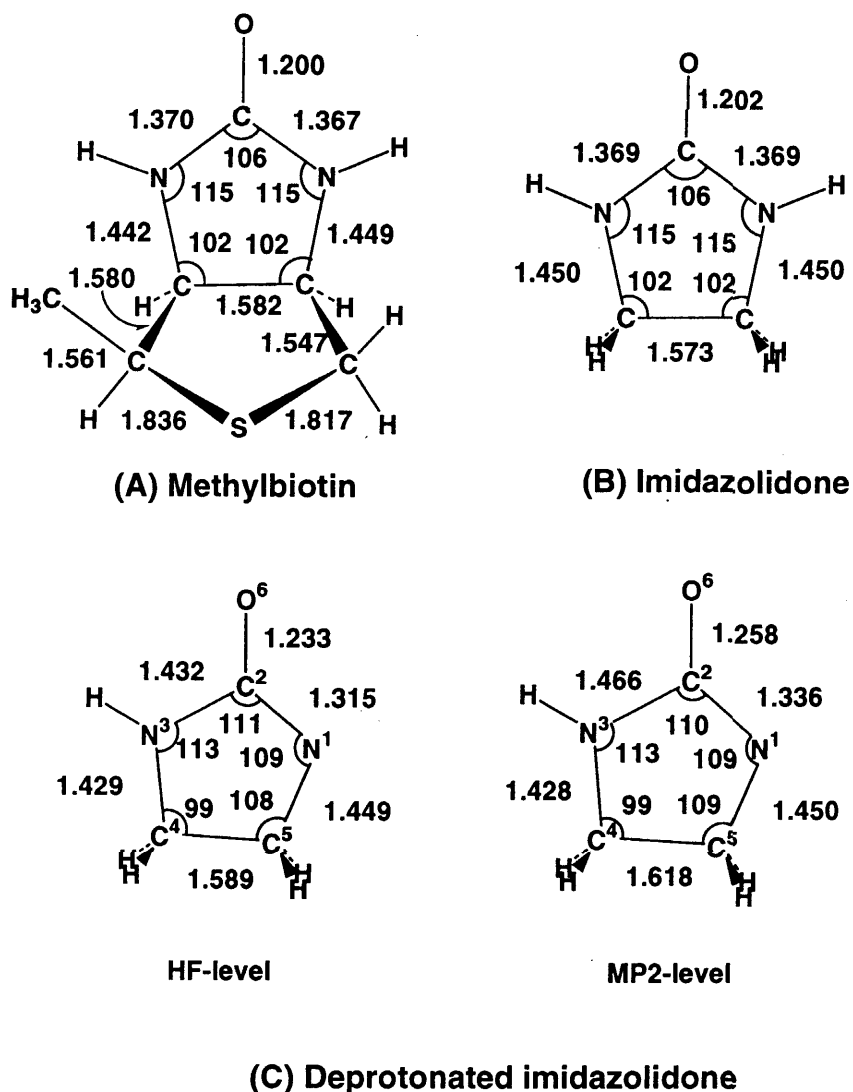
Figure 3.1 Optimized geometries of methylbiotin, imidazolidone, and deprotonated imidazolidone

adopted as a reasonable model of biotin or not. As shown in Figure 3.1A, the HF-optimized geometry of methylbiotin agrees well with the experimental structure of d(+)-biotin.[22] Also, the HF-optimized geometry of imidazolidone (Figure 3.1B) is almost the same as the corresponding part of the HF-optimized methylbiotin. Furthermore, imidazolidone has

53

Table 3.1 Atomic population and energy levels of π and π^* orbitals $((\varepsilon(\pi)$ end $\varepsilon(\pi^*))$ of methylbiotin and imidazolidone[a]

	methylbiotin	imidazolidone
	Atomic Population	
N^1	7.94	7.93
C^2	4.60	4.61
C^4	7.93	7.93
C^5	5.59	6.15
O^6	5.93	6.15
	8.79	8.79
	Orbital Energy (eV)	
$e(\pi)$	-10.19	-10.18
$e(\pi^*)$	7.35	7.36

a) The 6-31G basis set was used, where a d-polarization function was added to N and O atoms of imidazolidone and methylbiotin.

almost the same atomic populations and π and π^* orbitals at almost the same energy as those of methylbiotin, as compared in Table 3.1. From these results, imidazolidone seems to be a reasonable model of biotin.

In order to examine correlation effects on geometry, imidazolidone⁻ was optimized at both HF and MP2 levels (Figure 3.1C). Introduction of electron correlation expectedly lengthens the C^2-O^6, N^1-C^2, and C^4-C^5 bonds. The difference in geometry between MP2 and HF levels is not,

however, significant. For instance, discrepancies in bond length and bond angle are less than 0.05 Å and 4° respectively. Further, the energy levels of π and π^* orbitals do not change so much upon going to the MP2-optimized geometry from the HF-optimized one; $\varepsilon(\pi)$ = -4.26 eV, $\varepsilon(\pi^*)$ = 12.60 eV for the HF-optimized geometry, and $\varepsilon(\pi)$ = -4.31 eV, $\varepsilon(\pi^*)$ = 12.42 eV for the MP2-optimized geometry. Thus, the HF-optimized geometry of the imidazolidone ring seems reasonable for investigating the interaction between imidazolidone ring and CO_2.

3-3-2 Geometries and the CO_2 Binding Energies (be) of N-Carboxyimidazolidone and O-Carboxyimidazolidone

Optimized geometries of N-carboxyimidazolidone **1** and O-carboxyimidazolidone **2** are shown in Figure 3.2. Several interesting features are observed; (1) the CO_2 part significantly distorts in both **1** and **2**; the C=O distance is considerably longer than that of the free CO_2 molecule and the OCO angle is remarkably closed. The CO_2 part in **1** is more distorted than in **2**. (2) It is noted that the geometry of CO_2 in **1** and **2** resembles well the η^1-C coordinated CO_2 complexes of transition metal, such as $M[Co^I(R-salen)(CO_2)]$,[25] $Rh^ICl(diars)_2(CO_2)$,[26] and $Ru(bpy)_2(CO)(\eta^1-CO_2)$.[27] (3) In both **1** and **2**, the CO_2 part is on the molecular plane of imidazolidone. The perpendicular structure is less stable than the planar one by ca. 6 kcal/mol for **1** and 10 kcal/mol for **2** at the MP4(SDQ)/6-31G level. This energy difference is much smaller than that calculated previously for the simple model compound $(H_2NCONH-CO_2)$.[8] There are several reasons for this

(A) HF-level

(B) MP2-level[a]

N-Carboxyimidazolidone

(C) HF-level
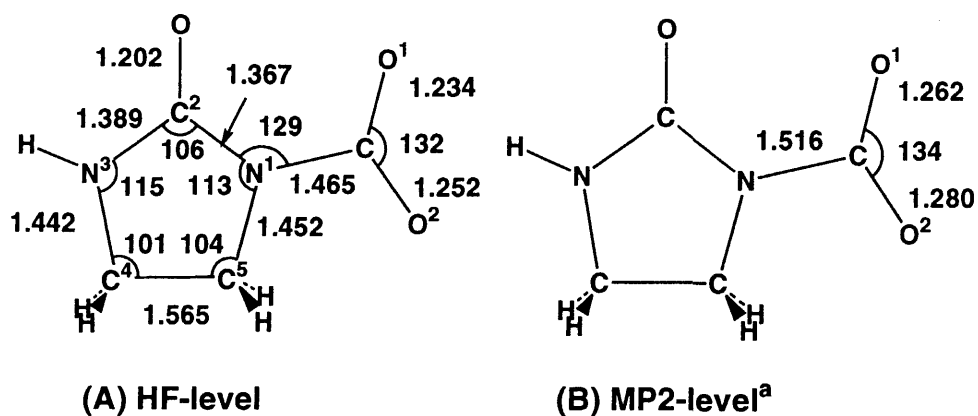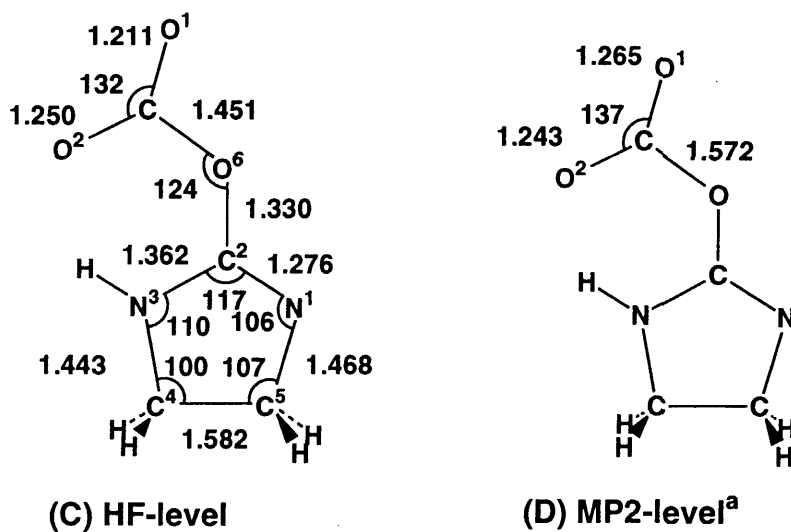
**(D) MP2-level[a]**

O-Carboxyimidazolidone

Figure 3.2 Optimized geometries of N-carboxyimidazolidone and O-carboxyimidazolidone

a) The CO_2 parts in **1** and **2** were re-optimized at the MP2 level, using 3-21G set, where the geometry of imidazolidone was assumed to be the same as the HF-optimized structure.

56

difference; the basis sets used are different, electron correlation is included in this thesis but was not in the previous work, and the more realistic model is adopted here than in the previous work.[8] Thus, the energy difference evaluated here seems more reliable. (4) Introduction of electron correlation lengthens the C=O distance like it in the free CO_2 molecule. Also, the N-CO_2 and O-CO_2 distances considerably lengthen upon introducing electron correlation, whereas the OCO angle little changes. This means that consideration of electron correlation is necessary for investigating model compounds of carboxybiotin.

In the η^2-side-on carboxyimidazolidone **3**, the C=O bond distances are optimized to be 1.16 and 1.17 Å, and the OCO angle is 167° at R(N-X) = 2.0 Å. This geometry of the CO_2 part is less distorted than in **1** and **2** (Figure 3), which suggests that the interaction between CO_2 and imidazolidone⁻ is weak in this η^2-CO_2 adduct (vide infra).

The binding energy of CO_2 in **1** and **2** was calculated with MP4SDQ/6-31G, MP4SDQ/6-31+G, SD-CI/6-31G and CCD/6-31G methods, where basis set super-position error was corrected with the counter-poise method.[28] Although the binding energy more or less fluctuates at MP2 and MP3 levels, almost the same binding energy was calculated at MP4, SD-CI, and CCD levels (see Table 3.2). Hereafter, we discuss relative stabilities of **1**, **2**, and **3**, based on MP4, SD-CI, and CCD calculations. Although use of the 6-31+G basis set including diffuse s and p functions on CO_2 yields somewhat smaller binding energy than the 6-31G basis set, the energy difference between **1** and **2** is little influenced by addition of such diffuse functions, and the CO_2 binding
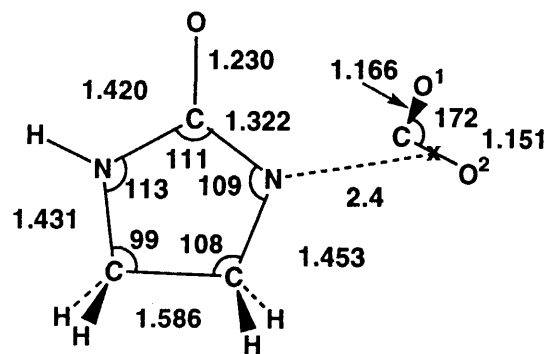
3a
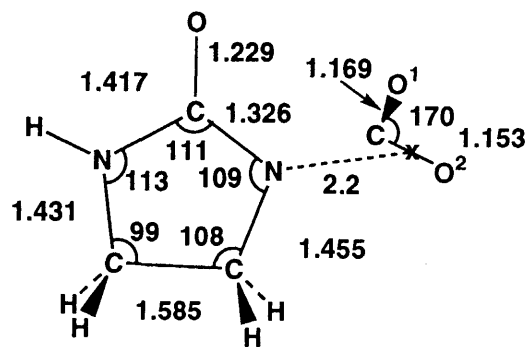
3b
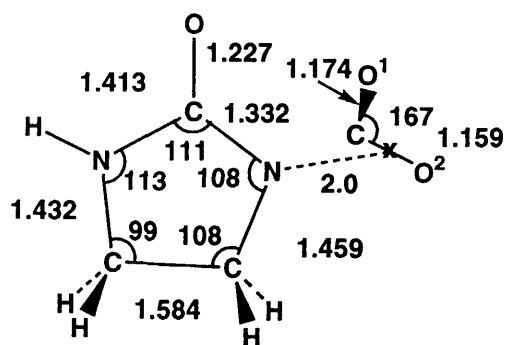
3c

Figure 3.3 Geometry of η^2-side-on carboxyimidazoidone[a]

a) Geometry optimization was performed under an assumption that the N-X line bisecting the CNC angle is perpendicularto the C=O bond, where X is the cneter of the C=O bond.

Table 3.2 Correlation and basis set effects on the CO_2 binding energy (be) of N-carboxyimidazolidone **1** and O-carboxy-imidazolidone **2** (kcal/mol)

	N-carboxy-imidazolidone 1	O-carboxy-imidazolidone 2	
	6-31G[a]		
	be	be	Δbe
HF	40.1(34.6)[c]	17.4(11.5)[c]	22.6(22.5)[c]
MP2	33.2(27.2)	22.5(16.5)	10.7(10.6)
MP3	39.9(33.8	27.9(21.9)	12.0(11.9)
MP4DQ	38.0(31.9)	25.7(19.7)	12.3(12.2)
MP4SDQ	37.4(31.3)	21.9(16.0)	11.6(11.5)
SDCI	40.0(33.9)	27.7(21.9)	18.1(18.0)
SDCI(D)[d]	39.9(33.8)	27.2(21.2)	12.0(11.9)
SDCI(DS)[e]	38.8(32.7)	27.2(21.8)	11.1(10.9)
SDCI(P)[f]	38.9(32.9)	27.2(21.2)	11.8(11.7)
CCD	38.1(32.0)	26.1(20.1)	12.0(11.9)

$$6\text{-}31\text{+}G^a$$

	be	be	Δbe
HF	34.7(29.3)	12.3(8.3)	22.4(21.0)
MP2	24.8(19.4)	15.0(11.0)	9.8(8.4)
MP3	32.6(27.2)	21.2(17.2)	11.4(10.0)
MP4DQ	30.5(25.1)	18.8(14.8)	11.7(10.3)
MP4SDQ	29.8(24.4)	18.7(14.7)	11.1(9.7)

a) A d-polarization function was added to N and O atoms of imidazolidone. b) Dbe = difference in binding energy between **1** and **2** c) In parenthesis; basis set super position error was corrected with the counter-poise method.[28] d) D = Davidson's correction for higher order excitations.[18] e) DS = Davidson-Silver's correction for higher order excitations.[19] f) P = Pople's correction for higher order excitations.[20]

energy of **1** is much larger than that of **2** in all the calculations. It should be, therefore, clearly concluded that N-carboxyimidazolidone is more stable than O-carboxyimidazolidone. This conclusion is in accord with the experimental result that N-carboxybiotin was isolated in the biotin-dependent enzymic reactions.[7c]

The binding energy of N-carboxybiotin was experimentally estimated to be ca. 20 kcal/mol.[29] This experimental value is much smaller than the binding energy calculated here. However, the experimental value of the binding energy would correspond to the energy difference between N-carboxyimidazolidone and the imidazolidone$^-$-H_2O adduct, because the binding energy was estimated in water. The

Table 3.3 Changes in total energy caused by η^2-side-on approach of CO_2 to deprotonated imidazolidone (kcal/mol)[a]

R(N-X)[b] (Å)	∞	2.4	2.4	2.4
HF	0.0	-4.3	3.9	20.6
MP2	0.0	-5.1	2.1	17.5
MP3	0.0	-5.7	1.6	17.0
MP4DQ	0.0	-5.3	2.2	17.7
MP4SDQ	0.0	-5.4	1.8	17.2

a) The 6-31G set was used, where a d-polarization function was added to N and O atoms of imidazolidone. Negative values mean stabilization. b) The N-X line which bisects the $C^2N^1C^5$ angle is perpendicular to the C=O bond of CO_2, where X is the center of the C=O bond (see Scheme 2).

energy difference between N-carboxyimidazolidone and the imidazolidone$^-$-H_2O adduct is calculated to be ca. 18 kcal/mol at the MP4SDQ/6-31G level. This value is almost the same as the experimental value. From these results, we can expect that the binding energy of carboxybiotin is correctly estimated at the present computational level.

The binding energy (BE) of **3** is given in Table 3.3. Although slight stabilization in energy is observed at R(N-X) = 2.4 Å, the binding energy is too small, compared with those of **1** and **2**. Furthermore, this structure becomes unstable rapidly, as the R(N-X) distance shortens to a usual interacting distance. Also, geometry optimization of **3**

without any constraint led to **1**. All these results clearly
indicate that the η^2-side-on carboxybiotin does not exist in
biotin-dependent enzymic reactions.

3-3-3 Electron Distribution of N-Carboxy-imidazolidone, O-Carboxyimidazolidone, and η^2-Side-on Carboxy-imidazolidone

Several interesting changes in Mulliken populations are
observed, as shown in Table 3.4: (1) The electron population
of the CO_2 part increases upon formation of carboxy-
imidazolidone **1**, **2**, and **3**, which indicates that the charge-
transfer from imidazolidone$^-$ to CO_2 strongly occurs. (2) The
electron population on CO_2 becomes greater in the order **3** <
2 < **1**, which corresponds to the increasing order of the CO_2
binding energy of CO_2. (3) The O^1 and O^2 atomic populations
expectedly increase but the C atomic population unexpectedly
decreases in spite of the strong charge-transfer from
imidazolidone$^-$ to CO_2. All these features of the electron
distribution are essentially the same as those reported in
η^1-C coordinated CO_2 complexes of transition-metal.[30]

This electron distribution is interpreted in terms of
the orbital mixing shown in Scheme 3.3. The HOMO of
imidazolidone$^-$ little interacts with the π^* orbital of CO_2
because it is a π-type orbital. The donor orbital (ϕ_{donor}) of
imidazolidone$^-$ is the next HOMO (Figure 3.4A), which is a
lone pair type orbital expanding on both N and O atoms. The
orbital mixing is mainly composed of the bonding overlap
between the ϕ_{donor} orbital and the CO_2 π^* orbital. The CO_2 π
orbital mixes into the ϕ_{donor}-π^* bonding overlap in an anti-
bonding way with ϕ_{donor} because the π orbital lies lower in

62

Table 3.4 Electron redistribution by the formation of carboxyimidazolidone[a]

	N-carboxy-imidazolidone **1**	O-carboxy-imidazolidone **2**	h^2-side-on-carboxy-imidazolidone[b] **3**
CO_2	+0.47(+0.35)[c]	+0.40(+0.34)[c]	+0.11
C	-0.17(-0.27)	-0.15(-0.12)	-0.03
O^1	+0.28(+0.28)	+0.31(+0.31)	+0.02
O^2	+0.35(+0.34)	+0.25(+0.24)	+0.12
N^1	+0.19(+0.25)	-0.07(-0.09)	-0.10
O^6	-0.15(-0.12)	-0.03(-0.13)	-0.03

a) The positive values mean increase of electron population. The 6-31G set was used, where a d-polarization function was added to N and O atoms of imdazolidone. b) R(N-X) = 2.4 Å (see Scheme 2 for R(N-X)). c) In parenthesis; The 6-31+G set was used, where a d-polarization function was added to N and O atoms of imidazolidone.

energy than ϕ_{donor}. As clearly shown in Scheme 3.3, this orbital mixing reduces the contribution of the C p_π orbital but enlarges the contribution of the O p_π orbitals. The 26a$_1$ orbital of **1** and **2** arises from this orbital mixing (Figure 3.4B and 3.4C), in which the C p_π orbital almost disappears but the O p_π orbitals are considerably large, according to the above-described orbital mixing. As a result, the C atomic population decreases but the O^1 and O^2 atomic
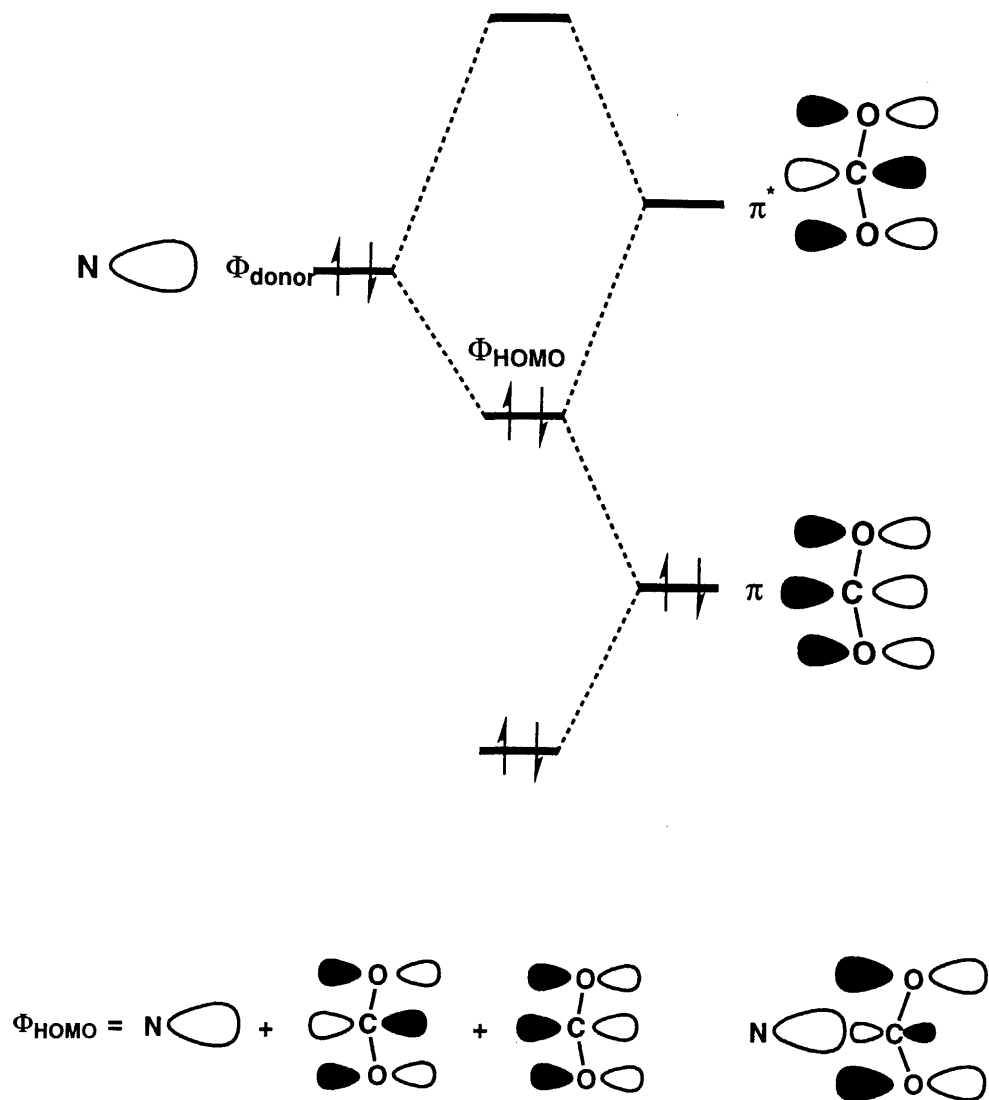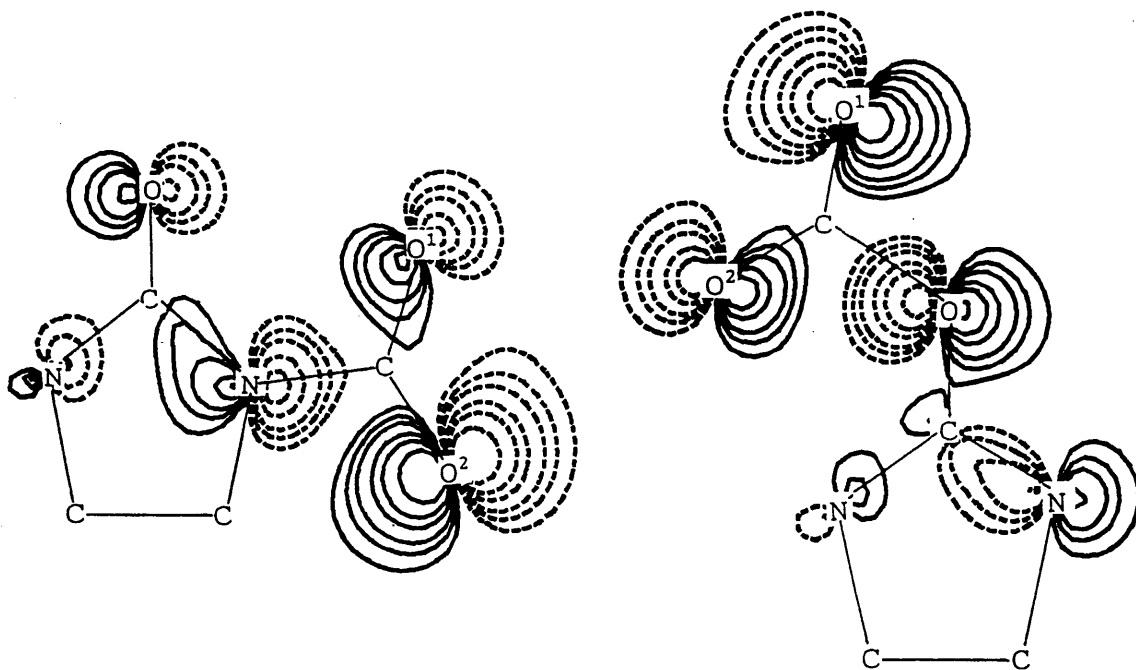
Scheme 3.3

populations increase upon formation of carboxyimidazolidone.

Finally, we will mention here the electron distribution of **3**. As described above, the CO_2 electron population of **3** increases least in three carboxy-imidazolidones, which is
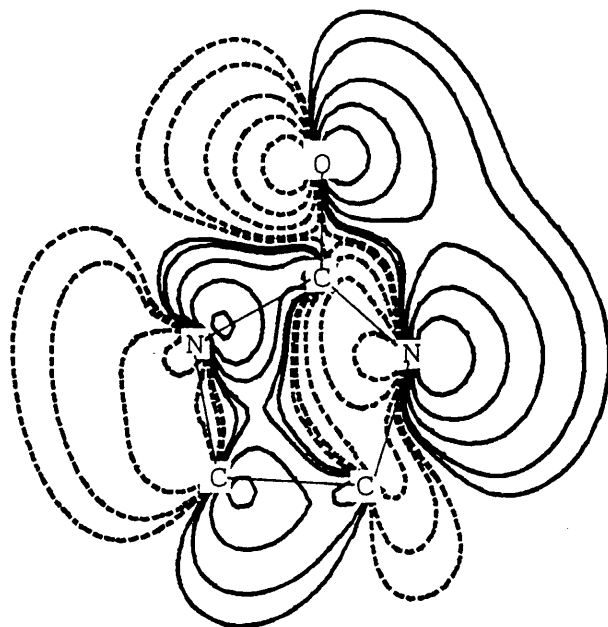
(A) next HOMO (Φ_{donor})

(B) $\Psi(26a_1)$ of N-Carboxyimidazolidone   **(C) $\Psi(26a_1)$ of N-Carboxyimidazolidone**

Figure 3.4 Contour maps of the next HOMO of deprotonated imidazolidone and next HOMO ($26a_1$) of N- and O-carboxy-imidazolidone

Contour values are ± 0.3, ± 0.2, ± 0.15, ± 0.1, ± 0.075, and ± 0.05.

consistent with the least distorted geometry of CO_2 in **3**.
These results are interpreted in terms of ϕ_{donor} of
imidazolidone$^-$; because ϕ_{donor} includes lone pair type
expansion at N and O atoms, the η^2-side-on approach of CO_2
cannot yield good overlap with ϕ_{donor}, as shown in Scheme 3.4.
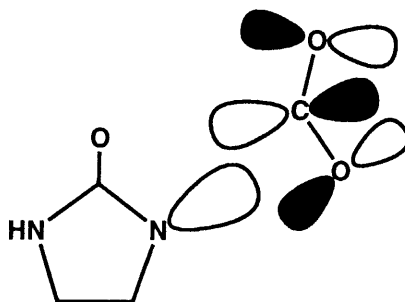
Scheme 3.4

Thus, the charge transfer from imidazolidone$^-$ to CO_2 does not
occur strongly in **3**. This seems to be the main reason that
the electron population of CO_2 increases only slightly and **3**
is much less stable than **1** and **2**.

3-3-4 Determining Factors for the Binding Energy of CO_2

Because **3** is apparently unfavorable as discussed above,
we will concentrate our discussion on the bonding nature of
1 and **2**. Their bonding nature was investigated with the
energy decomposition analysis (EDA).

First, we will inspect **1** because it is the most stable.
As shown in Table 3.5, the ES stabilization cannot overwhelm
the EX repulsion. This means that the static interaction,
which corresponds to the sum of ES and EX, does not
contribute to the stabilization of **1**, and the charge-

66

transfer interaction is necessary to stabilize **1**. Of CTPLXA and CTPLXB, the CTPLXA term yields much greater stabilization energy than the CTPLXB term. This is consistent with the electron distribution that the CO_2 electron population significantly increases upon formation of **1**, since this term involves the charge-transfer from imidazolidone$^-$ to CO_2 as a main contributor. Thus, the charge-transfer from imidazolidone$^-$ to CO_2 is primarily important in **1** not only from the point of view of electron distribution but also from the point of view of binding energy. Similar results are also observed in **2** (Table 3.5).

Now, let us compare **1** and **2**, in order to clarify the reason that **1** is more stable than **2**. **1** receives greater stabilization energies from ES, CTPLXA, and CTPLXB terms but suffers greater destabilization energy from the EX term than does **2** at their equilibrium geometries. Thus, we cannot find clearly factors to stabilize **1** more than **2** by comparing **1** and **2** at their equilibrium geometries. In our previous EDA studies of transition metal complexes,[23c,31] we compared two complexes, M^aL^a and M^bL^b, at the inter-fragment distance which yielded the same EX repulsion. When two complexes exhibit the same EX values, we can consider that M^a contacts with L^a to a similar extent that M^b does with L^b, because the EX repulsion arises from the overlap of electron clouds between M^a and L^a (or between M^b and L^b). When the R(O-CO_2) distance of **2** is shortened to 1.441 Å, the EX repulsion of **2** becomes almost the same as that of **1**. This geometry of **2** is named **2'** (see Table 3.5). Apparently, the outstanding difference is observed at the CTPLXA term; **1** can receive greater stabilization energy from this term than **2**. The ES

Table 3.5 Energy decomposition analysis of the interaction between CO_2 and deprotonated imidazolidone in N-carboxyimidazolidone **1** and O-carboxyimidazolidone **2** (kcal/mol)[a]

	1	**2**	**2**'[c]
R(X-CO_2)[b]	1.516	1.572	1.441
BE	-40.1	-17.4	-19.5
DEF			
total	58.6	60.5	60.5
CO_2	6.4	46.3	46.3
Imd	52.2	14.2 .	14.2
INT	-98.7	-77.9	-80.0
ES	-201.1	-139.5	-195.8
EX	321.2	209.2	322.5
CTPLXA(Imd→CO_2)	-160.9	-103.7	-139.5
CTPLXB(CO_2→Imd)	-52.7	-38.8	-62.3
R	-5.2	-5.1	-4.9

a) A negative value means stabilization in energy. The 6-31G basis set was used, where a d-polarization function was added to N and O atoms of imdazolidone. b) X = N or O. c) **2**'; The geometry was taken to be the same as **2** except that the O-CO_2 distance was shortened (1.441 Å) to give the same EX value as that of **1**.

stabilization energy is also larger in **1** than in **2**. Although **2** receives the greater stabilization energy from the CTPLXB term than **1** does, its difference is about one-half of the difference in the CTPLXA term. From these results, it is clearly concluded that the stronger CT interaction from imidazolidone$^-$ to CO_2 is a main factor to stabilize **1** more than **2**. This conclusion is easily understood by considering ϕ_{donor} of imidazolidone$^-$. As shown in Figure 3.4A, ϕ_{donor} expands more largely on the N atom than on the O atom. Thus, CO_2 can form the stronger CT interaction by approaching to the N atom than by approaching to the O atom.

3-3-5 Reactivity of CO_2 in Carboxyimidazolidone

The knowledge on the reactivity of CO_2 in carboxyimidazolidone is potentially useful in understanding the enzymic function of biotin. The reactivity would strongly depend on electron distribution and frontier orbitals. The O atom of CO_2 becomes much negatively charged in carboxyimidazolidone (vide supra). This means that the coulombic interaction between the O atom and a cationic species would be easily formed in carboxyimidazolidone. Frontier orbital energies are given in Table 3.6. The $26a_1$ orbital receives considerable contribution from the O p_π orbitals (Figure 3.4B and 3.4C). This $26a_1$ orbital lies at a higher energy than the non-bonding π orbital (HOMO) of the free CO_2 molecule like in $NiF(NH_3)_4(\eta^1\text{-}CO_2)$ which was calculated as a model of the $Ni^I(cyclam)(CO_2)$ complex.[30c] Furthermore, the $n\pi$ orbitals localized on the CO_2 part of carboxyimidazolidone lie much higher in energy than in the

Table 3.6 Frontier orbital energies of carboxy-imidazolidone[a]

Compound		Frontier Orbital	
N-carboxyimidazolidone	**1**	$26a_1$	-6.3 eV
		$n\pi_\perp$	-5.3 eV
		$n\pi_{''}$	-5.8 eV
O-carboxyimidazolidone	**2**	$26a_1$	-7.6 eV
		$n\pi_\perp$	-6.6 eV
		$n\pi_{''}$	-7.2 eV
$NiF(NH_3)_4(\eta^1\text{-}CO_2)$[30b]		HOMO	-8.2 eV
		$n\pi$	-11.0 eV
free CO_2		$n\pi$	-14.6 eV

a) The 6-31G set was used, where a d-polarization function was added to N and O atoms of imidazolidone. b) $n\pi_\perp$; non-bonding π orbital of the CO_2 part. The subscript "$\perp$" represents that $n\pi$ orbital is perpendicular to the molecular plane of carboxyimidazolidone. c) $n\pi_{''}$; non-bonding π orbital of CO_2 part. The subscript "$''$" represents that the $n\pi$ orbitals is on the molecular plane of the carboxyimidazolidone.

free CO_2 molecule, probably because of strong charge-transfer from imidazolidone$^-$ to the CO_2 π^* orbital. Thus, an electrophile can react with the CO_2 part of **1** and **2** more easily than with the free CO_2. In conclusion, CO_2 is much activated to an electrophile in both charge and frontier controlled reactions. This suggests the possibility that the CO_2 part in carboxybiotin would interact with some electrophile or cationic center and would be activated for the carboxyl-transfer reaction.

Also, we mention here that the above-described feature of CO_2 is quite the same as that observed in η^1-C coordinated CO_2 complexes of transition metal.[30] Considering that η^1-C coordinated CO_2 complexes of transition metal serve as a catalyst in many electrocatalytic reduction of CO_2,[32] we can expect that carboxyimidazolidone is useful as an organic catalyst for the similar electrochemical reduction of CO_2 like transition metal complexes.

3-3-6 Reliable Model of Carboxybiotin

It is necessary to adopt a simple but reliable model for investigating theoretically the function of biotin. $CH_3NH(CO_2)^-$ **4**, $CH_3N(CHO)(CO_2)^-$ **5**, $CH_3N=CH(OCO_2)^-$ **6**, $CH_3N(CONH_2)(CO_2)^-$ **7**, and $CH_3N=C(NH_2)(OCO_2)^-$ **8** are considered to be a candidate for a model of carboxybiotin. However, little has been known on the CO_2 binding energy, electron distribution, and energy levels of their frontier orbitals. We carried out MP4SDQ/6-31+G//MP2/3-21G calculations[33] on them and compared them with carboxyimidazolidone.

As shown in Figure 3.5, the geometry of **4** is considerably different from that of **1**; for instance, the N-
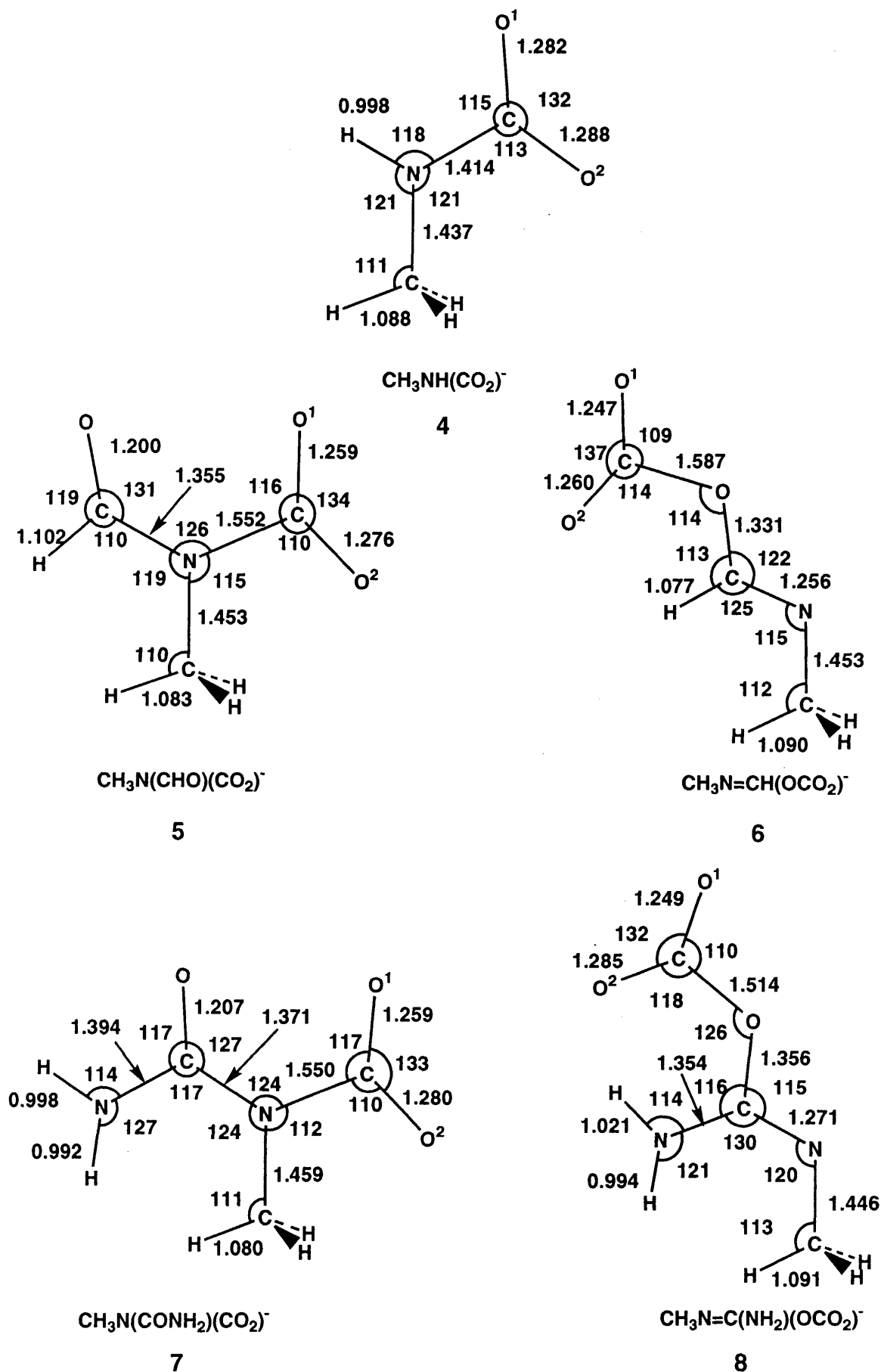
Figure 3.5 Optimized geometriesof $CH_3NH(CO_2)^-$ **4**, $CH_3N(CHO)(CO_2)^-$ **5**, $CH_3N=CH(OCO_2)^-$ **6**, $CH_3N(CONH_2)(CO_2)^-$ **7**, and $CH_3N=C(NH_2)(OCO_2)^-$ **8**

CO_2 distance of **4** is much shorter and the $C-O^1$ and $C-O^2$ distances are much longer than those in **1**. Consistent with these geometrical features, the binding energy (be) of **4** is much greater than that of **1** (Table 3.7). Also, the CO_2 electron population of CO_2 in **4** is considerably larger than that of **1** (Table 3.7). These results indicate that **4** is not appropriate as a model of carboxybiotin appropriate as a model of carboxybiotin.

5 is considered to be a better model than **4** because the carbonyl group exists at the neighboring position of the active N atom like biotin (see Figure 3.5). The $N-CO_2$ distance of **5** is somewhat longer than that of **1**, while the $C-O^1$ and $C-O^2$ distances of **5** are similar to those of **1**. Thus, the geometrical features are improved upon going to **5** from **4**. The CO_2 binding energy of **5** is, however, much smaller than that of **1**. **6** is also examined as a model of **2**. Although the $O-CO_2$ distance (1.59 Å) is almost the same as it in **2**, the CO_2 binding energy is much smaller than that of **2**. Although the difference in the binding energy (Δbe) is similar to that between **1** and **2**, the CO_2 electron population of **5** is unexpectedly smaller than that of **6** unlike **1** and **2**. From these results, **5** and **6** would be better models than **4**, but they are still unreasonable for quantitative investigation of biotin.

7 is considered to be a better model than **5**, because **7** has the urea structure like **1** (Figure 3.5). In fact, the CO_2 geometry in **7** is similar to that in **1**, whereas the $N-CO_2$ distance of **7** is calculated to be somewhat longer than that of **1**. The CO_2 binding energy is only 2~3 kcal/mol smaller than that of **1**. In **8** which is a model of **2**, the $O-CO_2$

73

Table 3.7 Binding ernergy (be) and the electron population of CO_2 in $CH_3NH(CO_2)^-$ **4**, $CH_3N(CHO)(CO_2)^-$ **5**, $CH_3N=CH(OCO_2)^-$ **6**, $CH_3NH(CONH_2)(CO_2)^-$ **7**, and $CH_3N=C(NH_2)(CO_2)^-$ **8** (kcal/mol).

	$CH_3NH(CO_2)^-$	$CH_3N(CHO)(CO_2)^-$	$CH_3N=CH(OCO_2)^-$
	4	**5**	**6**
be			
HF	78.4	30.2	19.2(11.0)[b]
MP2	61.8	21.4	5.9(15.5)
MP3	72.2	28.9	15.8(13.1)
Mp4DQ	69.7	26.8	13.0(13.8)
MP4SDQ	69.1	26.2	.11.2(15.0)
CO_2	+0.53	+0.38	+0.43

	$CH_3N(CONH_2)(CO_2)^-$	$CH_3N=C(NH_2)(OCO_2)^-$
	7	**8**
be		
HF	31.0	23.0(8.0)[c]
MP2	22.9	17.1(5.8)
MP3	30.3	25.6(4.7)
Mp4DQ	28.1	22.6(5.5)
MP4SDQ	27.5	21.4(6.1)
CO_2	+0.37	+0.38

a) The 6-31G+ set was used, where a d-polarization function was added to N and O atoms of CH_3NH^-, $CH_3N(CHO)^-$, $CH_3N(CONH_2)$, and deprotonated imidazolidone. b) In parentheses are differences in binding energy between $CH_3N(CHO)(CO_2)^-$ and $CH_3N=CH(OCO_2)^-$. c) In parentheses are differences in binding energy between $CH_3N(CONH_2)(CO_2)^-$ and $CH_3N=C(NH_2)(OCO_2)^-$.

distance is somewhat shorter and the CO_2 binding energy is slightly larger than those of **2**. These results show that **7** and **8** seem to be reasonable models of **1** and **2** respectively, and that the urea structure of biotin is important in the CO_2-binding function of biotin.

3.4 Conclusions

Imidazolidone can be adopted as a reasonable model of biotin because imidazolidone and methylbiotin have very similar geometry, electron distribution, and π and π^* orbital energies. However, more simple compounds such as CH_3NH_2 and $CH_3NH(CHO)$ are considered not to be a good model unlike imidazolidone. $CH_3NH(CONH_2)$ seems reasonable as a model of biotin, because the CO_2 binding energy to $CH_3NH(CONH_2)$ is almost the same as that of carboxy-imidazolidone. These results suggest that the urea structure is important in the CO_2 binding function of biotin.

In N-carboxyimidazolidone **1** and O-carboxyimidazolidone **2**, CO_2 lies on the molecular plane. The perpendicular structure is less stable than the planar one by ca. 6 kcal/mol for **1** and 10 kcal/mol for **2** at the MP4(SDQ)/6-31G level. The binding energy of CO_2 in **1** is much greater than that of **2** by ca. 12 kcal/mol, indicating that **1** is more stable than **2**. This is in accord with the experimental result that N-carboxybiotin was isolated in the biotin-dependent enzymic reactions.[7c] The CO_2 binding energy of η^2-side-on carboxyimidazolidone **3** is much smaller than those of **1** and **2**, and geometry optimization of **3** leaded to **1**. Thus, the η^2-side-on CO_2 adduct would not exist in the reaction of

biotin.

In carboxyimidazolidone, the charge-transfer from imidazolidone$^-$ to CO_2 strongly occurs. The electron population of CO_2 increases in the order **3** < **2** < **1**. The O^1 and O^2 atomic populations increase but the C atomic population decreases upon formation of carboxy-imidazolidones, **1** and **2**. This electron distribution can be interpreted in terms of the bonding interaction between ϕ_{donor} of imidazolidone$^-$ and the CO_2 π^* orbital into which the π orbital of CO_2 mixes in an anti-bonding way with ϕ_{donor}.

Energy decomposition analysis of the interaction between imidazolidone$^-$ and CO_2 also shows that the charge-transfer from imidazolidone$^-$ to CO_2 (the CTPLXA term) largely contributes to the CO_2 binding energy. The difference in stability between **1** and **2** mainly arises from this term. This is because the donor orbital (the next HOMO) of imidazolidone$^-$ expands more largely on the N atom than on the O atom. Consequently, **1** can receive greater stabilization energy from the CTPLXA term than **2**.

Geometries, electron distribution, and frontier orbitals of **1** and **2** resemble well those of η^1-C coordinated CO_2 complexes of transition metal, such as $[Co(alcn)_2(\eta^1\text{-}CO_2)]^-$ (alcn = $HNCHCHCHO^-$), $RhCl(AsH_3)_4(\eta^1\text{-}CO_2)]$, and $NiF(NH_3)_4(\eta^1\text{-}CO_2)$.[30] Considering that the several η^1-C coordinated CO_2 complexes of transition metal serve as a key intermediate in electrochemical reduction of CO_2,[32] we can expect that biotin, imidazolidone, and their analogues would be useful as an organic catalyst for CO_2 reduction.

The CO_2 part in **1** is considerably activated for an electrophile. Thus, there is a possibility that the

electrophile or cationic species interacts with the O atom of CO_2 to activate it for the carboxyl-transfer reaction.

References

(1)   (a) J. R. Knowles, <u>Annu. Rev. Biochem.</u>, **58**, 195 (1989). (b) G. R. Thatcher and R. Kluger, <u>Adv. Phys. Org. Chem.</u>, **25**, 99 (1989). (c) R. Kluger, <u>Chem. Rev.</u>, 1990, **90**, 1151.

(2)   F. Lynen, J. Knappe, E. Lorch, G. Jütting, and E. Ringelmann, <u>Angew. Chem.</u>, **71**, 481 (1959).

(3)   For instance; (a) R. Kluger and S. D. Taylor, <u>J. Am. Chem. Soc.</u>, **113**, 996 (1991). (b) S. D. Taylor and R. Kluger, <u>ibid.</u>, **115**, 867 (1993). References are therein.

(4)   J. Rétey and F. Lynen, <u>Biochem. Z.</u>, **342**, 256 (1965).

(5)   (a) J. Stubbe and R. H. Abeles, <u>J. Biol. Chem.</u>, **252**, 8338 (1977). (b) J. Stubbe, S. Fish, and R. H. Abeles, <u>J. Biol. Chem.</u>, **255**, 236 (1980).

(6)   (a) D. Kuo and I. A. Rose, <u>J. Am. Chem. Soc.</u>, **104**, 3235 (1982). (b) D. Kuo and I. A. Rose, <u>ibid.</u>, 1993, **115**, 387. References are therein.

(7)   (a) M. Caplow, <u>J. Am. Chem. Soc.</u>, **87**, 5774 (1965). (b) M. Caplow and M. Yager, <u>J. Am. Chem. Soc.</u>, **89**, 4513 (1967). (c) R. B. Guchhait, S. E. Polakis, P. Bimroth, E. Stoll, J. Moss, and M. D. Lane, <u>J. Biol. Chem.</u>, **249**, 6633 (1974).

(8)   G. R. J. Thatcher, R. Poirier, and R. Kluger, <u>J. Am. Chem. Soc.</u>, **108**, 2699 (1986).

(9)   C. L. Perrin and T. J. Dwyer, <u>J. Am. Chem. Soc.</u>, **109**, 5163 (1987).

(10)   J. Andrés, V. Moliner, J. Krechl, and E. Silla. <u>J. Chem. Soc., Perkin Trans.</u>, **2**, 521 (1993).

(11)   A. F. Hegarty and T. C. Bruice, <u>J. Am. Chem. Soc.</u>, **92**,

6561 (1970).

(12) (a) S. Sakaki, Transition Metal Complexes of N_2, CO_2, and Similar Small Molecules. Ab-initio MO studies of Their Stereochemistry and Coordinate Bonding Nature, in <u>Stereochemistry of Organometallic and Inorganic Compounds</u>, ed by I. Bernal, Elsevier (1990), vol. 4, pp. 95. (b) D. J. Darensbourg and R. A. Kudaroski, <u>Adv. Organometall. Chem.</u>, **22**, 129 (1983). (c) A. Behr, <u>Angew. Chem., Int. Ed. Engl.</u>, 1988, **27**, 661 (1988).

(13) (a) M. J. Frisch, J. S. Binkley, H. B. Schlegel, K. Raghavachari, C. F. Melius, L. R. Kahn, D. J. DeFrees, R. Seeger, R. A. Whiteside, D. J. Fox, E. M. Fleuder, S. Topiol, and J. A. Pople, <u>Gaussian 86</u>, GAUSSIAN Inc., Pittsburgh, PA, (1988). (b) M. J. Frisch, G. W. Trucks, M. H. Gordon, P. M. W. Gill, M. W. Wong, J. B. Foresman, B. G. Johnson, H. B. Schlegel, M. A. Robb, E. S. Replogle, R. Gomperts, J. L. Andres, K. Raghavachari, J. S. Binkley, C. Gonzalez, R. L. Martin, D. J. Fox, D. J. DeFrees, J. Baker, J. J. P. Stewart and J. A. Pople, <u>Gaussian 92</u>, GAUSSIAN Inc., Pittsburgh, PA, (1992).

(14) (a) J. S. Binkley, J. A. Pople, and W. J. Hehre, <u>J. Am. Chem. Soc.</u>, **102**, 939 (1980). (b) M. S. Gordon, J. S. Binkley, J. A. Pople, W. J. Pietro, and W. J. Hehre, <u>J. Am. Chem. Soc.</u>, **104**, 2797 (1982).

(15) W. J. Hehre, R. Ditchfield, and J. A. Pople, <u>J. Chem. Phys.</u>, **56**, 2257 (1972).

(16) T. Clark, J. Chandrasekhar, G. W. Spitznagel, and P. v. R. Schleyer, <u>J. Comp. Chem.</u>, **4**, 294 (1983).

(17) (a) W. J. Pietro, M. M. Francl, W. J. Hehre, D. J. DeFrees, J. A. Pople, and J. S. Binkley, J. Am. Chem. Soc., **104**, 5039 (1982). (b) P. C. Hariharan and J. A. Pople, Theor. Chim. Acta., **28**, 213 (1973).

(18) S. R. Langhoff and E. R. Davidson, Int J. Quant. Chem., **8**, 61 (1974).

(19) E. R. Davidson and D. W. Silver, Chem. Phys. Lett., **52**, 403 (1977).

(20) J. A. Pople, R. Seeger, and R. Krishnan, Int. J. Quant. Chem. Symp., **11**, 149 (1977).

(21) (a) J. A. Pople, R. Krishnan, H. B. Schlegel, and J. S. Binkley, Int. J. Quant. Chem., **14**, 545 (1978). (b) K. Ragavachari, J. Chem. Phys., **82**, 4607 (1985).

(22) G. T. DeTitta, J. W. Edmonds, W. Stallings, and J. Donohue, J. Am. Chem. Soc., **98**, 1920 (1976).

(23) (a) K. Morokuma, Acc. Chem. Res., **10**, 294 (1977). (b) K. Kitaura and K. Morokuma, Int. J. Quant. Chem., **10**, 325 (1976). (c) K. Kitaura, S. Sakaki, and K. Morokuma, Inorg. Chem., **10**, 2292 (1981).

(24) K. Morokuma, S. Kato, K. Kitaura, I. Ohmine, S. Sakai, and S. Obara, IMS Computer center library, No. 0372.

(25) (a) G. Fachinetti, C. Floriani, and P. F. Zanazzi, J. Am. Chem. Soc., **100**, 7405 (1978). (b) S. Gambarotta, F. Arena, C. Floriani, and P. F. Zanazzi, ibid., **104**, 5082 (1982).

(26) J. C. Calabrese, T. Herskovitz, and J. B. Kinney, J. Am. Chem. Soc., **105**, 5914 (1983).

(27) H. Tanaka, H. Nagao, S. M. Peng, and K. Tanaka, Organometallics, **11**, 1450 (1992).

(28) (a) S. F. Boys and F. Bernardi, Mol. Phys., **19**, 553

(1970). b) N. S. Ostlund and D. L. Merrifield, <u>Chem. Phys. Lett.</u>, **39**, 612 (1976).

(29) N. M. Green, <u>Biochem. J.</u>, **89**, 599 (1963).

(30) (a) S. Sakaki, T. Aizawa, N. Koga, K. Morokuma, and K. Ohkubo, <u>Inorg. Chem.</u>, **28**, 103 (1989). (b) S. Sakaki, <u>J. Am. Chem. Soc.</u>, **112**, 7813 (1990). (c) S. Sakaki, <u>J. Am. Chem. Soc.</u>, **114**, 2055 (1992).

(31) (a) S. Sakaki, K. Kitaura, K. Morokuma, and K. Ohkubo, <u>Inorg. Chem.</u>, **22**, 104 (1983). (b) S. Sakaki, K. Morokuma, and K. Ohkubo, <u>J. Am. Chem. Soc.</u>, **107**, 2686 (1985).

(32) For instance, (a) M. Beley, J. -P. Collin, R. Ruppert, and J, -P, Sauvage, <u>J. Am. Chem. Soc.</u>, **108**, 7461 (1986). (b) H. Ishida, T. Terada, K. Tanaka, and T. Tanaka, <u>Inorg. Chem.</u>, **29**, 905 (1990).

(33) This means that geometry is optimized at the MP2-level using the 3-21G basis set, and then, MP4SDQ calculation is carried out on the optimized geometry using the 6-31+G basis set. d-Polatization function was added to N and O of model compounds.

Part II

Catalyses of Transition-metal

Complexes Related to Activation of

Small Molecules

## CO$_2$ and C$_2$H$_4$ Insertion into a Cu(I)-R Bond (R = H, CH$_3$, or OH).

4.1 Introduction

CO$_2$ insertion into the M-R (R = H, CH$_3$, or OR) bond has received considerable interest in the chemistry of CO$_2$ fixation[1] because similar insertion reactions of alkene, alkyne and CO are involved as key processes in many homogeneous catalytic cycles.[2] Actually, many examples of the catalytic CO$_2$ conversion into organic chemicals involve the CO$_2$ insertion as an important elementary step.[3-12] General knowledge on the CO$_2$ insertion is, therefore, necessary to understanding well the CO$_2$ fixation and finding a new efficient catalyst for the CO$_2$ fixation. In this context, experimental investigation of the CO$_2$ insertion has been actively carried out, in which various valid information has been reported.[13-32] Not only experimental work but also theoretical one is expected to offer such general knowledge. However, only few MO studies have been carried out on the CO$_2$ insertion.[33,34] In those studies, the geometry of transition state (TS) has not been optimized, and calculations at the correlated level have not been performed except for preliminary MP2 calculations of the CO$_2$ insertion into the Cu(I)-H and Cu(I)-CH$_3$ bonds.[33]

In this chapter, the CO$_2$ insertion into the Cu(I)-R bond (R = H, CH$_3$, or OH) is theoretically investigated with the ab initio MO/MP4, SD-CI, and CCD (coupled cluster (doubles)) methods.

$$CuR(PH_3)_2 \quad + \quad CO_2 \quad \rightarrow \quad Cu(\eta^1\text{-}OCOR)(PH_3)_2$$

$$\rightarrow \quad Cu(\eta^2\text{-}O_2CR)(PH_3)_2 \quad\quad\quad (4.1)$$
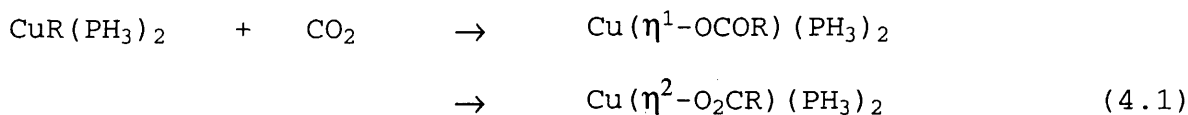
This reaction is selected here, considering that there are many experimental reports on the insertion reactions of CO_2 into Cu(I)-alkyl,[13c-e,16b,e,18,26,27q] Cu(I)-hydride,[28] and Cu-alkoxide bonds.[13g,16a,d,f] Aims of this chapter are (1) to optimize the geometry of the TS, (2) to estimate the activation energy and the energy of reaction, (3) to reveal characteristic features of the CO_2 insertion by comparing it with the C_2H_4 insertion (eq 4.2), and (4) to clarify the

$$CuR(PH_3)_2 \quad + \quad C_2H_4 \quad \rightarrow \quad Cu(CH_2CH_2R)(PH_3)_2 \quad\quad (4.2)$$
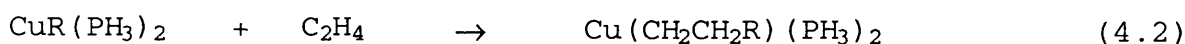
factors determining the ease of the CO_2 insertion. Points of departure from previous works[33,34] are on presenting (i) the detailed knowledge of the TS structure and (ii) discussion based on the calculations at the correlated level.

4.2 Computational Details

Ab initio closed-shell Hartree-Fock (HF), MP2 – MP4(SDQ), SD-CI, and coupled cluster (doubles; CCD) calculations were carried out with Gaussian 86[35a] and 92[35b] programs, where four kinds of basis sets were employed. In the small basis set (BS I), core electrons of Cu (up to 3p) were replaced with effective core potentials (ECP1) proposed by Hay et al.[36] and its 3d, 4s, and 4p valence orbitals were represented with a (3s 2p 5d)/ [2s 2p 2d] set. Usual MIDI-3[37] and (4s)/[2s][38] sets were used for C, O, and H respectively. STO-2G[39] sets were employed for PH_3. In the

84

second (BS II), core electrons of Cu (up to 2p) were replaced with effective core potentials (ECP2), and its valence orbitals (3s, 3p, 3d, 4s, and 4p) were represented with a (5s 5p 5d)/[3s 3p 3d] set.[40] Usual MIDI-4 sets[37] were used for C, O, and P, and the (4s)/[2s] set was employed for H.[38] In the third (BS III), an all electron type basis set was used for Cu; Huzinaga's (13s 7p 4d) primitive set[37] was augmented with one diffuse d primitive function (ζ = 0.141)[41] and two p primitive functions describing the valence 4p orbital, and the resultant (13s 9p 5d) primitive set was contracted to a [5s 4p 3d] set. For the other atoms, the same basis sets as those in the BS II were used. In the fourth (BS IV), (9s 5p)/[3s 2p][38] sets were used for C and O. For Cu, a (14s 9p 5d) primitive set of Wachters[42] was augmented with one diffuse d primitive function (ζ = 0.1491) presented by Hay[43] and two p primitive functions (ζ = 0.155065 and 0.046199) describing the valence 4p orbitals.[44] The resultant (14s 11p 6d) primitive set was contracted to a [5s 4p 3d] set. For PH_3, the same basis sets as those in the BS II and BS III were used. The BS I set was used only for geometry optimization, the BS II – IV for examination of basis set effects, and the BS III for investigation of energy changes, electron redistribution, and change in bonding nature by the insertion reactions. Calculations at the correlated level were performed with all the core orbitals excluded from an active space.

Both insertion reactions of CO_2 and C_2H_4 are considered to proceed via the precursor complexes (PC) and TS, as shown in Chart 4.1. Geometries of CO_2, C_2H_4, $CuR(PH_3)_2$ **1** (see Chart 4.1 for **1** – **10**), PC (**2**, **7**), TS (**3**, **8**), and products
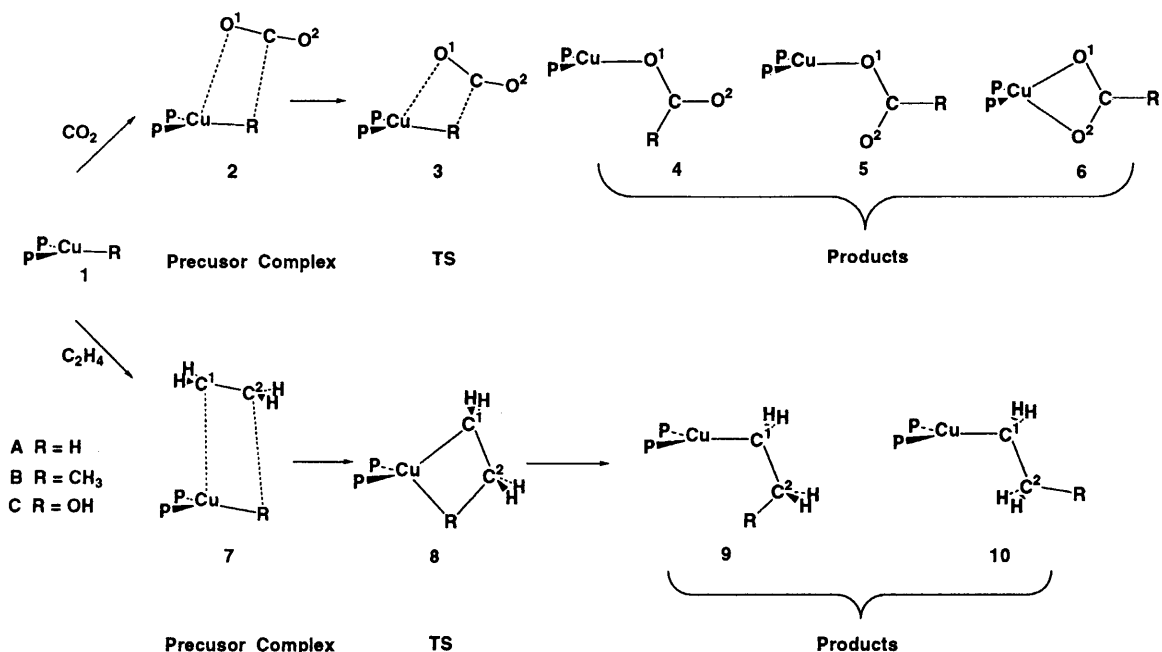
Chart 4.1

(**4 - 6, 9, 10**) were optimized with the energy gradient method at the HF level, in which the geometry of PH_3 was fixed to the experimental structure of the free PH_3 molecule.[45] There are several possible isomers in the products; See **4 - 6** in the CO_2 insertion and **9** and **10** in the C_2H_4 insertion. **4A** and **4B** could not be optimized since they converted to **5A** and **5B**, respectively, with no barrier,[33] where A and B represent R = H and R = CH_3, respectively. Their MO calculations were carried out under assumption that the geometry of the OC(O)R group and the Cu-O distance are the same as those in **5A** and **5B**. Because **5B** converted to **6B** with no barrier, the geometry of **5B** was optimized with the Cu-O^1 bond fixed on the $Cu(PH_3)_2$ plane. Geometries of **9A** and **9B** were optimized under constraint of the C_s symmetry. In the CO_2 insertion into the Cu-OH bond, PC and TS could not

be optimized because this reaction proceeded with no barrier at both HF and correlated levels (vide infra). Geometry changes by this insertion were optimized, taking the distance between O of OH and C of CO_2 as a reaction coordinate.

4.3 Results and Discussion
4-3-1 Effects of Basis Set and Electron Correlation on the CO_2 and C_2H_4 Insertions

Prior to detailed discussion, we will briefly examine basis set effects on the CO_2 insertion into the Cu-H bond. As shown in Table 4.1, the activation energy (E_a) and the energy difference between the PC and the product (ΔE) significantly decrease upon going to the BS V from the BS VI,[33b] whereas only the basis set for Cu is different between BS V and BS VI; in the BS VI, a (3s 2p 5d)/[2s 2p 2d] set is employed with the ECP1,[36] but in the BS VI, an all electron type basis set[42] is used (see footnotes a and b of Table 4.1 for BS V and BS VI). Similarly, E_a and ΔE considerably decrease upon going to BS II from BS I, where ECP's for Cu is changed on going to BS II from BS I. On the other hand, BS II, BS III, and BS IV yield similar values for E_a and ΔE, where basis sets for ligand atoms are improved upon going to BS IV from BS II. From these results, we can conclude that (1) E_a and ΔE little depend on the basis sets of ligand atoms but significantly depend on the ECPs for Cu, (2) Huzinaga's basis set and Wachters' one for Cu give similar results on E_a and ΔE, (3) the basis set involving the ECP1 yields considerably different results from others, and (4) the BS II involving ECP2 yields almost the same results as

Table 4.1 Effects of Basis Set and Electron Correlation for CO_2 Insertion into Cu-H Bond (kcal/mol)

	CO$_2$ Insertion						C$_2$H$_4$ Insertion
	BS-I	BS-II	BS-III	BS-IV	BS-V[a]	BS-VI[b]	BS-III
E_a[c]							
HF	7.0	3.7	4.2	1.6	12.5	5.4	24.9
MP2		7.9	8.3	9.0	12.9		2.7
MP3		1.3	2.2	2.1			11.6
MP4(DQ)			6.5				
MP4(SDQ)			7.9				
SD-CI		3.2	4.5	4.2			6.8
SD-CI+D[d]		2.8	5.3	5.0			2.0
SD-CI+DS[e]		2.3	4.2	4.1			12.6
SD-CI+P[f]		2.4	4.3	4.1			9.9
ΔE[g]							
HF	-38.9	-50.4	-48.5	-53.8	-37.5	-56.8	-13.5
MP2		-34.5	-30.1	-34.3	-29.1		-19.4
MP3		-49.0	-43.9	-48.3			-15.7
MP4(DQ)			-36.0				
MP4(SDQ)			-33.1				
SD-CI		-46.6	-43.1	-45.5			-16.9
SD-CI+D[d]		-45.2	-41.0	-43.3			-16.8
SD-CI+DS[e]		-42.9	-40.0	-41.0			-16.3
SD-CI+P[f]		-44.3	-39.7	-41.9			-16.4

a) BS V (BS II of ref. 33b); The basis set fo Cu was the same as it in BS I, while the basis sets for the other parts were the same as those in BS VI. b) BS VI (BS III of ref. 33b); The basis sets for Cu, C, and O were the same as those in BS III, while MIDI-3 was used for PH$_3$. c) E_a = the energy difference between the transition state and the precurosor complex (PC). d) D = the Davidson's correction for higher order excitations.[47] e) DS = the Davidson and Silver's corrections for higher order excitations.[48] f) P = the Pople's for higher order excitations.[49] g) ΔE = the energy difference between product and PC.

the better basis sets such as the BS III and BS IV. Thus, use of either BS II or better basis sets is necessary in estimating the energy change. Very recently, use of ECP2 has also been recommended.[46]

Then, we will inspect the correlation effects on E_a and ΔE. Unexpectedly, E_a of the CO_2 insertion little changes upon introducing electron correlation, except that the E_a value slightly fluctuates at the MP2 level. On the other hand, introduction of electron correlation considerably changes the E_a of the C_2H_4 insertion and the ΔE of both CO_2 and C_2H_4 insertion reactions. An important result to be noted is that both E_a of the C_2H_4 insertion and ΔE of CO_2 and C_2H_4 insertion reactions considerably fluctuate at MP2 – MP4(SDQ) levels, demonstrating that the MP2 – MP4(SDQ) methods are not reliable in investigating these insertion reactions. On the other hand, SD-CI and CCD methods give similar results on E_a and ΔE, suggesting that these methods are reliable. Discussion presented here is based on the SD-CI and CCD calculations with the BS-III.

4-3-2 Relative Stabilities of the Products and the Energy of Reaction

The energies of reaction are given in Tables 4.2 and 4.3 as an energy difference between the products and the sum of reactants, **1A** + CO_2, **1A** + C_2H_4, **1B** + CO_2, and **1B** + C_2H_4, where a negative value represents a stabilization energy (vice versa).

In the product of the CO_2 insertion, **6A** and **6B** are calculated to be the most stable in **4A** - **6A** and **4B** - **6B**, respectively, suggesting that $Cu(\eta^2\text{-}O_2CR)(PH_3)_2$ is a final

Table 4.2 Energy Change by the CO_2 Insertion into Cu-R (R = H, CH_3) bond (kcal/mol).

compd		HF	MP2	MP3	MP4 DQ	MP4 SDQ
$CuH(PH_3)_2 + CO_2 \rightarrow Cu(\eta^2-O_2CH)(PH_3)_2$						
$CuH(PH_3)_2$(**1A**)+CO_2		0.0^a	0.0^b	0.0^c	0.0^d	0.0^e
$CuH(PH_3)_2(CO_2)$	**2A**	-3.6	-4.4	-5.1	-4.4	-4.5
Transtion State	**3A**	0.6	3.9	-2.9	2.1	3.4
$Cu(\eta^1-OCOH)(PH_3)_2$	**4A**	-36.2	-19.6	-32.7	-25.5	-22.3
	5A	-50.9	-32.2	-46.0	-38.4	-35.2
$Cu(\eta^2-O_2CH)(PH_3)_2$	**6A**	-52.1	-34.5	-49.0	-40.4	-37.0
$Cu(CH_3)(PH_3)_2 + CO_2 \rightarrow Cu(\eta^2-O_2CCH_3)(PH_3)_2$						
$Cu(CH_3)(PH_3)_2$(**1B**)+CO_2		0.0^k	0.0^l	0.0^l	0.0^m	0.0^n
$Cu(CH_3)(PH_3)_2(CO_2)$	**2B**	-2.1	-5.4	-4.9	-5.0	-5.2
Transtion State	**3B**	7.3	9.8	0.6	7.9	10.5
$Cu(\eta^1-OCOCH_3)(PH_3)_2$	**4B**	-26.3	-10.5	-25.3	-17.4	-13.2
	5B	-58.4	-35.7	-52.1	-43.7	-39.0
$Cu(\eta^2-O_2CCH_3)(PH_3)_2$	**6B**	-59.5	-37.5	-54.2	-45.3	-40.7

		SD-CI				CCD
		no[aa]	D[ab]	DS[ac]	P[ae]	
$CuH(PH_3)_2$ (**1A**) $+CO_2$		0.0^k	0.0^l	0.0^m	0.0^n	0.0^o
$CuH(PH_3)_2(CO_2)$	**2A**	-4.5	-4.9	-5.0	-5.0	-4.7
Transtion State	**3A**	0.0	-0.4	-0.8	-0.7	-0.4
$Cu(\eta^1\text{-OCOH})(PH_3)_2$	**4A**	-31.5	-30.0	-28.4	-28.7	
	5A	-45.4	-43.6	-42.1	-42.0	
$Cu(\eta^2\text{-O}_2CH)(PH_3)_2$	**6A**	-47.6	-45.9	-44.5	-44.7	-44.7
$Cu(CH_3)(PH_3)_2$ (**1B**) $+CO_2$		0.0^p	0.0^q	0.0^r	0.0^s	
$Cu(CH_3)(PH_3)_2(CO_2)$	**2B**	-4.3	-4.8	-5.2	-5.1	
Transtion State	**3B**	5.6	4.9	4.1	4.2	
$Cu(\eta^1\text{-OCOCH}_3)(PH_3)_2$	**4B**	-23.5	-22.1	-20.6	-20.9	
	5B	-52.0	-49.5	-47.1	-47.5	
$Cu(\eta^2\text{-O}_2CCH_3)(PH_3)_2$	**6B**	-53.7	-51.4	-49.1	-49.5	

a) $E_t(HF)$	=	-2509.2289	k) $E_t(HF)$	=	-2548.2017
b) $E_t(MP2)$	=	-2510.0320	l) $E_t(MP2)$	=	-2549.1011
c) $E_t(MP3)$	=	-2509.9304	m) $E_t(MP3)$	=	-2549.0048
d) $E_t(MP4(DQ))$	=	-2510.0158	n) $E_t(MP4(DQ))$	=	-2549.0930
e) $E_t(MP_4(SDQ)$	=	-2510.0628	o) $E_t(MP_4(SDQ)$	=	-2549.1425
f) $E_t(SDCI)$	=	-2509.8562	p) $E_t(SDCI)$	=	-2548.8976
g) $E_t(SDCI+(D))$	=	-2509.9585	q) $E_t(SDCI+(D))$	=	-2549.0193
h) $E_t(SDCI+(DS))$	=	-2510.0080	r) $E_t(SDCI+(DS))$	=	-2549.0848
i) $E_t(SDCI+(P))$	=	-2509.9977	s) $E_t(SDCI+(P))$	=	-2549.0731
j) $E_t(CCD)$	=	-2509.9929	(hartree)		

aa) No correction was made for higher order excitations. ab) D = Davidson's correction for higher order excitations.[47] ac) DS = Davidson and Silver's correction for higher order excitations.[48] ad) P = Pople's correction for higher order excitations.[48]

Table 4.3 Energy Change by the C_2H_4 Insertion into Cu-R (R = H, CH_3) bond (kcal/mol).

compd		HF	MP2	MP3	MP4 DQ	SDQ
$CuH(PH_3)_2 + C_2H_4 \rightarrow Cu(C_2H_5)(PH_3)_2$						
$CuH(PH_3)_2$ (**1A**) $+C_2H_4$		0.0^a	0.0^b	0.0^c	0.0^d	0.0^e
$CuH(PH_3)_2(C_2H_4)$	**7A**	1.6	-1.3	-1.4	-0.9	-1.2
Transtion State	**8A**	24.9	1.4	10.2	5.9	0.8
	9A	-8.8	-17.6	-14.1	-14.8	-16.4
$Cu(C_2H_5)(PH_3)_2$	**10A**	-11.9	-20.7	-17.1	-16.1	-19.5
$Cu(CH_3)(PH_3)_2 + C_2H_4 \rightarrow Cu(C_3H_7)(PH_3)_2$						
$Cu(CH_3)(PH_3)_2$ (**1B**) $+C_2H_4$		0.0^k	0.0^l	0.0^m	0.0^n	0.0^o
$Cu(CH_3)(PH_3)_2(C_2H_4)$	**7B**	1.3	-3.0	-2.1	-2.4	-2.8
Transtion State	**8B**	39.1	20.4	24.2	24.7	22.5
	9B	-6.0	-12.7	-11.5	-11.3	-11.5
$Cu(C_3H_7)(PH_3)_2$	**10B**	-13.9	-20.3	-18.5	-18.6	-18.9

		SD-CI.				CCD
		no[aa]	D[ab]	DS[ac]	P[ad]	
$CuH(PH_3)_2$ (**1A**)$+C_2H_4$		0.0^f	0.0^g	0.0^h	0.0^i	0.0^j
$CuH(PH_3)_2(C_2H_4)$	**7A**	-0.4	-0.9	-1.3	-1.2	-0.8
Transtion State	**8A**	12.2	9.0	6.7	7.2	9.7
	9A	-14.2	-14.6	-14.5	-14.4	
$Cu(C_2H_5)(PH_3)_2$	**10A**	-17.3	-17.7	-17.6	-17.6	-16.4
$Cu(CH_3)(PH_3)_2$ (**1B**)$+C_2H_4$		0.0^p	0.0^q	0.0^r	0.0^s	
$Cu(CH_3)(PH_3)_2(C_2H_4)$	**7B**	-1.3	-0.4	1.0	-2.2	
Transtion State	**8B**	28.6	25.7	23.4	23.8	
	9B	-11.0	-11.4	-11.2	-11.2	
$Cu(C_3H_7)(PH_3)_2$	**10B**	-18.4	-18.6	-18.3	-18.3	

a) E_t (HF) = -2399.8294
b) E_t (MP2) = -2400.4584
c) E_t (MP3) = -2400.4085
d) E_t (MP4(DQ)) = -2400.4869
e) E_t (MP$_4$(SDQ) = -2400.5232
f) E_t (SDCI) = -2400.3548
g) E_t (SDCI+(D)) = -2400.4393
h) E_t (SDCI+(DS)) = -2400.4794
i) E_t (SDCI+(P)) = -2400.4701
j) E_t (CCD) = -2400.4669

k) E_t (HF) = -2438.3989
l) E_t (MP2) = -2439.5275
m) E_t (MP3) = -2439.4829
n) E_t (MP4(DQ)) = -2439.5641
o) E_t (MP$_4$(SDQ) = -2439.6029
p) E_t (SDCI) = -2439.5458
q) E_t (SDCI+(D)) = -2439.5020
r) E_t (SDCI+(DS)) = -2439.5565
s) E_t (SDCI+(P)) = -2439.5275
(hartree)

aa) No correction was made for higher order excitations. ab) D = Davidson's correction for higher order excitations.[47] ac) DS = Davidson and Silver's correction for higher order excitations.[48] ad) P = Pople's correction for higher order excitations.[48]

product of the CO_2 insertion.[33] Relative stabilities of
these products have been discussed in the previous work[33b]
and the discussion is omitted here. Both CO_2 insertion
reactions into the Cu-H and Cu-CH$_3$ bonds are significantly
exothermic, and the exothermicity of the former is slightly
greater than that of the latter.

In the product of the C_2H_4 insertion, **10A** and **10B** are
calculated to be more stable than **9A** and **9B** respectively,
indicating that **10A** and **10B** are final products. The
exothermicity of the C_2H_4 insertion reaction hardly depends
on the kind of R.

One of the differences between CO_2 insertion and C_2H_4
insertion is that the former is much more exothermic than
the latter. This difference is rationalized in terms of
bond energies.[50] In the CO_2 insertion into the Cu-CH$_3$ bond,
the CH_3-C(O)O- bond is newly formed, and the Cu-CH$_3$ and C=O
bonds change to the Cu-OC(O)CH$_3$ and C-O bonds respectively.
Thus, the exothermicity (E_{exo}) is approximately represented
by eq 4.3;

$$E_{exo} = E(Cu-OC(O)CH_3) + E(C-O) + E(CH_3-C(O)O-) - E(Cu-CH_3)$$
$$- E(C=O)$$

$$= \{E(Cu-OC(O)CH_3) - E(Cu-CH_3)\} + \{E(C-O) - E(C=O)\}$$
$$+ E(CH_3-C(O)O-) \quad (4.3)$$

In the C_2H_4 insertion into the Cu-CH$_3$ bond, the Cu-CH$_3$ and
C=C bonds change to the Cu-C$_3$H$_7$ and -CH$_2$-CH$_2$- bonds
respectively, and the -CH$_2$-CH$_3$ bond is newly formed. In this
case, E_{exo} is approximately represented, as follows;

$$E_{exo} = E(Cu-C_3H_7) - E(Cu-CH_3) + E(-CH_2-CH_3)$$

$$+ E(-CH_2-CH_2-) - E(C=C)$$

$$\sim \{E(-CH_2-CH_2-) - E(\underset{/}{\overset{\backslash}{C}}=\underset{\backslash}{\overset{/}{C}})\} + E(-CH_2-CH_3) \quad (4.4)$$

where $E(Cu-CH_3)$ is considered to be almost the same as $E(Cu-C_3H_7)$.

A difference between C=O and C-O bond energies which is involved in eq 4.3 can be estimated from the energy difference (ΔE_{r-1}) between right- and left-hand sides of eq 4.5, as follows;

$$CO_2 + H_2 \rightarrow H-C(O)OH \quad (4.5)$$

$$\Delta E_{r-1} = E(H-H) + E(=C=O) - E(=\overset{|}{C}-O) - E(=\overset{|}{C}-H) - E(H-H) \quad (4.6a)$$

$$E(=C=O) - E(=\overset{|}{C}-O) = \Delta E_{r-1} - E(H-H) + E(=\overset{|}{C}-H) + E(H-H) \quad (4.6b)$$

Similarly, a difference between the C=C and $-CH_2-CH_2-$ bond energies is estimated from ΔE_{r-1} of eq 4.7;

$$C_2H_4 + H_2 \rightarrow H_3C-CH_3 \quad (4.7)$$

$$\Delta E_{r-1} = E(H-H) + E(\underset{/}{\overset{\backslash}{C}}=\underset{\backslash}{\overset{/}{C}}) - E(\underset{/}{\overset{\backslash}{C}}-\underset{\backslash}{\overset{/}{C}}-) - 2\cdot E(\underset{/}{\overset{\backslash}{C}}-H) \quad (4.8a)$$

$$E(\underset{/}{\overset{\backslash}{C}}=\underset{\backslash}{\overset{/}{C}}) - E(\underset{/}{\overset{\backslash}{C}}-\underset{\backslash}{\overset{/}{C}}-) = \Delta E_{r-1} - E(H-H) + 2 E(\underset{/}{\overset{\backslash}{C}}-H) \quad (4.8b)$$

In these estimations, the H-H and -C-H bond energies are calculated with MP2 - MP4(SDQ) and SD-CI/BS III methods (Table 4.4), where geometries of $\bullet C_2H_5$, $\bullet C(O)OH$, and $H-C(O)O\bullet$ radicals are optimized with the ROHF/BS I method. A difference between $Cu-CH_3$ and $Cu-OC(O)R$ bond energies can be evaluated, considering the energy difference between right- and left-hand sides of eq 4.9;

$$Cu(CH_3)(PH_3)_2 + H-OC(O)R \rightarrow Cu(OC(O)R)(PH_3)_2 + H-CH_3 \quad (4.9)$$
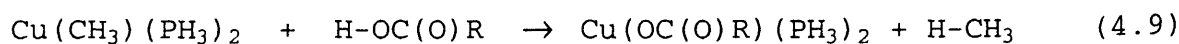
$$\Delta E_{r-1} = E(H-CH_3) + E(Cu-OC(O)R) - E(Cu-CH_3) - E(-O-H) \quad (4.10a)$$

Table 4.4 Bond Energies and Their Differences (kcal/mol unit)

	E(H-H)	E(H-COOH)	E(HCOO-H)	E(H-CH$_3$)	E(H$_3$C-CH$_3$)
MP2	93.2	96.3	106.3	99.4	95.0
MP3	96.5	99.2	102.5	100.1	95.6
MP4DQ	97.5	99.0	103.9	100.4	98.7
MP4SDQ	97.5	98.0	103.7	100.5	98.7
SD-CI+D[a]	97.9	95.0	101.6	100.2	95.6
SD-CI+DS[b]	97.9	93.8	102.1	100.4	96.5
SD-CI+P[c]	97.9	97.8	109.0	100.2	96.7

a) D = Davidson's correction for higher order excitations.[47] b) DS = Davidson-Silver's corrections for higher order excitations.[48] c) P = Pople's correction for higher order excitations.[49]

Table 4.4 (Continued)

	E(H-C$_2$H$_5$)	E(C=O)-E(C-O)	E(C=C)-E(C-C)	E(H$_3$C-COOH)
MP2	101.7	124.7	74.0	93.5
MP3	102.2	113.4	71.0	94.1
MP4DQ	102.4	111.0	71.8	93.0
MP4SDQ	102.3	106.5	72.0	92.0
SD-CI+D	101.9	101.2	72.0	84.0
SD-CI+DS	104.4	102.6	74.6	86.7
SD-CI+P	102.1	102.1	72.8	90.7

(Continued to be the next page)

Table 4.4 (Continued)

	E(HO-COOH)	E(HOCOO-H)	E(HO-H)	E(Cu-OC(O)CH$_3$) - E(Cu-H)
MP2	92.1	102.7	102.5	56.1
MP3	87.0	99.4	99.6	56.5
MP4DQ	86.9	100.9	100.7	51.5
MP4SDQ	87.1	100.7	100.8	49.4
SD-CI+D	62.3	98.1	83.5	61.2
SD-CI+DS	64.3	99.5	98.7	55.6
SD-CI+P	85.7	99.1	100.1	55.7

Table 4.4 (Continued)

	E(CuOC(O)H)-E(Cu-H)	E(CU-OCOOH)-E(Cu-OH)
MP2	47.5	32.3
MP3	43.7	39.7
MP4DQ	38.1	34.0
MP4SDQ	37.5	29.5
SD-CI+D	18.8	30.0
SD-CI+DS	34.4	29.5
SD-CI+P	34.9	28.8

$E(Cu-OC(O)R) - E(Cu-CH_3) = \Delta E_{r-1} - E(H-CH_3) - E(-O-H)$ (4.10b)

where $-O-H$ and $H-C(O)OR$ bond energies can be estimated as described above. Using these bond energies and their differences (Table 4.4), a difference in E_{exo} between CO_2 and C_2H_4 insertion reactions will be discussed. The difference between $C=O$ and $C-O$ bond energies is about 100 kcal/mol, about 30 kcal/mol greater than the difference between $C=C$ and $-CH_2-CH_2-$ bond energies. Thus, the $E(C-O) - E(C=O)$ term is not responsible for the higher exothermicity of the CO_2 insertion. The H_3C-CH_3 bond energy does not differ very much from the $H_3C-C(O)OR$ bond energy (see Table 4.4), yielding only a little difference in the exothermicity between the CO_2 and C_2H_4 insertion reactions. On the other hand, $E(Cu-OC(O)R)$ is larger than $E(Cu-CH_3)$ by ca. 50 kcal/mol, indicating that the term, $E(Cu-OC(O)R) - E(Cu-CH_3)$, results in the greater exothermicity of the CO_2 insertion than that of the C_2H_4 insertion. In other words, the greater exothermicity of the CO_2 insertion is due to the stronger $Cu-OC(O)CH_3$ bond than the $Cu-CH_3$ bond.

Similarly, exothermicities of the CO_2 and C_2H_4 insertion reactions into the Cu-H bond are represented by eqs 4.11 and 4.12, respectively.

$E_{exo} = E(Cu-OC(O)H) + E(C-O) + E(H-C(O)OR)$

$- E(Cu-H) - E(C=O)$

$= E(Cu-OC(O)H) + \{E(C-O) - E(C=O)\}$

$+ E(H-C(O)OR) - E(Cu-H)$ (4.11)

$E_{exo} = E(Cu-C_2H_5) + E(-CH_2-CH_2-) + E(H-C_2H_5)$

$- E(Cu-H) - E(\,\diagdown C=C\diagdown\,)$

$$= \text{E}(\text{Cu-C}_2\text{H}_5) + \{\text{E}(\text{-CH}_2\text{-CH}_2\text{-}) - \text{E}(\text{>C=C<})\}$$

$$+ \text{E}(\text{H-C}_2\text{H}_5) - \text{E}(\text{Cu-H}) \qquad (4.12)$$

The difference, $\text{E}(\text{C=O}) - \text{E}(\text{C-O})$, is larger than the difference, $\text{E}(\text{C=C}) - \text{E}(\text{-CH}_2\text{-CH}_2\text{-})$, as discussed above. $\text{E}(\text{H-C}(\text{O})\text{OR})$ is calculated to be similar to $\text{E}(\text{H-C}_2\text{H}_5)$, as shown in Table 4.4. Thus, these two terms do not lead to the greater exothermicity of the CO_2 insertion into the Cu-H bond. On the other hand, $\text{E}(\text{Cu-OC}(\text{O})\text{H})$ is much larger than $\text{E}(\text{Cu-C}_2\text{H}_5)$. This is a main reason for the greater exothermicity of the CO_2 insertion into the Cu-H bond than that of the C_2H_4 insertion.

4-3-3 Geometries of Precursor Complex and Transition State

Geometries of precursor complexes (PC) and transition states (TS) are shown in Figures 4.1 and 4.2, respectively. In the PCs, the Cu-CO_2 and $\text{Cu-C}_2\text{H}_4$ distances are considerably long. Correspondingly, geometries of CO_2, C_2H_4, and $\text{CuR}(\text{PH}_3)_2$ parts only slightly distort from those of reactants. Consistent with these geometrical features, stabilization energies of PCs (Tables 4.2 and 4.3) are much smaller than that of the usual coordinate bond, indicating that CO_2 and C_2H_4 weakly interact with $\text{CuR}(\text{PH}_3)_2$ like a van der Waals complex.

In the TS of the CO_2 insertion into the Cu-H bond (**3A** in Figure 4.2), both C-H and Cu-O^2 distances between CO_2 and $\text{CuH}(\text{PH}_3)_2$ are much longer than those in the product. The Cu-H and C-O^1 bonds somewhat lengthen by ca. 0.1 Å and ca. 0.05 Å respectively, and the CO_2 part starts to bend ($<$OCO = 150°). Similar features are observed in the TS of the CO_2 insertion into the Cu-CH$_3$ bond (**3B** in Figure 4.2). There is, however, a
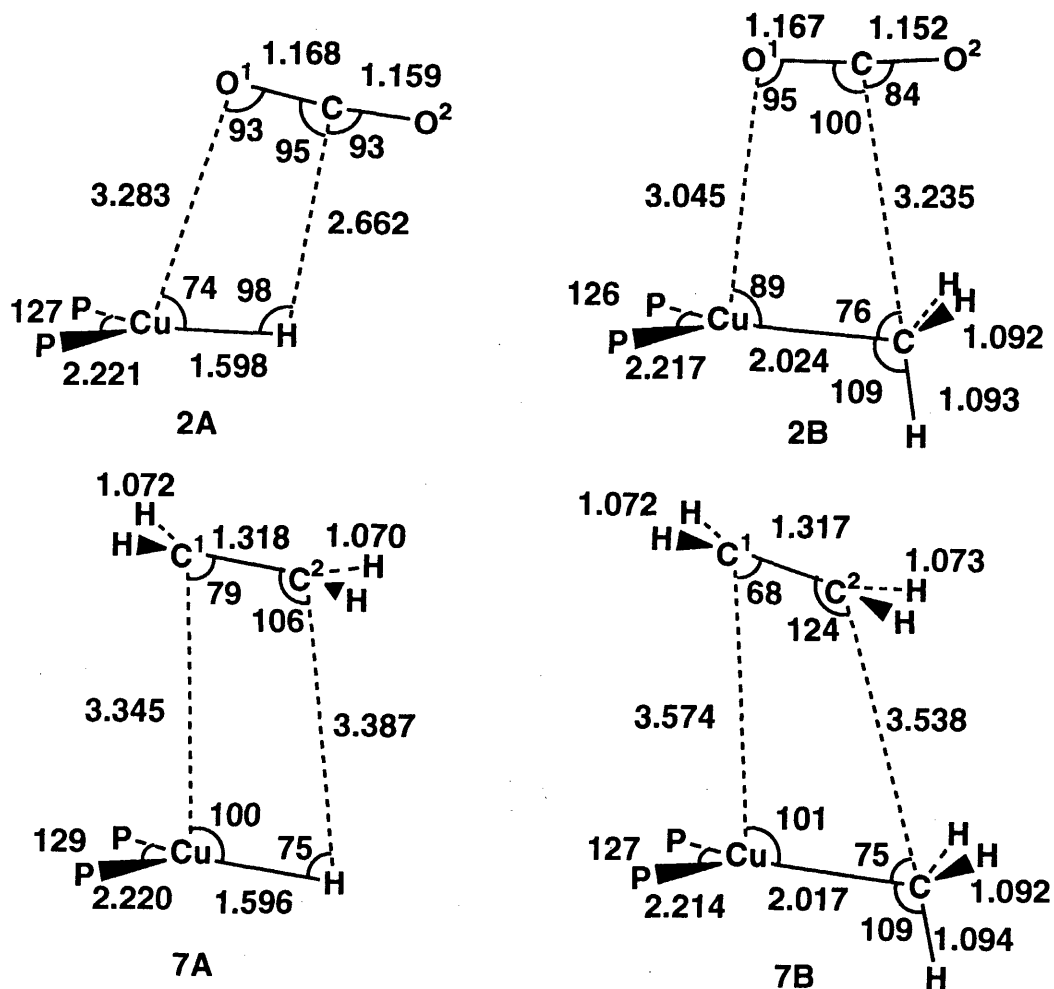
**Figure 4.1** Optimized geometries of precursor complexes in the CO_2 and C_2H_4 insertions into the Cu-H and Cu-CH$_3$ bonds. Bond length in Å and angle in degree.

critical difference between **3A** and **3B**; the CH$_3$ ligand considerably moves downward and changes its direction toward the incoming CO_2 molecule, whereas the H ligand only slightly moves downward at the TS. This difference between CuH(PH$_3$)$_2$ and Cu(CH$_3$)(PH$_3$)$_2$ is easily interpreted in terms of the valence orbitals of CH$_3$ and H ligands. Because of the highly directional sp^3 valence orbital, the CH$_3$ ligand must change its
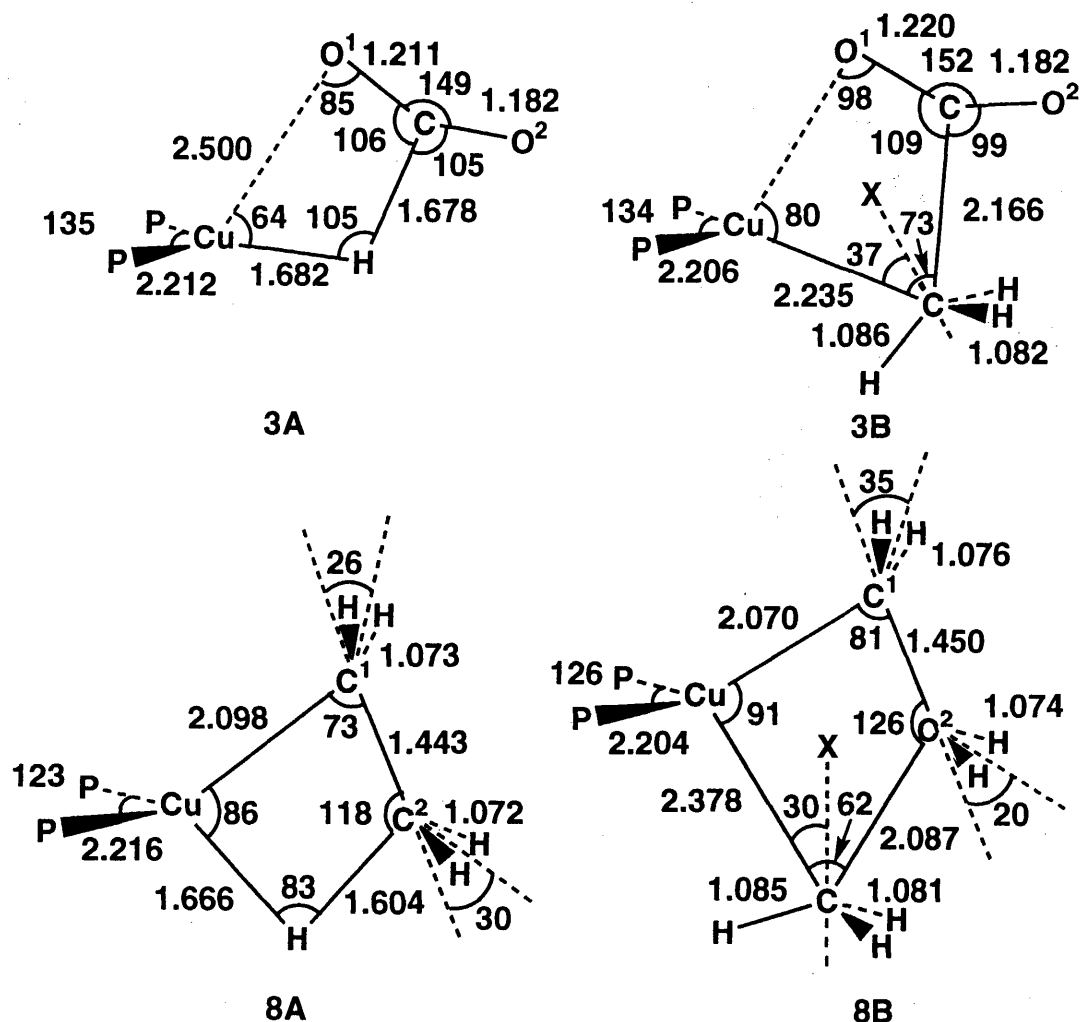
Figure 4.2 Optimized geometries of transition state in the CO_2 and C_2H_4 insertions into the Cu-H and Cu-CH_3 bonds. Bond length in Å and angle in degree. X represents the direction of CH_3.

direction toward CO_2 in order to form a new bond with CO_2. At the same time, the CH_3 ligand wants to keep a bonding interaction with Cu as much as possible. Thus, the downward movement of CH_3 occurs to satisfy these two requisites, as schematically shown in Chart 4.2A. On the other hand, the H ligand does not need to change its position because it can form a new bond with the incoming CO_2, keeping the coordinate
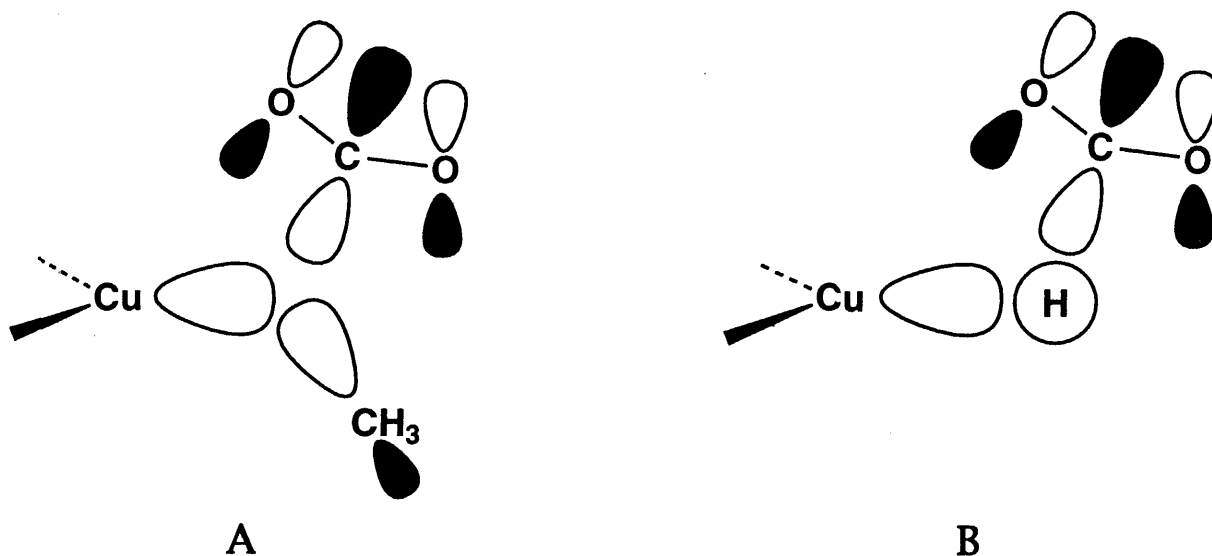
Chart 4.2

bond with Cu, due to its spherical 1s valence orbital (Chart 4.2B).

The TS of the C_2H_4 insertion into the Cu-R bond (H or CH_3) exhibits interesting features (Figure 4.2), as follows; (1) the Cu-H distance slightly lengthens but the Cu-CH_3 bond considerably lengthens, (2) both H and CH_3 ligands considerably move downward, (3) the C^1-C^2 bond of C_2H_4 considerably lengthens by 0.13 Å, and the C^1H_2 and C^2H_2 planes are remarkably bent by 26 and 30 degrees respectively, (4) the Cu-C^1 distance is short (2.1 Å) like it in the product, but the C^2-R bond is still long. These features suggest that the TS of the C_2H_4 insertion is product-like compared to the TS of the CO_2 insertion, and that the Cu-C^1 bond is formed prior to the formation of the C^2-R bond (remember that both Cu-O^1 and C-R bonds between CO_2 and $CuR(PH_3)_2$ are not formed yet at the TS

of the CO_2 insertion). These differences between CO_2 and C_2H_4 insertion reactions will be discussed below.

Activation energies (E_a) of these insertion reactions are given in Tables 4.2 and 4.3. Both CO_2 and C_2H_4 are inserted into the Cu-H bond with lower activation energies than into the Cu-CH_3 bond. This result can be interpreted in terms of the valence orbitals of H and CH_3 ligands, again; as described above, the $CuH(PH_3)_2$ part distorts at the TS to a lesser extent than the $Cu(CH_3)(PH_3)_2$ part because the 1s valence orbital of H is spherical but the sp^3 valence orbital of CH_3 is directional. Accordingly, the insertion into the Cu-CH_3 bond needs higher activation energy, due to the greater distortion energy of the $Cu(CH_3)(PH_3)_2$ part. Consistent with this result, Darensbourg et al. experimentally suggested that CO_2 could be inserted into the Ni-H bond but could be not into the Ni-CH_3 bond.[27m] The other interesting result to be noted is that the C_2H_4 insertion requires a higher activation energy than the CO_2 insertion, which will be discussed after investigating characters of the TS.

4-3-4 Electron Redistribution in the CO_2 and C_2H_4 Insertion Reactions and the Reasons for Low Activation Energy of the CO_2 Insertion.

Changes in Mulliken populations by these reactions are shown in Figure 4.3. In all the insertion reactions examined, electron populations of CO_2 and C_2H_4 remarkably increase as the reaction proceeds, indicating that the charge-transfer from $CuR(PH_3)_2$ to CO_2 or C_2H_4 takes place in these reactions. In the insertion into the Cu-H bond, electron populations of both Cu and H significantly decrease (Figures 4.3A and 4.3C). This
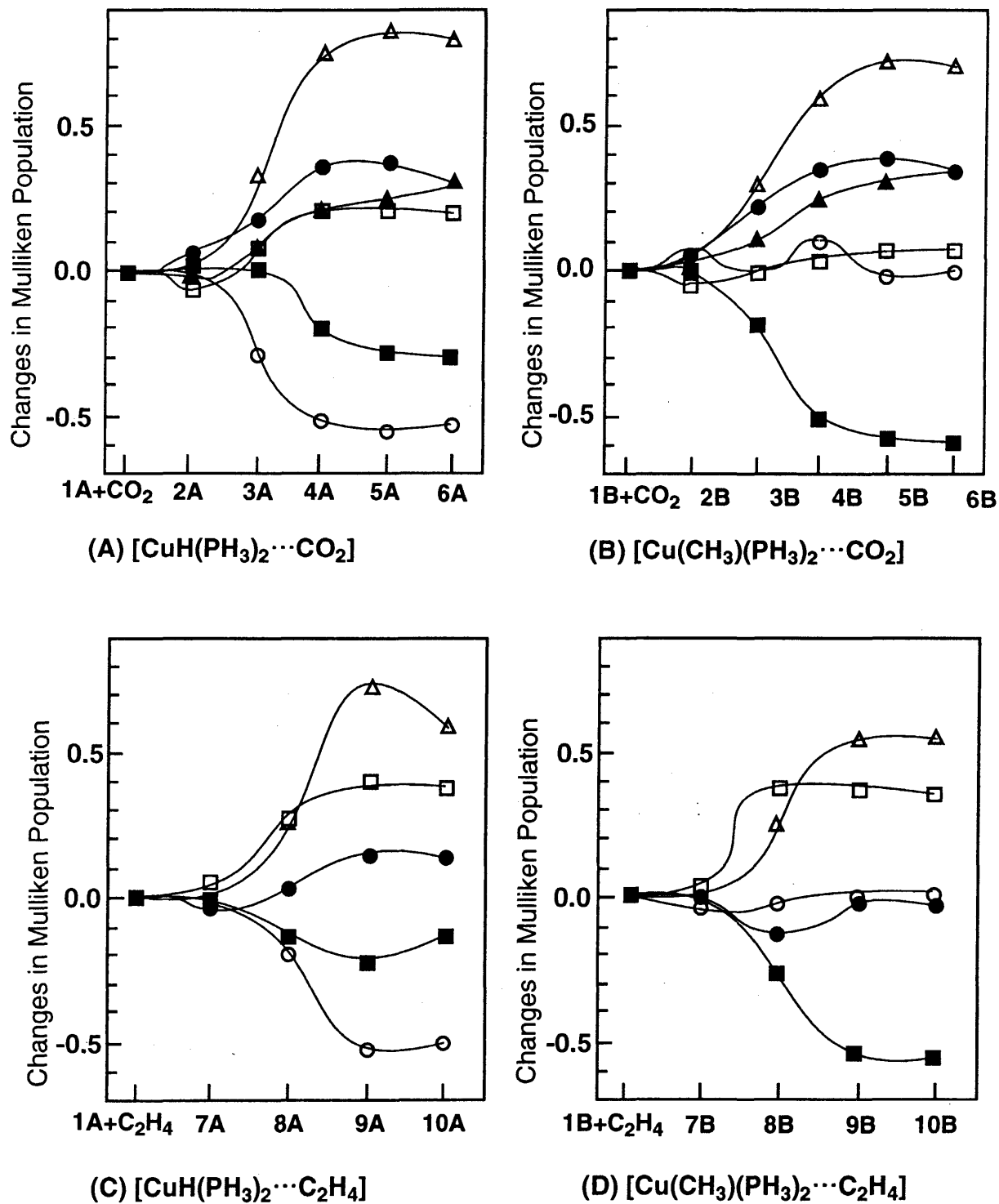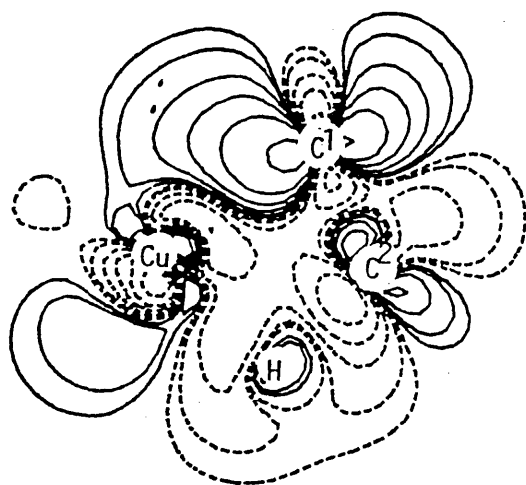
Figure 4.3 Changes in Mulliken populations caused by CO_2 and C_2H_4 insertions into Cu-H and Cu-CH$_3$ bonds. (A) CO_2 insertion into the Cu-H bond. (B) CO_2 insertion into the Cu-CH$_3$ bond. (C) C_2H_4 insertion into the Cu-H bond. (D) C_2H_4 insertion into the Cu-CH$_3$ bond.
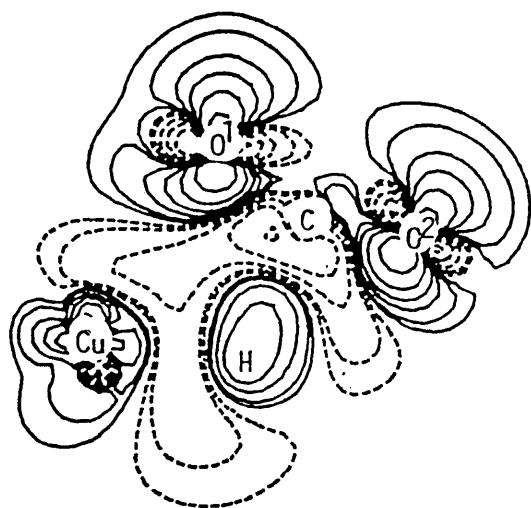
(A) CuH(PH₃)₂ + CO₂
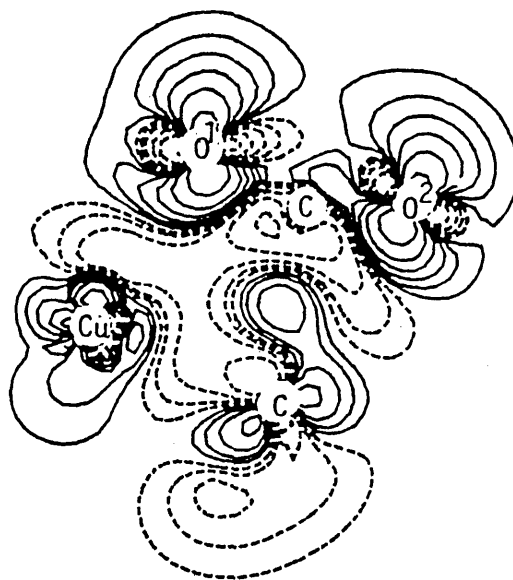
(B) Cu(CH₃)(PH₃)₂ + CO₂

(C) CuH(PH₃)₂ + C₂H₄
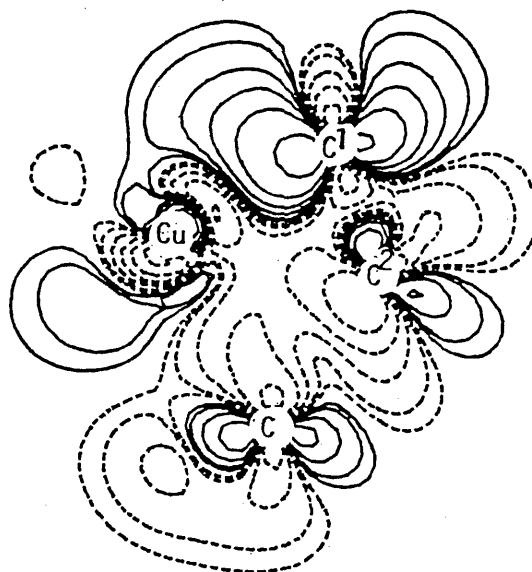
(D) Cu(CH₃)(PH₃)₂ + C₂H₄

Figure 4.4 Difference density maps at the transition state of CO_2 and C_2H_4 insertions into the Cu-H and Cu-CH₃ bonds (A) [CuH(PH₃)···(CO₂)], **3A**, (B) [Cu(CH₃)(PH₃)···(CO₂)], **3B**, (C) [CuH(PH₃)₂···(CO₂)], **9A**, (D) [Cu(CH₃)(PH₃)₂···(CO₂)], **9B**. Contour values are ±0.05, ±0.02, ±0.005, ±0.002, and ±0.01.

A   **B**
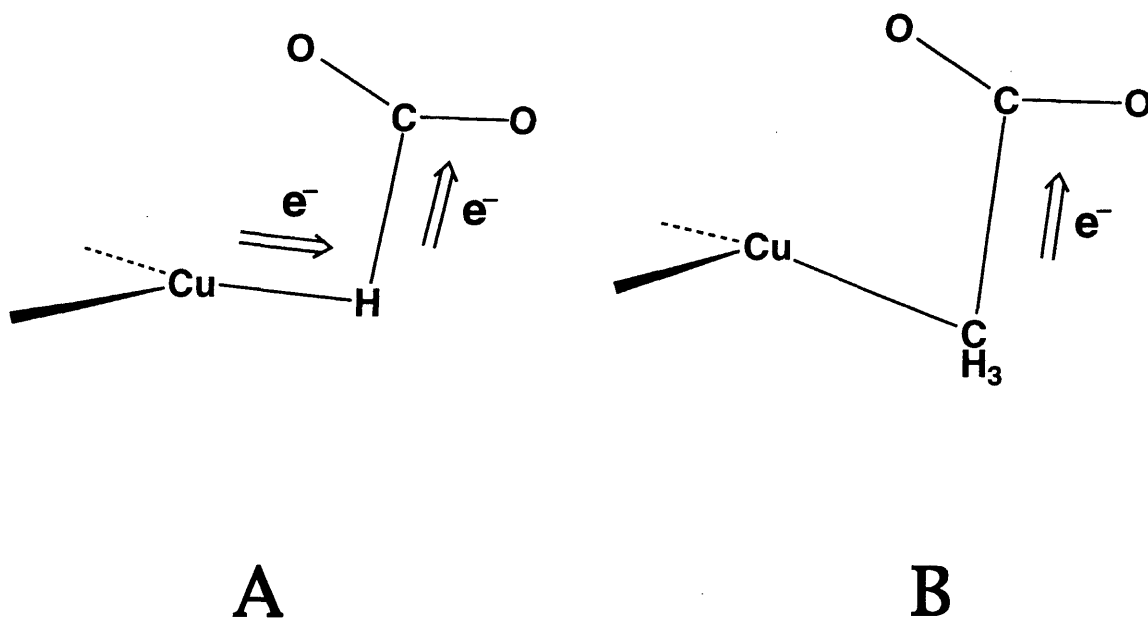
Chart 4.3

implies that the insertion into the Cu-H bond causes the charge-transfer from the H ligand to CO_2 or C_2H_4 concomitantly with the polarization of $CuH(PH_3)_2$ which induces electron flow from Cu to H (Chart 4.3A). In the insertion into the Cu-CH_3 bond, on the other hand, electron population of CH_3 considerably decreases but electron population of Cu hardly changes (Figures 4.3B and 4.3D), indicating that the insertion into the Cu-CH_3 bond causes only charge-transfer to CO_2 or C_2H_4 from the CH_3 ligand (Chart 4.3B) unlike the insertion into the Cu-H bond. This difference between R = CH_3 and R = H is easily interpreted in terms of the directionality of the valence orbital, again. Because the Cu-CH_3 bond must be broken to form a new CH_3-CO_2 bond at the TS due to the directional sp^3 valence orbital of CH_3, the electron flow from

106

Cu to CH_3 becomes difficult at around the TS. On the other hand, the electron flow from Cu to H can occur, because the Cu-H bond still exists at the TS due to the spherical 1s valence orbital of H.

Electron redistribution at the TS is investigated in more detail, inspecting the difference density maps (Figure 4.4); the difference density = $\rho[CuR(PH_3)_2\bullet\bullet\bullet Sub]_{TS}$ − $\rho[CuR(PH_3)_2]$ − $\rho[Sub]$, where Sub means CO_2 or C_2H_4. An important feature found in the CO_2 insertion (Figures 4.4A and 4.4B) is that electron density accumulates on the terminal O atoms but slightly decreases on the central C atom. This feature arises from the HOMO, $\psi_{HOMO}(CuR\bullet\bullet\bullet CO_2)$, of the reaction system. This $\psi_{HOMO}(CuR\bullet\bullet\bullet CO_2)$ resembles well the HOMO, $\psi_{HOMO}(CO_2\bullet\bullet\bullet R^-)$, of the $CO_2\bullet\bullet\bullet R^-$ system, as clearly shown in Figures 4.5A, 4.5B, 4.5E, and 4.5F. Both $\psi_{HOMO}(CuR\bullet\bullet\bullet CO_2)$ and $\psi_{HOMO}(CO_2\bullet\bullet\bullet R^-)$ mainly consist of the large p_π orbital of O, the very small p_π orbital of C, and the HOMO of R^-, which are formed through the orbital mixing among the π and π^* orbitals of CO_2 and the HOMO of R^-. As shown in Chart 4.4A, the HOMO of R^- overlaps with the π^* orbital of CO_2 in a bonding way, into which the π orbital of CO_2 mixes in an anti-bonding way with the HOMO of R^- because the former lies at a lower energy than the latter. This orbital mixing decreases the p_π orbital of C but enhances the p_π orbital of O, which leads to accumulation of electron density on the O atoms but a slight decrease of electron density on the C atom as we have seen in Figures 4.4A and 4.4B.

In the C_2H_4 insertion, electron density accumulates on the C^1 atom but decreases on the C^2 atom (Figures 4.4C and 4.4D). This feature is explained in terms of the HOMO of the
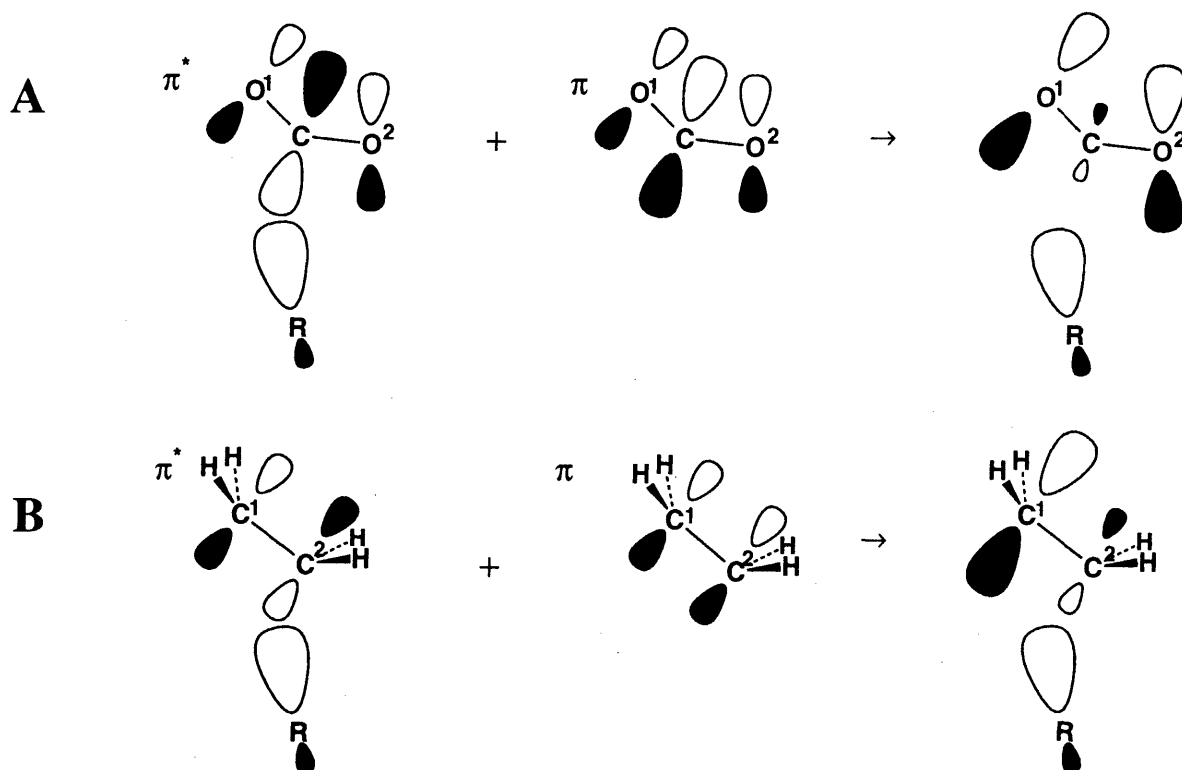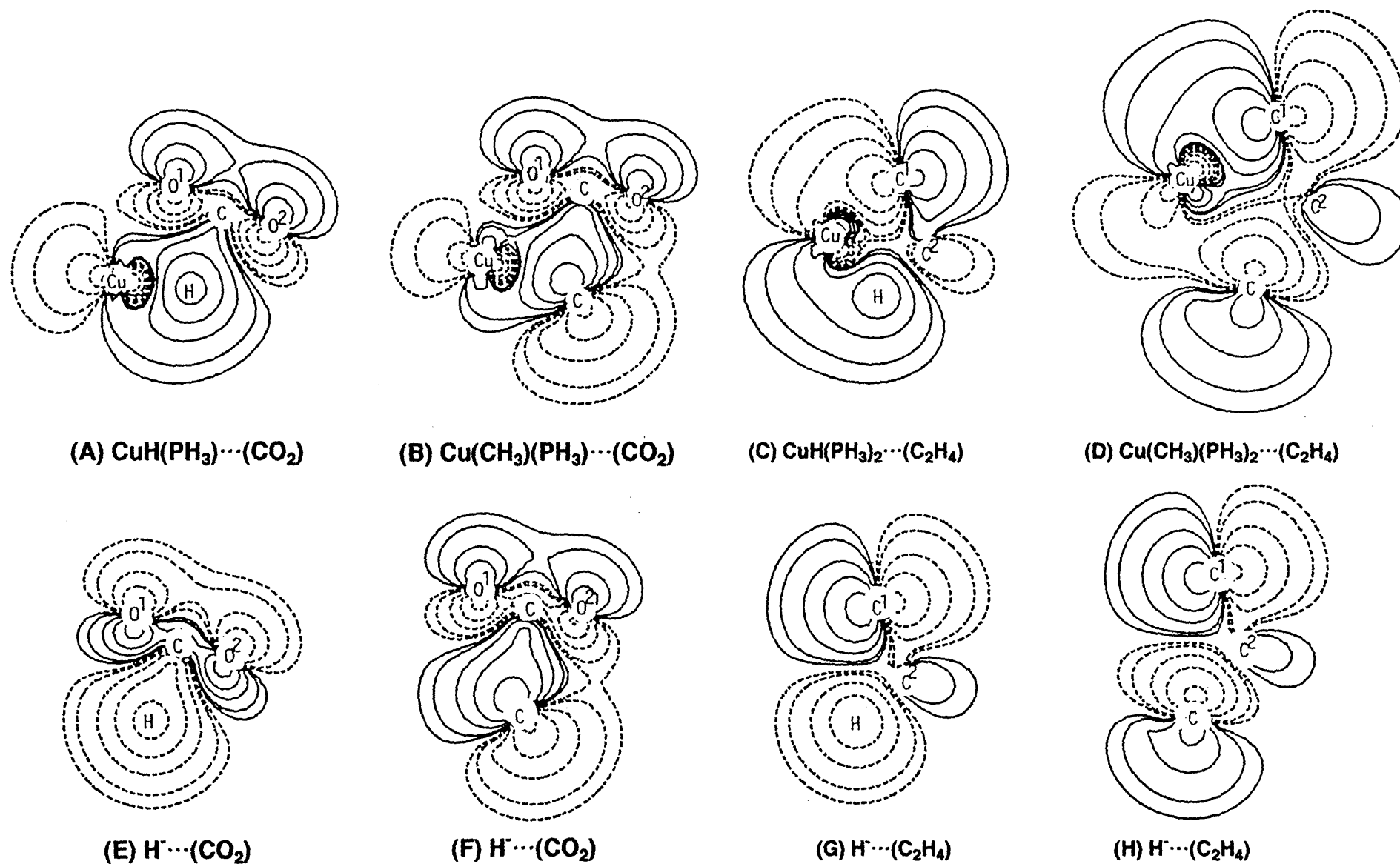
Chart 4.4

reaction system, $\psi_{HOMO}(CuR\bullet\bullet\bullet C_2H_4)$, again. As shown in Figures
4.5C, 4.5D, 4.5G, and 4.5H, this HOMO resembles well the HOMO
of the $C_2H_4\bullet\bullet\bullet R^-$ system, $\psi_{HOMO}(C_2H_4\bullet\bullet\bullet R^-)$. These HOMOs mainly
consist of the large p_π orbital of C^1, the small p_π orbital of
C^2 and the HOMO of R^-, which are formed through the orbital
mixing among the π and π^* orbitals of C_2H_4 and the HOMO of R^-;
the HOMO of R^- overlaps with the π^* orbital of C_2H_4 in a
bonding way, into which the π orbital of C_2H_4 mixes in an anti-
bonding way with the HOMO of R^- because the former lies at
lower energy than the latter, as shown in Chart 4.4B. This

orbital mixing enhances the C^1 p_π orbital but decreases the C^2 p_π orbital in $\psi_{HOMO}(C_2H_4 \bullet\bullet\bullet R^-)$ and $\psi_{HOMO}(CuR \bullet\bullet\bullet C_2H_4)$, which leads to an increase of electron density on the C^1 atom but a decrease of electron density on the C^2 atom.

Electron redistribution in the region between R and Sub (Sub = CO_2 or C_2H_4) is important for the insertion reaction. At the TS of the CO_2 insertion, electron density accumulates in this region (Figures 4.4A and 4.4B). Actually, the considerable C-R bonding overlap between CO_2 and $CuR(PH_3)_2$ is observed in $\psi_{HOMO}(CuR \bullet\bullet\bullet CO_2)$ (Figures 4.5A and 4.5B). At the TS of the C_2H_4 insertion, on the other hand, electron density decreases in this region (Figures 4.4C and 4.4D). Because $\psi_{HOMO}(CuR \bullet\bullet\bullet C_2H_4)$ involves the considerable C^2-R bonding overlap between C_2H_4 and $CuR(PH_3)_2$ like it in the CO_2 insertion (Figure 4.5), the decrease in the density arises not from $\psi_{HOMO}(CuR \bullet\bullet\bullet C_2H_4)$ but from the other interaction, i.e., exchange repulsion between the π orbital of C_2H_4 and the HOMO of R. Approach of C_2H_4 to R would be difficult due to this strong exchange repulsion, which disfavors the C_2H_4 insertion into the Cu-R bond and leads to the high activation energy. In the case of the CO_2 insertion, this kind of exchange repulsion would be small because the π orbital of CO_2 lies at considerably low in energy (-19.37 eV) than it of C_2H_4 (-9.63 eV).[51] Accordingly, the C_2H_4 insertion requires a higher activation energy than the CO_2 insertion.

Finally, an interaction between Cu and Sub will be investigated. At the TS of the CO_2 insertion, electron density decreases in the region between Cu and O^1 atoms (Figures 4.4A and 4.4B). At the TS of the C_2H_4 insertion, on the other hand, electron density increases in this region.

(A) CuH(PH$_3$)$\cdots$(CO$_2$)   **(B)** Cu(CH$_3$)(PH$_3$)$\cdots$(CO$_2$)   **(C)** CuH(PH$_3$)$_2\cdots$(C$_2$H$_4$)   **(D)** Cu(CH$_3$)(PH$_3$)$_2\cdots$(C$_2$H$_4$)

(E) H$^-\cdots$(CO$_2$)   **(F)** H$^-\cdots$(CO$_2$)   **(G)** H$^-\cdots$(C$_2$H$_4$)   **(H)** H$^-\cdots$(C$_2$H$_4$)

Figure 4.5 Contour maps at the HOMOs of (A) [CuH(PH$_3$)$\cdots$(CO$_2$)], **3A**, (B) [Cu(CH$_3$)(PH$_3$)$\cdots$(CO$_2$)], **3B**, (C) [CuH(PH$_3$)$_2\cdots$(CO$_2$)], **9A**, (D) [Cu(CH$_3$)(PH$_3$)$_2\cdots$(CO$_2$)], **9B**. (E) CO$_2\cdots$H$^-$, (F) CO$_2\cdots$CH$_3^-$, (G) C$_2$H$_4\cdots$H$^-$, (H) C$_2$H$_4\cdots$CH$_3^-$. Contour values are ±0.2, ±0.1, ±0.05, ±0.02, and ±0.01.

Consistent with this result, $\psi_{HOMO}(CuR\bullet\bullet\bullet C_2H_4)$ at the TS of the C_2H_4 insertion involves a strong bonding interaction between Cu and C^1 atoms (Figures 4.5C and 4.5D), while $\psi_{HOMO}(CuR\bullet\bullet\bullet CO_2)$ at the TS of the CO_2 insertion involves an apparently weaker bonding interaction between Cu and O^1 atoms than that between Cu and C^1 atoms in $\psi_{HOMO}(CuR\bullet\bullet\bullet C_2H_4)$ (Figures 4.5A and 4.5B). All these results are consistent with the TS structure in which the $Cu-C^1$ distance is short at the TS of the C_2H_4 insertion but the $Cu-O^1$ distance is long at the TS of the CO_2 insertion. The short $Cu-C^1$ and the long $Cu-O^1$ distances are explained in terms of HOMOs, $\psi_{HOMO}(C_2H_4\bullet\bullet\bullet R^-)$ and $\psi_{HOMO}(CO_2\bullet\bullet\bullet R^-)$. These HOMOs (Figure 4.5) are calculated to be -2.61 eV for $CO_2\bullet\bullet\bullet H^-$, -2.52 eV for $CO_2\bullet\bullet\bullet CH_3^-$, 0.56 eV for $C_2H_4\bullet\bullet\bullet H^-$, and 0.07 eV for $C_2H_4\bullet\bullet\bullet CH_3^-$, where geometries are taken to be the same as those in the TS. This means that approach of R^- to C_2H_4 yields the HOMO at a considerably high energy but approach of R^- to CO_2 yields the HOMO at a rather low energy; Accordingly, $\psi_{HOMO}(C_2H_4\bullet\bullet\bullet R^-)$ can form much stronger charge transfer interaction with Cu than does $\psi_{HOMO}(CO_2\bullet\bullet\bullet R^-)$, leading to the short $Cu-C^1$ distance at the TS of the C_2H_4 insertion. The $Cu-O^1$ distance is, however, rather long at the TS because the charge-transfer from $\psi_{HOMO}(CO_2\bullet\bullet\bullet R^-)$ to Cu is not strong very much.

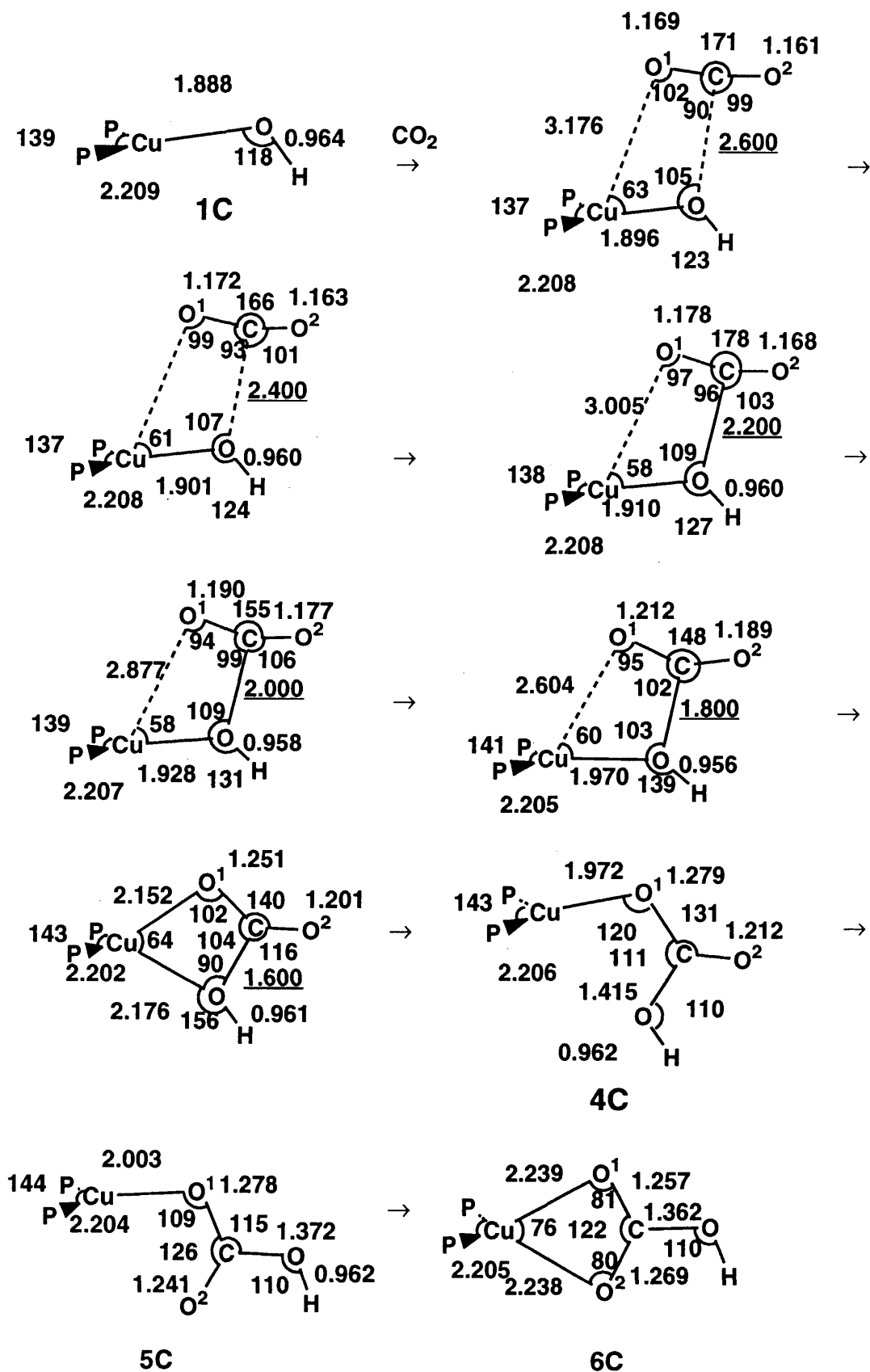## 4-3-5 CO_2 Insertion Reaction into the Cu-OH Bond of $Cu(OH)(PH_3)_2$

Interestingly, the CO_2 insertion into the Cu-OH bond proceeds with no barrier, as clearly shown in Figure 4.6. Following geometry changes are observed (Figure 4.7); the Cu-OH distance is getting longer, the $Cu-O^1$ distance is getting

111

shorter, and the $<O^1CO^2$ angle gradually closes. All these results represent that the Cu-OH bond is gradually broken and the Cu-O^1 bond is gradually formed, and the Cu-OC(O)OH bond is smoothly produced. The geometry at the late stage of this reaction is very close to that of the product, Cu(η^1-OCOH)(PH$_3$)$_2$ **4C** (see the geometry at R(O-CO$_2$) = 1.6 Å). After the insertion, **4C** converts to **5C** with very small barrier (ca. 2.6 kcal/mol at the MP2/BS III level), and **5C** converts to the final product, Cu(η^2-O$_2$COH)(PH$_3$)$_2$ **6C**, with no barrier (Figure 4.6).
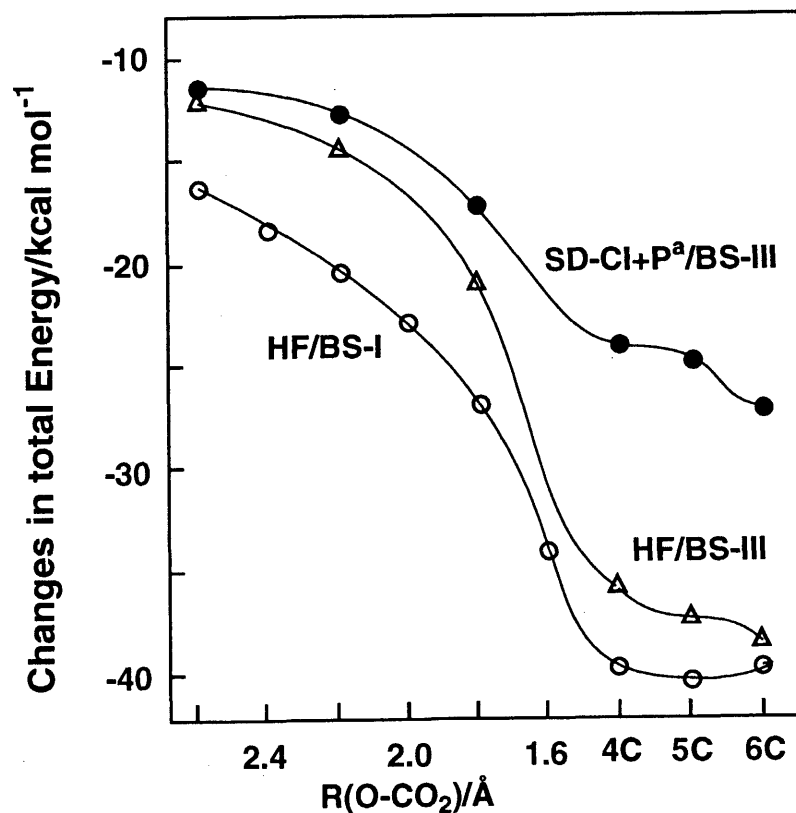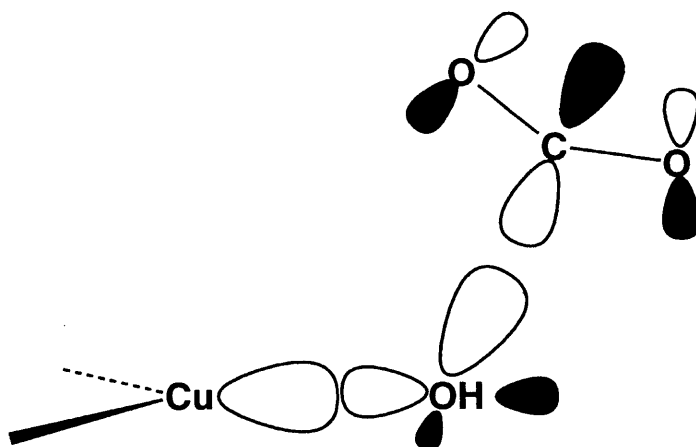

Figure 4.6 Changes in total energy caused by the CO$_2$ insertion into the Cu-OH bond of Cu(OH)(PH$_3$)$_2$ **1C**.
a) P = Pople's higher order excitaton correction.

Unexpectedly, the exothermicity of this insertion (27.1

Figure 4.7 Changes in geometry caused by the CO_2 insertion into the Cu-OH bond of $Cu(OH)(PH_3)_2$ **1C**. Bond distance in Å and bond angle in degree.

Chart 4.5

kcal/mol for **6C** (SD-CI(P)/BS III)) is calculated to be much
smaller than that of the CO_2 insertion into Cu-H and $Cu-CH_3$
bonds, whereas CO_2 can insert into the Cu-OH with no barrier.
The exothermicity of this insertion is approximately
represented by eq 4.13,[50] The HO-C(O)OH bond energy is

$$E_{exo} = E(Cu-OC(O)OH) + E(C-O) + E(HO-C(O)OH)$$
$$- E(Cu-OH) - E(C=O)$$
$$= E(Cu-OC(O)OH) + \{E(C-O) - E(C=O)\}$$
$$+ E(HO-C(O)OH) - E(Cu-OH) \qquad (4.13)$$

estimated to be 87 kcal/mol, only slightly smaller than the C-
C(O)OH bond energy (92 kcal/mol) (Table 4.4). On the other
hand, the term of E(Cu-OC(O)OH) - E(Cu-OH) is calculated to be
29 kcal/mol, much smaller than the term of E(Cu-OC(O)R) -
E(Cu-R), as shown in Table 4.4. Consequently, this insertion
is less exothermic than the CO_2 insertion into the Cu-H and
$Cu-CH_3$ bonds.

114

No activation energy of this insertion can be interpreted in terms of the HOMO of $Cu(OH)(PH_3)_2$ **1C**. Unlike the HOMOs of **1A** and **1B**, the HOMO of **1C** mainly consists of a lone-pair type orbital of OH^- which is not used for a coordinate bond with Cu (Chart 4.5). As a result, the LUMO of CO_2 can easily interact with this orbital. This means that the bonding interaction between CO_2 and OH is formed without weakening the Cu-OH bond. On the other hand, both H and CH_3 ligands have only one valence orbital which is used for bonding with Cu in **1A** and **1B**. Accordingly, the CO_2 insertion into the Cu-H bond weakens the Cu-H bond even though the 1s valence orbital of H is spherical, and the CO_2 insertion into the Cu-CH_3 bond considerably weakens the Cu-CH_3 bond because of the directional sp^3 valence orbital of CH_3. Thus, the CO_2 insertion into the Cu-OH bond more easily occurs than the CO_2 insertion into the Cu-H and Cu-CH_3 bonds.

4.4 Conclusions

Ab initio MO/MP4, SD-CI, and CCD calculations are carried out on the insertion reactions of CO_2 and C_2H_4 into the Cu-R bond (R=H, CH_3, and OH). The activation energy (E_a) is calculated to be very low (ca. 4 - 5 kcal/mol) for the CO_2 insertion, relatively high (9 - 10 kcal/mol) for the C_2H_4 insertion into the Cu-H bond, and very high (23 - 30 kcal/mol) for the C_2H_4 insertion into the Cu-CH_3 bond. These results suggest that the C_2H_4 insertion into the Cu-R bond is more difficult than the CO_2 insertion into the Cu-R bond. The difference of E_a between CO_2 and C_2H_4 insertion reactions can be interpreted in terms of the exchange repulsion between R and Sub (Sub = CO_2 or C_2H_4); because the π orbital of C_2H_4 lies

higher in energy than that of CO_2, the exchange repulsion between C_2H_4 and R is much larger than that between CO_2 and R, leading to the higher E_a value of the C_2H_4 insertion. The exothermicity of the CO_2 insertion is much greater than that of the C_2H_4 insertion. The main reason for the greater exothermicity of the CO_2 insertion is that $E(Cu-OC(O)H)$ is larger than $E(Cu-C_2H_5)$ and $E(Cu-CH_3)$ by ca. 50 kcal/mol. The CO_2 insertion into the Cu-OH bond proceeds with no barrier. This is because the HOMO of $Cu(OH)(PH_3)_2$ is mainly consists of the lone-pair type orbital of OH^- and the bonding interaction between CO_2 and OH can be formed without weakening of the Cu-OH bond. However, the E_{exo} of this insertion is smaller than that of the other CO_2 insertion, since the $Cu-OC(O)OH$ bond energy is about 29 kcal/mol larger than the Cu-OH bond energy (remember that $Cu-OC(O)R$ bond energy is about 50 kcal/mol larger than the $Cu-CH_3$ bond energy).

From these results, one can predict a primarily important factor for the CO_2 insertion that the presence of a lone-pair type orbital of R which is not used for coordination to Cu in the CO_2 insertion. When the R ligand possesses such a lone-pair type orbital, the bonding interaction between this lone-pair type orbital and the LUMO of CO_2 can be formed without weakening of the Cu-OH bond. This situation facilitates the CO_2 insertion into the Cu-OH bond.

References

(1) For instance; (a) D. J. Darensbourg and R. A.
     Kudaroski, <u>Adv. Organomet. Chem.</u>, **22**, 129 (1983).
     (b) D. A. Palmer and R. van Eldik, R. <u>Chem. Rev.</u>,
     83, 651 (1983). (c) D. Walther, <u>Coord. Chem.
     Rev.</u>, **79**, 135 (1987). (d) A. Behr, <u>Angew. Chem.,
     Int. Ed. Engl.</u>, **27**, 661 (1988). (e) P. Braustein,
     D. Matt, and D. Nobel, <u>Chem. Rev.</u>, **88**, 747 (1988).
     (f) A. R. Culter, P. K. Hanna, and J. C. Vites,
     <u>Chem. Rev.</u>, **88**, 1363 (1988). (g) A. Behr "Carbon
     Dioxide Activation by Metal Complexes," VCH
     Publishing, Weinheim, West Germany (1988).

(2) For instance; (a) J. J. Alexander, In "The Chemistry of
     the Metal-Carbon Bond," F. R. Hartley and S. Patai, ed.
     John Wiley & Sons, New York (1985), vol. 2, p 339. (b)
     F. R. Hartley and S. Patai, "The Chemistry Metal-Carbon
     Bond," ed. by F. R. Hartley and S. Patai, S. John Wiley
     & Sons, New York (1985), vol. 3. (c) R. H. Crabtree,
     "The Organometallic Chemistry of Transition Metals,"
     John Wiley & Sons, New York (1988).

(3) (a) S. Inoue and N. Takeda, <u>Bull. Chem. Soc. Jpn.</u>,
     50, 984 (1977). (b) T. Aida and S. Inoue, <u>J. Am.
     Chem. Soc.</u>, **105**, 1304 (1983). (c) F. Kojima, T.
     Aida, and S. Inoue, <u>J. Am. Chem. Soc.</u>, **108**, 391
     (1986) (d) T. Aida, M. Ishikawa, and S. Inoue,
     <u>Macromolecules</u>, **19**, 8 (1986). (e) Y. Hirai, T.
     Aida and S. Inoue, <u>J. Am. Chem. Soc.</u>, **111**, 3062
     (1989). (f) M. Komatsu, T. Aida, and S. Inoue, <u>J.
     Am. Chem. Soc.</u>, **113**, 8492 (1991).

(4) A. Rokicki and W. Kuran, <u>J. Macromol. Sci. Rev.</u>

<u>Macromol. Chem.</u>, **135**, C21 (1981).

(5)   K. Soga, E. Imai, and I. Hattori, <u>Polym. J.</u>, **13**, 407 (1981).

(6)   S. Gambarotta, S. Strologo, C. Floriani, A. Chiesi-Villa, and C. Guastini, <u>J. Am. Chem. Soc.</u>, **107**, 6278 (1985).

(7)   (a) E. Carmona, P. Palma, M. Paneque, and M. L. Poveta, <u>J. Am. Chem. Soc.</u>, **108**, 6424 (1986). (b) E. Carmona, E. Gutiérrez-Puebla, J. M. Marin, A. Monge, M. Paneque, M. L. Poveta, and C. Ruiz, <u>J. Am. Chem. Soc.</u>, **111**, 2883 (1989).

(8)   P. Braunstein, D. Matt, and D. Nobel, <u>J. Am. Chem. Soc.</u>, **110**, 3207 (1988).

(9)   D. J. Darensbourg and C. Ovalles, <u>J. Am. Chem. Soc.</u>, **109**, 3330 (1989).

(10)   K. T. Aye, L. Gelmini, N. C. Payne, J. J. Vittal, and R. J. Puddephatt, <u>J. Am. Chem. Soc.</u>, **112**, 2464 (1990).

(11)   (a) C. Amatore and A. Jutand, <u>J. Am. Chem. Soc.</u>, **113**, 2819 (1991). (b) C. Amatore and A. Jutand, <u>J. Electroanal. Chem.</u>, **306**, 141 (1991).

(12)   J. C. Tsai and K. M. Nicholas, <u>J. Am. Chem. Soc.</u>, **114**, 5117 (1992).

(13)   (a) L. S. Pu, A. Yamamoto, and S. Ikeda, <u>J. Am. Chem. Soc.</u>, **90**, 3896 (1968). (b) S. Komiya and A. Yamamoto, <u>J. Organomet. Chem.</u>, **46**, C58 (1972). (c) A. Miyashita and A. Yamamoto, <u>J. Organomet. Chem.</u>, **49**, C57 (1973). (d) T. Ikariya and A. Yamamoto, <u>J. Organomet. Chem.</u>, **72**, 145 (1974). (e) A. Miyashita and A. Yamamoto, <u>J. Organomet. Chem.</u>, **113**, 187 (1976). (f) S. Komiya and A. Yamamoto, <u>Bull. Chem. Soc. Jpn.</u>, **49**, 784 (1976). (g) T.

Yamamoto, M. Kubota, and A. Yamamoto, <u>Bull. Chem. Soc.</u> <u>Jpn.</u>, **53**, 680 (1980).

(14) A. Misono, Y. Uchida, M. Hidai, and T. Kuse, <u>J. Chem.</u> <u>Soc., Chem. Commun.</u>, **1968**, 981.

(15) V. Zucchini, E. Albizzati, and V. Giannini, <u>J.</u> <u>Organomet. Chem.</u>, **26**, 357 (1971).

(16) (a) T. Tsuda and T. Saegusa, <u>Inorg. Chem.</u>, **11**, 2561 (1972). (b) T. Tsuda and T. Ueda, <u>J. Chem. Soc., Chem.</u> <u>Commun.</u>, **1974**, 380. (c) T. Tsuda, Y. Chujo, and T. Saegusa, <u>J. Chem. Soc., Chem. Commun.</u>, **1975**, 963. (d) T. Tsuda, S. Sanada, K. Ueda, and T. Saegusa, <u>Inorg</u> <u>Chem.</u>, **15**, 2329 (1976). (e) T. Tsuda, Y. Chujo, and T. Saegusa, <u>J. Am. Chem. Soc.</u>, **100**, 630 (1978). (f) T. Tsuda, Y. Chujo, and T. Saegusa, <u>J. Am. Chem. Soc.</u>, **102**, 431 (1980).

(17) I. S. Kolomnikov, A. I. Gusev, G. G. Aleksandrov, T. S. Lobeeva, Yu. I. Struchkov, and M. E. Vol'pin, <u>J.</u> <u>Organomet. Chem.</u>, **59** 349 (1973).

(18) G. Cahiez, J. F. Normant, D. Bernard, <u>J. Organomet.</u> <u>Chem.</u>, **94**, 463 (1975).

(19) H. H. Karsch, <u>Chem. Ber.</u> **110**, 2213 (1977).

(20) H. Koinuma, Y. Yoshida, and H. Hirai, <u>Chem. Lett.</u>, **1975**, 1223.

(21) Y. Inoue, H. Izumida, Y. Sasaki, and H. Hashimoto, <u>Chem.</u> <u>Lett.</u>, **1976**, 863.

(22) (a) M. H. Chisholm, W. W. Reichert, F. A. Cotton, and C. A. Murillo, <u>J. Am. Chem. Soc.</u>, **99**, 1652 (1977). (b) M. H. Chisholm, F. A. Cotton, M. W. Extine, and W. W. Reichert, <u>J. Am. Chem. Soc.</u>, **100**, 1727 (1978).

(23) T. Yoshida, D. L. Thorn, T. Okano, J. A. Ibers, and S.

Ohtsuka <u>J. Am. Chem. Soc.</u>, **101**, 4212 (1979).

(24) R. Van Eldik, D. A. Palmer, H. Kelm, and G. M. Harris, <u>Inorg. Chem.</u>, **19**, 3679 (1980).

(25) G. A. Razuvaef, L. I. Vyshinskaya, V. V. Drobotenko, G. Y. Malkova, and N. N. Vysinski, <u>J. Organomet. Chem.</u>, **239**, 335 (1982).

(26) N. Marsich, A. Camus, and G. Nardin, <u>J. Organomet. Chem.</u>, **239**, 429 (1982).

(27) (a) D. J. Darensbourg and A. Rokicki, <u>J. Am. Chem. Soc.</u>, **104**, 349 (1982). (b) S. G. Slater, R. Lusk, B. F. Schumann, and M. Darensbourg, <u>Organometallics</u>, **1**, 1685 (1982). (c) D. J. Darensbourg and A. Rokicki, <u>Organometallics</u>, **1**, 1685 (1982). (d) D. J. Darensbourg, M. Pala, and J. Waller, <u>Organometallics</u>, **2**, 1285 (1983). (e) D. J. Darensbourg and R. Kudaroski, <u>J. Am. Chem. Soc.</u>, **106**, 3672 (1984). (f) D. J. Darensbourg and C. Ovalless, <u>J. Am. Chem. Soc.</u> **106**, 3750 (1984). (g) D. J. Darensbourg and M. Pala, <u>J. Am. Chem. Soc.</u>, **107**, 5687 (1984). (h) D. J. Darensbourg, R. K. Hanckel, C. G. Bauch, M. Pala, D. Simmons, and J. White, <u>J. Am. Chem. Soc.</u>, **107**, 7463 (1985). (i) D. J. Darensbourg and G. Grötsch, <u>J. Am. Chem. Soc.</u>, **107**, 7473 (1985). (j) D. J. Darensbourg, C. G. Bauch, and A. L. Rheingold, <u>Inorg. Chem.</u>, **26**, 977 (1987). (k) D. J. Darensbourg, K. M. Sanchez, and A. L. Rheingold, <u>J. Am. Chem. Soc.</u>, **109**, 290 (1987). (l) D. J. Darensbourg, G. Grötsch, P. Wiegreffe, and A. L. Rheingold, <u>Inorg. Chem.</u>, **26**, 3827 (1987). (m) D. J. Darensbourg, M. Y. Darensbourg, L. Y. Goh, M. Ludvig, and H. P. Wiegreffe, <u>J. Am. Chem. Soc.</u>, **109**, 7539 (1987). (n) D. J. Darensbourg, K. M. Sanchez,

J. H. Reibenspies, and A. L. Rheingold, <u>J. Am. Chem. Soc.</u>, **111**, 7094 (1989). (o) D. J. Darensbourg, H. P. Wiegreffe, and C. G. Riordan, <u>J. Am. Chem. Soc.</u>, **112**, 5759 (1990). (p) D. J. Darensbourg, H. P. Wiegreffe, and P. W. Wiegreffe, <u>J. Am. Chem. Soc.</u>, **112**, 9252 (1990). (q) D. J. Darensbourg, B. L. Mueller, C. J. Bischoff, and S. S. Chojnacki, <u>Inorg. Chem.</u>, **30**, 2418 (1991).

(28) C. Bianchini, C. A. Ghilardi, A. Meli, S. Midollini, and A. Orlandini, <u>Inorg. Chem.</u>, **24**, 924 (1985).

(29) P. Cocolios, R. Guilard, D. Bayeul, and C. Lecomte, <u>Inorg. Chem.</u> **24**, 2058 (1985).

(30) W. C. Kaska, S. Nemeh, A. Shirazi, and S. Potuznik, <u>Organometallics</u>, **7**, 13 (1988).

(31) T. Arai, Y. Sato, and S. Inoue, <u>Chem. Lett.</u> **1990**, 551.

(32) J. F. Hartwig, R. G. Bergman, and R. A. Andersen, <u>J. Am. Chem. Soc.</u> **113**, 6499 (1991).

(33) (a) S. Sakaki and K. Ohkubo, <u>Inorg. Chem.</u>, **27**, 2020 (1988). (b) S. Sakaki and K. Ohkubo, <u>Inorg. Chem.</u>, **28**, 2583 (1989). (c) S. Sakaki and K. Ohkubo, <u>Organometallics</u>, **8**, 2970 (1989).

(34) C. Bo and A. Dedieu, <u>Inorg. Chem.</u>, **28**, 304 (1989).

(35) (a) M. J. Frisch, J. S. Binkley, H. B. Schlegel, K. Raghavachari, C. F. Melius, R. L. Martin, J. J. P. Stewart, F. W. Bobrowicz, C. M. Rohlfing, L. R. Kahn, D. J. DeFrees, R. Seeger, R. A. Whiteside, D. J. Fox, E. M. Fluder, S. Topiol, and J. A. Pople, <u>Gaussian 86</u>, Carnegie-Mellon Quantum Chemistry Publishing Unit, Pittsburg, PA, (1986). (b) M. J. Frisch, G. W. Trucks, M. Head-Gordon, P. M. W.

Gill, M. W. Wong, J. B. Foresman, B. G. Johnson, H. B. Schlegel, M. A. Robb, E. S. Replogle, R. Gomperts, J. L. Andres, K. Raghavachari, J. S. Binkley, C. Gonzalez, R. L. Martin, D. J. Fox, D. J. DeFrees, J. Baker, J. J. P. Stewart and J. A. Pople, Gaussian 92, Gaussian, Inc., Pittsburgh, PA, (1992).

(36) P. J. Hay and W. R. Wadt, J. Chem. Phys., **82**, 270 (1985).

(37) S. Huzinaga, J. Andzelm, M. Kobukowski, E. Radzio-Andzelm, Y. Sakai, and H. Tatewaki, "Gaussian Basis Sets for Molecular Calculations," Elsevier, Amsterdam (1984).

(38) T. H. Dunning and P. J. Hay, In Methods of Electronic Structure Theory", ed. by H. F. Schaefer, Plenum, New York (1977), p. 1.

(39) W. J. Hehre, R. F. Stewart, and J. A. Pople, J. Chem. Phys., **51**, 2657 (1969).

(40) P. J. Hay and W. R. Wadt, J. Chem. Phys., **82**, 299 (1985).

(41) This exponent was determined, according to an even-tempered criterion.

(42) A. J. H. Wachters, J. Chem. Phys., **52**, 1033 (1970).

(43) P. J. Hay, J. Chem. Phys. **66**, 4377 (1977).

(44) Original exponents which mainly represent 4p orbitals of Cu were used not directly but after scaling up by a factor 1.5, to make them suitable for molecular calculation.[42]

(45) G. Herzberg, "Molecular Spectra and Molecular Structure," D. Van Nostrand Co. Inc., Princeton, NJ

(1967), vol. 3, p. 610.

(46) (a) P. J. Hay, <u>New. J. Chem.</u>, **15**, 735 (1991). (b) T. Leininger, J. -F. Riehl, G. -H. Jeung, and M. Pélissier, <u>Chem. Phys. Lett.</u>, **205**, 301 (1993).

(47) S. R. Langhoff and E. R. Davidson, <u>Int. J. Quantum Chem.</u>, **8**, 61 (1974).

(48) E. R. Davidson and D. W. Silver, <u>Chem. Phys. Lett.</u>, **52**, 403 (1977).

(49) J. A. Pople, R. Seeger, and R. Krishnan, <u>Int. J. Quantum Chem. Symp.</u> **11**, 149 (1977).

(50) We discuss the exothermicity of $Cu(\eta^1\text{-}OC(O)R)(PH_3)_2$ **5A**, **5B**, or **5C** here, because the final product, $Cu(\eta^2\text{-}O_2CR)(PH_3)_2$, **6A**, **6B** and **6C** are only slightly more stable than **5A**, **5B** and **5C** respectively (see Table 4.2 and Figure 4.6).

(51) Geometries of CO_2 and C_2H_4 were taken to be the same as the distorted structures like in the TSs of their insertion reactions into the Cu-H bond.
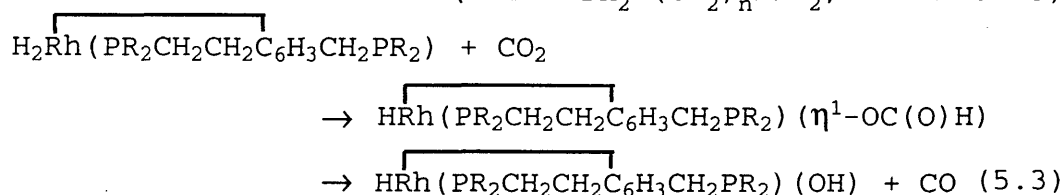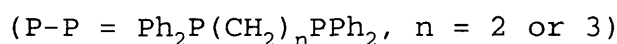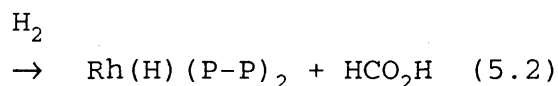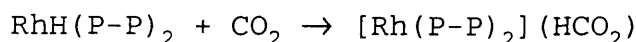
CO_2 Insertion Into a Rh(I)-H Bond

5.1 Introduction

Because insertion reactions of alkene, alkyne, and CO into M-H and M-R bonds are involved as key elementary processes in various catalytic cycles by transition metal complexes,[1] the insertion reaction of CO_2 into M-H and M-R bonds is believed to be of significant importance in transition-metal catalyzed CO_2 conversion into useful chemicals.[2] In this context, detailed knowledge of the insertion reaction of CO_2 is necessary to understanding well the catalytic CO_2 conversion and making its further development. To obtain such knowledge, not only experimental works but also theoretical works should be carried out on the CO_2 insertion because theoretical works can offer meaningful information of changes in geometry, transition state, bonding nature, electron distribution, activation energy etc. However, only a few MO studies have been reported on the insertion reactions of CO_2 into Cu(I)-R (R = H or CH_3)[3] and Cr(0)-H bonds.[4]

Besides insertion reactions of CO_2 into the Cu(I)-R and Cr(0)-H bonds, the CO_2 insertion reaction into the Rh-R bond (R = H, CH_3, or Ph) is considered to be important because Rh complexes perform various catalytic reactions.[1] So far several rhodium hydride and rhodium alkyl complexes have been reported to undergo the CO_2 insertion. For instance, CO_2 reacts with $RhPh(PR_3)_3$, yielding $Rh(\eta^1-OC(O)Ph)(PR_3)_3$ and $Rh(\eta^2-O_2CPh)(PH_3)_2$ (eq 5.1).[5] Similar insertion reactions of

$$RhPh(PR_3)_3 + CO_2 \rightarrow Rh(\eta^1\text{-OC(O)Ph})(PR_3)_3 \rightarrow$$

$$Rh(\eta^2\text{-O}_2CPh)(PR_3)_2 + PR_3 \qquad (5.1)$$
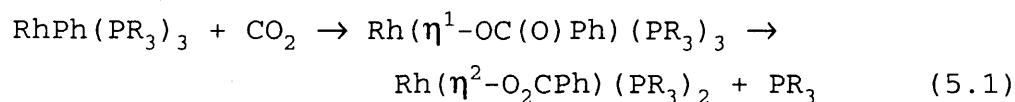
CO_2 into Rh(I)-H and Rh(III)-H bonds are involved as key
processes in catalytic hydrogenation of CO_2 to formic acid
(eq 5.2)[6,7] and catalytic reduction of CO_2 to CO (eq 5.3)[8]

$$RhH(P-P)_2 + CO_2 \rightarrow [Rh(P-P)_2](HCO_2)$$

$$\xrightarrow{H_2} Rh(H)(P-P)_2 + HCO_2H \quad (5.2)$$

$$(P-P = Ph_2P(CH_2)_nPPh_2, \; n = 2 \text{ or } 3)$$

$$H_2\overline{Rh(PR_2CH_2CH_2C_6H_3CH_2PR_2)} + CO_2$$

$$\rightarrow HRh\overline{(PR_2CH_2CH_2C_6H_3CH_2PR_2)}(\eta^1\text{-OC(O)H})$$

$$\rightarrow HRh\overline{(PR_2CH_2CH_2C_6H_3CH_2PR_2)}(OH) + CO \quad (5.3)$$

CO_2 into Rh(I)-H and Also, the reverse reaction of the CO_2
insertion (eq 5.4) has been reported as a key process of the

$$Rh(\eta^1\text{-OC(O)H})(PR_3)_3 \rightarrow Rh(H)(PR_3)_3 + CO_2 \qquad (5.4)$$
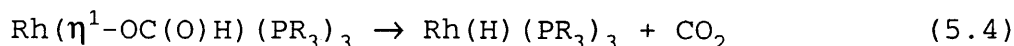
decomposition of formic acid.[9] From these reactions, we can
expect that rhodium complexes serve as an efficient catalyst
for the CO_2 conversion into useful chemicals. Thus, there
is a considerable need to investigate theoretically the CO_2
insertion into the Rh-R bond.

In the present chapter, the insertion reaction of CO_2
into the Rh(I)-H bond of $RhH(PH_3)_3$ (eq 5.5) is investigated

$$RhH(PH_3)_3 + CO_2 \rightarrow Rh(\eta^1\text{-OC(O)H})(PR_3)_3 \qquad (5.5)$$
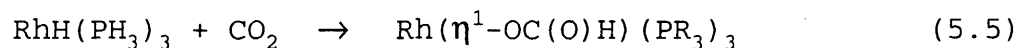
with ab initio MO/MP4, SD-CI and coupled cluster methods.
This reaction (eq 5.5) is selected here as a model of eqs
5.1 and 5.4. Purposes in this chpater are (1) to present
detailed understanding of this insertion reaction, (2) to
evaluate theoretically the activation energy and the energy
of reaction, and (3) to compare this insertion reaction with

a similar insertion reaction of CO_2 into the Cu(I)-H bond
(see, chapter 4).[3] Through this investigation, we hope to

$$CuH(PH_3)_2 + CO_2 \rightarrow Cu(\eta^1-OC(O)H)(PH_3)_2$$

$$\rightarrow Cu(\eta^2-O_2CH)(PH_3)_2 \qquad (5.6)$$
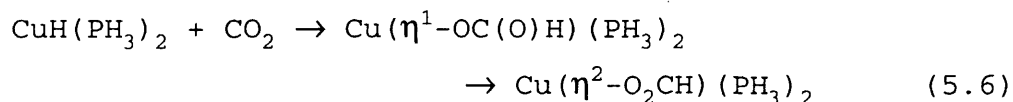
clarify differences between Cu(I) and Rh(I) in the CO_2
insertion reaction.

5.2 Computational Details

Ab Initio MO/MP4SDQ, SD-CI and coupled cluster with
double excitations (CCD) calculations were carried out by
means of Gaussian 86[10] and 92[11] programs, using several kinds
of basis sets (BS). In the BS I, core electrons (up to 4p)
of Rh were replaced with Hay-Wadt's effective core
potentials (ECP1), and valence orbitals (4d, 5s and 5p) were
represented with a (3s 3p 4d)/[2s 2p 2d] set.[12] For C and O,
MIDI-3 sets were adopted,[13] while STO-2G was used for PH_3.[14]
A (4s)/[2s] basis set[15] was employed for the active H atom
that coordinated to Rh first and then reacted with CO_2. In
the BS II, valence orbitals of Rh were represented with
almost the same basis set (3s 3p 4d)/[2s 2p 3d] as in the BS
I, and the ECP1 was used for core electrons (up to 4p) of
Rh.[12] MIDI-4[13] sets were used for C, O and P, and the
(4s)/[2s] set[15] was employed for H. Only for the active H
atom, a p-polarization function ($\zeta = 1.0$) was added.[15] In
the BS III, core electrons (up to 3d) were replaced with
Hay-Wadt's effective core potentials (ECP2), and valence
orbitals (4s, 4p, 4d, 5s and 5p) were represented with a
(5s 5p 4d)/[3s 3p 3d] set.[16] For H, C, O and P, the same
basis sets as those of the BS II were adopted. In the BS
IV, not ECP but an all electron basis set (16s 12p 8d)/[6s 5

p 4d] was used for Rh,[13] where two p primitive functions[13] and one d primitive function ($\zeta = 0.08$)[17] were added to represent well valence 5p and 4d orbitals respectively. In the BS V, (9s 5p)/[3s 2p] sets were adopted for C and O,[16] while the same basis sets as those in the BS IV were used for the other atoms.

Geometries of reactants, transition state (TS) and products were optimized at the Hartree-Fock (HF) level with the energy gradient technique, using the BS I,[18] where the geometry of PH_3 was taken to be the same as the experimental structure of a free PH_3 molecule.[19,20] The TS was determined by evaluating the hessian matrix. MP2 ~ MP4SDQ, SD-CI and CCD calculations were carried out with all core orbitals excluded from an active space. In SD-CI calculations, contributions from higher order excited configurations were estimated, according to Davidson-Silver[21] and Pople et al.[22] In the CCD calculations, the contribution of single and triple excitations were evaluated through forth order using double excitation wave functions. Instability of HF wave functions[23] was not observed for all the reactants, TS, and product.[24] Because solvent effects were not considered here, the present computations are meaningful because CO_2 insertion into Rh(I)-H bond of $RhH(PH_3)_3$ was carried out in non-polar solvent.[5,8]

In order to investigate bonding nature at the TS, we carried out energy decomposition analysis proposed by Morokuma et al.[25] In this analysis, the interaction energy (INT) is defined as the stabilization energy of the reaction system relative to reactants, CO_2 and $RhH(PH_3)_3$, taking the distorted structures like in the TS (see eq 5.7). The

deformation energy (DEF) is defined as the destabilization energy which is necessary to distort CO_2 and $RhH(PH_3)_3$ from their equilibrium structures to their distorted ones taken in the TS (see eq 5.8);

$$INT = E_t[RhH(PH_3)_3 \bullet\bullet\bullet CO_2]_{TS} - E_t[RhH(PH_3)_3]_{dist}$$
$$- E_t(CO_2)_{dist} \qquad (5.7)$$

$$DEF = E_t[RhH(PH_3)_3]_{dist} - E_t[RhH(PH_3)_3]_{eq}$$
$$+ E_t(CO_2)_{dist} - E_t(CO_2)_{eq} \qquad (5.8)$$

The sum of INT and DEF corresponds to the activation energy (E_a) relative to reactants (eq 5.9). INT is further divided into several chemically meaningful terms, as shown in eq

$$E_a = INT + DEF$$
$$= E_t[RhH(PH_3)_3 \bullet\bullet\bullet CO_2]_{TS} - E_t[RhH(PH_3)_3]_{eq}$$
$$- E_t(CO_2)_{eq} \qquad (5.9)$$

$$INT = ES + EX + CTPLXA \ (RhH(PH_3)_3 \ --> \ CO_2)$$
$$+ CTPLXB \ (CO_2 \ --> \ RhH(PH_3)_3) + R \qquad (5.10)$$

5.10. ES is the electrostatic term arising from the coulombic interaction between $RhH(PH_3)_3$ and CO_2. EX is the exchange repulsion due to Pauli exclusion principle. CTPLXA consists of the charge-transfer from $RhH(PH_3)_3$ to CO_2, the polarization of CO_2, and their coupling terms. CTPLXB consists of the charge-transfer from CO_2 to $RhH(PH_3)_3$, the polarization of $RhH(PH_3)_3$ and their coupling terms. R is a higher order coupling term. From the definition, a negative value means stabilization in energy for all these terms. Although this analysis is based on the HF approximation,[25] bonding nature of the TS is expected to be successfully investigated with this analysis because the activation energy of this insertion reaction is not influenced very much by electron correlation, as will be described below.

The IMSPAC program was used for this analysis.[26]

5.3 Results and Discussion

5-3-1 Geometries of Precursor Complex, Transition State and Product

In many catalytic reactions by transition metal complexes, a substrate first coordinates to (or interacts with) a transition metal complex, to form a precursor complex before reaching the TS. We will mention the precursor complex, first. In the precursor complex (**2** in Figure 5.1), CO_2 is considerably distant from Rh, and both $RhH(PH_3)_3$ and CO_2 parts little distort (compare **2** with **1**), suggesting that an interaction between Rh and CO_2 is very weak (vide infra). These features are also observed in the insertion reaction of CO_2 into the Cu(I)-H bond as described in chapter 4.[27,28] When a substrate strongly coordinates to Rh(I), the precursor complex is a d^8 five-coordinate system. In such a case, there are many possible isomers including trigonal bipyramidal and square pyramidal structures, and the reaction course of the CO_2 insertion is much complicated in the trigonal bipyramidal structure, as has been theoretically investigated in the insertion reaction of ethene into the Rh(I)-H bond of $RhH(CO)_2(PH_3)(C_2H_4)$.[29] In the present case, however, we do not need to consider a five-coordinate trigonal bipyramidal structure because the interaction between CO_2 and Rh(I) is very weak.

In the transition state (TS), the C-H distance between $RhH(PH_3)_3$ and CO_2 is 1.46 Å, the Rh-H distance slightly lengthens by only 0.12 Å and the H ligand barely moves downward from the RhP_3 plane (see **3—TS** of Figure 5.1).[30]
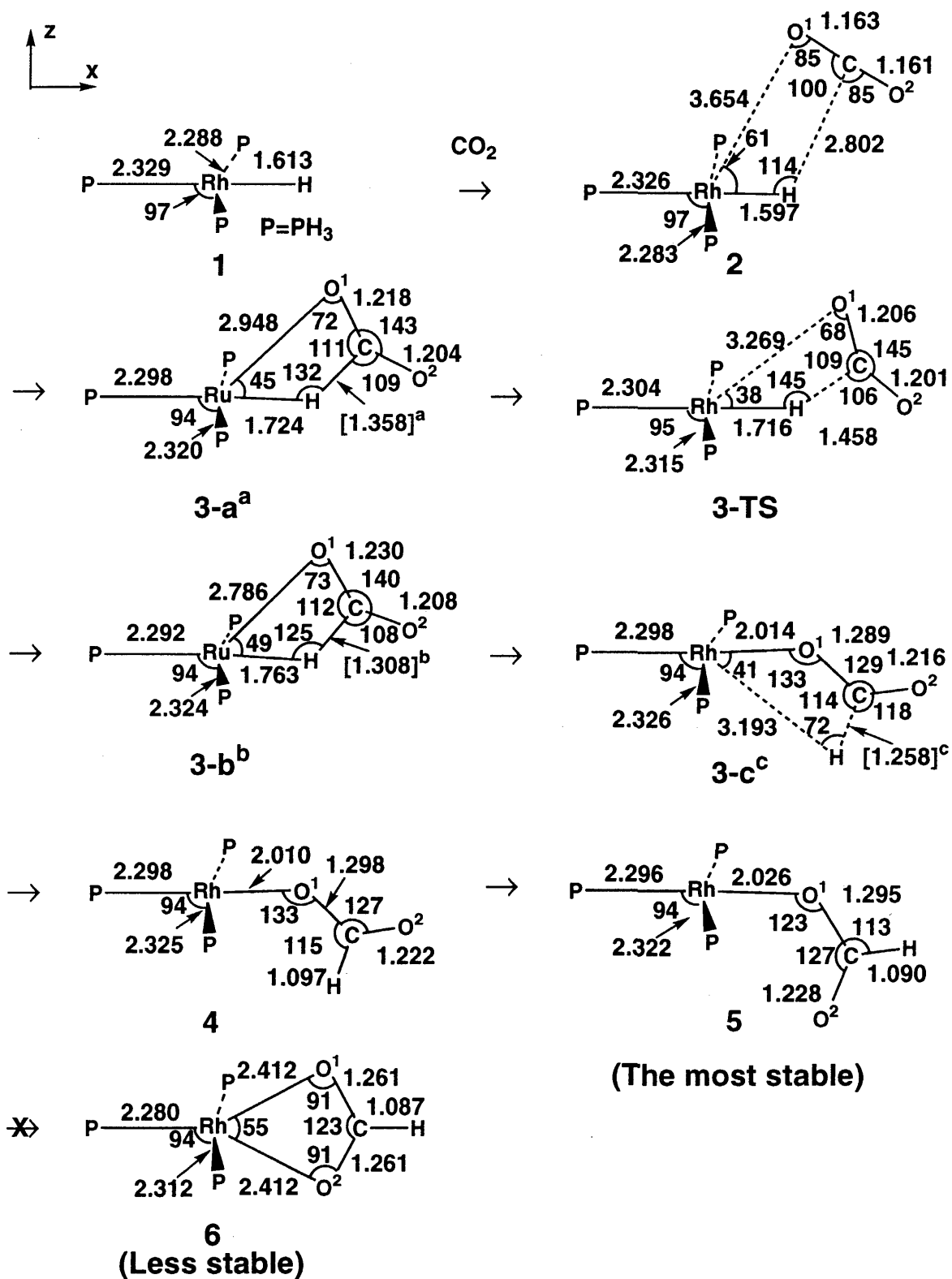
Figure 5.1 Geometry changes in the CO_2 insertion into a Rh(I)-H bond of $RhH(PH_3)_3$. Bond distance in Å and bond angle in degree. a), b), and c) The geometry was optimized under assumption that R(C-H) was 1.358, 1.308, and 1.258 A for a), b), and c), respectively.

130

These geometrical features of the TS are common in both insertion reactions of CO_2 into Rh(I)-H and Cu(I)-H bonds.[3][b,27,31] Interesting differences are, however, observed between them; the C-H distance (1.46 Å) between CO_2 and $RhH(PH_3)_3$ is shorter than that (1.68 Å) of the Cu reaction system, indicating that the TS of the Rh reaction system is more product-like than that of the Cu reaction system. Nevertheless, the Rh(I)-O^1 distance (3.27 Å) is much longer than the Cu(I)-O^1 distance (2.50 Å), and the RhHC angle (145°) is much larger than the CuHC angle (105°). The C-O^1 distance (1.21 Å) is almost equal to the C-O^2 distance (1.20 Å) in the Rh reaction system, while the C-O^1 distance (1.21 Å) is longer than the C-O^2 distance (1.18 Å) in the Cu reaction system. These differences indicate that the Cu-O^1 bond is partially formed but the Rh-O^1 bond is not formed yet at the TS. It should be, therefore, reasonably concluded that a four-center type interaction is hardly involved in the TS of the Rh reaction system but involved in the TS of the Cu reaction system.[3b]

Geometry changes after the TS were examined, shortening the C-H distance between CO_2 and $RhH(PH_3)_3$ to 1.358 Å, 1.308 Å and 1.258 Å. The reaction system is getting similar to the product **4**, as the C-H distance is getting shorter (see **3-a**, **3-b** and **3-c** in Figure 5.1). This geometry change suggests that although a four-center type interaction is not formed at the TS, the CO_2 insertion yields the Rh-(η^1-OC(O)H) species as the product.

In the product, there are three possible structures, as shown in Figure 5.1. **4** and **5** include a monodentate η^1-formate ligand and **6** a bidentate η^2-formate ligand. Of

them, **5** is the most stable, as will be discussed below.

In a recent experiment,[6] CO_2 reacts with a five-coordinate rhodium(I)-hydride complex, $[RhH(P-P)_2]$ $(P-P = Ph_2(CH_2)_nPPh_2$, n = 2 or 3), in DMSO, affording not a Rh-$(\eta^1$-OC(O)H) species but $[Rh(P-P)_2](HCO_2)$ in which formate exists as a counter anion (eq 5.2). This experimental result is consistent with the geometrical feature of the TS presented here; because the Rh-O^1 bond is hardly formed at the TS, the insertion reaction of CO_2 into the Rh(I)-H bond would not always yield a Rh-$(\eta^1$-OC(O)H) species but yield a free formate anion when coordinating species (coordinating solvent, four phosphine ligands per Rh etc.) exist in the reaction system.

Table 5.1 Basis set effects on the activation energy (E_a) and the exothermicity (E_{exo}) at the HF level for the CO_2 insertion into the Rh(I)-H bond of $RhH(PH_3)_3$ (kcal/mol)

	BS I	BS II	BS III	BS IV	BS V
$E_a{}^a$	9.3	14.3	13.3	12.2	11.2
$E_{exo}{}^b$	42.5	37.3	34.9	37.3	38.2

a) $E_a = E_t(TS) - E_t(precursor, \mathbf{2})$.
b) $E_{exo} = E_t(\mathbf{1} + CO_2) - E_t(\mathbf{5})$.

5-3-2 Activation Energy (E_a) and Exothermicity (E_{exo})

Prior to detailed discussion of E_a and E_{exo}, basis set effects on E_a and E_{exo} will be mentioned here, where E_a is defined as an energy difference between the TS and the precursor complex **2**, and E_{exo} is an energy difference between the final product **5** and the sum of reactants, **1** + CO_2. As shown in Table 5.1, the BS I yields a smaller E_a value and a

larger E_{exo} value than the others. On the other hand, the BS II yields a larger E_a value than the others (note ECP1 was employed in both BS I and BS II). Recently, use of ECP2 has been recommended for calculating energy change.[32,33] Also in our calculations of the CO_2 insertion into the Cu(I)-R bond,[27] the BS II yielded much different E_{exo} value from the value calculated with the BS III. Thus, it is necessary to use the BS III or a better one in investigating the CO_2 insertion into the Rh(I)-H bond. In the present work, the BS IV was mainly used, except that the BS III was used in comparing several computational methods at the correlated level.

Then we will examine electron correlation effects on the E_a and the energy of reaction (ΔE). As clearly shown in Table 5.2, introduction of electron correlation somewhat increases the E_a value, but considerably decreases the exothermicity (the negative ΔE means the exothermicity). Thus, introduction of electron correlation is indispensable for quantitative estimation of E_a and ΔE. The other important result to be noted is that MP2 and MP3 methods are not reliable in investigating the CO_2 insertion, because E_a and ΔE significantly fluctuate at MP2 and MP3 levels. On the other hand, MP4DQ, MP4SDQ, and SD-CI calculations yield similar E_a values, while the ΔE values at the SD-CI level are a little bit larger than the value at the MP4SDQ level. In Table 5.3, we can also see that SD-CI and CCD calculations yield almost the same E_a value and that the E_{exo} value calculated at the CCD level is intermediate between E_{exo} values at MP4SDQ and SD-CI levels. Thus, the method of higher quality than MP4 should be applied to the present

Table 5.2 Electron correlation effects on energy changes[a] by the CO_2 insertion into a Rh(I)-H bond

compd		HF	MP2	MP3	MP4 DQ	MP4 SDQ	SDCI(DS)[b]	SDCI(P)[c]
RhH(PH$_3$)$_2$ + CO$_2$	**1**[d]	0.0[e]	0.0[f]	0.0[g]	0.0[h]	0.0[i]	0.0[j]	0.0[k]
Precursor complex	**2**	-1.6	-3.3	-3.3	-3.1	-3.2	-3.4	-3.3
TS	**3-TS**	11.7	14.8	9.8	13.5	12.4	12.8	12.8
		(13.3)	(18.1)	(13.1)	(16.6)	(15.6)	(16.2)	(16.1)
Rh(η^1-OC(O)H)(PH$_3$)$_3$	**4**	-29.0	-1.0	-20.1	-11.3	-9.7	-16.2	-16.5
	5	-34.9	-6.7	-25.9	-17.0	-15.3	-22.0	-22.4
Rh(η^2-O$_2$CH)(PH$_3$)$_3$	**6**	-21.7	2.5	-15.4	-6.8	-6.3	–	–

a) BS-III was used. b) Correction by Davidson and Silver for higher order excitations.[20] c) Correction by Pople et al. for higher order excitations.[21]

d) See Figure 5.1 for these numbers.

e) E_t(HF) = -1322.6328. f) E_t(MP2) = -1323.3920. g) E_t(MP3) = -1323.3619.

h) E_t(MP4DQ) = -1323.4118. i) E_t(MP4SDQ) = -1323.4400. j) E_t(SDCI(DS)) = -1323.4231. k) E_t(SDCI(P)) = -1323.4118 (hartree unit for all these total energies. l) In paretheses; energy difference between **2** and **3-TS**, which corresponds to the activation energy.

Table 5.3 Stabilization energy of a precursor complex, BE, activation energy, E_a, and exothermicity, E_{exo}, of the CO_2 insertion into Rh(I)-H and Cu(I)-H bonds (kcal/mol)[a]

| | RhH(PH_3)$_3$ | | | CuH(PH_3)$_2$[34] | | |
	BE	$E_a{}^b$	$E_{exo}{}^b$	BE	$E_a{}^b$	$E_{exo}{}^b$
HF	1.5	12.2	-37.3	3.5	3.7	-51.4
MP4DQ	3.2	21.0	-17.8	4.5	5.9	-43.6
MP4SDQ	3.2	20.5	-15.6	4.4	7.1	-40.1
SDCI(DS)	3.5	15.7	-24.0	5.0	3.5	-39.4
SDCI(P)	3.5	15.6	-24.2	5.0	3.6	-39.7
CCD[c]	3.1	15.9	-18.7	---	---	---

a) The BS IV was used. E_t of RhH(PH_3)$_2$ + CO_2 is -5896.1584 at HF, -5896.9380 at MP4DQ, -5896.9676 at MP4SDQ, -5896.9066 at SDCI(DS), -5896.8954 at SDCI(P), and -5898.9824 at CCD (hartree unit). E_t of CuH(PH_3)$_2$ + CO_2 is -2509.2300 at HF, -2510.0240 at MP4DQ, -2510.0713 at MP4SDQ, -2510.0162 at SDCI(DS), and -2510.0057 at SDCI(P) (hartree unit).

b) See footnotes a) and b) of Table 1 for the definition.

c) The contribution of single and triple excited configurations is evalueted through double excited configurations.

study. The SD-CI method was mainly used in comparing the Rh reaction system with the Cu reaction system.

As given in Table 5.3, the stabilization energy (BE) of the precursor complex is very small at all computational levels adopted here. This small stabilization energy is consistent with the long Rh-CO_2 distance and the very small distortion of RhH(PH_3)$_3$ and CO_2 parts (vide supra). This is not surprising because a coordinate bond of CO_2 with a transition metal is, in general, weak. The activation

energy was calculated to be ca. 12 kcal/mol at the HF level and ca. 16 kcal/mol at the SD-CI level (after correction of higher order excited configurations). This activation energy is considerably higher than that of the CO_2 insertion into the Cu(I)-H bond (3.5 kcal/mol).[34]

Before discussing the energy of reaction, we must examine the relative stabilities of the products. As shown in Table 5.2, **5** is the most stable, **4** is the next and **6** is the least stable at HF, MP2 - MP4SDQ and SD-CI levels. These relative stabilities differ from those of the products in the CO_2 insertion into the Cu(I)-H bond of $CuH(PH_3)_2$. This difference is easily interpreted in terms of the electron configurations of Rh(I) and Cu(I); Rh(I) prefers a four-coordinate square planar structure, **5**, to a five-coordinate pseudo-trigonal bipyramid structure, **6**, due to its d^8 electron configuration, whereas Cu(I) prefers a four-coordinate pseudo-tetrahedral structure due to its d^{10} electron configuration. In a recent experiment of the CO_2 insertion into the Rh(I)-Ph bond of $RhPh(PR_3)_3$,[5] the η^1-formate species is formed first and then it converts to the η^2-formate species after one PR_3 ligand dissociates from Rh (eq 5.1). Our calculation is consistent with this experimental result.

For the Rh reaction system, the exothermicity is calculated to be 24 kcal/mol at the SD-CI level and 19 kcal/mol at the CCD level (Table 5.3). This value is much smaller than the exothermicity of the CO_2 insertion into the Cu(I)-H bond (ca. 40 kcal/mol).[3b,34] Comparing the E_a and E_{exo} values between Rh and Cu reaction systems, we can conclude that the CO_2 insertion into the Rh(I)-H bond occurs less

136

easily than the CO_2 insertion into the Cu(I)-H bond of $CuH(PH_3)_2$.

5-3-3 Electron Redistribution in the CO_2 Insertion and Bonding Interactions at the Transition State

Changes in Mulliken populations are shown in Figure 5.2, in which several interesting features are observed, as follows: (1) Electron population of CO_2 considerably increases, while Rh and Cu atomic populations remarkably decrease, indicating that the charge transfer from $RhH(PH_3)_3$ to CO_2 is important in the CO_2 insertion. (2) The O^1 and O^2 atomic populations increase more than the C atomic population in both Rh and Cu reaction systems. This electron redistribution arises from the orbital mixing in which the π orbital of CO_2 mixes into the bonding overlap between the π^* orbital of CO_2 and HOMO of $RhH(PH_3)_3$. This kind of orbital mixing is in general observed in transition-metal CO_2 complexes and their reactions. Detailed explanation has been presented in our previous works[3,35] and is omitted here. (3) In the Rh reaction system, the H atomic population increases at the TS, unexpectedly. Because the electron population of CO_2 considerably increases at the TS, the increase in the H atomic population cannot be attributed to the charge-transfer from CO_2 to $RhH(PH_3)_3$. One plausible explanation is that the $\delta+$ charge on the C atom of CO_2 causes the polarization of $RhH(PH_3)_3$ in which electrons are accumulated on the H ligand so as to strengthen the $C^{\delta+} \bullet\bullet\bullet H^{\delta-}$ coulombic interaction between CO_2 and $RhH(PH_3)_3$. In the Cu reaction system, on the other hand, the H atomic population
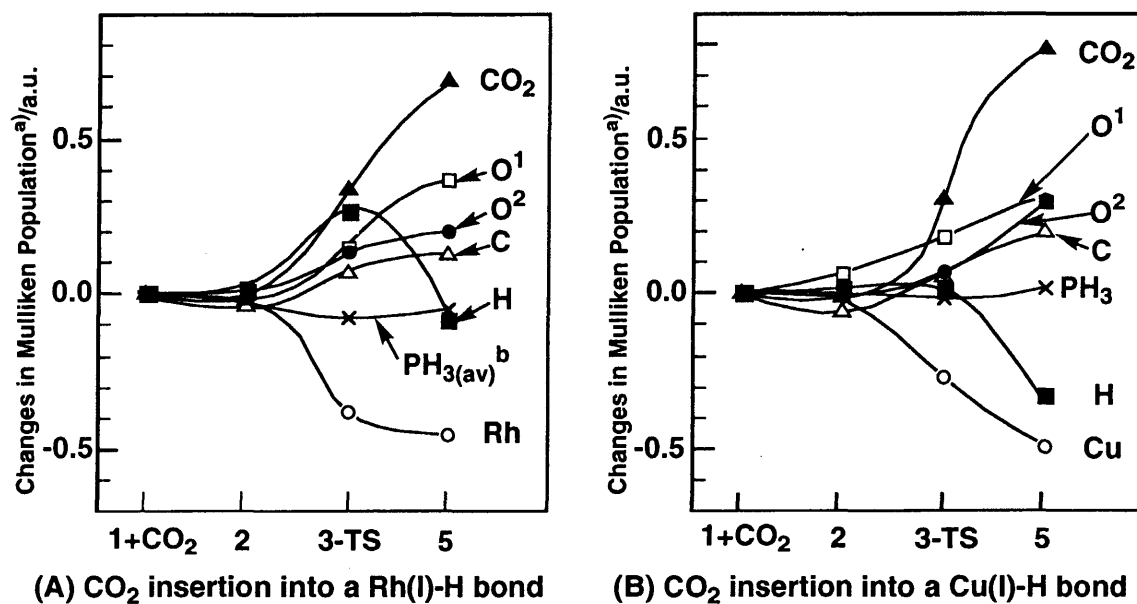
Figure 5.2 Changes in Mulliken population[a] in the CO_2 insertion into a $Rh(I)$-H or $Cu(I)$-H bond.

a) A positive value means an increase in population. The infinite separation between CO_2 and $RhH(PH_3)_3$ is taken to be the standard (change 0). The BS IV was used. b) The averaged value of three PH_3 ligands.

hardly increases at the TS (Figure 5.2B). This difference suggests that $RhH(PH_3)_3$ is much more polarizable than $CuH(PH_3)_2$, which will be discussed below in more detail.

To inspect the bonding interaction at the TS, energy decomposition analysis was performed, as shown in Tables 5.4 and 5.5 The ES stabilization cannot overwhelm the EX repulsion, as is often found in the reactions of transition metal complexes.[3b,36] This means that the static interaction, which corresponds to the sum of ES and EX, is

Table 5.4 Energy decomposition analysis of an interaction between CO_2 and $MH(PH_3)_n$ (M = Cu or Rh, n = 2 or 3) at the transition state (TS) (kcal/mol)[a]

θ[b]	RhH(PH$_3$)$_3$···CO$_2$		CuH(PH$_3$)$_2$···CO$_2$	
	145° (TS)	106°[c]	145° (TS)	106°[c]
ΔE	10.6	23.1 (19.2)[d]	5.1	0.4
DET total	25.7	25.7 (25.7)	21.7	21.7
MH(PH$_3$)$_n$	0.8	0.8 (0.8)	2.1	2.1
CO$_2$	24.9	24.9 (24.9)	19.6	19.6
INT	-15.1	-2.6 (-6.5)	-16.6	-21.3
ES	-55.9	-103.6 (-63.0)	-47.5	-71.0
EX	106.5	189.3 (105.7)	70.5	101.7
CTPLXA (MH(PH$_3$)$_n$→CO$_2$)	-44.7	-59.3 (-35.2)	-28.6	-37.9
CTPLXB (CO$_2$→MH(PH$_3$)$_n$)	-13.8	-20.7 (-10.8)	-7.4	-8.9
R	-7.2	-8.4 (-3.2)	-3.6	-5.2

a) The BS IV was used. A positive value means destabilization in energy (vice versa). b) The MHC angle (see Figure 5.1).

c) The only θ angle (= the MHC angle) is changed with the geometry of the other part unchanged.

d) In parentheses; The C-H distance between CO_2 and RhH(PH$_3$)$_3$ is lengthend to 1.678 Å which is the C-H distance in the TS of the Cu reaction system.

Table 5.5 Partitioning of population changes[a] at the
transition state

|	RhH(PH$_3$)$_3$				CuH(PH$_3$)$_2$			
	Rh	H	PH$_{3(av)}$	CO$_2$	Cu	H	PH$_3$	CO$_2$
EX	0.013	-0.024	0.008	0.000	-0.014	0.013	0.001	0.000
CTPLXA	-0.152	-0.134	-0.014	0.329	-0.140	-0.163	0.000	0.303
CTPLXB	-0.425	0.476	-0.045	-0.023	-0.170	0.198	0.008	-0.038

a) Difference from the population at the infinite separation between CO$_2$
and MH(PH$_3$)$_n$ (M = Cu or Rh, n = 2 or 3). A positive value means an
increase in the population (vice versa).

repulsive and the contribution from the CTPLXA and CTPLXB
terms is necessary to stabilize the TS of the CO$_2$ insertion
reaction. CTPLXA yields much greater stabilization than
CTPLXB. This result is consistent with the electron
redistribution discussed above, since the CTPLXA term
includes the charge-transfer from RhH(PH$_3$)$_3$ to CO$_2$ as a main
contributor. Actually, the electron population of CO$_2$
increases but atomic populations of Rh and H decrease
through this term (Table 5.5). Although the CTPLXB
stabilization is small, its contribution cannot be
neglected. The electron population of CO$_2$ is little
decreased, the Rh atomic population is considerably
decreased but the H atomic population is remarkably
increased by this term (Table 5.5). These results indicate
that the charge-transfer from CO$_2$ to RhH(PH$_3$)$_3$ does not
contribute to the CTPLXB term very much but the polarization
of RhH(PH$_3$)$_3$ considerably contributes to this term. In the
Cu reaction system, the H atomic population increases

through this term to a much lesser extent than in the Rh reaction system (Table 5.5). This is because $CuH(PH_3)_2$ is much less polarizable than $RhH(PH_3)_3$. The increase in the H atomic population through the CTPLXB term is almost compensated by its decrease through the CTPLXA term (Table 5.5). Thus, the H atomic population hardly changes at the TS of the Cu reaction system, as has been shown in Figure 5.2B.

5-3-4 Differences Between $RhH(PH_3)_3$ and $CuH(PH_3)_2$ in the CO_2 Insertion Reaction

One of the great differences between these two reaction systems is that the CO_2 insertion into the Rh(I)-H bond is much less exothermic than the insertion into the Cu(I)-H bond (Table 5.3). The exothermicity is mainly determined by bond energies. In the CO_2 insertion into the M-H bond, the M-H bond is broken, while the M-OC(O)H and the H-C(O)OM bonds are formed. The formation of the H-C(O)OM bond is common in both insertion reactions of CO_2 into the Rh(I)-H and Cu(I)-H bonds. Thus, the difference in exothermicity mainly arises from Rh(I)-H, Cu(I)-H, Rh(I)-(η^1-OC(O)H) and Cu(I)-(η^1-OC(O)H) bond energies. Considering the assumed

$$[Rh(PH_3)_3]^+ + HCu(PH_3)_2 \rightarrow RhH(PH_3)_3 + [Cu(PH_3)_2]^+ \quad (5.11)$$
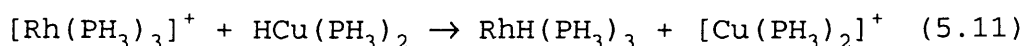
eq 5.10, we can estimate the difference between Rh(I)-H and Cu(I)-H bond energies, as shown in eq 5.11 where $\Delta E_{r-1} =$

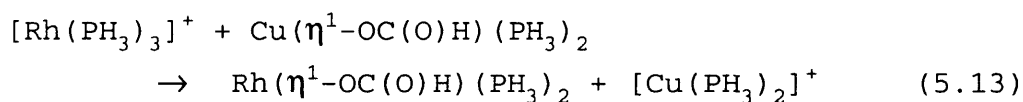$$\Delta E_{r-1} = E(Cu-H) - E(Rh-H) \quad (5.12)$$

E_t(right hand side of eq 5.11) $- E_t$(left-hand side of eq 5.10). Similarly, we can estimate the difference between Rh(I)-(η^1-OC(O)H and Cu(I)-(η^1OC(O)H) bond energies from the following assumed eq 5.11;

141

Table 5.6 Differences in bond energies between Rh(I)-X and Cu(I)-X (X = H or h^1-OC(O)H) (kcal/mol)[a]

	E(Rh-H) −E(Cu-H)	E(Rh-OC(O)H) −E(Cu-OC(O)H)
MP2	37.2	9.2
MP3	29.6	8.1
MP4DQ	30.7	6.9
MP4SDQ	28.3	5.5

a) The BS IV was uwsed.

$$[Rh(PH_3)_3]^+ + Cu(\eta^1\text{-}OC(O)H)(PH_3)_2$$
$$\rightarrow \quad Rh(\eta^1\text{-}OC(O)H)(PH_3)_2 + [Cu(PH_3)_2]^+ \qquad (5.13)$$
$$\Delta E_{r-1} = E(Cu\text{-}OC(O)H) - E(Rh\text{-}OC(O)H) \qquad (5.14)$$

where geometries of $[Cu(PH_3)_2]^+$ and $[Rh(PH_3)_3]^+$ were optimized at the HF level, using the BS I. As shown in Table 5.6, E(Rh-H) is larger than E(Cu-H) by 28-31 kcal/mol at the MP4 level, while E(Rh-OC(O)H) is slightly larger than E(Cu-OC(O)H) by only 6-7 kcal/mol. In the Rh reaction system, therefore, the considerably stronger Rh(I)-H bond is broken but the only slightly stronger Rh(I)-(η^1-OC(O)H) bond is formed than those in the Cu reaction system, which leads to the smaller exothermicity of the Rh reaction system than that of the Cu reaction system.

It should be also noted that the Rh reaction system requires the higher activation energy than the Cu reaction system. The interaction between CO_2 and $MH(PH_3)_n$ (M = Cu or Rh; n = 2 or 3) at the TS was investigated with energy

decomposition analysis (EDA), which was performed at θ (the MHC angle) = 145° and 105°, one corresponding to the TS of the Rh reaction system and the other to the TS of the Cu reaction system. A clear reason for the higher activation energy of the Rh reaction system is not, however, found by comparing these two reaction systems at the same θ value, because the Rh reaction system suffers greater destabilization from DEF and EX terms and greater stabilization from ES, CTPLXA and CTPLXB terms than the Cu reaction system (Table 5.4). To inspect the differences between two reaction systems, we carried out further EDA of the Rh reaction system in which the C-H distance and the RhHC angle were taken to be the same as those of the Cu reaction system (results are given in parentheses of Table 5.4). Comparing this assumed structure of the Rh reaction system with the TS of the Cu reaction system, the Rh reaction system suffers larger destabilization energies from the DEF and EX terms and receives a smaller stabilization energy from the ES term than the Cu reaction system. Thus, the higher activation energy of the former can be attributed to the larger DEF value, the smaller ES stabilization and the larger EX repulsion. The large DEF value is due to the large distortion of the CO_2 part (Table 5.4). In order to break the strong Rh(I)-H bond, CO_2 more strongly interacts with the H ligand in the TS of the Rh reaction system than in the TS of the Cu reaction system, which causes the larger distortion of the CO_2 part in the former than in the latter (Figure 5.1). Thus, the large DEF value of the Rh reaction system is related to the strong Rh(I)-H bond. The smaller ES stabilization is interpreted in terms of the

143
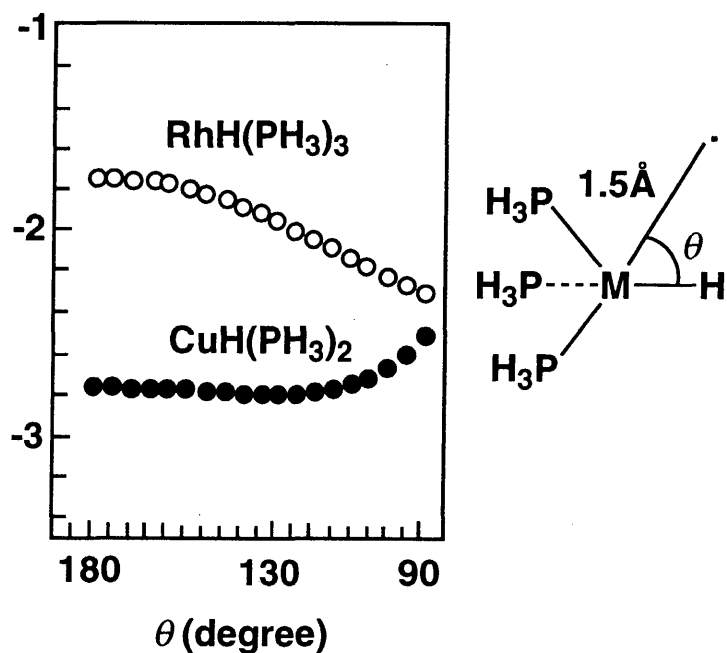
Figure 5.3 Electrostatic potential of $RhH(PH_3)_3$ and $CuH(PH_3)_2$.

a) A positive value means destabilization of positive charge. The BS IV set was used.

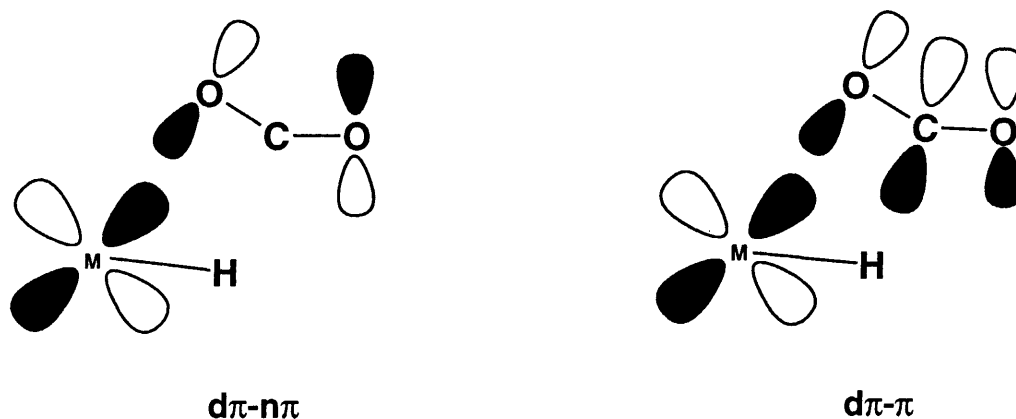electrostatic potential. The electrostatic potentials of $RhH(PH_3)_3$ and $CuH(PH_3)_2$ are compared at the position 1.5 Å distant from the H ligand (Figure 5.3). At both $\theta = 105°$ and 145°, the electrostatic potential of $CuH(PH_3)_2$ is more negative than that of $RhH(PH_3)_3$, probably because the H ligand is more negatively charged in $CuH(PH_3)_2$ (-0.161 e) than in $RhH(PH_3)_3$ (-0.043 e). Because CO_2 exhibits positive electrostatic potential toward the H ligand (Figure 5.4), the Cu reaction system can receive the larger ES stabilization than the Rh reaction system. The greater EX
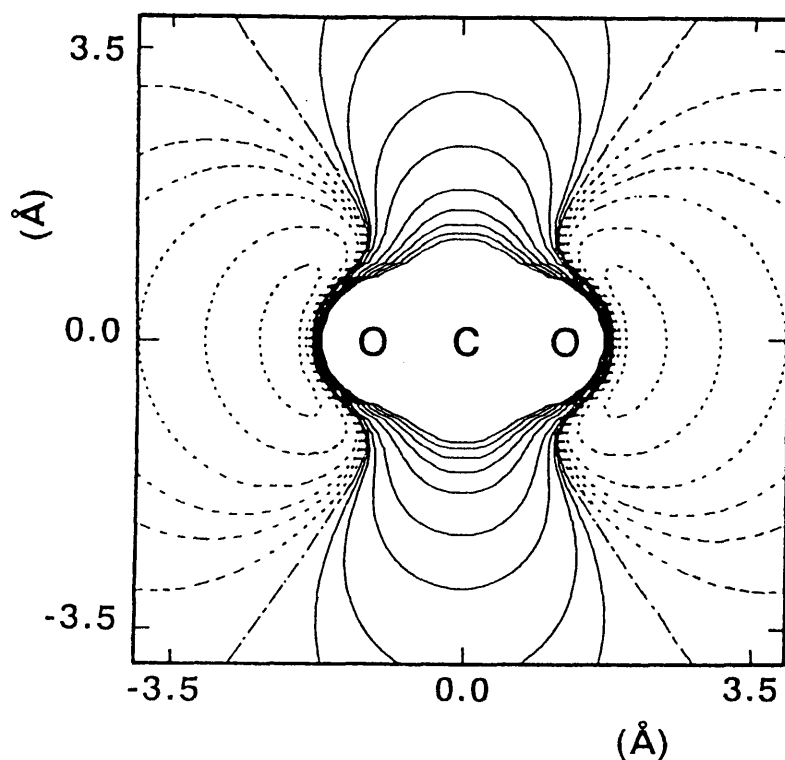
Figure 5.4 Map of electrostatic potential of CO_2

a) The BS IV set was used. Contour values (eV unit) are 0.0, ±0.05, ±0.01, ±0.15, ±0.25, ±1.0, ±1.5, ±2.0, ±2.5, and ±3.0 The solid lines indicate positive values, the dotted lines indicate negative values, and the --- lines indicate the values of 0.0.

repulsion of the Rh reaction system can be understood, considering the occupied $4d_{xz}$ orbital of Rh. In general, the 4d orbital expands to a greater extent than the 3d orbital, and furthermore, the Cu atom possesses the least expanding 3d orbital in the elements of the first transition series. Thus, the Rh $4d_{xz}$ orbital gives rise to larger EX repulsion with the π and $n\pi$ orbitals of CO_2 than the Cu $3d_{xz}$ orbital

dπ-nπ

dπ-π

Scheme 5.1

(Scheme 5.1). These results reasonably lead to a conclusion that the higher activation energy of the Rh reaction system arises from the stronger Rh(I)-H bond, the smaller electrostatic potential of $RhH(PH_3)_3$, and the more largely expanding $4d_{xz}$ orbital of Rh than those of the $CuH(PH_3)_2$.

There are outstanding differences in the TS structure between two reaction systems. The first is that the C-H distance between CO_2 and the H ligand is much shorter in the TS of the Rh reaction system than in the TS of the Cu reaction system (Figure 5.1). This is because CO_2 must interact strongly with the H ligand at the TS of the Rh reaction system, to break the strong Rh(I)-H bond (vide supra). The next is that the RhHC angle is much larger than the CuHC angle (vide supra). As clearly shown in Table 5.4, both destabilization from the EX term and stabilization from the ES and CTPLXA terms increase, as the θ angle becomes small. The increase of the EX repulsion energy cannot be

146

overwhelmed by the increases of ES and CTPLXA stabilization
energies in the Rh reaction system but can be in the Cu
reaction system. This difference is easily explained, as
follows. The decrease in θ enlarges the overlap of the Rh
$4d_{xz}$ orbital with the π and $n\pi$ orbitals of CO_2 (Scheme I),
which increases the EX repulsion between them. Because of
the smaller expanse of the Cu 3d orbital (vide supra), the
EX repulsion is intrinsically weak in the Cu reaction
system. Thus, the decrease in θ strengthens the exchange
repulsion of the Cu reaction system to a lesser extent than
that of the Rh reaction system. Accordingly, the θ angle is
large at the TS of the Rh reaction system but small at the
TS of the Cu reaction system. Although the dependence of ES
and CTPLXA terms on the θ angle can be explained in terms of
the electrostatic potential and the expanse of d_{xz} orbital,
we leave the explanation here, because their dependence is
not the point in main discussion.

5.4 Conclusions

The CO_2 insertion into the Rh(I)-H bond easily occurs
with an activation barrier of ca. 16 kcal/mol and
exothermicity of ca. 24 kcal/mol (at the SD-CI level),
yielding $Rh(\eta^1-OC(O)H)(PH_3)_3$. This activation barrier is
higher and the exothermicity is lower than those of the
similar CO_2 insertion into the Cu(I)-H bond of $CuH(PH_3)_2$ (E_a
= 3.5 kcal/mol and E_{exo} = ca. 40 kcal/mol at the SD-CI
level). The higher activation energy of the Rh reaction
system results from the facts that the Rh(I)-H bond is
stronger than the Cu(I)-H bond, the negative electrostatic
potential of $RhH(PH_3)_3$ is smaller than that of $CuH(PH_3)_2$, and

the EX repulsion between CO_2 and $RhH(PH_3)_3$ is greater than that between CO_2 and $CuH(PH_3)_2$. The lower exothermicity is due to the stronger Rh(I)-H bond. The TS of the Rh reaction system has a shorter C-H distance between CO_2 and the H ligand than the TS of the Cu reaction system. The strong Rh(I)-H bond is the reason for the short C-H distance; in the TS of the Rh reaction system, CO_2 must approach the H ligand to a greater extent than in the TS of the Cu reaction system, so as to break the strong Rh(I)-H bond. The θ angle at the TS is much different between two reaction systems; this angle is 145° in the Rh reaction system but only 105° in the Cu reaction system. The larger RhHC angle of the Rh reaction system arises from the strong EX repulsion between the $4d_{xz}$ orbital of Rh and the π and $n\pi$ orbitals of CO_2. The Rh $4d_{xz}$ orbital more expands than the Cu $3d_{xz}$ orbital, which gives rise to the stronger EX repulsion in the Rh reaction system. From these results, we can predict that the CO_2 insertion into the M-H bond easily occurs when the M-H bond is weak, the electrostatic potential of the metal hydride complex is negatively large, and the expanse of the d_π orbital is small.

References

(1)   (a) F. R. Hartley and S. Patai, "The Chemistry of Metal-Carbon Bonds," John Wiley & Sons, New York (1985), vol.3. (b) R. H. Crabtree, "The Organometallic Chemistry of Transition Metals," John Wiley & Sons, New York (1988).

(2)   (a) D. J. Darensbourg and R. A. Kudaroski, <u>Ad. Organomet. Chem.</u>, **22**, 129 (1983). (b) A. Behr, <u>Angew. Chem., Int. Ed. Engl.</u>, **27**, 661 (1988).

(3)   (a) S. Sakaki and K. Ohkubo, <u>Inorg. Chem.</u>, **27**, 2020 (1988). (b) S. Sakaki and K. Ohkubo, <u>Inorg. Chem.</u>, **28**, 2583 (1989). (c) S. Sakaki and K. Ohkubo, <u>Organometallics</u>, **8**, 2970 (1989).

(4)   C. Bo and A. Dedieu, <u>Inorg. Chem.</u>, **28**, 304 (1989).

(5)   D. J. Darensbourg, G. Grötsch, P. Wiegreffe, and A. L. Rheingold, <u>Inorg. Chem.</u>, **26**, 3827 (1987).

(6)   T. Burgemeiser, F. Kastner, and W. Leitner, <u>Angew. Chem., Int. Ed. Engl.</u>, **32**, 739 (1993).

(7)   J. -C. Tsai and K. M. Nicholas, <u>J. Am. Chem. Soc.</u>, **114**, 5117 (1992).

(8)   W. C. Kaska, S. Nemeh, A. Shiraze, and S. Potunik, <u>Organometallics</u>, 1988, **7**, 13.

(9)   S. H. Strauss, K. H. Whitmire, and D. F. Shriver, <u>J. Organomet. Chem.</u>, **174**, C59 (1979).

(10)   M. J. Frisch, J. S. Binkley, H. B. Schlegel, K. Raghavachari, C. F. Melius, R. L. Martin, J. J. P. Stewart, F. W. Bobrowicz, C. M. Rohlfing, L. R. Kahn, D. J. DeFrees, R. Seeger, R. A. Whiteside, D. J. Fox, E. M. Fluder, S. Topiol, and J. A. Pople,

Gaussian 86, Carnegie-Mellon Quantum Chemistry Publishing Unit; Pittsburg, PA (1986).

(11)   M. J. Frisch, G. W. Trucks, M. Head-Gordon, P. M. W. Gill, M. W. Wong, J. B. Foresman, B. G. Johnson, H. B. Schlegel, M. A. Robb, E. S. Replogle, R. Gomperts, J. L. Andres, K. Raghavachari, J. S. Binkley, C. Gonzalez, R. L. Martin, D. J. Fox, D. J. DeFrees, J. Baker, J. J. P. Stewart, and J. A. Pople, Gaussian 92, Gaussian Inc., Pittsburgh, PA (1992).

(12)   P. J. Hay and W. R. Wadt, J. Chem. Phys., **82**, 270 (1985).

(13)   S. Huzinaga, J. Andzelm, M. Klobukowski, E. Radzio-Andzelm, Y. Sakai, and H. Tatewaki, "Gaussian basis sets for molecular calculations," Elsevier, Amsterdam (1984).

(14)   W. J. Hehre, R. Ditchfield, R. F. Stewart, and J. A. Pople, J. Chem. Phys., **52**, 2769 (1970).

(15)   T. H. Dunning and P. J. Hay, "Methods of Electronic Structure Theory," ed. by H. F. Schaefer, Plenum, New York (1977), p. 1.

(16)   P. J. Hay and W. R. Wadt, J. Chem. Phys., **82**, 299 (1985).

(17)   This value was determined, according to an even-tempered criterion.

(18)   (a) The HF optimization with BS I offers reasonable geometries; For $Rh(CO)(PH_3)_2(\eta^1-OCO_2H)$, $R(Rh-O) = 2.009$ (2.075), $R(Ph-P) = 2.338$ (2.333), $R(Rh-CO) = 1.826$ (1.798), and for $RhH_2(PH_3)_2(\eta^2-O_2COH)$, $R(Rh-O)$

150

= 2.237, 2.239, 2.279, 2.306), R(Rh-P) =
2.306(2.302), R(Rh-H) = 1.512 and 1.513 (1.41 and
1.47), where values are in Å unit, and in
parentheses are experimental values for
Rh(CO)(PPh$_3$)$_2$(η^1-OCO$_2$H)[18b] and RhH$_2$(PPr$^i_3$)$_2$(η^2-O$_2$COH).[18c]
(b) S. F. Hossain and K. M. Nicholas, <u>J. Chem. Soc.,
Chem. Commun.</u>, **1981**, 268. (c) T. Yoshida, D. L.
Thorn, T. Okano, J. A. Ibers, and S. Otsuka, <u>J. Am.
Chem. Soc.</u>, **101**, 4212 (1979).

(19)   G. Herzberg, "Molecular Spectra and Molecular
Structure," D. Van Nostrand Co. Inc., Princeton, NJ
(1967), vol. 3, p. 610.

(20)   (a) PH$_3$ is considered as a model of PMe$_3$.[20b] This
means that the results presented here are meaningful
for the reaction system including non-bulky
phosphine. (b) J. O. Noell and P. J. Hay, <u>J. Am.
Chem. Soc.</u>, **104**, 4578 (1982).

(21)   E. R. Davidson and D. W. Silver, <u>Chem. Phys. Lett.</u>,
52, 403 (1977).

(22)   J. A. Pople, R. Seeger, and R. Krishnan, <u>Int. J.
Quantum. Chem. Symp.</u>, **11**, 149 (1977).

(23)   R. Seeger and J. A. Pople, <u>J. Chem. Phys.</u>, **66**, 3045
(1977). References are therein.

(24)   Eigenvalues of the instability matrix are 0.05,
0.013, and 0.016 for reactant, TS and product, where
BS IV was used. The E$_a$ and E$_{exo}$ values calculated at
the CCD level are very similar to those calculated
at the SD-CI level (Table 5.3).

(25)   (a) K. Morokuma, <u>Acc. Chem. Res.</u>, **10**, 294 (1977).

(b) K. Kitaura and K. Morokuma, <u>Int. J. Quant. Chem.</u>,

10, 325 (1976). (c) K. Kitaura, S. Sakaki, and K.

Morokuma, <u>Inorg. Chem.</u>, **20**, 2292 (1981).

(26)   K. Morokuma, S. Kato, K. Kitaura, I. Ohmine, S.

Sakai, and S. Obara, IMS Computer center library, No.

0372.

(27)   S. Sakaki and Y. Musashi, submitted for <u>Inorg. Chem.</u>

(28)   In the precursor complex, $CuH(PH_3)_2\bullet\bullet\bullet CO_2$, the $Cu-O^1$

distance is 3.28 Å, the C-H distance is 2.66 Å, the

$C-O^1$ and $C-O^2$ distances are 1.168 and 1.159 Å, the OCO

angle is 172°, and the Cu-H distance lengthens by

0.06 Å.[27]

(29)   N. Koga, S. Q. Jin and K. Morokuma, <u>J. Am. Chem.</u>

<u>Soc.</u>, **110**, 3417 (1988).

(30)   The geometry of the reaction system, $RhH(PH_3)_3\bullet\bullet\bullet CO_2$,

was optimized by taking the C-H distance as the

reaction coordinate (R(C-H) = 1.558, 1.458 (TS at the

HF level), 1.358, 1.308 and 1.258 Å), and then CCD

calculations were carried out on these optimized

geometries. The TS was roughly determined at R(C-H)

= 1.35 Å from the least-square fitting of CCD total

energies. This C-H distance is 0.1 Å longer than the

HF-optimized TS geometry, but E_a (16.9 kcal/mol) for

this geometry is very similar to E_a (15.9 kcal/mol)

for the HF-optimized geometry, where E_a is calculated

with the CCD/BS-IV method. These results suggest

that HF-optimization of TS followed by single point

correlated calculation seems to provide reasonable E_a

value, while the HF-optimization provides slightly more reactant-like TS than the optimization at the correlated level.

(31)   The TS structure was roughly determined in our previous work[3b] and correctly optimized at the HF level with the energy gradient technique in our recent work.[27] The basis sets used for ligand atoms were the same as the BS I, and the basis set and ECPs used for Cu were of the same quality as those used for Rh in the BS I (see ref. 3). The C-H distance is 1.68 Å, the Cu-O^1 distance is 2.50 Å, the CuHC angle is 105°, the OCO angle is 149°, the C-O^1 and C-O^2 distances are 1.21 and 1.18 Å respectively, and the Cu-H distance is 1.68 Å (about 0.15 Å longer than in CuH(PH$_3$)$_2$).

(32)   P. J. Hay, New J. Chem., **15**, 735 (1991).

(33)   T. Leininger, J. -F. Riehl, G. -H. Jeung, and M. Pèlissier, Chem. Phys. Lett., **205**, 301 (1993).

(34)   The E$_a$ and E$_{exo}$ values for the Cu reaction system were calculated at the SD-CI level, using the BS IV, where geometries were optimized in our previous works.[3b,27]

(35)   (a) S. Sakaki, T. Aizawa, N. Koga, K. Morokuma, and K. Ohkubo, Inorg. Chem., **28**, 103 (1989). (b) S. Sakaki, J. Am. Chem. Soc., **114**, 2055 (1992).

(36)   (a) S. Sakaki, K. Maruta, and K. Ohkubo, J. Chem. Soc., Dalton Trans., **1987**, 361. (b) S. Sakaki, K. Maruta, and K. Ohkubo, Inorg. Chem., **26**, 2499 (1987).

Chapter 6

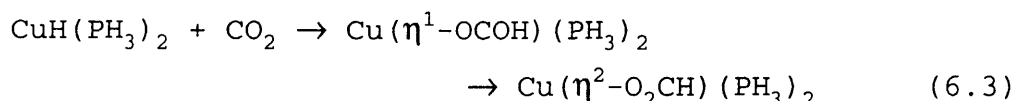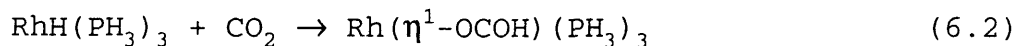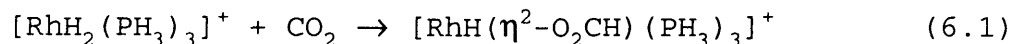## CO$_2$ Insertion Into a Rh(III)-H Bond

6-1 Introduction

Insertion reactions of alkenes and alkynes into metal-hydride and metal-alkyl bonds are involved as a key process in many catalytic reactions by transition metal complexes. In this regard, many theoretical works have been reported on those insertion reactions.[1] Considering the importance of the insertion reactions in catalytic cycles,[2] we can expect that the CO$_2$ insertion into the metal-hydride and metal-alkyl bonds would be utilized to construct a good catalytic system for CO$_2$ fixation. In fact, several interesting catalytic systems for the CO$_2$ fixation involve the CO$_2$ insertion into the metal-hydride bond, as have been reported so far.[3-5] However, only a few of theoretically works have been carried out on the CO$_2$ insertion reactions,[6,7] whereas the theoretical knowledge is indispensable to finding a good catalytic system for the CO$_2$ fixation. Furthermore, the CO$_2$ insertion reaction is worthwhile investigating from the point of view of theoretical chemistry because CO$_2$ has different frontier orbitals from those of alkene and alkyne; the HOMO of CO$_2$ is non-bonding π (nπ) orbital and the LUMO of CO$_2$ is the polarized π^* orbital which expands more at the C atom than at the O atoms.

In this chapter, the CO$_2$ insertion into the Rh(III)-H (Rh^{III}-H) bond (eq 6.1) is investigated with ab initio MO/MP4, SD-CI and CCD methods, and compared with the similar

CO_2 insertion into the Rh^I-H and Cu(I)-H (Cu^I-H) bonds (eqs 6.2 and 6.3).

$$[RhH_2(PH_3)_3]^+ + CO_2 \rightarrow [RhH(\eta^2-O_2CH)(PH_3)_3]^+ \qquad (6.1)$$

$$RhH(PH_3)_3 + CO_2 \rightarrow Rh(\eta^1-OCOH)(PH_3)_3 \qquad (6.2)$$

$$CuH(PH_3)_2 + CO_2 \rightarrow Cu(\eta^1-OCOH)(PH_3)_2$$

$$\rightarrow Cu(\eta^2-O_2CH)(PH_3)_2 \qquad (6.3)$$

Similar CO_2 insertion reactions have been experimentally reported for Cu^I-CH_3,[8] Cu^I-H,[9] Rh^I-H,[10] and Rh^{III}-H complexes.[4] Purposes of this chapter are (1) to examine basis set effects and electron correlation effects on these reactions, (2) to compare the reactivities of $CuH(PH_3)_2$, $RhH(PH_3)_3$, and $[RhH_2(PH_3)_3]^+$ in the CO_2 insertion reaction, and (3) to clarify what factors determine the ease of CO_2 insertion reaction.

6-2 Computational Details

Geometries of reactants, transition states (TS), and products were optimized at the Hartree-Fock (HF) level with the energy gradient technique, and then MP2 to MP4SDQ, SD-CI and coupled cluster with double substitution (CCD) calculations were carried out on those optimized geometries, where core orbitals were excluded from the active space. In SD-CI calculations, the contributions of higher-order excited configurations were estimated, according to Davidson,[11] Davidson-Silver,[12] and Pople's methods.[13] In CCD calculations, the contributions of single and triple substitutions were evaluated through forth-order with CCD wave functions.[14] Gaussian 86[15] and 92[16] programs were used for these calculations.

Several kinds of basis sets were used in these

Table 6.1 Basis sets used in this work

	BS-I	BS-II	BS-III	BS-IV
Cu	ECP(~3p) +(21/21/31)[a]	ECP(~3p) +(21/21/211)[a]	ECP(~2p) +(311/311/311)[d]	ECP(~2p) +(311/311/311)[d]
Rh	ECP(~4p) +(21/21/31)[a]	ECP(~4p) +(21/21/211)[a]	ECP(~3d) +(311/311/211)[d]	ECP(~3d) +(311/311/211)[d]
PH_3	STO-2G	MIDI-4[b]	MIDI-4[b]	MIDI-4[b]
CO_2	MIDI-3[b]	MIDI-4[4]	MIDI-4[4]	MIDI-4[4]
$H_{(hydride)}$	(31)[c]	(31/1)[c]	(31/1)[c]	(31/1)[c]

	BS-V	BS-VI	BS-VII
Cu	ECP(~2p) +(311/311/311)[d]	(43321/4311 /311)[e]	(43321/4311 /311)[e]
Rh	ECP(~3d) +(311/311/211)[d]	(433321/43311 /4211)[e]	(433321/43311 /4211)[e]
PH_3	MIDI-4[b]	MIDI-4[b]	MIDI-4[b]
CO_2	(621/41/1)[c]	MIDI-4[4]	MIDI-4[*b]
$H_{(hydride)}$	(31/1)[c]	(31/1)[c]	(31/1)[c]

a) Ref. 13. b) Ref. 14 c) Ref. 15. d) Ref. 16. e) The (43333/43/4)[14] for Cu and (43333/433/43)[14] for Rh basis sets were augumented with a diffuse function, ζ = 0.141 and ζ = 0.08, respectively.

calculations. As summarized in Table 6.1, the quality becomes higher going to BS-VII from BS-I. The BS-I was employed for geometry optimization, and the other better basis sets were used for correlated calculations. The reliability of effective core potentials was investigated by

comparing BS-II, BS-III, BS-IV, BS-VI, and BS-VII, where BS-II involves a large ECP(up to 4p electron of Rh), BS-III and BS-IV involve a small ECP(up to 3d electron of Rh), BS-VI and BS-VII involve an all electron basis set for Rh. Effects of polarization functions are also examined by comparing BS-III and BS-VI with BS-IV and BS-VII respectively, where polarization functions were added to CO_2 in the latter two basis sets.

6-3 Results and Discussion

6-3-1 Geometries of Reactants, Transition States, and Products

The CO_2 insertion into the Rh^{III}-H bond proceeds via the precursor complex **2** and the transition state (TS) **3**, finally affording the η^2-O_2CH complex **5**, as shown in Figure 6.1. In **2**, both CO_2 and $RhH_2(PH_3)_3$ parts little distort, which suggests that the interaction between CO_2 and Rh^{III} is very weak. These geometrical features of precursor complex are common to the CO_2 insertion into $CuH(PH_3)_2$ and $RhH(PH_3)_3$.[21] This is not surprising because the coordinate bond of CO_2 to transition metal is in general weak. The geometry of TS **3** is, however, much different from TS of the CO_2 insertion into Cu^I-H and Rh(I)-H (Rh^I-H) bonds (see **6** and **7** in Figure 6.1). In **3**, the Rh-O^1 and C-H distances are shorter, and the OCO angle is more closed than those in **6** and **7**. This Rh-O^1 distance seems to be almost the same as the usual coordinate bond distance, and surprisingly, it is much shorter than in the product. These features indicate that **3** is product-like, while **6** and **7** are rather reactant-like. There is the other difference to be noted; CO_2 little
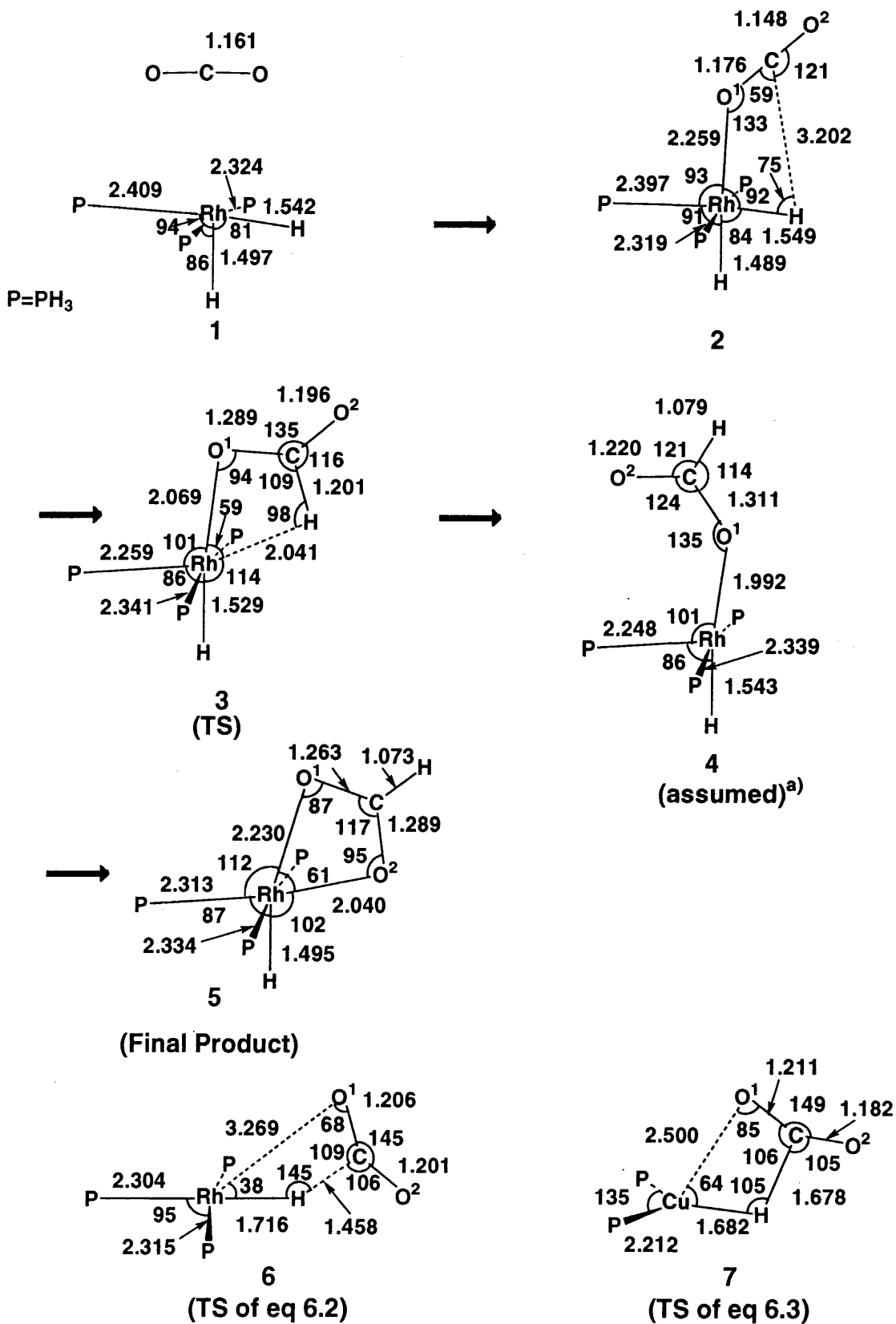
Figure 6.1 Geometry changes in the CO_2 insertion into the Rh^{III}-H bond of $[RhH_2(PH_3)_3]^+$.

Bond distance in Å and bond angle in degree.

changes its coordination site but the hydride ligand attacks CO_2 in **3**, whereas CO_2 moves toward the hydride ligand and inserts into the M-H bond in **6** and **7**.

Geometries of products are also discussed briefly here. The CO_2 insertion reaction with $[RhH_2(PH_3)_3]^+$ affords the η^2-formate complex $[RhH(PH_3)_3(\eta^2-O_2CH)]^+$ **5**. This is because the Rh^{III} complex is a d^6 system and tends to form a six-coordinate system. The similar η^2-formate complex $Cu(PH_3)_2(\eta^2-O_2CH)$ is the product of the CO_2 insertion reaction with $CuH(PH_3)_2$,[6b] because Cu^I has a d^{10} electron configuration and tends to take a tetrahedral-like four-coordinate complex. On the other hand, the CO_2 insertion reaction with $RhH(PH_3)_3$ yields the η^1-formate complex $Rh(\eta^1-OCOH)(PH_3)_3$ as a product, where the η^2-formate complex $Rh(\eta^2-O_2CH)(PH_3)_3$ is less stable than the η^1-formate complex. The reason for this result is that Rh^I takes a d^8 electron configuration and tends to form a planar four-coordinate complex unlike Cu^I and Rh^{III}.

6-3-2 Electron Correlation and Basis set Effects on Activation Energy and Reaction Energy

The activation energy (E_a) is defined as an energy difference between the precursor complex and the TS, the reaction energy (ΔE) is an energy difference between sum of reactants, MHL_n and CO_2, and the final product, and the binding energy (BE) is a stabilization energy of the precursor complex relative to reactants. A negative ΔE value means exothermicity. First, correlation effects on BE, E_a, and ΔE of the CO_2 insertion into the Rh^{III}-H bond will be examined, using BS-VI. As shown in Table 6.2, BE hardly

Table 6.2 Electron correlation effects[a] on stabilization energy (BE) of precusor complex,[b] activation energy (E_a)[c] and reaction energy (ΔE).[d]

	HF	MP2	MP3	MP4DQ	MP4SDQ	SD-CI(D)
$[RhH_2(PH_3)_3]^+$ + CO_2 → $[Rh(\eta^2\text{-}O_2CH)H(PH_3)_3]^+$						
BE	6.8	13.1	11.0	12.3	13.2	11.6
E_a	44.2	52.9	44.2	48.8	46.8	45.5
ΔE	-14.2	-3.3	-13.9	-8.8	-10.5	-13.6
$RhH(PH_3)_3$ + CO_2 → $Rh(\eta^1\text{-}OCOH)H(PH_3)_3$						
BE	1.5	3.4	3.6	3.2	3.2	3.3
E_a	12.2	24.6	15.1	21.0	20.5	15.7
ΔE	-37.3	-7.7	-27.9	-17.8	-15.6	-26.2

	SD-CI(DS)	SD-CI(P)	CCD(ST)
$[RhH_2(PH_3)_3]^+$ + CO_2 → $[Rh(\eta^2\text{-}O_2CH)H(PH_3)_3]^+$			
BE	6.8	11.0	12.3
E_a	44.2	44.2	48.8
ΔE	-14.2	-13.9	-8.8
$RhH(PH_3)_3$ + CO_2 → $Rh(\eta^1\text{-}OCOH)H(PH_3)_3$			
BE	1.5	3.6	3.2
E_a	12.2	15.1	21.0
ΔE	-37.3	-27.9	-17.8

a) BS VI was used. b) The energy difference between sum of reactants and the precursor complex. c) The energy difference between the precursor complex and the TS. d) The energy difference between the sum of reactants and the most stable product. A negative value means the exothermicity.

Table 6.3 Eigenvalues of instability matrix at the TS of CO_2 insertion reactions

	$[RhH_2(PH_3)_3]^+$	$RhH(PH_3)_3$	$CuH(PH_3)_2$
Internal RHF	0.122	0.089	0.215
RRHF $\rightarrow$ CRHF	0.094	0.058	0.201
RRHF $\rightarrow$ RUHF	0.056	0.018	0.099

depends on the computational method except for the HF level. E_a and ΔE somewhat fluctuate upon going from HF to MP4DQ but only a little upon going from MP4SDQ to CCD. In the CO_2 insertion into the Rh^I-H bond of $RhH(PH_3)_3$, E_a and ΔE somewhat change upon going to SD-CI and CCD from MP4SDQ. However, it should be noted that CCD calculations provide intermediate BE, E_a, and ΔE values between MP4SDQ and SD-CI calculations. This suggests that single-reference wave function can be used for these reaction systems. Consistent with this suggestion, no instability of HF wave functions was observed for TS of these three CO_2 insertion reactions; as shown in Table 6.3, the minimum eigenvalue of the instability matrix is not large but apparently positive.

Then, basis set effects were examined at the MP4SDQ level, because MP4SDQ calculations yield similar E_a and ΔE values to CCD calculations with only one exception that E_a of the CO_2 insertion into the Rh^I-H bond is slightly different between CCD and MP4SDQ methods (vide supra). As shown in Table 6.4, several significant effects are observed; (1) Addition of d-polarization functions to CO_2

161

Table 6.4 Basis set effects on BE, E_a and ΔE[a]

		BS-II	BS-III	BS-IV	BS-V	BS-VI	BS-VII
(a) $RhH(PH_3)_3 + CO_2 \rightarrow Rh(\eta^1\text{-}OCOH)H(PH_3)_3$							
BE	HF	1.9	1.6	1.3	0.5	1.5	0.8
	MP4SDQ	3.3	3.2	7.5	2.8	3.2	2.8
E_a	HF	13.8	13.8	20.2	18.5	12.2	21.0
	MP4SDQ	14.7	15.6	19.5	18.0	20.5	24.6
ΔE	HF	-39.4	-34.9	-10.2	-13.6	-37.3	-12.2
	MP4SDQ	-22.1	-15.3	-5.2	-4.1	-15.6	-0.4
(b) $[RhH_2(PH_3)_3]^+ + CO_2 \rightarrow [Rh(\eta^2\text{-}O_2CH)H(PH_3)_3]^+$							
BE	HF	11.6	6.8	4.3	2.9	6.8	4.1
	MP4SDQ	15.8	12.5	14.8	10.3	13.2	10.9
E_a	HF	42.2	46.5	58.0	54.7	44.2	56.8
	MP4SDQ	45.1	48.2	53.0	50.9	46.8	52.3
ΔE	HF	-23.5	-12.2	7.5	5.3	-14.2	6.6
	MP4SDQ	-17.7	-8.3	-2.5	-0.3	-10.5	0.8

BS VII was used (kcal/mol). a) See footnote b)~d) of Table 2.

decreases exothermicity and enlarges the E_a value (compare BS-III and BS-VI with BS-IV and BS-VII respectively). Effects of polarization functions are significantly larger at the HF level than at the correlated level. (2) Use of all electron basis set for Rh instead of ECP does not cause significant change on E_a and ΔE, whereas the E_a value of the

CO_2 reaction with $RhH(PH_3)_3$ slightly increases by 4 kcal/mol upon going to all electron basis set from ECP (compare BS-III with BS-VI). The same result is observed in comparing BS-IV with BS-VII. (3) Improvement of the basis set for s and p orbitals of CO_2 little changes the E_a and ΔE values (compare BS-IV with BS-V). (4) Introduction of electron correlation decreases the exothermicity independently on the presence of the polarization functions on C and O atoms, slightly increases E_a in the absence of the polarization functions but little changes E_a in the presence of the polarization functions. The above results are summarized as follows; the addition of d-polarization functions on CO_2 considerably changes E_a and ΔE, and electron correlation effects on E_a and ΔE are not significant when the polarization functions are added on CO_2. This indicates that the d-polarization functions should be added on C and O atoms to estimate quantitatively E_a and ΔE.

6-3-3   Comparison of Exothermicity in the Rh^{III}, Rh^{I}, and Cu^{I} Reaction Systems

The CO_2 reaction with $[RhH_2(PH_3)_3]^+$ requires the highest E_a value and yields the smallest exothermicity (see Table 6.5). First, we will compare the exothermicity between three insertion reactions. Because a comparison between $CuH(PH_3)_2$ and $RhH(PH_3)_3$ has been made in chapter 5 and ref. 21, its comparison is briefly repeated here. The difference between Cu^I-H and Rh^I-H bond energies and that between Cu^I-$(\eta^2$-$O_2CH)$ and Rh^I-$(\eta^2$-$O_2CH)$ bond energies were estimated, according to the following assumed eqs 6.8 and 6.10 respectively:
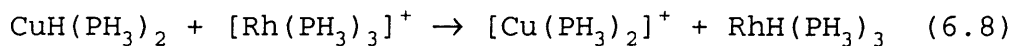
Table 6.5 $E_a{}^a$ and ΔE^a of the CO_2 insertion reactions with $RhH(PH_3)_3$, $[RhH_2(PH_3)_3]^+$, and $CuH(PH_3)_2$

	$CuH(PH_3)_2$			$RhH(PH_3)_3$		
	HF	MP4SDQ	SDCI(DS)	HF	MP4SDQ	SDCI(DS)
E_a	10.3	7.1	6.5	21.0	24.6	21.2
ΔE	-31.7	-32.1	-33.5	-12.2	-0.4	-7.0

	$[RhH_2(PH_3)_3]^+$		
	HF	MP4SDQ	SDCI(DS)
E_a	56.8	52.3	51.3
ΔE	6.6	0.8	-1.1

BS-VII was used (kcal/mol unit). a) See footnote c) and d) of Table 2.
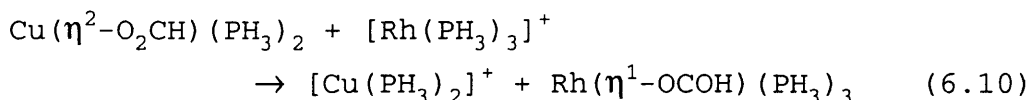
$$CuH(PH_3)_2 + [Rh(PH_3)_3]^+ \rightarrow [Cu(PH_3)_2]^+ + RhH(PH_3)_3 \quad (6.8)$$
$$\Delta E_{r-1} = D(Cu^I-H) - D(Rh^I-H) \quad (6.9)$$
$$Cu(\eta^2-O_2CH)(PH_3)_2 + [Rh(PH_3)_3]^+$$
$$\rightarrow [Cu(PH_3)_2]^+ + Rh(\eta^1-OCOH)(PH_3)_3 \quad (6.10)$$
$$\Delta E_{r-1} = D(Cu^I-(\eta^2-O_2CH)) - D(Rh^I-(\eta^1-OCOH)) \quad (6.11)$$

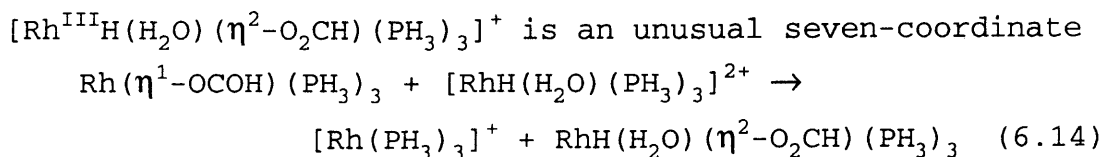where $D(X-Y)$ = the X-Y bond energy and $\Delta E_{r-1} = E_t$ (the right hand side of the eq) - E_t (the left hand side of the eq). These energy differences were calculated at the MP4SDQ level because MP4SDQ calculations provide similar E_a and ΔE values to those of CCD calculations (vide supra). As shown in Table 6.6, the Rh^I-H bond is considerably stronger than the Cu^I-H bond, whereas the Rh^I-$(\eta^1$-OCOH) is slightly stronger

164

than the $Cu^I-(\eta^2-O_2CH)$ bond. Thus, the stronger Rh^I-H bond
than the Cu^I-H bond is the main reason that the CO_2 insertion
into the Rh^I-H bond is much less exothermic than that into
the Cu^I-H bond. Then, the similar comparison is made
between $RhH(PH_3)_3$ and $[RhH_2(PH_3)_3]^+$. The difference between
the Rh^I-H and $Rh^{III}-H$ bond energies was estimated,
considering the following assumed eq 6.12.

$$Rh^IH(PH_3)_3 + [Rh^{III}H(H_2O)(PH_3)_3]^+$$

$$\rightarrow [Rh^I(PH_3)_3]^+ + [Rh^{III}H_2(H_2O)(PH_3)_3]^+ \qquad (6.12)$$
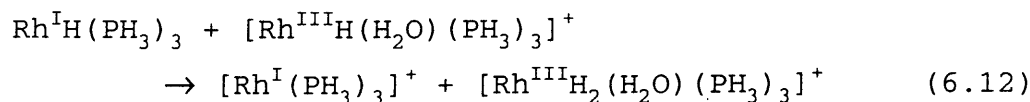
$$\Delta E_{r-1} = D(Rh^I-H) - D(Rh^{III}-H) \qquad (6.13)$$

where H_2O was coordinated to $[Rh^{III}H(PH_3)_3]^{2+}$ to stabilize the
four coordinate d^6 system because the four coordinate d^6
system such as $[Rh^{III}H(PH_3)_3]^{2+}$ was unstable. The term of
$D(Rh^{III}-H) - D(Rh^I-H)$ is 117 kcal/mol at the MP4SDQ level,
indicating that the $Rh^{III}-H$ bond is much stronger than the
Rh^I-H bond. The similar eq 6.14, however, could not be
employed for estimating the difference between the $Rh^I-(\eta^1-OCOH)$ and $Rh^{III}-(\eta^2-O_2CH)$ bond energies because
$[Rh^{III}H(H_2O)(\eta^2-O_2CH)(PH_3)_3]^+$ is an unusual seven-coordinate

$$Rh(\eta^1-OCOH)(PH_3)_3 + [RhH(H_2O)(PH_3)_3]^{2+} \rightarrow$$

$$[Rh(PH_3)_3]^+ + RhH(H_2O)(\eta^2-O_2CH)(PH_3)_3 \quad (6.14)$$

system. So, we estimated the difference, considering the
following two eqs 6.15 and 6.17.

$$Rh^{III}H(\eta^2-O_2CH)(PH_3)_3 + H_2 \rightarrow$$

$$[Rh^{III}H_2(PH_3)_3]^+ + HCOOH \quad (6.15)$$
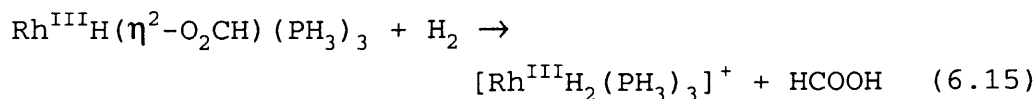
$$\Delta E_{r-1}(eq\ 6.15) = D(Rh^{III}-(\eta^2-O_2CH)) + D(H-H)$$

$$- D(Rh^{III}-H) - D(C-H) \ (6.16)$$

$$Rh^I(\eta^1-OCOH)(PH_3)_3 + H_2 \rightarrow Rh^IH(PH_3)_3 + HCOOH \qquad (6.17)$$
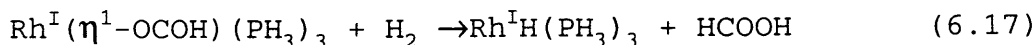
$$\Delta E_{r-1}(eq\ 6.17) = D(Rh^I-(\eta^1-OCOH)) + D(H-H)$$

$$- D(Rh^I-H) - D(C-H) \ (6.18)$$

165

From eqs 6.16 and 6.18, the following eq 6.19 is obtained;

$$\Delta E_{r-1}(\text{eq } 6.15) - \Delta E_{r-1}(\text{eq } 17) = D(Rh^{III}-(\eta^2-O_2CH))$$
$$- D(Rh^I-(\eta^1-OOCH)) + D(Rh^I-H) - D(Rh^{III}-H) \quad (6.19)$$

Because the term of $D(Rh^I-H) - D(Rh^{III}-H)$ has been estimated above, the term of $D(Rh^{III}-(\eta^2-O_2CH)) - D(Rh^I-(\eta^1-OCOH))$ can

Table 6.6 Difference in bond energy calculated with MP2~MP4SDQ/BS-VII method (kcal/mol)

|	MP2	MP3	MP4DQ	MP4SDQ
$D(Rh^{III}-(\eta^2-O_2CH))-D(Rh^I-(\eta^1-OCOH))$[a]	109	131	119	111
$D(Rh^{III}-H)-D(Rh^I-H)$[a]	109	121	114	109
$D(Rh^I-(\eta^1-OCOH))-D(Cu^I-(\eta^1-OCOH))$[a]	9	8	6	5
$D(Rh^I-H)-D(Cu^I-H)$[a]	37	30	31	28
$D(Rh^{III}-H)$	64	60	64	63

a) For heterolytic bond breaking. b) For homolytic bond breaking.

be estimated from eq 6.19. As given in Table 6.6, the $Rh^{III}-(\eta^2-O_2CH)$ and $Rh^{III}-H$ bonds are much stronger than the $Rh^I-(\eta^1-OCOH)$ and Rh^I-H bonds respectively. However, the difference between $Rh^{III}-H$ and Rh^I-H bond energies is slightly smaller than the difference between $Rh^I-(\eta^1-OCOH)$ and $Rh^{III}-(\eta^2-O_2CH)$ bond energies. Thus, the CO_2 insertion into the $Rh^{III}-H$ bond is slightly less exothermic than the CO_2 insertion into the Rh^I-H bond.

At the end of this section, it is necessary to mention the meaning of the bond energy given in Table 6.6. The $D(Rh^{III}-H)$ bond energy was estimated to be about 63 kcal/mol at the MP4SDQ level, considering the following eq 6.20.

$$[Rh(PH_3)_3]^+ + H_2 \rightarrow cis-[RhH_2(PH_3)_3]^+ \qquad (6.20)$$
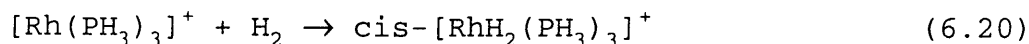
The similar value was reported by Koga et al. from eq 6.23.[22]

$$RhCl(PH_3)_2 + H_2 \rightarrow cis-RhH_2Cl(PH_3)_2 \qquad (6.21)$$
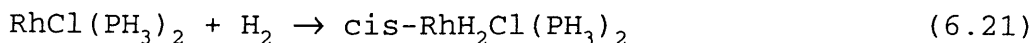
This $D(Rh^{III}-H)$ value and the value of $D(Rh^{III}-H)-D(Rh^I-H)$ in Table 6.6 lead to a negative $D(Rh^I-H)$ value. This is strange apparently, if we do not pay attention to the fact that the meaning of the bond energy is different between eqs 6.13 and 6.20. The $Rh^{III}-H$ bond energy from eqs 6.20 and 6.21 was estimated from the homolytic bond fission, while $Rh^{III}-H$ and Rh^I-H bond energies in eq 6.13 were from the heterolytic bond fission. Thus, the term of $D(Rh^{III}-H)-D(Rh^I-H)$ in eq 6.13 cannot be related to the $D(Rh^{III}-H)$ value estimated from eq 6.20. This is the reason that the term of $D(Rh^{III}-H)-D(Rh^I-H)$ seems too large. Also, we must comment here that the exothermicity of the CO_2 insertion is reasonably discussed in terms of the bond energies based on the heterolytic bond fission because the H ligand moves toward CO_2 as a hydride, as will be described below.

6-3-4 Bonding Nature of the Transition State and the Activation Energy

As shown in Table 6.6, the CO_2 insertion into the $Rh^{III}-$H bond requires the much higher activation energy than the CO_2 insertion into the Rh^I-H and Cu^I-H bonds. This high activation energy would be related to the geometry and the bonding nature at the TS **3** (Figure 6.1).

First, let us see the electron redistribution by the CO_2 insertion to shed some light on the bonding nature. Several interesting features are observed in Mulliken population changes. As shown in Figure 6.2, the electron
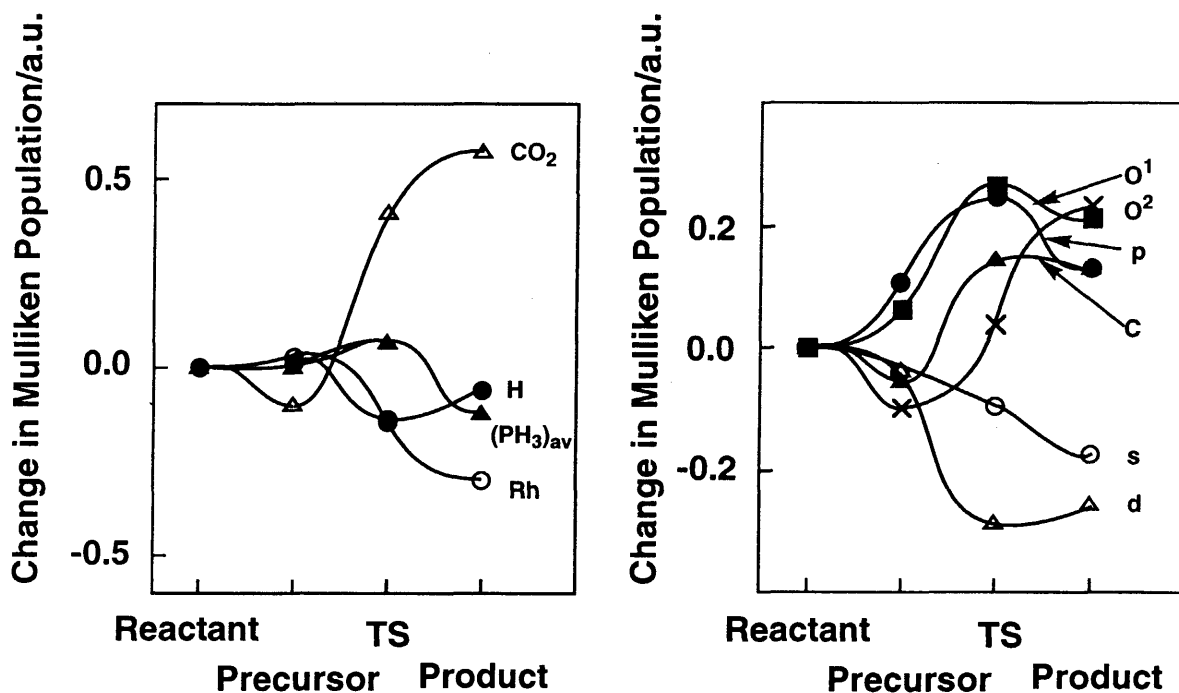
Figure 6.2 Changes in Mulliken population[a] in the CO_2 insertion into the Rh^{III}-H bond of $[RhH_2(PH_3)_3]^+$.

a) A positive value represents the increase in population and vice versa. The standard (change zero) is taken for the sum of reactants, $[RhH_2(PH_3)_3]^+ + CO_2$.

population of CO_2 significantly increases as the CO_2 insertion proceeds. In CO_2, the O^1 and O^2 atomic populations remarkably increase but the C atomic population increases less than the O atomic population. These features are common in the CO_2 insertion. They are explained in terms of orbital mixing **A** shown in Scheme 6.1. The charge transfer from the occupied orbitals of $[Rh^{III}H_2(PH_3)_3]^+$ to the π^* orbital of CO_2 occurs in the CO_2 insertion, and at the same time, the π orbital of CO_2 mixes into the charge-transfer
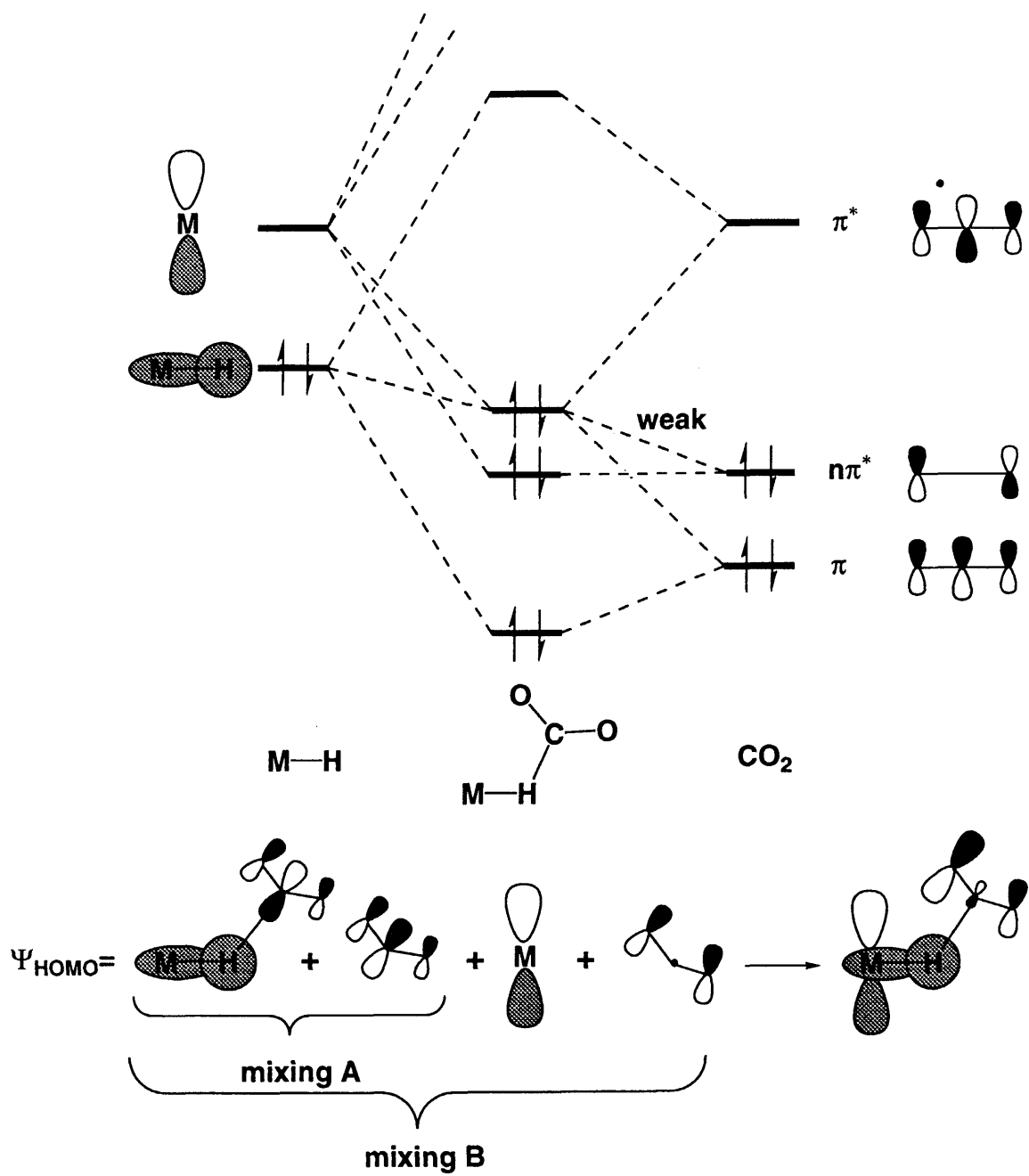
Scheme 6.1

interaction in an anti-bonding way with the occupied orbital of $[Rh^{III}H_2(PH_3)_2]^{2+}$. This mixing enhances the p_π orbitals of O but weakens the p_π orbital of C, which increases the O atomic population much more than the C atomic population, as we have seen in Figure 6.2. These features also suggest that the bonding interaction between CO_2 and the H ligand is produced by the charge transfer from HOMO of $[Rh^{III}H_2(PH_3)_3]^+$ to the π^* orbital of CO_2. The HOMO includes the significant contribution of the H 1s orbital. Thus, the CO_2 insertion into the $Rh^{III}-H$ bond is characterized as a nucleophilic attack of the H ligand to CO_2, in other word, the H ligand moves toward CO_2 as a hydride.

It is necessary to discuss here the origin of the strong charge-transfer interaction from the metal-hydride to CO_2. CO_2 causes the bending distortion, as the CO_2 insertion proceeds. Although the π^* orbital of the undistorted CO_2 lies at a relatively high energy level like C_2H_4, it considerably lowers in energy upon bending of CO_2, as shown in Figure 6.3A. Comparing CO_2 with C_2H_4 at the same distortion energy, the π^* orbital of CO_2 lies at a much lower energy than that of C_2H_4. This is because the bonding overlap between two O atoms emerges in the π^* orbital when CO_2 causes the bending distortion (see contour map in Figure 6.3B). Such bonding overlap dose not emerge at all in the π^* orbital of C_2H_4 even if C_2H_4 causes the distortion. Thus, it is reasonably concluded that the strong charge-transfer interaction is one of the characteristic features of the CO_2 insertion reaction.

Although qualitatively the same electron redistribution is observed in the other CO_2 insertion into the Rh^I-H and
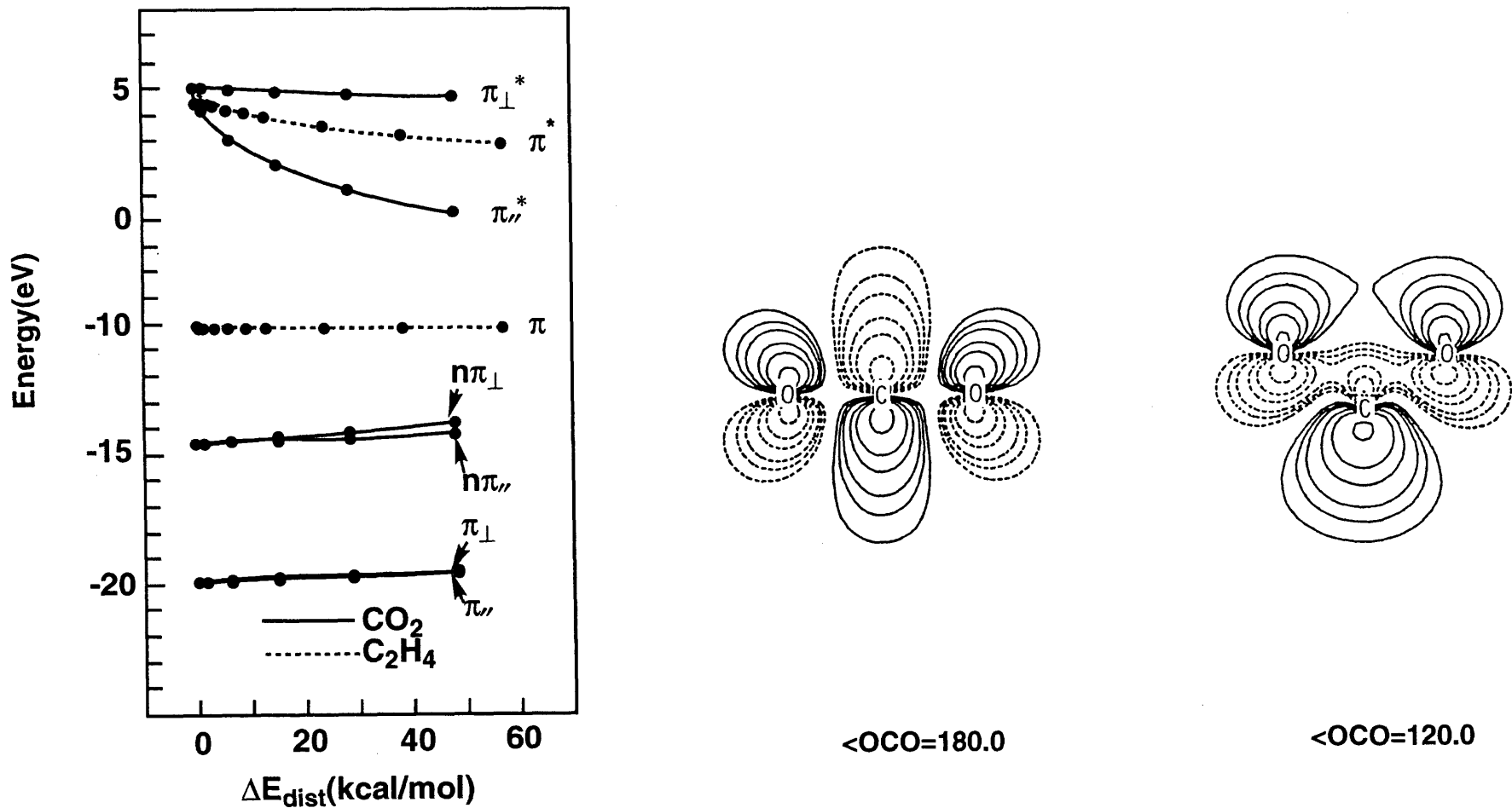
(A) π, nπ, and π^* orbital energies vs. distrotion energy.[a]

(B) Contour map of the CO_2 π^* orbital.[b]

Figure 6.3 The frontier orbital energy leveles vs. the distortion energy,[a] and the contour map of the CO_2 π^* orbital.

a) MP4SDQ/MIDI-4. nπ means non-bonding π orbital. $\pi_{\prime\prime}$ etc. represents the π orbital in the molecular

Table 6.7 Comparison of Mulliken populaitons

	[RhH$_2$(PH$_3$)$_3$]$^+$			RhH(PH$_3$)$_3$	
	Reactant	(TS)^a	TS	Reactant	TS
H	0.937	1.089	1.005	1.039	1.268
CO$_2$	22.000	22.176	22.414	22.000	22.320

	CuH(PH$_3$)$_2$	
	Reactant	TS
H	1.174	1.184
CO$_2$	22.000	22.258

a) R(C-H) was taken to be the same as it in the TS of the CO$_2$ insertion into the Rh^I-H bond.

Cu^I-H bonds, important differences between them are found in Table 6.7. The CO$_2$ electron population at the TS is the greatest in the CO$_2$ insertion into the Rh^{III}-H bond. However, the greatest electron population of CO$_2$ would arise from the short C-H distance between CO$_2$ and the H ligand at the TS of this insertion reaction. In this insertion, the CO$_2$ electron population increases least, when the C-H distance between CO$_2$ and the H ligand is taken to be the same as it in the TS of the CO$_2$ insertion into the Rh^I-H bond. This means that the charge-transfer from the H ligand to CO$_2$ occurs least in the CO$_2$ insertion into the Rh^{III}-H bond. The most weak charge-transfer from [RhH$_2$(PH$_3$)$_3$]$^+$ to CO$_2$ would be related to the smallest H atomic population in the

reactant, $[RhH_2(PH_3)_3]^+$ (see Table 6.7). This is one of the reasons for the considerably high E_a of this insertion reaction.

Now, let us start to discuss the TS geometry in terms of the bonding nature and the electron distribution at the TS. The TS of the CO_2 insertion into the Rh^{III}-H bond is much product-like, as has been described above. This product-like TS can be explained by considering that the Rh^{III}-H bond is much stronger than the Rh^I-H and Cu^I-H bonds (vide supra). To break the strong Rh^{III}-H bond and to form the C-H bond between CO_2 and the H ligand, CO_2 must closely approach the H ligand, which leads to the short C-H distance and causes the highly bending distortion of the CO_2 part. Corresponding to this geometry, the strong charge-transfer occurs from $[Rh^{III}H_2(PH_3)_3]^+$ to CO_2, which accumulates considerable electron density on the O^1 atom through the orbital mixing **A** of Scheme 6.1. As a result, CO_2 can strongly interact with the unoccupied orbital of Rh^{III}, as shown in the orbital mixing **B** in Scheme 6.1. In fact, the $Rh-O^1$ distance is very short the in TS like the usual coordinate bond, which suggests that the coordinate bond of formate is mostly formed at the TS. This situation of the TS would be considerably affected by the trans-influence of the co-existing ligand. It is well-known that the H ligand exhibits the strong trans-influence. To investigate the trans-influence of the η^1-formate ligand, we optimized the assumed structure **4** (see Figure 6.1) in which the $PRhO^1$ angle was taken to be the same as it in TS. In **4**, the $Rh-O^1$ distance is significantly short and the Rh-H distance is much longer than it in the reactant **1** and the product **5**.

This geometrical feature strongly suggests that the η^1-formate ligand exhibits the strong trans-influence. The geometry of TS is, therefore, much unfavorable because formate is going to be mostly formed at the trans-position of the H ligand. On the other hand, the unfavorable situation of this kind does not emerge in the CO_2 insertion into the Rh^I-H and Cu^I-H bonds, as clearly shown in Figure 6.1 (see **6** and **7**). This is, therefore, one of the reasons for the considerably high E_a value of CO_2 insertion into the Rh^{III}-H bond. This is also a reason that the Rh-H and Rh-O^1 distances are longer in the TS **3** than in the product **5**; in **5**, formate can coordinate to Rh^{III} as a bidentate ligand and does not need to strongly coordinate to Rh through the O^1 atom because η^2-formate can interact with Rh via the other O^2 atom.

6-4 Conclusion

Basis set effects were examined in the CO_2 insertion into the Rh^I-H and Rh^{III}-H bonds. Although use of ECP instead of all electron basis set for Rh causes little effects on the activation energy (E_a) and the reaction energy (ΔE), introduction of polarization functions on CO_2 considerably increases E_a and remarkably decreases the exothermicity. Electron correlation effects were investigated by using such methods as MP2 – MP4SDQ, SD-CI, and CCD. Although E_a and ΔE somewhat fluctuate at MP2 and MP3, similar values of E_a and ΔE are calculated with MP4, SD-CI, and CCD methods, and CCD values are intermediate between MP4SDQ and SD-CI values. When polarization functions were added on CO_2, introduction of electron

174

correlation changes E_a and ΔE only a little. Consistent with these results, no instability of the HF wave-function was observed at the TS. This is not surprising because the H ligand moves toward CO_2 as a hydride ligand, in other words, the C-H bond between CO_2 and H ligand is formed not in a homolytic way but in a heterolytic way accompanied with the strong charge transfer from the H ligand to CO_2.

The CO_2 insertion into the Rh^{III}-H bond reaches TS much more late than the other CO_2 insertion into the Rh^{I}-H and Cu^{I}-H bonds, whereas the former is only slightly less exothermic than the CO_2 insertion into the Rh^{I}-H bond. This is because the charge-transfer from $[RhH_2(PH_3)_3]^+$ to CO_2 is weak and CO_2 must approach closely the H ligand to break the strong Rh^{III}-H bond. In the TS, therefore, formate is mostly formed and strongly interacts with Rh in a η^1-coordinating way at the trans-position of the H ligand. This geometrical feature is unfavorable because of the strong trans-influence of the H ligand. Thus, the CO_2 insertion into the Rh^{III}-H bond requires the highest activation energy. In the other CO_2 insertion into the Rh^{I}-H and Cu^{I}-H bonds, such situation does not emerge, and therefore, the activation energy of these insertion reactions is much lower than the CO_2 insertion into the Rh^{III}-H bond.

References

(1)   For example; N. Koga and K. Morokuma, <u>Chem. Rev.</u>, **91**, 823 (1991).

(2)   For example; R. H. Crabtree, "The Organometallic Chemistry of the Transition Metals," John-Wiley & Sons, New York (1988).

(3)   W. C. Kaska, S. Nemeh, A. Shirazi, and S. Potunik, <u>Organometallics</u>, **7**, 13 (1988).

(4)   J. -C. Tsai and K. M. Nicholas, <u>J. Am. Chem. Soc.</u>, **114**, 5117 (1992).

(5)   T. Burgemeiser, F. Kastner, and W. Leitner, <u>Angew. Chem., Int. Ed. Engl.</u>, **32**, 739 (1993).

(6)   (a) S. Sakaki and K. Ohkubo, <u>Inorg. Chem.</u>, **27**, 2020 (1988). (b) S. Sakaki and K. Ohkubo, <u>ibid.</u>, **28**, 2583 (1989). (c) S. Sakaki and K. Ohkubo, <u>Organometallics</u>, **8**, 2970 (1989).

(7)   C. Bo and A. Dedieu, <u>Inorg. Chem.</u>, **28**, 304 (1988).

 8)   A. Miyashita and A. Yamamoto, <u>J. Organomet. Chem.</u>, **49**, C57 (1973).

(9)   C. Bianchini, C. A. Ghilardi, A. Meli, S. Midollini, and A., Orlandini, <u>Inorg. Chem.</u>, **24**, 924 (1985).

(10)   D. J. Danensbourg, G. Grötsch, P. Wiegreffe, and A. L. Rheingold, <u>Inorg. Chem.</u>, **26**, 3827 (1987).

(11)   (a) E. R. Davidson, In "The World of Quantum Chemistry," ed. by R. Daudel and B. Pullman, Reidel, Dordrecht (1974). (b) S. R. Langhoff and E. R. Davidson, <u>Int. J. Quant. Chem.</u> **8**, 61 (1974).

(12)   E. R. Davisdon and D. W. Silver, <u>Chem. Phys. Lett.</u>, **52**, 403 (1977).

(13)   J. A. Pople, R. Seeger, and R. Krishnan, <u>Int. J.</u>

Quant. Chem. Symp., **11**, 149 (1977).

(14) K. Raghavachari, J. Chem. Phys., **82**, 4607 (1985).

(15) M. J. Frisch, J. S. Binkley, H. B. Schlegel, L. Raghavachari, C. F. Melius, R. L. Martin, J. J. P. Stewart, F. W. Bobrowicz, C. M. Rohlfing, L. R. Kahn, D. J. DeFrees, R. Seeger, R. A. Whiteside, D. J. Fox, E. M. Fluder, S. Topiol, and J. A. Pople, Gaussian 86, Carnegie-Mellon Quantum Chemistry Publishing Unit; Pittsburg, PA (1986).

(16) M. J. Frisch, G. W. Trucks, M. Head-Gordon, P. M. W. Gill, M. W. Wong, J. B. Foresman, B. G. Johnson, H. B. Schlegel, M. A. Robb, E. S. Replogle, R. Gomperts, J. L. Andres, K. Raghavachari, J. S. Bindley, C. Gonzalez, R. L. Martin, D. J. Fox, D. J. DeFrees, J. Baker, J. J. P. Stewart and J. A. Pople, Gaussian 92, GAUSSIAN Inc., Pittsburgh, PA (1992).

(17) P. J. Hay and W. R. Wadt, J. Chem. Phys., **82**, 270 (1985).

(18) S. Huzinaga, J. Andzelm, M. Klobukowski, E. Radzio-Andzelm, Y. Sakai, and H. Tatewaki, "Gaussian basis sets for molecular calculations," Elsevier, Amsterdam (1984).

(19) T. H. Dunning and P. J. Hay, "Methods of Electronic Structure Theory," ed. by H. F. Schaefer, Plenum, New York (1977), p. 1.

(20) P. J. Hay and W. R. Wadt, J. Chem. Phys., **82**, 299 (1985).

(21) S. Sakaki and Y. Musashi, submitted to Inorg. Chem. and J. Chem. Soc., Dalton Trans.

(22) C. Daniel, N. Koga, J. Han, X. Y. Fu, and K. Morokuma, J. Am. Chem. Soc., **110**, 3773 (1988).

177

Oxidative Addition of The Si-X σ-Bond to (X = H, C, or Si) Palladium (0) and Platinum (0) Complexes

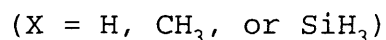### 7.1 Introduction

Oxidative addition of the Si-X σ-bond (X = H, CH_3, SiH_3 etc.) to transition metal complexes is of central significance in syntheses of various organosilicon compounds.[1] For instance, the oxidative addition of the Si-Si σ-bond is considered to be involved as a key process in platinum- and palladium-catalyzed bis-silylation of carbon-carbon,[2-9] carbon-nitrogen,[10] and carbonoxygen[11] multiple bonds. In this context, interesting experimental works have been reported on stoichiometric oxidative addition of the Si-X σ-bond to transition metals.[1,12-19]

Although palladium(0) complexes have often been used as catalysts in the above-mentioned bis-silylation,[1a,3-7,8c,d,9-11] a previous theoretical work revealed that the palladium(0) complex was unfavorable for the oxidative addition of H-H, C-H, and C-C bonds.[20] Thus, knowledge of the Si-X oxidative addition to the palladium(0) complex is necessary to understanding well palladium-catalyzed syntheses of organosilicon compounds. Experimentally, bis(silyl)palladium complexes have been investigated well and several interesting results have been presented on their reductive elimination (i.e., the reverse reaction of the oxidative addition).[21,22] Besides the experimental work, the theoretical work is also expected to offer valid information on the Si-X oxidative addition to palladium(0) complexes.

In this chapter, oxidative addition of the Si-X σ-bond to Pd(PH$_3$)$_2$ (eq 7.1) is theoretically investigated with the

$$Pd(PH_3)_2 + H_3Si-X \rightarrow cis-Pd(X)(SiH_3)(PH_3)_2 \qquad (7.1)$$

$$(X = H, CH_3, \text{ or } SiH_3)$$
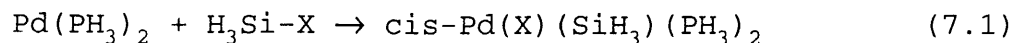
ab initio MO/MP4 method, and compared with the same reaction of Pt(PH$_3$)$_2$.[23] Aims of this chapter are (1) to estimate the activation energy (E$_a$) and the energy of reaction (ΔE) of eq 7.1, (2) to show similarities and differences between Pd(PH$_3$)$_2$ and the Pt analogue, Pt(PH$_3$)$_2$, in the Si-X oxidative addition, and (3) to clarify the factors determining the reactivity of Pd(PH$_3$)$_2$ in this oxidative addition.

7.2 Computational Details

Ab initio MO/MP4 calculations were carried out with the Gaussian 86[24a] and 92[24b] programs. MP2 ~ MP4(SDQ) calculations were carried out with all the core orbitals excluded from the active space. Two kinds of basis sets, BS-I and BS-II, were mainly employed in this work; the BS-I was used for geometry optimization and the BS-II was used for MP2 ~ MP4(SDQ) calculations. In the BS-I, the 4s, 4p, 4d, 5s, and 5p orbitals of Pd were represented by a (5s 5p 4d)/[3s 3p 2d] set, where inner core electrons (up to 3d) were replaced with relativistic effective core potentials (ECPs).[25] MIDI-3 sets[26] were used for ligand atoms, except for MINI-1 set employed for PH$_3$.[26,27a] In the BS-II, the 4s, 4p, 4d, 5s, and 5p orbitals of Pd were represented with a (5s 5p 3d)/[3s 3p 3d] set, where inner core electrons (up to 3d) were replaced with the same ECPs as those in the BS-I.[25] MIDI-4 sets[26] were used for Si, P, and C, and a (4s)/[2s] set was employed for H.[27b] In both BS-I and BS-II, the basis set

of Si was augmented with a d-polarization function.[28] In the BS-II, a p-polarization function[27b] was added to the basis set of H, when it directly coordinates to Pd.[29]

In the Si-Si, Si-C, and C-C oxidative additions, geometries of reactants, transition states (TS), and products were optimized with the energy gradient technique at Hartree-Fock (HF) level, where the geometry of PH_3 was taken from the experimental structure of the free PH_3 molecule[30] and the TS was determined by calculating the Hessian matrix. In the Si-H oxidative addition, however, geometries of reactants and product were optimized at the MP2 level, using the BS-I, because optimization of cis-$Pd(H)(SiH_3)(PH_3)_2$ at the HF level was failed (it leaded to the precursor complex, $Pd(PH_3)_2(SiH_4)$). Geometry changes during this oxidative addition were optimized at the HF level, taking the Pd-Si distance as the reaction coordinate in the early stage of the reaction, the Si-H distance in the middle stage of the reaction, and the HPdSi angle in the late stage of the reaction. The TS was roughly determined from MP4(SDQ)/BS-II calculations performed for HF-optimized geometries (see below and Figure 7.3 for details).

In order to ascertain the reliability of the computational method employed here, the reductive elimination (eq 7.2) of a model complex, $M(CH_3)_2$ (M = Pd or Pt), was examined because this reaction has been investigated well with theoretical methods of high

$$M(CH_3)_2 \rightarrow M + H_3C\text{-}CH_3 \qquad (M = Pd \text{ or } Pt) \qquad (7.2)$$
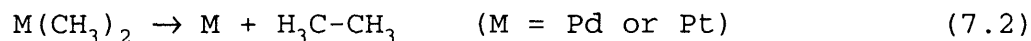
quality.[20,31] Geometries of $M(CH_3)_2$ and the TS of eq 7.2 were optimized with the energy gradient technique at the HF level, using the BS-I. MP2 ~ MP4(SDQ), SD-CI, and coupled

cluster calculations were carried out with BS-II and BS-III; in the latter, Huzinaga-Dunning (9s 5p)/[3s 2p] set[27b] was used for C, but the same basis sets and ECPs as those in the BS-II were adopted for Pd and H. For Pt, a (5s 5p 3d)/[3s 3p 3d] set was employed with ECPs used for core electrons (up to 4f).[25]

7.3 Results and Discussion
7-3-1 Reliability of Our Computational Method

Prior to discussion of the Si-X oxidative addition to $Pd(PH_3)_2$, we will compare our results on the reductive elimination of $M(CH_3)_2$ (eq 7.2) with the results reported by Low and Goddard (LG)[20] and Siegbahn and Blomberg (SB),[31] in order to examine the reliability of our computational method employed here. In both the equilibrium structure of $M(CH_3)_2$ and the TS structure of eq 7.2, the $M-CH_3$ distance optimized here is similar to that reported by SB, and the optimized bond angle is almost the same as those reported by LG and SB, whereas the $M-CH_3$ distance optimized by LG slightly differs from that of SB and ours (Table 7.1). The activation energy (E_a) of the reductive elimination little depends on the basis sets (BS-II and BS-III) and the computational methods such as MP2 ~ MP4(SDQ), SD-CI, and CCD(ST4) methods (Table 7.2; see its footnote (d) for CCD(ST4)). Our E_a value for M = Pd agrees well with the E_a value of SB, but is larger than the E_a value of LG by ca. 10 kcal/mol. In the case of M = Pt, our E_a value is about 5 kcal/mol larger than the E_a value reported by LG. For the purpose of comparing the Pd reaction system with the Pt system, a difference in E_a between M = Pd and M = Pt should

181

Table 7.1 Optimized Geometrical Parameters of $M(CH_3)_2$ and the TS of Reductive Elimination (M = Pd or Pt)

		M = Pd			M = Pt	
		This Work	LG[a]	SB[b]	This Work	LG[a]
$M(CH_3)_2$	$R(M-CH_3)$	2.046	1.96	2.03	2.030	1.97
	$\angle CMC$	88	92	89.9	98	98
TS	$R(M-CH_3)$	2.185	2.34	2.17	2.258	2.34
	$\angle CMC$	58	56	58.3	50	50
	$R(C-C)$	2.133	2.14	2.114	1.969	2.14

Bond length in Å and bond angle in degree.

a) Low and Goddard (Ref. 20). Pd; Basis sets and ECPs of Hay et al,[32] C; Dunning double-ζ contraction of Huzinaga's (9s 5p) primitive set,[27b] H; double-ζ contraction of Huzinaga's (4s) pritmitive set.[27b]

b) Siegbahn and Blomberg (Ref. 31). Pd; (17s 13p 9d 3f)/[7s 6p 4d 1f),[33] C; (9s 5p)/[3s 2p],[27b] H; (5s 1p)/[3s 1p].[27c]

be correctly calculated. This difference (36.6 kcal/mol) calculated here does not differ very much from that (40.8 kcal/mol) reported by LG. All these results suggest that the MP4(SDQ)/BS-II//HF/BS-I calculation (the MP4(SDQ)/BS-II calculation of the HF/BS-I optimized structure) is reliable at least in a semi-quantitative sense and in comparing the Si-X oxidative addition to $Pd(PH_3)_2$ with the same reaction to $Pt(PH_3)_2$.

Table 7.2 Activation Energy of the Reductive Elimination of $M(CH_3)_2$ (kcal/mol unit)

		M = Pd		M = Pt	
		BS-II	BS-III	BS-II	BS-III
This	HF	20.0	19.9	57.4	57.3
Work	MP2	20.5	20.5	57.5	56.9
	MP3	23.6	23.7	60.1	59.9
	MP4DQ	22.5	22.5	59.0	58.7
	MP4SDQ	20.5	20.4	57.1	57.0
	SDCI(D)[a]	22.3	22.4	58.9	58.6
	SDCI(DS)[b]	22.9	22.9	58.9	58.8
	SDCI(P)[c]	22.7	22.7	59.1	58.7
	CCD(ST4)[d]	22.8	--	59.1	--
LG	GVB-CI[e]	12.6[f]		53.4	
SB	CCSD(T)[g]	23.3[h]		--	

a) Davidson's correction for quadratic excitations. S. R. Langhoff and E. R. Davidson, Int. J. Quat. Chem., **8**, 61 (1974).

b) Davidson and Silver's correction for quadratic excitations.[40e]

c) Pople's correction for quadratic excitations. J. A. Pople, R. Seeger, and R. Krishnan, Int. J. Quant. Chem., Quant. Chem., **11**, 149 (1977).

d) Coupled Cluster (doubles) calculation with evaluation of contribution of single and triple excitations through forth order using the CCD wavefunctions.

e) Low and Goddard (Ref. 20).
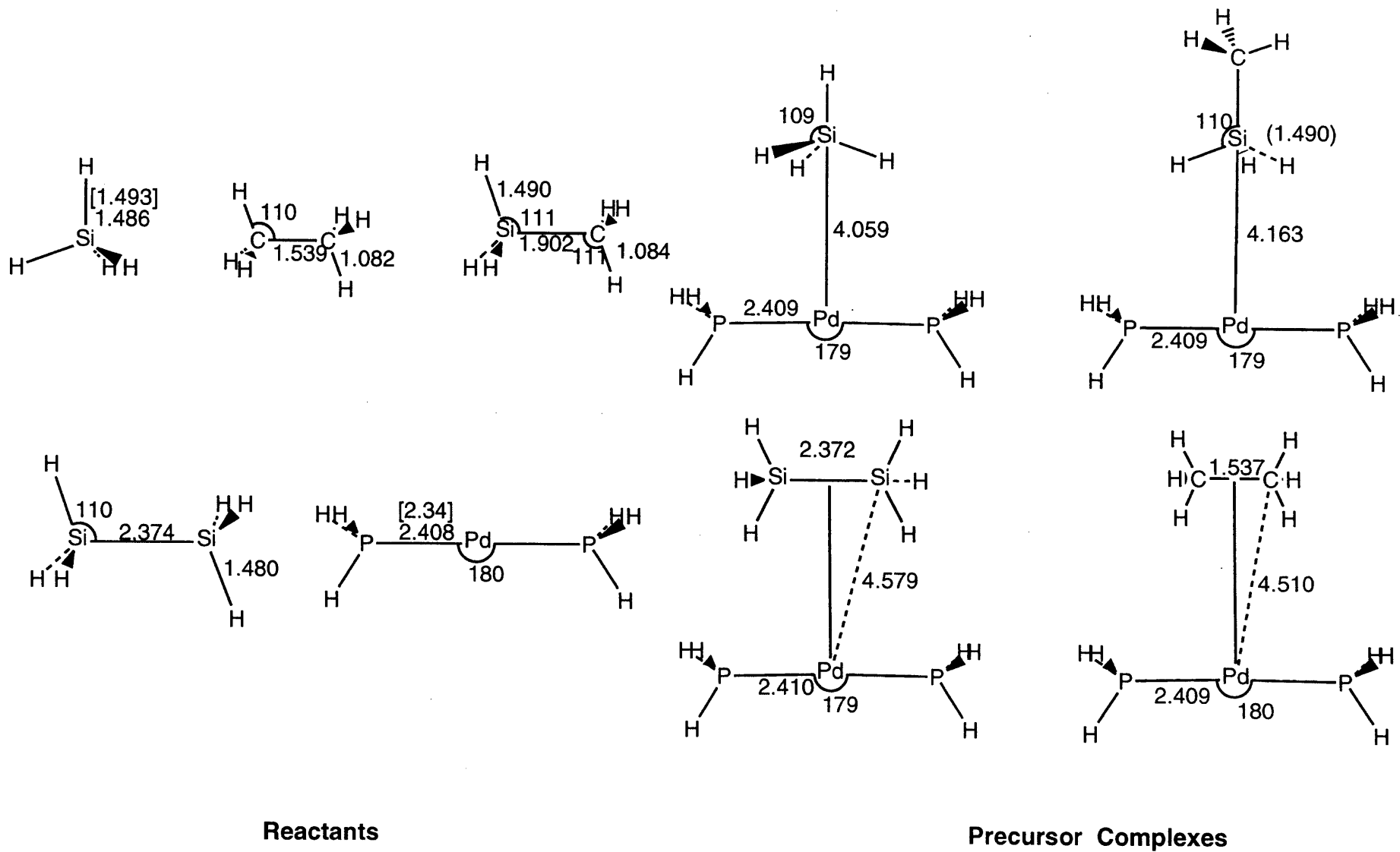
f) See footnote a) of Table 1 for the basis sets used.
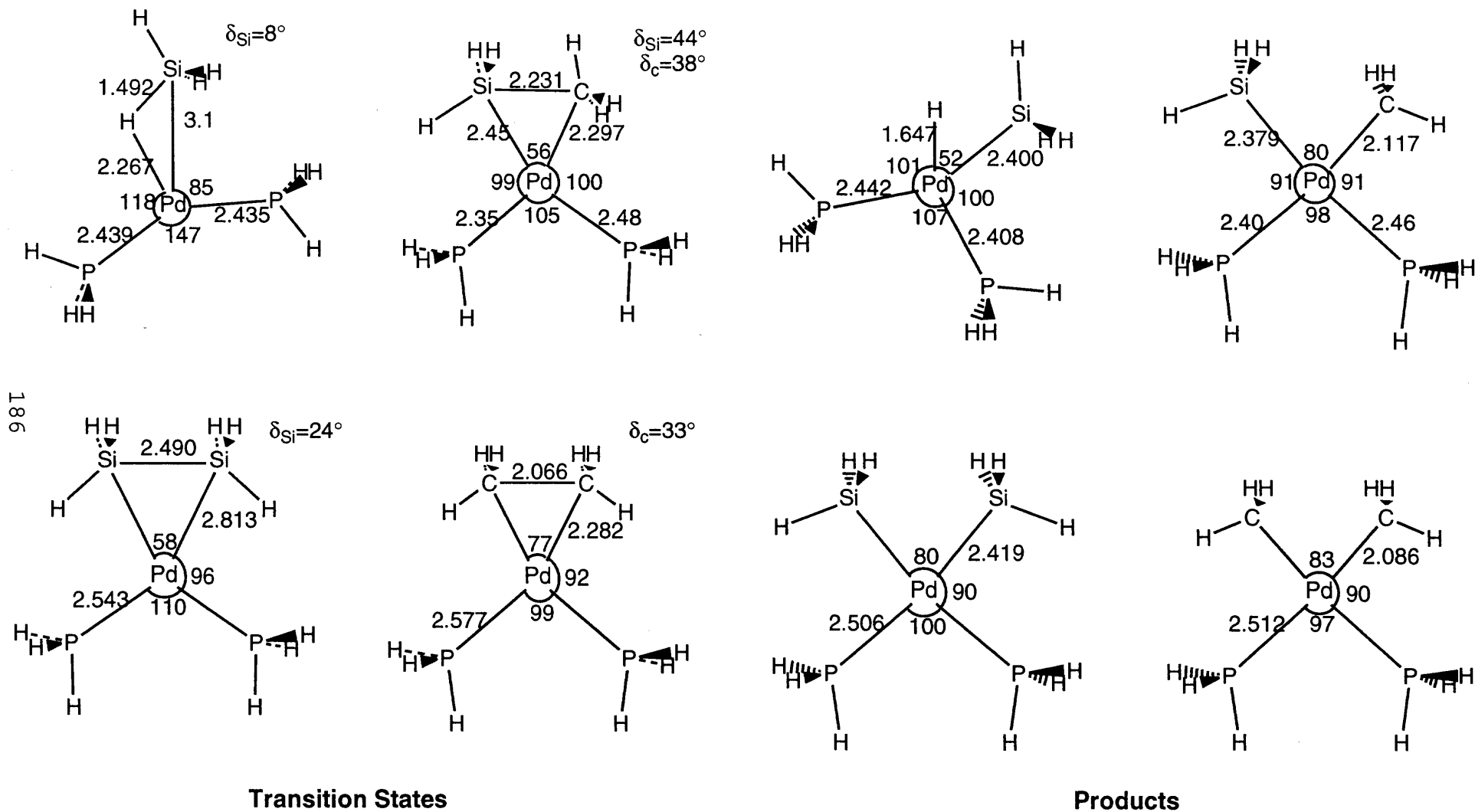
g) Siegbahn and Blomberg (Ref. 31).

h) See footnote b) of Table 1 for the basis sets used.

7-3-2 Changes in Geometry and Energy in the Si-X Oxidative Addition

Now, we will start to consider the Si-X oxidative addition. It is often considered in this kind of oxidative addition that a substrate forms a precursor complex with a transition metal before reaching the TS.[23,34] Optimized geometries of reactants and precursor complexes are shown in Figure 7.1. In a precursor complex, $Pd(PH_3)_2(Si_2H_6)$, having a C_{2v}-like structure,[35a,36] the Pd-Si distance is very long (4.58 Å) and both $Pd(PH_3)_2$ and Si_2H_6 parts little distort (<PPdP=180°, R(Si-Si)=2.37 Å) like the precursor complex of the Pt analogue, $Pt(PH_3)_2(Si_2H_6)$.[23] The similar features are observed in the other precursor complexes, $Pd(PH_3)_2(C_2H_6)$,[36] $Pd(PH_3)_2(SiH_4)$,[35b,36] and $Pd(PH_3)_2(SiH_3CH_3)$.[36] Consistent with these geometrical features, all the precursor complexes yield very small stabilization energies like the Pt analogues[23] (Table 7.3): for instance, the stabilization energy of $Pd(PH_3)_2(Si_2H_6)$ is only 3 kcal/mol (MP4(SDQ)) without the correction of basis set super position error (BSSE) and 1.6 kcal/mol with BSSE correction.[37] These values are too small for the usual coordinate bond, indicating that these complexes can be considered as a van der Waals complex.

At the TS of the Si-Si oxidative addition (Figure 7.2), the Si-Si distance (2.490 Å) is 0.12 Å longer than it in the free Si_2H_6 (Figure 7.1), the SiH_3 group is changing its direction toward Pd, and the Pd-SiH_3 distance is still 0.4 Å longer than it in the product, while the PPdP angle (110°) is very close to that in the product. At the TS of the Si-C oxidative addition,[38] the $Pd(PH_3)_2$ part remarkably distorts

184

Reactants

Precursor Complexes

Figure 7.1 Optimized geometries of reactants and precursor complexes (Bond length in A and bond angle in dergree. Bond distance and bond angles which are given no value)

Figure 7.2 Optimized geometries of transition states and products of the Si-X oxidative addition to $Pd(PH_3)_2$ (Bond length in Å and bond angle in degree)

(<PPdP=105°), the Si-C distance lengthens by 0.33 Å, and the Pd-Si (2.450 Å) and Pd-C (2.297 Å) distances are longer than those in the product by only 0.07 and 0.18 Å respectively, suggesting that this TS is more product-like than the TS of the Si-Si oxidative addition. In the TS of the C-C oxidative addition, the PPdP angle is very small (99°) and the C-C distance is considerably long (2.066 Å), about 0.53 Å longer than it in the free C_2H_6, indicating that this TS is further product-like compared to the TS of the Si-C oxidative addition. It is noted that the PPdP angles in these TSs are much smaller than those in the TSs of the Pt reaction systems; for instance, the PPdP angle is 110° and PPtP angle is 132° for the Si-Si oxidative addition, the PPdP angle is 95° and the PPtP angle is 110° for the C-C oxidative addition, whereas Si_2H_6 and C_2H_6 parts in the TSs of Pd reaction systems are distorted to a similar extent to those in the TSs of Pt reaction systems. This interesting feature relates to the Pd d orbital energy, as will be discussed below.

As shown in Figure 7.3, the Si-H oxidative addition occurs with a very small barrier at the MP4(SDQ) level. Apparently, the HF optimization of cis-Pd(H)(SiH$_3$)(PH$_3$)$_2$ leads to a precursor complex, Pd(PH$_3$)$_2$(SiH$_4$), and therefore, we abandoned HF optimization of the TS. From the MP4(SDQ)/BS-II//HF/BS-I calculations of Figure 7.3, the TS is roughly determined at around R(Pd-Si) = 3.1 Å. In its geometry (Figure 7.2), the PPdP angle is 147°, much smaller than it in the reactant, whereas the SiH$_4$ part little distorts and the Si-H distance little lengthens.

The activation barrier (E_a) and the energy of reaction
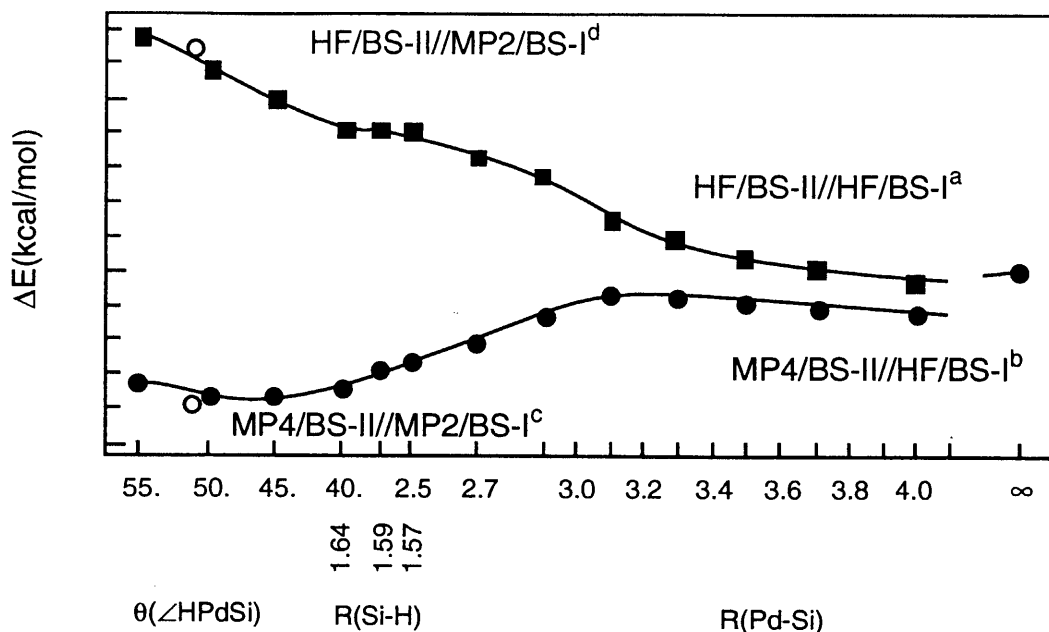
Figure 7.3 Energy changes[a] during the Si-H oxidative addition to Pd(PH$_3$)$_2$. **R(Pd-Si)** and **R(Si-H)** in Å and θ in degree.

a) HF/BS-II calculation for the geometry optimized by HF/BS-I calculation.

b) MP4SDQ/BS-II calculation for the geometry optimized by HF/BS-I calculation.

c) MP4SDQ/BS-II calculation for the geometry optimized by MP2/BS-I caclulation.

d) HF/BS-II calculation for the geometry optimized by MP2/BS-I calculation.

(ΔE) of these reactions are compared in Table 7.3. The C-C oxidative addition to Pd(PH$_3$)$_2$ occurs with a considerably high activation energy and a remarkably high endothermicity, as expected. The Si-Si oxidative addition, however, proceeds with a rather small activation energy and a considerable exothermicity, indicating that although the C-C oxidative addition to Pd(PH$_3$)$_2$ is difficult very much, the

188

Table 7.3 Energy Change in Oxidative Additions[a] (kcal/mol unit)

	M = Pd					M = Pt
	HF	MP2	MP3	MP4DQ	MP4SDQ	MP4SDQ
(A) C-C Oxidative Addition						
Reactants[c]	-889.0641	-889.5403	-889.5659	-889.5938	-889.6042	-881.9800
Precursor	-0.2(0.4)	-1.3(-1.1)	-1.2(-0.36)	-1.2(-0.6)	-1.4(-0.8)	-1.1(-0.8)
TS	82.8(85.3)	56.9(59.3)	63.5(65.9)	61.0(63.5)	56.8(59.3	66.0(68.5)
Product	50.9	27.9	29.5	30.7	30.5	5.2
(B) Si-Si Oxidative Addition						
Reactants[c]	-1390.6068	-1391.0659	-1391.0976	-1391.1259	-1391.1380	-1383.5124
Precursor	-0.6(0.8)	-2.9(-1.4)	-2.7(-1.3)	-2.7(-1.2)	-3.0(-1.6)	-3.7(-2.6)
TS	21.2(24.8)	9.8(13.4)	11.9(15.5)	11.1(14.7)	8.2(11.9)	13.7(17.0)
Product	9.0	-21.1	-13.3	-16.7	-18.1	-46.4
(C) Si-C Oxidative Addition						
Reactants[c]	-1139.8416	-1140.3050	-1140.3346	-1140.3625	-1140.3740	-1132.7497
Precursor	-0.6(0.5)	-2.3(-1.2)	-2.1(-1.0)	-2.2(-1.1)	-2.5(-1.4)	-2.3(-1.4)
TS	42.9(46.6)	-15.1(18.9)	22.2(25.9)	19.2(22.9)	16.3(20.1)	24.9(28.1)
Product	34.0	5.9	9.9	8.7	8.1	-14.1

(D) Si-Si Oxidative Addition

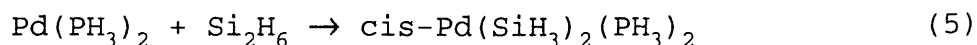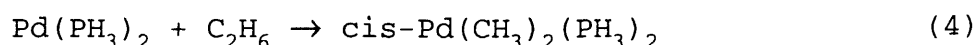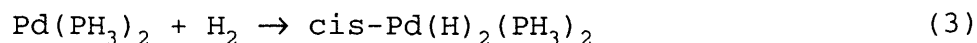|						
Reactants[c]	-1100.8494	-1101.2327	-1101.2542	-1101.2809	-1101.2920	-1093.6616[e]
Precursor	-2.2(-1.2)	-1.8(-0.8)	-2.5(-1.5)	-2.1(-1.1)	-2.4(-1.4)	-6.1(-5.8)
TS	2.6(4.4)	-0.3(1.5)	-0.4(1.5)	-0.3(1.6)	-1.3(0.5)	-6.3(-4.0)
Product	12.5	-9.5	-4.1	-6.6	-8.1	-31.1

a) In parethesis; basis set superposition error (BSSE) was corrected with the counter-poise method.[37]
b) ref. 23. c) Sum of the total energies of reactants (hartree unit). d) $Pd(PH_3)_2$ and SiH_4 were optimized at the MP_2 levle, using the BS-I. (e) Values differ from those of ref. 23, because a p-polarization function was added to H coordinating to Pt.

Si-Si oxidative addition to $Pd(PH_3)_2$ can proceed easily. The Si-C oxidative addition is endothermic, and the activation energy of this reaction is much lower than that of the C-C oxidative addition but considerably higher than that of the Si-Si oxidative addition. The Si-H oxidative addition can proceed with a very small barrier (ca. 2 kcal/mol at MP4(SDQ)/BS-II) and a moderate exothermicity (8 kcal/mol at MP4(SDQ)/BS-II). In summary, the activation energy of oxidative addition to $Pd(PH_3)_2$ increases in the order Si-H < Si-Si < Si-C << C-C, and the exothermicity increases in the order C-C < Si-C < Si-H < Si-Si. These orders are the same as those in the oxidative addition to $Pt(PH_3)_2$, and the reasons have been discussed previously.[23]

7-3-3 A Comparison of Reactivity between $Pd(PH_3)_2$ and $Pt(PH_3)_2$

First, let us examine the C-C oxidative addition. A significant difference between $Pd(PH_3)_2$ and $Pt(PH_3)_2$ is observed in this reaction; the C-C oxidative addition to $Pd(PH_3)_2$ is significantly endothermic in contrast to the same reaction to $Pt(PH_3)_2$ which is only slightly endothermic (Table 7.3). The other Si-X oxidative addition to $Pd(PH_3)_2$ is also much less exothermic (or much more endothermic) than the corresponding reaction to $Pt(PH_3)_2$. This difference between $Pt(PH_3)_2$ and $Pd(PH_3)_2$ is easily interpreted in terms of bond energies. Bond energies are estimated at the MP2 ~ MP4(SDQ) levels, considering the following reactions;

$$Pd(PH_3)_2 + H_2 \rightarrow cis\text{-}Pd(H)_2(PH_3)_2 \qquad (3)$$
$$Pd(PH_3)_2 + C_2H_6 \rightarrow cis\text{-}Pd(CH_3)_2(PH_3)_2 \qquad (4)$$
$$Pd(PH_3)_2 + Si_2H_6 \rightarrow cis\text{-}Pd(SiH_3)_2(PH_3)_2 \qquad (5)$$

Table 7.4 Estimated Pd-X and Pt-X (X = H, CH_3, or SiH_3) Bond Energies (kcal/mol unit)

	Pd-H	Pd-CH_3	Pd-SiH_3	Pt-H	Pt-CH_3	Pt-SiH_3
MP2	47.0	29.5	47.0	59.9	42.2	64.4
MP3	49.1	27.7	43.3	62.2	40.2	60.3
MP4DQ	49.5	26.9	44.6	62.1	39.4	59.4
MP4SDQ	48.9	27.1	45.4	61.7	39.7	61.5

a) Values differ fromthose of ref. 23, because a p-polarization was added to H coordinating to Pt

Apparently shown in Table 7.4, the Pd-X bond energy is smaller than the corresponding Pt-X bond energy. Thus, the oxidative additions of the Si-Si, Si-C, Si-H, and C-C bonds to $Pd(PH_3)_2$ are much less exothermic (or much more endothermic) than the corresponding reaction with $Pt(PH_3)_2$.

Interestingly, the activation energy (E_a) of the Si-X oxidative addition to $Pd(PH_3)_2$ is slightly lower than (or similar to) that of the corresponding reaction with $Pt(PH_3)_2$, whereas the former is much less exothermic (or much more endothermic) than the latter. If the bond energy was an only determining factor for the E_a value, the oxidative addition to $Pd(PH_3)_2$ would always require a considerably higher E_a value than the corresponding oxidative addition to $Pt(PH_3)_2$. Thus, the rather low E_a value indicates that the other factor is important in determining the activation barrier. At the TS, the charge-transfer from the d_{xz} orbital of $Pd(PH_3)_2$ to the σ^*-orbital of the Si-X bond is necessary
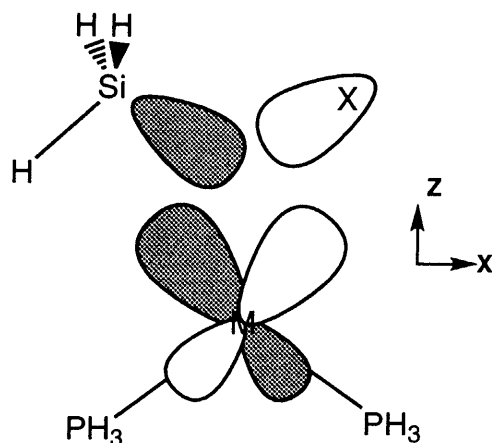
Chart 7.1

to break the Si-X σ-bond (see Chart 7.1 for d_{xz} and σ*), as well known.[34,39] This charge-transfer interaction is, in general, considered to be weaker in the Pd atom than in the Pt atom because Pd takes a d^{10} electron configuration as its ground state but Pt takes a d^9s^1 configuration.[20] The situation, however, changes upon going to $M(PH_3)_2$ from the bare M atom (M = Pd or Pt). The d^{10} state of $Pt(PH_3)_2$ was calculated at the SD-CI level[40] to be 62 kcal/mol more stable than the $^1B_1(d^9s^1)$ state, where the BS-II was used and the geometry of $Pt(PH_3)_2$ as taken to be the same as in the TS of the Si-Si oxidative addition.[23] This result suggests that the situation of d orbital is similar in $Pd(PH_3)_2$ and $Pt(PH_3)_2$. Furthermore, $Pd(PH_3)_2$ is more flexible for the PPdP bending and needs smaller distortion energy (E_{dist}) to cause the bending than $Pt(PH_3)_2$ (note that $Pd(PH_3)_2$ is linear at the equilibrium structure but takes a bending structure at the TS, as shown in Figures 7.1 and 7.2); when the PMP
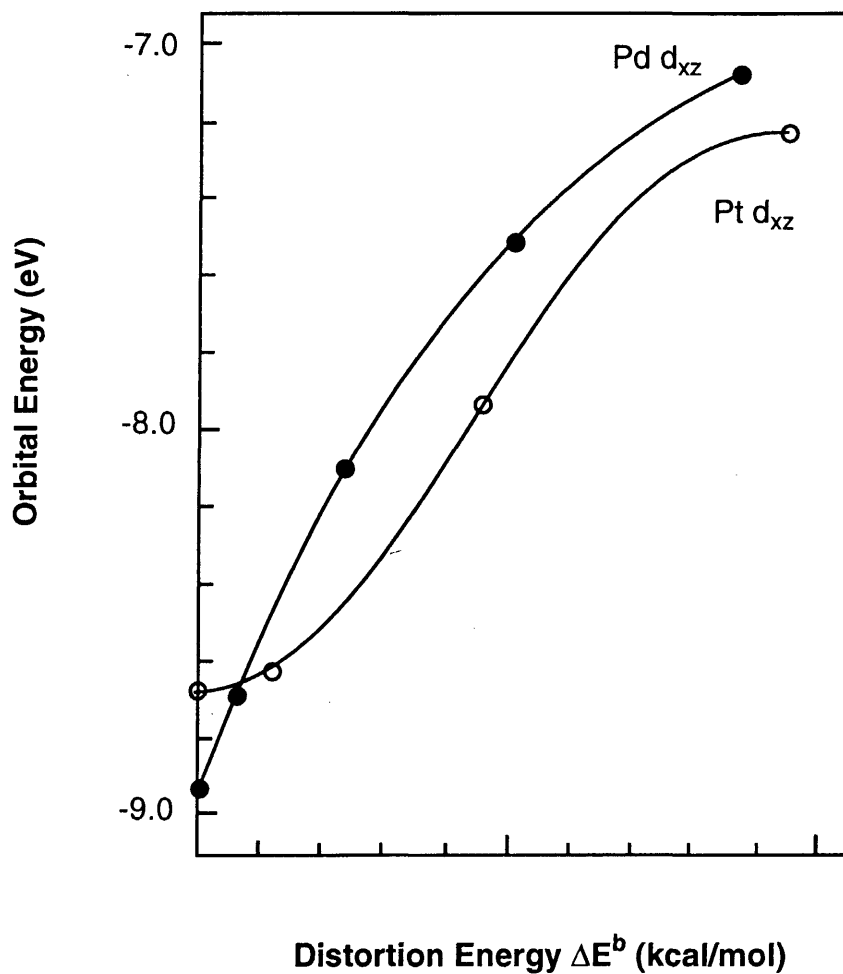
Figure 7.4 Relation between the d_{xz} orbital energy and the bending of $M(PH_3)_2$ ($M = Pd$ or Pt)[a]

a) Only the PMP angle was changed with the M-P distance fixed to that of the equibrium structure.

b) E_{dist} was calculated at the MP4SDQ level.

Table 7.5 Distortion Energy (E_{dist}), d_{xz} orbital energy ($\varepsilon(d_{xz})$), and Ionization Potential ($I_p(d_{xz})$).

	$Pd(PH_3)_2$	$Pt(PH_3)_2$
$E_{dist}{}^a$	47.0	29.5
$\varepsilon(d_{xz})^b$	49.1	27.7
$I_p(d_{xz})$	49.5	26.9

a) $E_t(M(PH_3)_2)_{at\ TS} - E_t(M(PH_3)_2)_{eq}$ at the MP4SDQ level. b) HS/BS-II calculation. c) SD-CI/BS-II. See ref. 40 and 41 for details of calculation.

angle (M = Pd or Pt) is taken to be 120°, E_{dist} = 19.1 kcal/mol for $Pt(PH_3)_2$ and 10.2 kcal/mol for $Pd(PH_3)_2$ (at the MP4(SDQ) level). This bending of $M(PH_3)_2$ pushes up the d_{xz} orbital energy. As shown by a relation between E_{dist} and the d_{xz} orbital energy (Figure 7.4), the d_{xz} orbital in $Pd(PH_3)_2$ rises in energy to a greater extent than it in $Pt(PH_3)_2$, and the former lies higher in energy than the latter at the same distortion energy. The d_{xz} orbital energy ($\varepsilon(d_{xz})$), the ionization potential from the d_{xz} orbital ($Ip(d_{xz})$),[41] and the E_{dist} value are compared between $Pd(PH_3)_2$ and $Pt(PH_3)_2$ in Table 7.5, where geometries of $Pd(PH_3)_2$ and $Pt(PH_3)_2$ were taken to be the same as the distorted structures in the TS of the Si-Si oxidative addition. It is noted that although the bending (<PPdP = 110°) of $Pd(PH_3)_2$ is much greater than that (<PPtP = 132°) of $Pt(PH_3)_2$, the E_{dist} value of the former is slightly larger than that of the latter by only 1.7 kcal/mol (MP4(SDQ)). Furthermore, the d_{xz} orbital in

Pd(PH$_3$)$_2$ lies at a slightly higher energy than it in Pt(PH$_3$)$_2$, and the I$_p$(d$_{xz}$) is almost the same in both Pd(PH$_3$)$_2$ and Pt(PH$_3$)$_2$. All these results indicate that Pd(PH$_3$)$_2$ can easily distort with the smaller distortion energy than Pt(PH$_3$)$_2$, and the d$_{xz}$ orbital of Pd(PH$_3$)$_2$ taking the distorted structure like in the TS lies at a relatively high energy level, similar to it in Pt(PH$_3$)$_2$. Accordingly, the charge-transfer interaction is easily formed between the d$_{xz}$ orbital of Pd(PH$_3$)$_2$ and the Si-X σ^* orbital. Thus, the Si-X oxidative addition to Pd(PH$_3$)$_2$, as well as the oxidative addition to Pt(PH$_3$)$_2$, easily occurs in spite of the low exothermicity of the former.

7.4 Conclusions

Finally, let us mention here the reductive elimination of cis-M(SiH$_3$)$_2$(PH$_3$)$_2$. The activation barrier of the reductive elimination is estimated at the MP4(SDQ) level to be 31.3 kcal/mol for M = Pd and 60.0 kcal/mol for M = Pt,[23] suggesting that the reductive elimination is much difficult in cis-Pt(SiH$_3$)$_2$(PH$_3$)$_2$ but rather easy in cis-Pd(SiH$_3$)$_2$(PH$_3$)$_2$. The activation barrier of the Si-C reductive elimination from cis-Pd(SiH$_3$)(CH$_3$)(PH$_3$)$_2$ is also estimated to be 8.2 kcal/mol at the MP4(SDQ) level, showing that this reductive elimination proceeds much more easily than the Si-C reductive elimination from cis-Pt(SiH$_3$)(CH$_3$)(PH$_3$)$_2$ (E$_a$=42.2 kcal/mol). Thus, we can expect that the palladium(0) complex is more useful as a catalyst for the reaction including both oxidative addition and reductive elimination of Si compounds than the platinum(0) complex; for instance, if the insertion of alkene and alkyne into the Pd-SiH$_3$ bond

easily occurs, the palladium(0) complex is more appropriate
for the bis-silylation of alkenes, alkynes, dienes, etc.
than the platinum(0) complex.

References

(1)   For instance: (a) T. D. Tilley, "The Chemistry of
        Organic Silicon Compounds," ed by S. Patai, Z.
        Rappoport, John Wiley & Sons, New York (1989), p.1415.
        (b) I. Ojima, "The Chemistry of Organic Silicon
        Compounds," ed by S. Patai, Z. Rappoport, John Wiley &
        Sons, New York (1989), p.1479.

(2)   (a) K. Yamamoto, J. Okinoshima, and M. Kumada, J.
        Organomet. Chem., **27**, C31 (1971). b) H. Okinoshima,
        K. Yamamoto, and M. Kumada, J. Organomet. Chem., **86**,
        C27 (1975). c) K. Tamao, S. Okazaki, and M. Kumada,
        J. Organomet. Chem., **146**, 87 (1978).

(3)   a) H. Sakurai, Y. Kamiyama, and Y. Nakadaira, J. Am.
        Chem. Soc., **97**, 931 (1975). (b) H. Sakurai, T.
        Kobayashi, and Y. Nakadaira, J. Organomet. Chem., **162**,
        C43 (1978). (c) H. Sakurai, Y. Eriyama, Y. Kamiyama,
        and Y. Nakadaira, J. Organomet. Chem., **264**, 229
        (1984).

(4)   (a) H. Matsumoto, K. Shono, A. Wada, I. Matsubara, H.
        Watanabe, and Y. Nagai, J. Organomet. Chem., **199**, 185
        (1980). (b) H. Watanabe, M. Saito, N. Sutou, and Y.
        Nagai, J. Chem. Soc., Chem. Commun., **1981**, 617. (c)
        H. Watanabe, M. Saito, K. Kishimoto, J. Inose, and Y.
        Nagai, J. Organomet. Chem., **225**, 343 (1982).

(5)   C. W. Carlson and R. West, Organometallics, **2**, 1801
        (1983).

(6)   D. Seyferth, E. W. Goldman, and J. Escudié, J.
        Organomet. Chem., **271**, 337 (1984).

(7)   (a) T. Hayashi, A. Yamamoto, T. Iwata, and Y. Ito, J.
        Chem. Soc., Chem. Comm., **1987**, 398. (b) T. Hayashi,

Y. Matsumoto, and Y. Ito, J. Am. Chem. Soc., **110**, 5579 (1988). (c) M. Murakami, P. G. Andersson, M. Suginome, and Y. Ito, J. Am. Chem. Soc., **113**, 3987 (1991).

(8) (a) T. Hayashi, A. M. Kawamoto, T. Kobayashi, and M. Tanaka, J. Chem. Soc., Chem. Comm., **1990**, 563. b) T. Hayashi, T. Kobayashi, A. M. Kawamoto, H. Yamashita, and M. Tanaka, Organometallics, **9**, 280 (1990). c) H. Yamashita, M. Catellani, and M. Tanaka, Chem. Lett., **1991**, 241. d) H. Yamashita and M. Tanaka, Chem. Lett., **1992**, 1547.

(9) (a) Y. Tsuji, R. M. Lago, S. Tomohiro, and H. Tsuneishi, Organometallics, **11**, 2353 (1992). (b) Y. Obara, Y. Tsuji, and T. Kawamura, Organometallics, **12**, 2853 (1993).

(10) (a) Y. Ito, S. Nishimura, and M. Ishikawa, Tetrahedron Lett., **28**, 1293 (1987). (b) Y. Ito, M. Suginome, and M. Murakami, J. Am. Chem. Soc., **110**, 3692 (1988).

(11) H. Yamashita, N. P. Reddy, and M. Tanaka, Chem. Lett., **1993**, 315.

(12) P. Hoffmann, H. Heiss, P. Neiteler, G. Müller, and J. Lachmann, Angew. Chem., Int. Ed. Engl., **29**, 880 (1990).

(13) (a) H. Yamashita, T. Hayashi, T. Kobayashi, M. Tanaka, and M. Goto, J. Am. Chem. Soc., **110**, 4417 (1988). (b) H. Yamashita, T. Kobayashi, T. Hayashi, and M. Tanaka, Chem. Lett., **1990**, 1447. c) H. Yamashita, M. Tanaka, and M. Goto, Organometallics, **11**, 3227 (1992).

(14) X. L. Luo, G. K. Schulte, P. Demou, and R. H.

Crabtree, <u>Inorg. Chem.</u>, **29**, 4268 (1990).

(15) D. L. Thorn and R. L. Harlow, <u>Inorg. Chem.</u>, **29**, 2017 (1990).

(16) (a) R. H. Heyn and T. D. Tilley, <u>J. Am. Chem. Soc.</u>, **114**, 1917 (1992). (b) N. S. Radu, T. D. Tilley, and A. L. Rheingold, <u>J. Am. Chem. Soc.</u>, **114**, 8293 (1992).

(17) M. A. Esteruelas, L. A. Oro, and C. Valero, <u>Organometallics</u>, **11**, 3362 (1992).

(18) D. M. Hester, J. Sun, A. W. Harper, and G. K. Yang, <u>J. Am. Chem. Soc.</u>, **114**, 5234 (1992).

(19) (a) Y. Pan, J. T. Mague, and M. J. Fink, <u>Organometallics</u>, **11**, 3495 (1992). (b) M. J. Michalczyk, C. A. Recatto, J. C. Calabrese, and M. J. Fink, <u>J. Am. Chem. Soc.</u>, **114**, 7955 (1992).

(20) (a) J. J. Low and W. A. Goddard, III, <u>J. Am. Chem. Soc.</u>, **108**, 6115 (1986). (b) J. J. Low and W. A. Goddard, III, <u>Organometallics</u>, **4**, 1468 (1985).

(21) U. Schubert and C. Müller, <u>J. Organomet. Chem.</u>, **373**, 165 (1989).

(22) Y. Pan, J. T. Mague, and M. J. Fink, <u>Organometallics</u>, **11**, 3495 (1992).

(23) (a) S. Sakaki and M. Ieki, <u>J. Am. Chem. Soc.</u>, **113**, 5063 (1991). (b) S. Sakaki and M. Ieki, <u>J. Am. Chem. Soc.</u>, **115**, 2373 (1993).

(24) (a) M. J. Frisch, J. S. Binkley, H. B. Schlegel, K. Raghavachari, C. F. Melius, R. L. Martin, J. J. P. Stewart, J. W. Bobrowicz, C. M. Rohlfing, L. R. Kahn, D. J. DeFrees, R. Seeger, R. A. Whiteside, D. J. Fox, E. M. Fluder, S. Topiol, and J. A. Pople, <u>Gaussian 86</u>, GAUSSIAN INC., Pittsburg, PA (1988). (b) M. J.

Frisch, G. W. Trucks, M. H. Gordon, P. M. W. Gill, M. W. Wong, J. B. Foresman, B. G. Johnson, H. B. Schlegel, M. A. Robb, E. S. Replogle, R. Gomperts, J. L. Andres, K. Raghavachari, J. S. Binkley, C. Gonzalez, R. L. Martin, D. J. Fox, D. J. DeFrees, J. Baker, J. J. P. Stewart, and J. A. Pople, <u>Gaussian 92</u>, GAUSSIAN INC., Pittsburg, PA (1992).

(25) P. J. Hay and W. R. Wadt, <u>J. Chem. Phys.</u>, **82**, 299 (1985).

(26) S. Huzinaga, J. Anzelm, M. Klobukowski, E. Radio-Andzelm, Y. Sakai, and H. Tatewaki, "Gaussian Basis Sets for Molecular Calculations," Elsevier, Amsterdam (1984).

(27) (a) F. B. Van Duijneveldt, "Gaussian Basis Sets for the Atoms H-Ne for Use in Molecular Calculations," <u>IBM. J. Res. Dev.</u> 1971, 945. (b) T. H. Dunning and P. J. Hay, "Methods of Electronic Structure Theory," ed by H. F. Schaefer, Plenum, New York (1977), p. 1. (c) T. H. Dunning, <u>J. Chem. Phys.</u>, **53**, 2823 (1970).

(28) Y. Sakai, H. Tatewaki, and S. Huzinaga, <u>J. Comput. Chem.</u>, **2**, 108 (1981).

(29) When the activation energy and the energy of reaction of the Si-H oxidative addition were calculated, the p-polarization function was added to one H atom of SiH_4.

(30) G. Herzberg, "Molecular Spectra and Molecular Structure," Academic Press, New York (1974), vol.3, p. 267.

(31) P. E. M. Siegbahn and M. R. A. Blomberg, <u>J. Am. Chem. Soc.</u>, **114**, 10548 (1992).

(32) J. O. Noell and P. J. Hay, <u>Inorg. Chem.</u>, **21**, 14

(1982).

(33) (a) Huzinaga's basis set[33b] was augmented with one
diffuse d, two p, and three f functions. See ref. 31
for details. (b) S. Huzinaga, $\underline{\text{J. Chem. Phys.}}$, **66**,
4245 (1977).

(34) For instance, (a) P. J. Hay, $\underline{\text{J. Am. Chem. Soc.}}$, **109**,
705 (1987). (b) G. R. Haynes, R. L. Martin, and P. J.
Hay, $\underline{\text{J. Am. Chem. Soc.}}$, **114**, 28 (1992). (c) C.
Daniel, N. Koga, J. Han, X. Y. Fu, and K. Morokuma, $\underline{\text{J.}}$
$\underline{\text{Am. Chem. Soc.}}$, **110**, 3773 (1988). (d) N. Koga, and K.
Morokuma, $\underline{\text{J. Phys. Chem.}}$, **94**, 5454 (1990).

(35) (a) The C_{2v}-like structure, in which the Si-Si bond was
perpendicular to the PPdP bond, was also optimized.
In this structure, both $Pd(PH_3)_2$ and Si_2H_6 parts little
distort, and the stabilization energy is almost the
same as that of the C_{2v}-like structure of Figure 7.1.
(b) The C_s-structure of $Pd(PH_3)_2(SiH_4)$ was also
optimized (see Figure 7.2 of ref. 23 for the C_s-
structure), but its stabilization energy was almost
the same as that of the C_{3v}-like structure (Figure
7.1).

(36) The structure shown in Figure 7.1 corresponds to the
most stable structure of the Pt's precursor complex.[23]
The other structures were not calculated. Even if the
other structure was more stable than that in Figure
7.1, the energy stabilization would be absolutely
small, and therefore, E_a would be little influenced,
like in the Pt analogues.[23]

(37) S. F. Boys and F. Bernardi, $\underline{\text{Mol. Phys.}}$ **19**, 553 (1970).
N. S. Ostlund, D. L. Merrifield, $\underline{\text{Chem. Phys. Lett.}}$

39, 612 (1976).

(38) (a) In optimizing this TS, the Pd-P bond distance considerably fluctuated, which made the optimization much difficult. Thus, the full optimization was abandoned, and the optimization was performed as follows; the Pd-P distances were optimized for the roughly optimized geometry[38b)] of the Pd(SiH$_3$CH$_3$) part, then the Pd(SiH$_3$CH$_3$) part was optimized with Pd-P distances fixed, and finally, again the Pd-P distances were re-optimized. Through the re-optimization, the Pd-P distances were changed by only 0.02 Å. (b) The maximum change of geometrical parameter was ca. 0.018 Å for bond distance and ca. 2° for bond angle.

(39) For instance, K. Tatsumi, R. Hoffmann, A. Yamamoto, and J. K. Stille, Bull. Chem. Soc. Jpn., **54**, 1857 (1981).

(40) (a) MELD plogram[40b] was used for these SD-CI calculations. A single reference wavefunction was constructed from either HF closed shell MOs or Roothaan's restricted open-shell MOs, and the virtual orbitals were transformed to K-orbitals,[40c] where all core orbitals were excluded from the active space. To reduce numbers of excited configurations, all possible spin-adapted configuration functions were screened through the second-order Rayleigh-Schödinger perturbation theory,[40d] and remaining excited configurations underwent variational CI calculation. The total energy from the limited SD-CI calculation was corrected by adding the correlation energy arising from the discarded excited configuration functions,

and then further correction was made by estimating higher order CI expansions.[40e] (b) E. R. Davidson, L. McMurchie, S. R. Elbert, S. R. Langhoff, D. Rawlings, and D. Feller, MELD; University of Washington, Seattle, WA; IMS Computer Center Library, No. 030. (c) D. Feller and E. R. Davidson, <u>J. Chem. Phys</u>, **84**, 3997 (1981). (d) S. R. Langhoff and E. R. Davidson, <u>Int. J. Quantum Chem</u>., **8**, 61 (1974). (e) E. R. Davidson and D. W. Silver, <u>Chem. Phys. Lett</u>., **52**, 403 (1977).

(41) Ip(d_{xz}) is calculated as an energy difference between $^1A(d^{10})$ and $^2B_1(d^9)$ states of Pd(PH), where their total energies were calculated with the SD-CI method.[40]

Chapter 8

General Conclusion

In part I of this thesis, coenzyme functions of thiamin diphosphate and biotin are investigated theoretically. Thiamin diphosphate participates in enzymic decarboxylation of pyruvic acid and biotin performs carboxylation of organic substrate by utilizing bicarbonate and ATP.

In chapter 2, the decarboxylation reaction of lactylthiazolium was investigated with AM1 and ab initio MO/MP2 methods, where 2-lactylthiazolium was adopted here as a model of thiamin diphosphate. The decarboxylation step is much difficult to investigate experimentally, probably owing to high reactivity of 2-lactylthiazolium. Theoretical method is useful and expected to offer detailed knowledge on the reaction. The results and new findings obtained are summarized as follows.

(1)   In the decarboxylation of 2-lactylthiazolium, the activation barrier (E_a) is estimated to be very small and the calculated exothermicity (E_{exo}) is considerably large; E_a = 1.5 kcal/mol (AM1), 3.9 kcal/mol (MP2/MIDI-4), 4.4 kcal/mol (MP2/6-31G), and E_{exo} = 23.8 kcal/mol (AM1). Thus, decarboxylation of lactylthiazolium smoothly occurs.

(2)   Two water molecules increase the activation barrier to 5.6 kcal/mol and decrease the exothermicity to 14.7 kcal/mol (AM1). An additional water molecule interacting with the thiazolium ring further increases the activation barrier to 19.0 kcal/mol and significantly decreases the exothermicity to -2.1

kcal/mol (i.e., the reaction becomes endothermic). This
result agrees well with Lienhard's experiment, and
clearly indicates that the main role of thiamin is
desolvation.

(3) As the decarboxylation proceeds, the C^2-$C^{2\alpha}$ and C^2-N
bonds are changing to the corresponding double and
single bonds respectively, and the product takes the
typical enamine structure. This result, as well as
Jordan's experiments, clearly supports that the enamine
intermediate is indeed on the reaction pathway.

(4)   Decarboxylation reactions of 2-lactyloxazolium and
2-lactylimidazolium are theoretically investigated with
the AM1 method, to compare their reactivities with that
of 2-lactylthiazolium. Products of their
decarboxylations also take the enamine structure. In
their decarboxylations, the activation barrier is
slightly higher than that of 2-lactylthiazolium; 2.8
kcal/mol for 2-lactyloxazolium and 6.4 kcal/mol for 2-
lactylimidazolium, but the exothermicity is somewhat
smaller in 2-lactyloxazolium and significantly smaller
in 2-lactylimidazolium (3.9 kcal/mol) than in 2-
lactylthiazolium. Thus, the decarboxylation reactivity
decreases in the order thiazolium > oxazolium >
imidazolium. This decreasing order is interpreted in
terms of the π^* orbital of the azolium ring. Since the
energy level of its π^* orbital lowers in the order
imidazolium > oxazolium > thiazolium, HOMO of 2-
hydroxyethylazolium lowers in the same order, which
results in the most weak $C^{2\alpha}$-CO_2 binding of 2-
lactylthiazolium. Accordingly, the decarboxylation of
2-lactylthiazolium proceeds most easily. The π^* orbital

of the azolium ring would be stabilized in energy by highly polarizable and diffuse orbitals of the S atom.

In chapter 3, structure and bonding nature of carboxy-imidazolidone were theoretically investigated as a model of carboxybiotin with ab initio MO/MP4, SD-CI, and CCD methods. Three isomers, N-carboxyimidazolidone **1**, O-carboxy-imidazolidone **2**, and the η^2-side-on carboxyimidazolidone **3** were examined here. The important results are summarized as follows:

(1)   Imidazolidone can be adopted as a reasonable model of biotin because imidazolidone and methylbiotin have very similar geometry, electron distribution, and π and π^* orbital energies. However, more simple compounds such as CH_3NH_2 and $CH_3NH(CHO)$ cannot be considered as a good model of biotin unlike imidazolidone. $CH_3NH(CONH_2)$ seems reasonable as a model of biotin, because the CO_2 binding energy to $CH_3NH(CONH_2)$ is almost the same as that of carboxyimidazolidone. These results suggest that the urea structure is important in the CO_2 binding with biotin.

(2)   In **1** and **2**, CO_2 lies on the molecular plane. The perpendicular structure is less stable than the planar one by ca. 6 kcal/mol for **1** and 10 kcal/mol for **2** at the MP4SDQ/6-31G level. The binding energy of CO_2 in **1** is much greater than that of **2** by ca. 12 kcal/mol, indicating that **1** is more stable than **2**. This is in accord with the experimental result that N-carboxybiotin is isolated in the biotin-dependent enzymic reactions. It is noted that geometries, electron distribution, and frontier orbitals of **1** and **2** resemble well those of η^1-C

coordinated CO_2 complexes of transition metal. The CO_2 binding energy of η^2-side-on carboxyimidazolidone **3** is much smaller than those of **1** and **2**, and geometry optimization of **3** led to **1**. Thus, the η^2-side-on CO_2 adduct would not exist in the reaction of biotin. The CO_2 part in **1** is considerably activated for an electrophile like it in the transition metal complex. Considering that the several η^1-C coordinated CO_2 complexes of transition metal serve as a key intermediate in electrochemical reduction of CO_2, we can expect that biotin, imidazolidone, and their analogues would be useful as an organic catalyst for electro-chemical reduction of CO_2.

(3)   In carboxyimidazolidone, the charge-transfer from deprotonated imidazolidone to CO_2 strongly occurs. The electron population of CO_2 increases in the order **3** < **2** < **1**. The O^1 and O^2 atomic populations increase but the C atomic population decreases upon formation of carboxyimidazolidone, **1** and **2**. This electron distribution can be interpreted in terms of the bonding interaction between the donor orbital (ϕ_{donor}) of deprotonated imidazolidone and the CO_2 π^* orbital into which the π orbital of CO_2 mixes in an anti-bonding way with ϕ_{donor}.

(4)   Energy decomposition analysis of the interaction between deprotonated imidazolidone and CO_2 also shows that the charge-transfer from deprotonated imidazolidone to CO_2 (the CTPLXA term) largely contributes to the CO_2 binding energy. The difference in stability between **1** and **2** mainly arises from this term. This is because ϕ_{donor} of deprotonated imidazolidone expands more largely

on the N atom than on the O atom. Consequently, **1** can receive greater stabilization energy from the CTPLXA term than **2**.

(5)   The electron distribution and frontier orbitals indicate the possibility that the electrophile and cationic species interact with the O atom of CO_2 to activate it for the carboxyl-transfer reaction.

In Part II, several elementary reactions involved in transition-metal catalytic cycles are theoretically investigated. The first is the CO_2 insertion into the M-H and M-R (R = alkyl) bonds, the next is the C_2H_4 insertion into the Cu(I)-R bond, and the last is the oxidative addition of the Si-X σ-bond to the palladium (0) complex.

In chapter 4, ab initio MO/MP4, SD-CI, and CCD (coupled cluster with double substitution calculations were carried out on the CO_2 insertion into the Cu(I)-R bond (R = H, CH_3, or OH) and the C_2H_4 insertion into the Cu(I)-R (R = H and CH_3). Many important findings are reported, as follows;

(1)   The activation energy (E_a) is calculated to be very low (ca. 4 - 5 kcal/mol) for the CO_2 insertion into the Cu-H bond, relatively high (9 - 10 kcal/mol) for the C_2H_4 insertion into the Cu-H bond, and very high (23 - 30 kcal/mol) for the C_2H_4 insertion into the Cu-CH_3 bond. These results suggest that the C_2H_4 insertion into the Cu-R bond is much more difficult than the CO_2 insertion into the Cu-R bond.

(2)   The difference of E_a between CO_2 and C_2H_4 insertion reactions can be interpreted in terms of π and π^* orbitals of CO_2 and C_2H_4; because the π orbital of C_2H_4 lies higher in energy than that of CO_2, the exchange

209

repulsion between C_2H_4 and R is much larger than that between CO_2 and R, leading to the higher E_a value of the C_2H_4 insertion. Since the π^* orbital of CO_2 becomes more stable than that of C_2H_4 with increasing distortion, the charge-transfer from the metal part to CO_2 is greater than the charge-transfer from the metal part to C_2H_4.

(3)   The exothermicity of the CO_2 insertion is much greater than that of the C_2H_4 insertion. The main reason for the greater exothermicity of the CO_2 insertion is that the Cu-OC(O)H bond energy is larger than the $Cu-C_2H_5$ and $Cu-CH_3$ bond energy by ca. 50 kcal/mol. CO_2 is inserted into the Cu-OH bond with no barrier. This is because the HOMO of $Cu(OH)(PH_3)_2$ mainly consists of the lone-pair type orbital of OH^- and the bonding interaction between CO_2 and OH can be formed without weakening of the Cu-OH bond. However, the exothermicity of this insertion is smaller than that of the other CO_2 insertion, since the Cu-OC(O)OH bond energy is about 29 kcal/mol larger than the Cu-OH bond energy (remember that Cu-OC(O)R bond energy is about 50 kcal/mol larger than the $Cu-CH_3$ bond energy).

(4)   From the above result (3), one can predict that a primarily important factor for the CO_2 insertion is the presence of a lone-pair type orbital of R which is not used for coordination to Cu. When the R ligand possesses such a lone-pair type orbital, the bonding interaction between this lone-pair type orbital and the LUMO of CO_2 can be formed without weakening of the Cu-R bond. This situation facilitates the CO_2 insertion into the Cu-R bond.

In chapter 5, the CO_2 insertion into the Rh(I)-H bond of RhH(PH$_3$)$_3$ was theoretically investigated by ab initio MO/MP4, SD-CI and coupled cluster (CCD) calculations. Results to be noted are summarized as follows:

(1)   The CO_2 insertion into the Rh(I)-H bond easily occurs with an activation barrier of ca. 16 kcal/mol and exothermicity of ca. 24 kcal/mol at the SD-CI level, yielding Rh(η^1-OC(O)H)(PH$_3$)$_3$. This activation barrier is higher and the exothermicity is lower than those of the similar CO_2 insertion into the Cu(I)-H bond of CuH(PH$_3$)$_2$ in which activation barrier is 3.5 kcal/mol and the exothermicity is ca. 40 kcal/mol at the SD-CI level.

(2)   The higher activation energy of the Rh reaction system results from the facts that the Rh(I)-H bond is stronger than the Cu(I)-H bond by ca. 28 kcal/mol at the MP4SDQ level, the negative electrostatic potential of RhH(PH$_3$)$_3$ is smaller than that of CuH(PH$_3$)$_2$, and the EX repulsion between CO_2 and RhH(PH$_3$)$_3$ is greater than that between CO_2 and CuH(PH$_3$)$_2$. The lower exothermicity of CO_2 insertion into the Rh(I)-H bond is also due to the stronger Rh(I)-H bond than the Cu(I)-H bond, because the difference between Rh(I)-OC(O)H and Cu(I)-OC(O)H bonds is considerably small.

(3)   The transition state of the Rh reaction system has a shorter C-H distance between CO_2 and the H ligand than it in the transition state of the Cu reaction system. The reason of the short C-H distance is the strong Rh(I)-H bond; in the transition state of the Rh reaction system, CO_2 must approach the H ligand to a greater extent than in the transition state of the Cu reaction system, so as to break the strong Rh(I)-H bond. The

211

RhHC angle at the transition state is much different between two reaction systems; this angle is 145° in the Rh reaction system but only 105° in the Cu reaction system. The larger RhHC angle arises from the strong EX repulsion between the occupied $4d_{xz}$ orbital of Rh and the occupied π and $n\pi$ orbitals of CO_2. The Rh $4d_{xz}$ orbital more expands than the Cu $3d_{xz}$ orbital, which gives rise to the stronger EX repulsion with CO_2 in the Rh reaction system.

(4)   From these results, one can predict that the CO_2 insertion into the M-H bond easily occurs, when the M-H bond is weak, the electrostatic potential of the metal hydride complex is negatively large, and the expanse of the d_{π} orbital is small.


In chapter 6, the CO_2 insertion into the Rh^{III}-H bond was theoretically investigated with ab initio MO/MP4, SD-CI and CCD methods. Electron correlation effects and basis set effects on the activation energy (E_a) and the reaction energy (ΔE) are also examined. The CO_2 insertion into the Rh^{III}-H bond are compared with the similar CO_2 insertion into the Rh^{I}-H and Cu^{I}-H bonds investigated in chapters 4 and 5.

(1)   Electron correlation effects were investigated by using such methods as MP2 - MP4SDQ, SD-CI, and CCD. Although E_a and ΔE somewhat fluctuate at MP2 and MP3, similar values of E_a and ΔE are calculated with MP4, SD-CI, and CCD methods. This result clearly shows that discussion of the E_a and ΔE of CO_2 insertion into the M-H bond should be based on calculations including electron correlation effects, at least, at the MP4SDQ level.

(2)   Basis set effects were examined in the CO_2 insertion

212

into the Rh^I-H and Rh^{III}-H bonds. Although use of the effective core potential (ECP) instead of all electron basis set for Rh causes little effects on the E_a and ΔE, introduction of polarization functions on CO_2 considerably increases E_a and remarkably decreases the exothermicity. These results indicate that the polarization function is very important and indispensable to estimate the activation energy and the reaction energy.

(3)   When polarization functions were added on CO_2, introduction of electron correlation changes the activation energy and the reaction energy only a little. Consistent with these results, no instability of the HF wave-function was observed at the transition state. This is because the H ligand moves toward CO_2 as a hydride ligand, in other words, the C-H bond between CO_2 and H ligand is formed not in a homolytic way but in a heterolytic way accompanied with the strong charge transfer from the H ligand to CO_2.

(4)   The CO_2 insertion into the Rh^{III}-H bond reaches the transition state much more late than the other CO_2 insertion into the Rh^I-H and Cu^I-H bonds, whereas the former is only slightly less exothermic than the CO_2 insertion into the Rh^I-H bond. This is because the charge-transfer from $[RhH_2(PH_3)_3]^+$ to CO_2 is weak and CO_2 must closely approach the H ligand to break the strong Rh^{III}-H bond. In the transition state, therefore, formate is mostly formed and strongly interacts with Rh in a η^1-coordinating way at the trans-position of the H ligand. This geometrical feature is unfavorable because of the strong trans-influence of the H ligand. Thus,

213

the CO_2 insertion into the Rh^{III}-H bond requires the highest activation energy. In the other CO_2 insertion into the Rh^I-H and Cu^I-H bonds, such situation does not emerge, and therefore, the activation energy of these insertion reactions is much lower than the CO_2 insertion into the Rh^{III}-H bond. From this result, we can predict that the structure B of $RhH_2(PH_3)_3$ shown in Scheme 8.1 is more favorable for the CO_2 insertion, because the formate is formed at the *trans* position of not the H ligand but the PH_3 ligand.
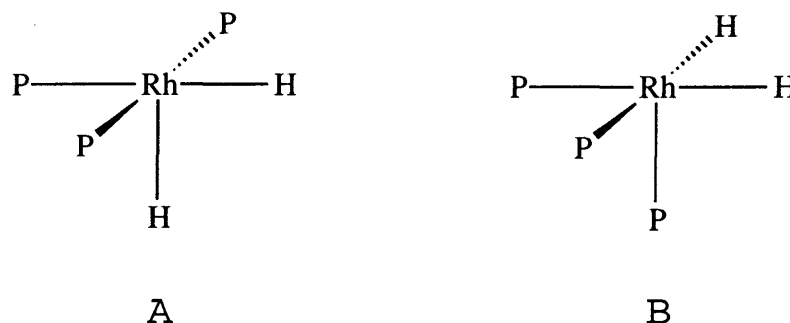
Scheme 8.1

In chapter 7, ab initio MO/MP4 studies were carried out on the oxidative addition of the Si-X σ-bond (X = H, C, or Si) to $Pd(PH_3)_2$. This reaction is involved in several catalytic reactions such as hydrosilation and bis-silation of alkenes and alkynes as an important elementary process. The results obtained are compared with several previous works, and detailed insight into this kind of reaction is presented, as follows:

(1)   The Si-X oxidative addition to $Pd(PH_3)_2$ proceeds with lower activation energy but lower exothermicity than it to $Pt(PH_3)_2$. The lower exothermicity arises from the fact that the Pd-X bond is weaker than the Pt-X bond, as

expectedly. Unexpected result of the lower activation energy is attributed to the lower distortion energy and the relatively high d_π orbital energy of Pd(PH$_3$)$_2$ at the transition state.

(2)   An interesting prediction is also possible for the reductive elimination which is the reverse reaction of the oxidative addition. For instance, the reductive elimination of Pd(SiH$_3$)(CH$_3$)(PH$_3$)$_2$ is calculated to proceed with only 8 kcal/mol of the activation energy while that of Pt(SiH$_3$)(CH$_3$)(PH$_3$)$_2$ is calculated to require the 39 kcal/mol of the activation energy. This result suggests that the reductive elimination is much more difficult in cis-Pt(SiH$_3$)(PH$_3$)$_2$ but rather easy in the Pd-analogue.

(3)   From these results, we can expect that the palladium(0) complex is more useful as a catalyst for the reaction including both oxidative addition and reductive elimination of Si compounds than the platinum(0) complex; for instance, if the insertion of alkene and alkyne into the Pd-SiH$_3$ bond easily occurs, the palladium(0) complex is more useful for the bis-silylation of olefin, acetylene, butadiene, etc. than the platinum(0) complex.

In this thesis, theoretical studies with the ab initio MO method were carried out on several elementary reaction steps involved in catalytic reactions by enzymes and transition-metal complexes. We obtained detailed theoretical informations, such as geometries, electronic structures, and bonding natures of the intermediates and transition states, activation energies and reaction energies

215

in the examined reaction steps. These informations are very
useful to understand well the catalytic reactions. Thus,
the ab initio MO method is considered to be powerful means
in investigating catalytic reactions, and in designing a
good catalyst.